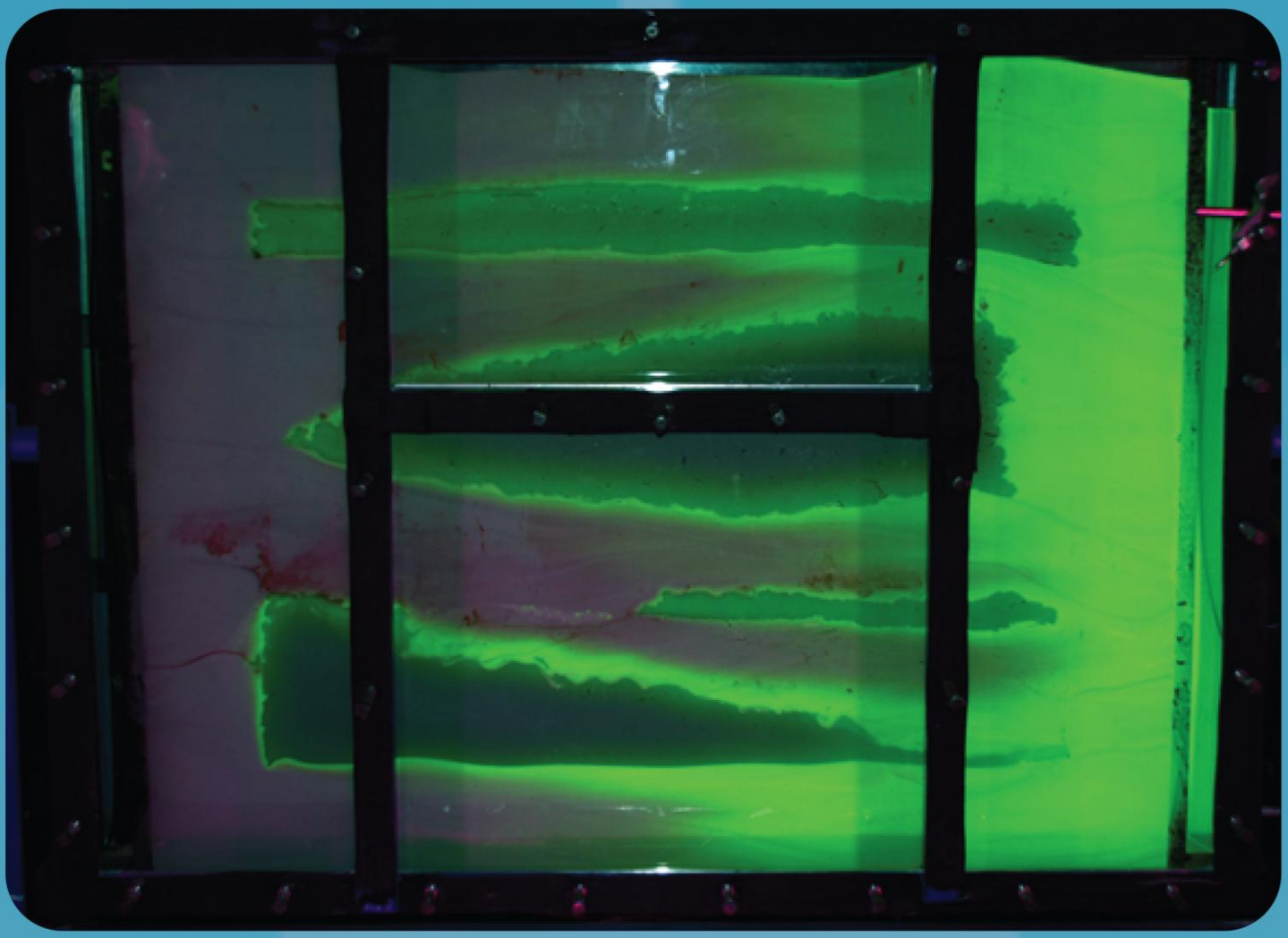

Modern Subsurface Contaminant Hydrology

Tom Sale and Joe Scalia

THE GROUNDWATER PROJECT

Modern Subsurface Contaminant Hydrology

The Groundwater Project

Tom Sale

Emeritus Professor
Department of Civil and Environmental Engineering
Colorado State University
Fort Collins, Colorado, USA

Joe Scalia

Associate Professor
Department of Civil and Environmental Engineering
Colorado State University
Fort Collins, Colorado, USA

Modern Subsurface Contaminant Hydrology

The Groundwater Project
Guelph, Ontario, Canada

The Groundwater Project relies on private funding for book production and management of the Project.

Please consider sponsoring The Groundwater Project so our books will continue to be freely available. https://gw-project.org/donate/↗

Thank you.

Published by The Groundwater Project, Guelph, Ontario, Canada, 2025.

Modern Subsurface Contaminant Hydrology - First Edition / Tom Sale and Joe Scalia - Guelph, Ontario, Canada, 2025.
269 pages
DOI: https://doi.org/10.62592/IQDO4854↗.
ISBN: 978-1-77470-131-7

Please consider signing up for GW-Project mailing list to stay informed about new book releases, events, and ways to participate in the GW-Project. When you sign up for our email list, it helps us build a global groundwater community. Sign up↗.

APA (7th ed.) Citation

Sale, T., & Scalia, J. (2025). *Modern Subsurface Contaminant Hydrology, first edition*. The Groundwater Project. https://doi.org/10.62592/IQDO4854↗.

Cover Image: Laboratory sand tank study demonstrating the concept of back diffusion from low permeability zones; work by Lee Ann Doner and Tom Sale in 2008.

Dedication

We are standing on the shoulders of many. Firstly, we want to recognize the transformational work and inspirations provided by Drs. John Cherry, David McWhorter, and Ralph Peck. Secondly, we wish to acknowledge individuals contributing to the themes in this book. They include Beth Parker, Chuck Newell, Steve Chapman, Robert Gillham, Fred Payne, Alan Freeze, Rick Johnson, Mark Lyverse, Jens Blotevogel, Harley Hopkins, David Ellis, Ed Seger, Hans Stroo, and innumerable students and academic research associates. Generous funding and thematic inspiration have come from the industry sponsors of the University Consortium for Field Focused Groundwater Research (since 1987) and the US Department of Defense's SERDP and ESTCP programs.

Table of Contents

The Groundwater Project Foreword

The United Nations (UN)-Water Summit on Groundwater, held from 7 to 8 December 2022, at the UNESCO headquarters in Paris, France, concluded with a call for governments and other stakeholders to scale up their efforts to better manage groundwater. The intent of the call to action was to inform relevant discussions at the UN 2023 Water Conference held from 22 to 24 March 2023 at the UN headquarters in New York City. One of the required actions is *strengthening human and institutional capacity*, for which groundwater education is fundamental.

The UN-Water website↗ states that *more than three billion people worldwide depend on water that crosses national borders*. There are 592 transboundary aquifers, yet most do not have an intergovernmental cooperation agreement in place for sharing and managing the aquifer. Moreover, while groundwater plays a key role in global stability and prosperity, it also makes up 99 percent of all liquid freshwater—accordingly, groundwater is at the heart of the freshwater crisis. *Groundwater is an invaluable resource*.

The Groundwater Project (GW-Project), a registered Canadian charity founded in 2018, pioneers in advancing understanding of groundwater and, thus, enables *building the human capacity for the development and management of groundwater.* The GW-Project is not government funded and relies on donations from individuals, organizations, and companies. The GW-Project creates and publishes high-quality books about *all things groundwater* that are scientifically significant and/or relevant to societal and ecological needs. Our books synthesize knowledge, are rigorously peer reviewed and translated into many languages. Groundwater is hidden and, therefore, our books emphasize visualizations essential to support the spatial thinking and conceptualization in space and time of processes, problems, and solutions. Based on *our philosophy that high-quality groundwater knowledge should be accessible to everyone*, The GW-Project provides all publications for free.

The GW-Project embodies a new type of global educational endeavor made possible by the contributions of a dedicated international group of over 1,000 volunteer professionals from a broad range of disciplines and from 70 countries on six continents. Academics, practitioners, and retirees contribute by writing and/or reviewing books aimed at diverse levels of readers including children, youth, undergraduate and graduate students, groundwater professionals, and the general public.

The GW-Project started publishing books in August 2020; by the end of 2024, we had published 55 original books and 77 translations (55 languages). Revised editions of the books are published from time to time. In 2024, interactive groundwater education tools and groundwater videos were added to our website, gw-project.org↗.

We thank our individual and corporate sponsors for their ongoing financial support. Please consider sponsoring the GW-Project so we can continue to publish books free of charge.

The Groundwater Project *Board of Directors*, January 2025

Foreword

Groundwater contamination is a critical issue, as water extracted from aquifers around the world contains contaminants, some harmless, others potentially hazardous. Regardless of their nature, understanding these contaminants is increasingly important given worsening global trends. This book *Modern Subsurface Contaminant Hydrogeology* discusses the processes and concepts that are needed to understand groundwater contamination. The Groundwater Project has issued other books concerning particular aspects of contamination, including Robertson (2021), Rittman (2023), Mumford and others (2024), and Mackay and others (2024), but this book by Sale and Scalia is the most integrative and has the most general relevance.

This book presents a new paradigm for contaminant transport. It is truly modern in that it covers all of the concepts and processes that have come to be recognized as important by 1) embracing heterogeneity in physical properties governing transport with the primary conceptualization of the subsurface as transmissive zones interspersed with low-*k* zones; 2) recognizing diffusion as a critical process with dispersion as a weak process; 3) elevating the role of natural assimilation processes with reactions being consequentially different in transmissive and low-*k* zones; and 4) providing alternatives to widely employed advective-dispersive models. For example, with respect to transport of contaminants, it recognizes that Fick's law for diffusion is as important as Darcy's law for groundwater flow and enthusiastically incorporates the complexity of geological heterogeneity.

This comprehensive coverage of contaminant hydrology combines quantitative tools for analysis of contaminant behavior with conceptual model development for the different forms of contamination including dissolved chemicals as well as oily liquids both more and less dense than water. The authors help us cope with the uncertainties associated with contaminants in groundwater by stressing that we proceed with thoughtfully assembled site conceptual models, anticipate a range of plausible model alternatives, monitor the site to compare field findings with the conceptual model, develop contingencies for consequential alternatives, and implement the contingencies as needed.

Numerous photographs and videos of laboratory experiments using dye as tracers are presented in addition to results of simulations using analytic and numerical models to help readers conceptualize effects of different processes and magnitudes parameter values.

This book has an outstanding combination of rigor, balance, and diversity that reflect the non-traditional education and experience of the authors including multiple types of academic programs, consulting, teaching, and research. Dr. Tom Sale is a professor emeritus and Dr. Joe Scalia, Associate Professor, both in the Department of Civil & Environmental Engineering at Colorado State University, USA.

John Cherry, The Groundwater Project Leader

Guelph, Ontario, Canada, July 2025

Preface

This text grows from the graduate course notes of Professor Tom Sale in the Department of Civil & Environmental Engineering at Colorado State University in Fort Collins, Colorado, USA, which he passed along to then Assistant Professor Joe Scalia when he retired. Professor Sale built his graduate course through integration of his professional experience at untold contaminated sites and the transformative work of Drs. John Cherry, David McWhorter, Beth Parker, Steve Chapman, Chuck Newell, Robert Gillham, Fred Payne, Alan Freeze, Rick Johnson, Mark Lyverse, Jens Blotevogel, Harley Hopkins, David Ellis, Ed Seger, Hans Stroo, and innumerable students and academic research associates. Much of our knowledge presented herein was built within the University Consortium for Field Focused Groundwater (since 1987), originally led by Professor John Cherry, and more recently captained by Professor Beth Parker. We are standing on the shoulders of many.

Dr. Sale started working in the remediation industry in 1981, where he found himself standing in the middle of a petroleum refinery on the banks of the Arkansas River in Oklahoma. He pulled up to a well, got out of his truck, and shook hands with Steve Blake – destined to be the CEO of ARCADIS and a lifelong friend. Steve took Dr. Sale to a well and pointed down an 8-inch steel casing. Below he saw a shimmering surface. In a eureka moment, he exclaimed "groundwater!" to which Steve exclaimed "gasoline!" They installed dual pump recovery wells across the refinery, on their best day recovering 2,200 barrels of petroleum liquids. Tom's journey towards writing this book had begun.

In 1983 Dr. Sale returned to school under Dr. John Thames at the University of Arizona where he interacted with some of the finest hydrologists of the day including Drs. John Thames, Stan Davis, Marty Fogel, Eugene Simpson, and Shlomo Neuman. Per the standards of the time, the conceptual basis for subsurface contaminant transport was largely that of C. V. Theis's solution for flow to a pumped well—uniform horizontal flow in infinite homogeneous-isotropic media, or "classroom aquifers." In hindsight, Dr. Simpson had nascent ideas about transport and the importance of low permeability inclusions (low-*k* zones) in transmissive media that come into focus in this book.

Dr. Sale returned to work in 1985 with a leading engineering firm. Over ten years he rose through the company's ranks and got to see the curtains pulled back at an untold number of sites with subsurface contamination. A notable project (1987–1990) was a multimillion dollar in-situ treatment development program at a former wood treating plant on the banks of the Laramie River in Wyoming. Simply put, all the king's horses and all the king's men couldn't put humpy dumpty (the site) back together again. The principal actors in our failure were ubiquitous fine-grained low permeability (low-*k*) zone inclusions that 1) preferentially held contaminants and 2) were absent in the predictive tools we used to anticipate the performance of our remedy.

In 1994 Dr. Sale returned to school to a PhD program in Engineering from Chemical and Agricultural Engineering at Colorado State University under Dr. David McWhorter. Dr. McWhorter is an inspirational first principles scholar. At the time Dr. McWhorter was making novel contributions regarding diffusion driven storage and release of contaminants in low-*k* zones. Other faculty at Colorado State University whose work is reflected in this text include Drs. Art Corey and Willard Lindsay. Dr. McWhorter and Dr. Sale explored advection-diffusion-controlled mass transfer from DNAPL pools in homogeneous-isotropic subsurface domains and learned that 1) partial depletion of DNAPL can have limited near-term benefits with respect to attaining drinking water standards and 2) resolving the benefits of subsurface remediation requires an understanding of hysteretic storage and release of contaminants in low-*k* zones via diffusion. Funding for Dr. Sale's PhD came from the industry funded University Consortium for Field-Focused Groundwater Research (since 1987) led by Dr. John Cherry. Tom then embarked on an academic career in the Department of Civil & Environmental Engineering at CSU that spanned the ranks of Research Assistant (2001–2008), Associate (2009–2017), Full (2018–2022), and Emeritus Professor (2022–present). The intellectual hub for his research and teaching endeavors was Dr. Cherry's University Consortium.

Building on University Consortium research at the Universities of Waterloo and of Guelph in Ontario, high resolution transects and longsects from multiple-level point sampling systems brought critical new light to our understanding of contaminant transport in natural subsurface settings. Quoting a consultant collecting high resolution site characterization data, "once seen there's no going back." Insights from high-resolution site characterization data include the prevalence of steep local concentration gradients and the magnitude of contaminants stored in low-*k* zones. High resolution data provide a point of embarkation from traditional views of contaminant transport seen through the lenses of monitoring wells. Notably, monitoring wells provide vertically integrated aqueous concentrations weighted to the concentrations in the most transmissive layers. Integral water-quality data from monitoring wells have 1) created misconceptions regarding mixing in transmissive zones dominated by laminar flow and 2) obscured our realization of hysteretic storage in and release of contaminants from less-transmissive zones via diffusion. Arguably, studying subsurface contaminant transport through the lens of monitoring wells can be misleading.

Dr. Scalia has a shorter story. He began working in the remediation industry for a specialty consulting firm in 2012 after completing his PhD in Geological Engineering at the University of Wisconsin-Madison. During his studies he had the opportunity to interact with a broad range of geoenvironmental scholars, including groundwater hydrogeologists Drs. Mary Anderson and Herb Wang, and geotechnical engineers Drs. Craig Benson and Tuncer Edil. Dr. Benson introduced Dr. Scalia to the applied and adaptive thinking of Drs. Ralph Peck, Roy Olson, and Dave Daniel, his academic grandfather, great-grandfather, and

great-great grandfathers, respectively. His work at UW-Madison focused on environmental containment systems intentionally engineered to attempt to achieve homogeneity.

Much of Dr. Scalia's work involved forensic investigations of contaminated sites and failed environmental containment systems. He benefited immensely from the mentorship of Peter Mesard, Walt Shields, Gary Bigham, Melissa Kleven, Mark Johns, and many other brilliant minds. He had the opportunity to see firsthand consequences of ignoring heterogeneity, back diffusion, the importance of mathematical models as a tool to building and exploring interdependent processes in support of conceptual models, and what happens when you attempt to clean up a contaminated site without adaptive site management, or as Ralph Peck famously articulated for geotechnical engineers, the observational method. In 2015, Dr. Scalia left consulting to join Dr. Sale in the Department of Civil & Environmental Engineering at CSU. He had the opportunity to work with diffusion guru Professor Chuck Shackelford—the PhD advisor of the undergraduate professor, Dr. Mike Malusis, that introduced him to geoenvironmental engineering.

This text provides the authors' conceptualization of contaminant transport in subsurface media predicated on heterogeneous hydrogeologic settings. This book departs from prior works by embracing heterogeneity in physical properties governing transport, diffusion as a critical process, dispersion as a weak process, natural assimilation processes, and provides alternatives to widely employed advective-dispersive models. The primary conceptualization is transmissive zones interspersed with low-*k* zones. Transport in transmissive zones is dominated by advection with weak hydrodynamic mixing and diffusion. Transport in low-*k* zones is dominated by diffusion with slow advection. Exchanges between transmissive and low-k zones are dominated by diffusion. Reactions, that can be consequentially different in transmissive and low-*k* zones, modify transport. Conceptualizations built on idealized heterogeneous (as opposed to homogeneous) representative volumes provide the reader a rigorous foundation for understanding and managing anthropogenic contaminants in the subsurface.

Acknowledgments

We deeply appreciate the thorough and useful reviews of and contributions to this book by the following individuals:

- Dr Chuck Newell, GSI Environmental, Houston Texas, USA.
- Dr. Rick Johnson, School of Public Health at the Oregon Health and Science University, Portland Oregon, USA.

We appreciate technical assistance provided by:

- Dr. David McWhorter (mathematics), Colorado State University (retired), Masonville, Colorado, USA.
- Dr. Jens Blotevogel (reactions), CSIRO, Adelaide, South Australia, Australia.

Furthermore, we are grateful to Amanda Sills and the Formatting Team of The Groundwater Project for their oversight and copyediting of this book. We thank Eileen Poeter (Colorado School of Mines, Golden, Colorado, USA) for reviewing, editing, and producing this book.

The sources of figures and/or tables are cited in their captions. Where a citation does not appear, the figures and/or tables are original to this book.

1 Overture

Demonstratively, 99 percent of all the unfrozen freshwater on our planet is groundwater. Nearly half of the earth's citizens rely on groundwater for their daily drinking water (e.g., Poeter et al., 2020). In the face of climate change, environmental-economic constraints, a growing global population, and challenges to surface water development, rational stewardship of groundwater is critical to the sustainable future of humanity.

Unfortunately, agricultural, industrial, and defense activities over previous centuries have led to releases of innumerable contaminants of concern (CoCs) to soil and groundwater systems (National Research Council (NRC), 1994, 2005). Sweeping laws have been passed by many nations, and an interdisciplinary army of scientists, engineers, and others have been engaged to mitigate negative impacts after broad recognition of threats to human health and the environment. Positively, large global investments have limited exposures to CoCs and limited new releases. Negatively, much of the footprint of legacy releases remains despite decades of promised cleanup, and problems continue to emerge. Notably, the National Research Council (NRC) Committee on Ground Water Cleanup Alternatives in a 1994 report (NRC 1994) recognizes growing concern "*that the nation might be wasting large amounts of money on ineffective remediation efforts* (pp. 1)." Three subsequent NRC reports addressing remediation (2003, 2005, 2013) do little to dispel concerns regarding limited progress in resolving impacts of subsurface releases.

Our intent in writing this book is to offer a modern conceptual foundation for contaminant transport in natural subsurface settings to support rational management of CoCs and better use of the finite resources available for their cleanup. This book departs from the classical conceptualization of homogeneous *classroom aquifers* and stylistically embraces the complexity and inherent uncertainties of natural systems, including the 11 points that follow.

1. Subsurface porous media are heterogeneous with spatial variations in permeability (transmissive and low-permeability (low-*k)* zones), diffusion coefficients, contaminant concentrations (in all phases), natural organic carbon, mineralogy, redox conditions, and microbial ecology.
2. Diffusion is a critical process governing storage and release of CoCs to and from low-*k* zones.
3. Reactions governing transport can be distinctly different in transmissive and low-*k* zones.
4. Assimilation of CoCs via transformation reactions are typically governed by thermodynamic conditions imposed by natural settings and interdependent biological and geochemical (*biogeochemical*) processes.
5. Transverse mixing of contaminants in plumes is typically a weak process.

6. Concentrations at the leading and tailing ends of plumes in transmissive zones are primarily governed by storage and release of contaminants in low-*k* zones via diffusion and slow advection, as opposed to longitudinal dispersion.
7. Integral aqueous concentrations weighted to transmissive zones from monitoring wells are generally rejected as a basis for studying transport processes.
8. All plausible contaminant phases, including gases, nonaqueous, aqueous, and sorbed, are interdependent and must be recognized.
9. Mathematical models provide a critical means of building tools to explore often-complex interdependent processes in support of advancing sound conceptual models and decisions.
10. Mathematical models: a) require approximations of actual conditions and processes, and b) can fail to recognize consequential aspects of transport and reactions that we have yet to discover.
11. Absolute characterization of sites and forecasting of future conditions is functionally impossible; therefore, uncertainty must be embraced.

The need to move beyond idealized classroom aquifers and manage uncertainties for contaminant transport is not a new concept. C. V. Theis (1967) stated that

> *"the type of aquifer in which our homogeneous model of groundwater flow is most grossly inadequate is that of dealing with transport phenomena… the simple and useful model for problems of well field development will mislead us if we apply it to problems of transport, in which we are concerned with the actual detailed movement of water"* (pp. 139 and 146).

Following Terzaghi and Peck's observational method (Peck, 1969), uncertainties can be managed by: a) proceeding with thoughtfully assembled *site conceptual models* (SCMs): b) anticipating a range of plausible alternatives: c) monitoring to evaluate actual outcomes; d) developing contingencies for consequential alternatives; and e) implementing contingencies as needed.

Primary audiences for this book are university students in an upper-level course in contaminant transport and professionals needing a technical reference. It is assumed readers 1) have a basic knowledge of hydrogeology and 2) are interested in managing contaminants in natural subsurface media. Our goal is to set a rigorous foundation of first principles for modern contaminant transport wherein the term "*modern*" embraces points 1 through 11 delineated in this section. Leading references are provided for those who want to know more. Sources for additional information include a remarkable set of books developed through The Groundwater Project, written by outstanding scientists and engineers under the leadership of Dr. John Cherry.

The content of this book is organized into foundational science and math, reviews of critical concepts and processes, and tools for evaluating contaminant transport. Each section includes practice questions the reader can use to gauge their comprehension.

Readers are encouraged to work the provided problems, as quantitative analyses are often the best route to understanding. We encourage all to jump in and find the joys of math and science as they master the tools needed to advance rational management of CoCs in soils and groundwater.

Lastly, we acknowledge that contaminant transport in the subsurface is an evolving field that has seen exponential growth in knowledge over a handful of decades. We have come so far in discovering the truth and serially realizing what we have missed. We look forward to inevitable advancements and expect there will be future editions of *Modern Subsurface Contaminant Transport*, as our profession continues to advance.

2 Foundations

As a point of embarkation, this section provides foundational information about modern contaminant hydrology as to subsurface settings, CoCs, releases, partitioning between phases, transport processes, reactions, conceptual models, and mathematics, and a demonstrative thought experiment. Central to this section is the theme of embracing heterogeneous subsurface media with respect to properties and processes that govern the nature, distribution, and fate of subsurface contaminants. At the end of this section the reader should be able to successfully complete Exercises 1 through 6 of Section 7. Links to each of those exercises are provided in Section 2.11.

2.1 Subsurface Settings

2.1.1 Domain of Interest

Our domain of interest includes diverse types of subsurface media wherein continuity in pore space allows transport of contaminants through the media. At a pore scale, subsurface porous media may include solid-phase inorganic minerals, solid-phase natural organic material (NOM), an aqueous phase, an immiscible nonaqueous phase, and a gas phase. Geologic processes govern the architecture of transmissive and low-hydraulic-conductivity (low-k) zones in subsurface media at both large and small scales. A knowledge of depositional environments provides a primary basis for developing a stylistic understanding of the spatial distribution of transmissive and low-k zones. Transmissive and low-k zones can have distinctly different permeabilities, diffusion coefficients, contaminant concentrations (in all phases), natural organic materials, mineralogy, redox conditions, and microbial ecology. Herein, following Dr. Beth Parker, we use the term stylistic for generalized, as compared to comprehensive and site specific, characterizations of subsurface conditions.

Figure 1 presents a stylistic introduction to transport in heterogeneous subsurface media, including advective transport through a transmissive subset of a subsurface body accompanied by storage and release of contaminants in low-k zones via diffusion and/or slow advection.

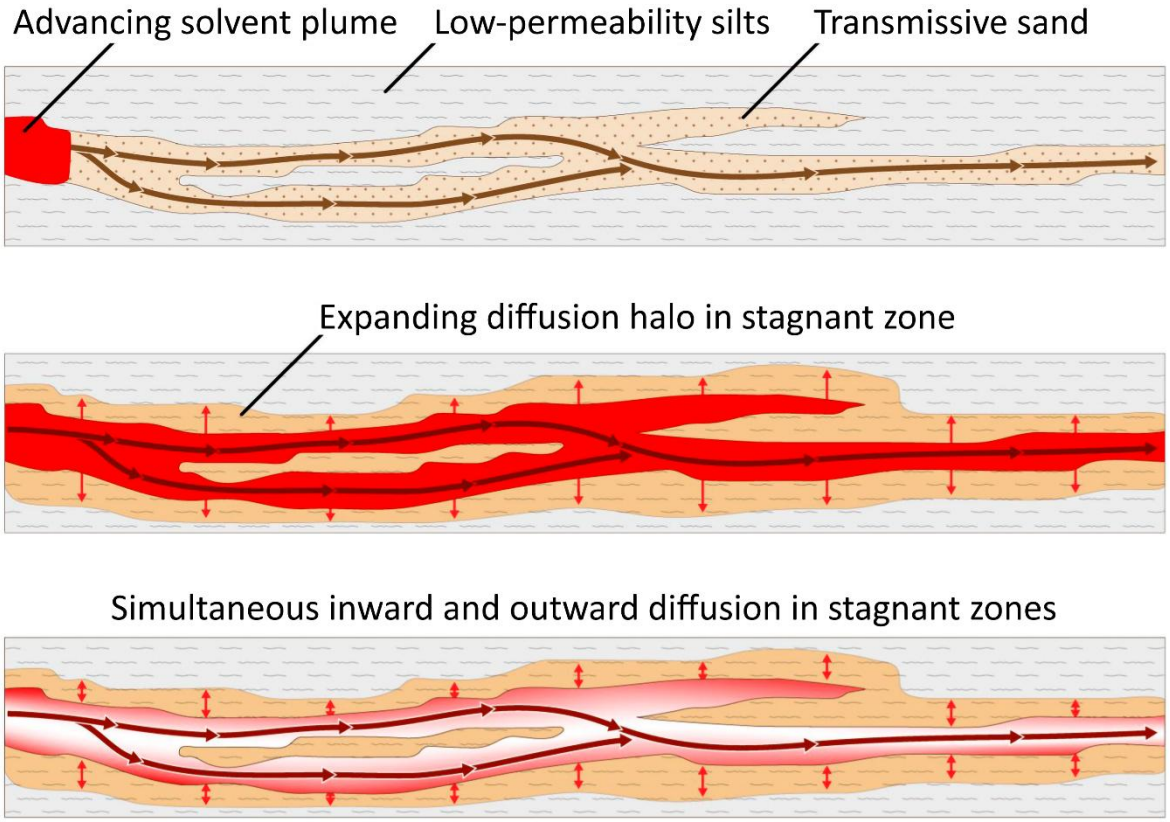

Figure 1 - Stylistic introduction to subsurface transport illustrating advective flow through transmissive zones with storage and release of contaminants in/from low-*k* zones (modified after Sale et al., 2007; Sale & Newell, 2010).

2.1.2 14 Compartment Model

Figure 2 introduces another thematic cornerstone of modern contaminant hydrology, the 14 compartment (14C) model (Sale et al., 2007; Sale & Newell, 2010). Some key attributes of the 14C model include:

- differentiation of subsurface source zones and plumes (NRC, 2005);
- recognition of transmissive and low-*k* porous media in source zones and plumes; and
- recognition of four potential contaminant phases in source zones and three potential contaminant phases in plumes.

The 14C model forces a holistic view of subsurface contamination that addresses plausible subsurface compartments and exchanges between compartments.

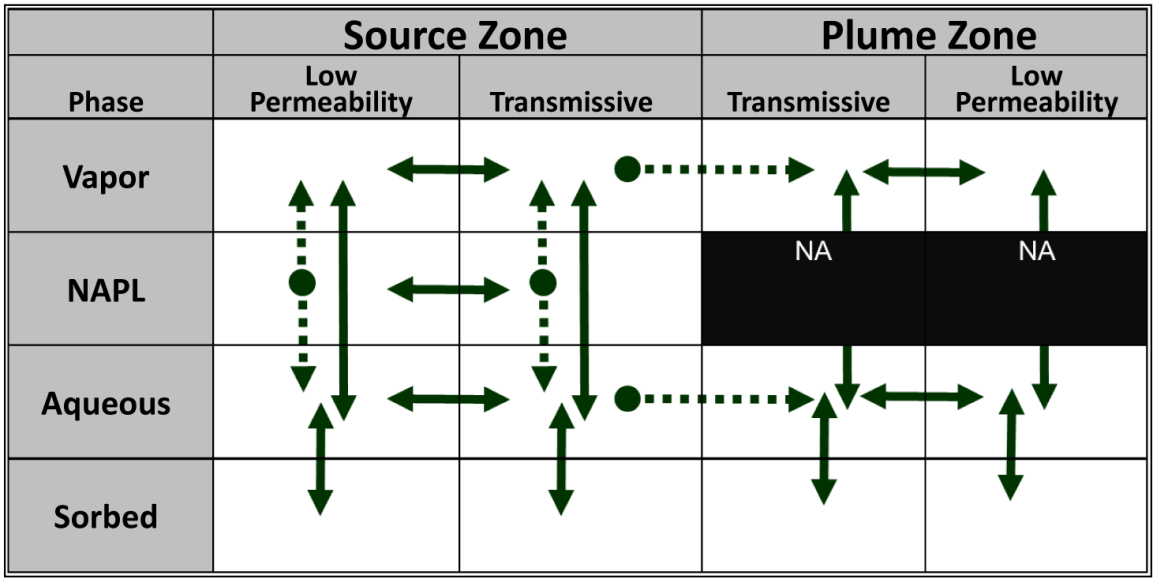

Figure 2 - The 14C model dividing the system into four zones by incorporating source zones and plumes, each with transmissive and low-*k* zones. Four contaminant phases include nonaqueous, aqueous, gas, and sorbed phases. Interconnecting fluxes are shown as solid arrows for reversible processes and dashed arrows for irreversible processes. Two cells are labeled not applicable (NA) because the presence of NAPL in a transmissive or low-*k* zone is a source, not a plume (modified after Sale et al., 2013).

2.1.3 Pore-Scale Subsurface Characteristics

Following Corey (1994), porous media, by definition, have the following characteristics:

- nonsolid space (voids) in a matrix with interconnected pores;
- pore dimensions larger than a representative fluid particle; and
- pore dimensions small enough that interfacial forces between solids, liquids, and gases control the spatial distribution of fluids.

To further define porous media, Figure 3 presents a photo from Wilson and others (1990) with added labels. Per Figure 3, porous media contain two or more of the following phases:

- *solid-phase* minerals (e.g. quartz sand grains);
- a liquid *wetting phase* in direct contact with the solid phase (typically water);
- a *nonwetting phase* in the center of the pores (typically gas); and
- an *intermediate wetting phase* between the wetting and nonwetting phases (typically an immiscible nonaqueous phase liquid [NAPL]).

The distribution of fluids at a pore scale is governed by interfacial forces. As a first-order approximation, *like* compounds are attracted such that polar solids attract polar aqueous solutions (vis-à-vis like likes like). Similarly, *dislike* compounds are repelled, and nonpolar fluids are repelled by polar liquids. Where present, intermediate wetting fluids are more polar than gases and less polar than aqueous solutions. Pausing to reflect on the complexities inherent in Figure 3 is warranted. Complexities include the following:

- pore spaces can contain up to three immiscible fluids (e.g., air, water, and NAPL);

- CoCs which may occur in gas, aqueous, nonaqueous, and sorbed phases; and
- diverse microbial communities, which are near-ubiquitously present.

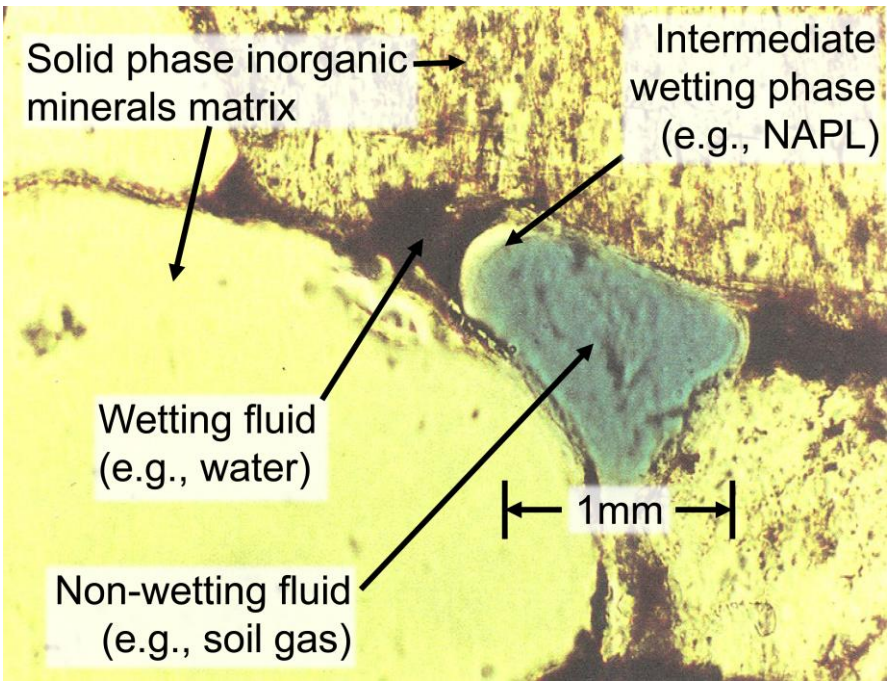

Figure 3 - Porous media composed of solid-phase inorganic mineral matrix (yellow), an aqueous wetting phase (brown), an immiscible nonaqueous intermediate wetting phase (light brown), and a nonwetting gas phase (blue-grey) (modified after Sale, 2001; photo from Wilson et al., 1990).

2.1.4 Macro-Scale Subsurface Characteristics

At a macro scale, subsurface domains are a product of diverse geologic processes that create a vast abundance of subsurface settings. Inclusive of governing geologic processes are life (including carbon cycling), climate evolution, post-depositional secondary alterations, and anthropogenic activities. Figure 4 provides a conceptual family tree for common depositional environments. When studying transport, an initial question should always be "*What is the site's depositional environment?*" Understanding the style of what one is getting into is central to managing subsurface contamination. Alternatively, ignoring the implications of depositional environments (e.g., assuming a classroom aquifer) can be a source of flawed conceptualizations and costly mistakes.

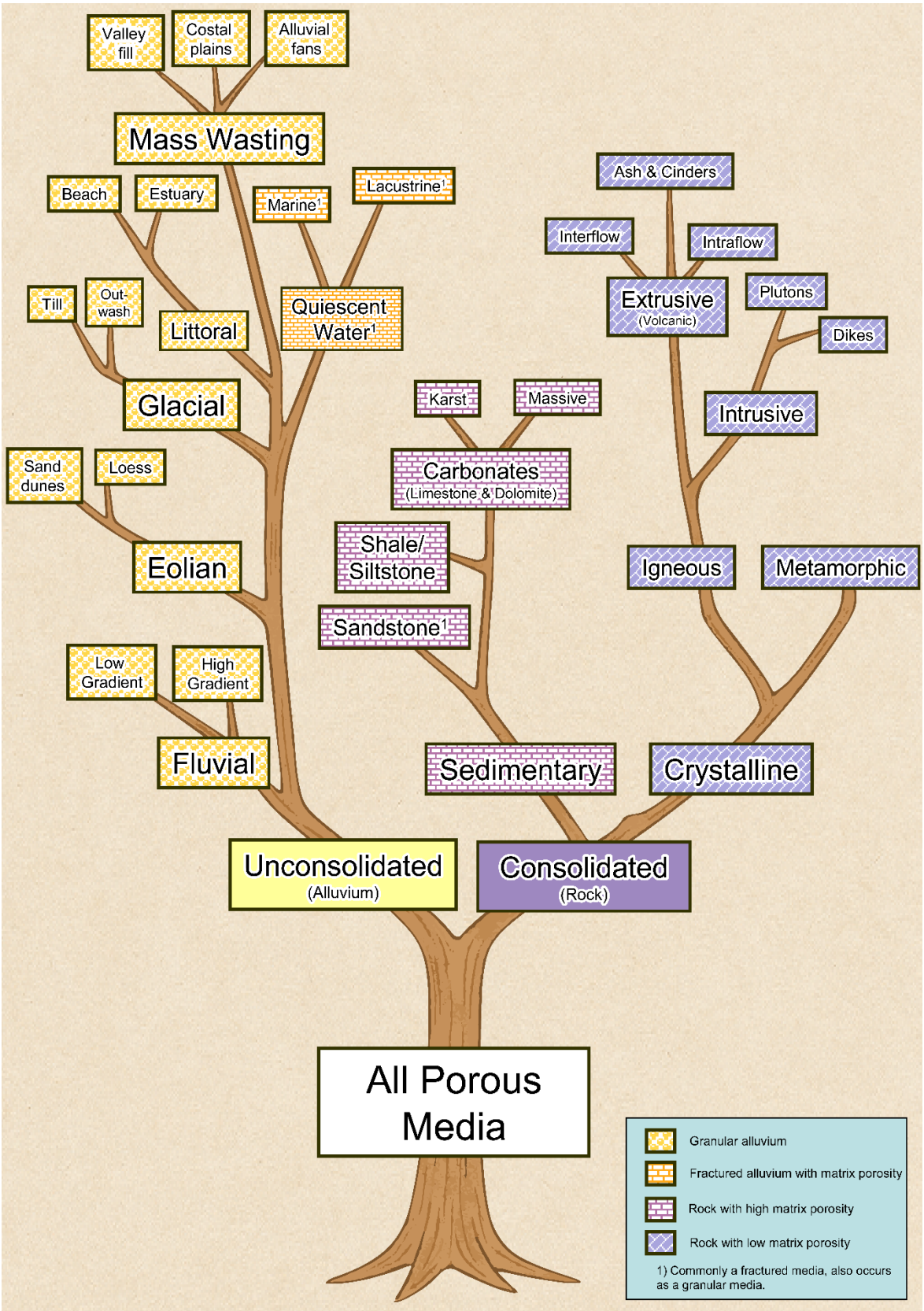

Figure 4 - Conceptual family tree for common depositional environments.

The first branch in the tree in Figure 4 occurs with unconsolidated and consolidated media. In unconsolidated media, flow of groundwater and, correspondingly, advective transport occurs through interconnected pore networks with preferential advective transport occurring in transmissive zones. Zones with permeabilities two or more orders of magnitude less than transmissive zones are called low-*k* zones. Fractured alluvium, where flow-through pore networks are common, are included in Figure 4. In contrast, flow of groundwater in consolidated media (the right branch of Figure 4) commonly exhibits advective transport primarily through joints and fractures. Similar preferential flow in fractures is common in unconsolidated fractured clay bodies.

The left branch of the tree in Figure 4 shows depositional environments for unconsolidated media including fluvial (rivers), eolian (wind), glacial (glaciers), littoral (shorelines), and lacustrine (lakes). The style and distributions of transmissive and low-*k* zones are governed by depositional processes. High-energy fluvial, glacial, and eolian settings often result in subsurface environments dominated by transmissive zones. In contrast, low-energy fluvial, littoral, and lacustrine settings tend to produce subsurface environments dominated by low-*k* zones.

Ascending the right branch of the tree in Figure 4 are depositional environments for consolidated media including sedimentary and crystalline rocks. With respect to transport, sedimentary and crystalline rock are differentiated by: a) porous matrix blocks in sedimentary rocks can act as vast low-*k* reservoirs that can store and release contaminants and b) matrix blocks in crystalline rocks generally have low porosities and limited roles in storing and releasing contaminants. Care is needed when applying the generalities described in (a) and (b). Examples of exceptions include 1) post-depositional cementation in sedimentary rock can fill in pores and 2) low porosities in crystalline rock can at times lead to consequential storage in low-*k* zones.

In fractured porous media, including rock and low-permeability sediments (i.e., clays or silts with secondary permeability features), low-*k* zones occupy on the order of 99 to 99.99 percent of the porous media volume. Correspondingly, transmissive zone fractions in fracture porous media are small—on the order of 0.01 to 1 percent.

Figure 5, based on Roads (2020), plots ranked cumulative percentages of low-*k* (black) zones based on 10- to 20-ft sections of cryogenically collected soil cores from 24 core holes at eight sites from across the USA. Cryogenic coring is described in Kiaalhosseini and others (2025). The complements to the low-k zones are transmissive. Figure 5 illustrates that low-*k* zones are ubiquitous features in unconsolidated media and the relative fractions of low-k and transmissive zones are variable and location specific.

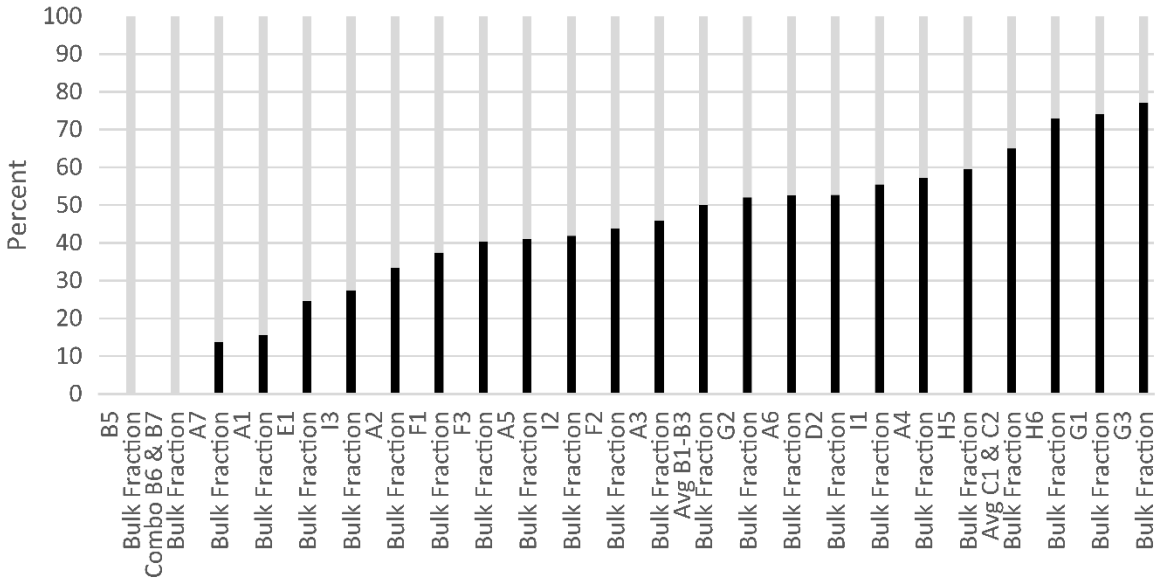

Figure 5 - Percentagesjump of boring composed of transmissive and low-*k* zones from 24 cryogenic core hole locations (Roads, 2020). Significance of the identification letters:
A and B indicate glacial-fluvial sand and gravel with interbedded silt layers;
C indicates a fluvial overbank deposit—silt and sand beds;
D and E indicate a braided stream deposit—silt and sand overlying coarse sand and gravel;
F and G indicate eolian deposits over sandstone—heterogeneous layers of conglomerate, sand, silt;
H indicates a tidal estuary—fine grained sands and silts.

Rigorous exploration of the implications of depositional environments is beyond the scope of this text. For many, proficiency in a handful of depositional environments can take a lifetime of field work. Two suggestions are offered regarding coming to grips with depositional settings. First, talk to people with extensive local experience in settings you are interested in. Second, look to the literature, including Back and others (1988), Davis and DeWiest (1966), Ritter and others (1995) and Woessner and Poeter (2020).

2.1.5 Geologic Type Settings

As a departure from classroom aquifers (defined as homogeneous aquifers), NRC (2005) and Sale and Newell (2011) advance five stylistic type settings as a basis for studying contaminant transport (Figure 6).

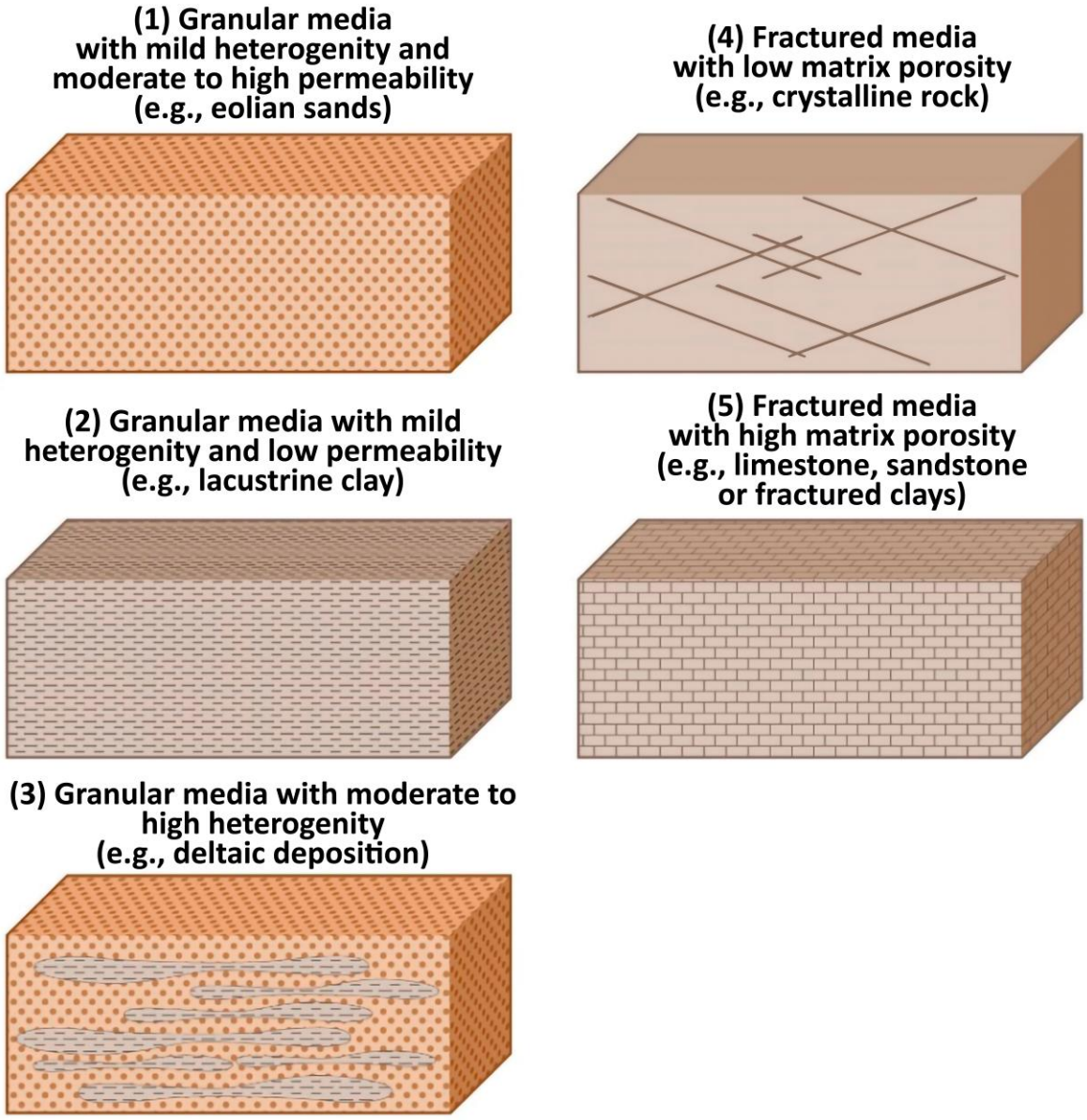

Figure 6 - Five stylistic type settings type settings for studying contaminant transport, following NRC (2005) and Sale and Newell (2011).

Type 1 settings are largely homogeneous-isotropic transmissive sand bodies. Outside of classrooms or carefully constructed laboratory sand tanks, we have never seen a true Type 1 setting. Type 1 settings have limited relevance other than as a bounding concept or a basis for reflection on the limitations of transport theory predicated on classroom aquifers (homogeneous-isotropic transmissive media). Type 1 settings form the theoretical foundation for much of what is encountered in historical contaminant transport texts.

Type 2 settings are largely homogeneous-isotropic low-permeability silt or clay bodies with no secondary permeability features such as fractures or root casts. Given their low permeability and no secondary permeability features, getting contaminants into Type 2 settings is difficult.

Type 3 settings involve low-*k* zones interspersed in an interconnected body of transmissive media. Type 3 settings are common. Most unconsolidated alluvial deposits are Type 3 settings. An example of a Type 3 setting is presented in the upper layer in Figure 7.

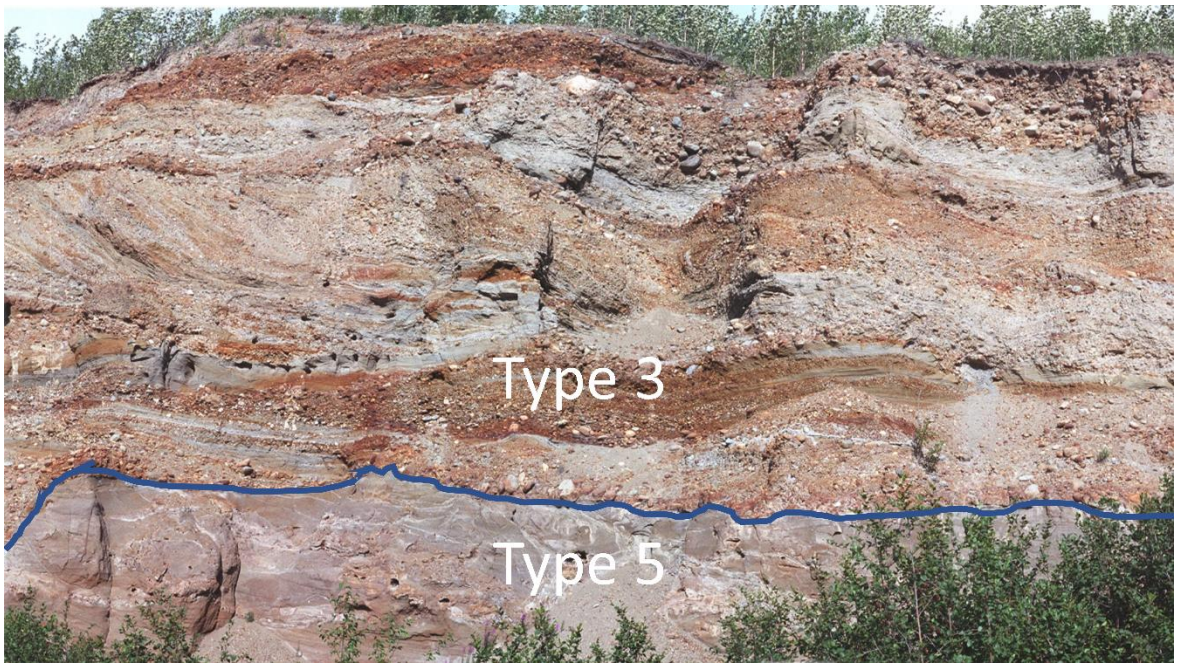

Figure 7 - Type 3 alluvium overlying Type 5 rock, Alaska, USA. Photo courtesy of Fred Payne.

Type 4 settings include fractured media with low-porosity matrix blocks. Crystalline rock is commonly a Type 4 setting. Limited porosity in matrix blocks constrains storage and release of contaminants to and from low-*k* zones.

Type 5 settings are fractured media wherein low-*k* matrix blocks have interconnected pore space that can store and release contaminants. Sedimentary rocks and fractured silts/clays commonly form Type 5 settings. Type 5 settings have a high ratio of porous low-*k* zones to transmissive zones and, correspondingly, a strong propensity to store and release contaminants to and from low-*k* zones.

Combined type settings: Due to geologic unconformities some sites are best viewed as a combination of one or more type settings. As an example, Figure 7 presents Type 3 alluvium overlying Type 5 sedimentary rock. Expanded discussions of type settings are presented in NRC (2005) and Sale and Newell (2011).

2.2 Hydrologic Cycle

Figure 8 illustrates the concept of the hydrologic cycle. The hydrologic cycle drives the movement of water and soil gases in subsurface settings. The hydrologic cycle also drives depositional and post depositional processes in sedimentary settings. As shown in Figure 8, subsurface settings are part of a larger systems that includes surface water and the atmosphere. Processes that occur at groundwater-surface water interfaces (e.g.

Woessner, 2020) and soil-atmosphere interfaces (e.g., Sale and others, 2021) often govern subsurface processes. Simple examples include: 1) infiltration of aerobic rainfall or snowmelt and 2) fluxes of O_2 and CO_2 at soil-atmosphere interfaces above subsurface petroleum liquid releases. In many instances understanding subsurface settings requires appreciation of surface water and atmospheric systems. Critical to subsurface contaminant hydrology is recognition that site-specific subsurface settings are part of a larger system.

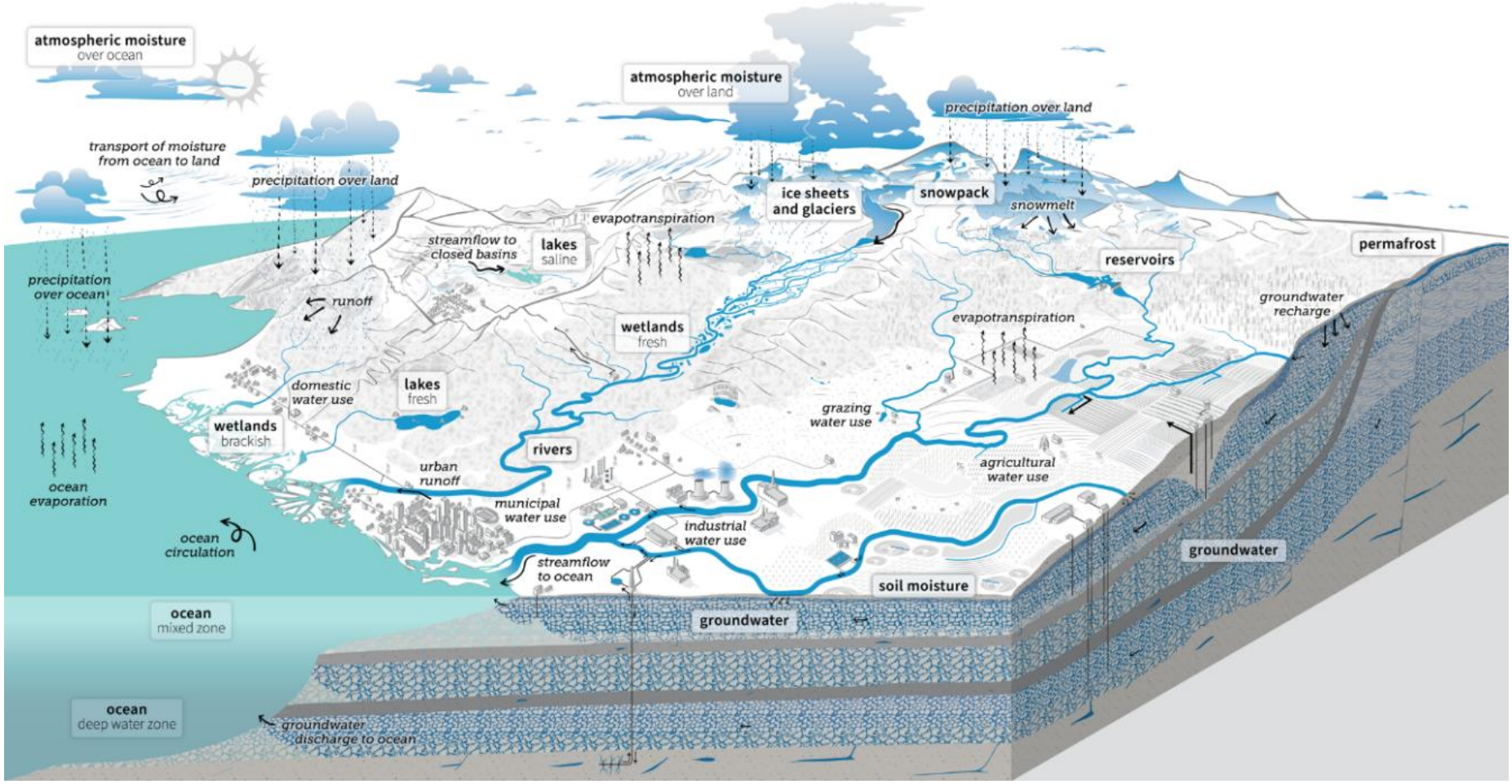

Figure 8 - The hydrologic cycle describing the location and movement of water on earth in the atmosphere, on the land, and below the subsurface (as groundwater) (modified after Corson-Dosch et al., 2023).

2.3 Common Contaminants of Concern

This subsection introduces common CoCs. Drinking water–based standards for CoCs generally fall in the range of low µg/L to low ng/L. Putting drinking water standards in perspective, low µg/L is equivalent to tens of people out of the earth's total human population. Low ng/L are equivalent to less than one person out of the earth's total human population. The challenges of treating water to low µg/L and ng/L concentrations can be large. One can imagine how difficult it might be to find a single person among all the people on our planet. Physical properties of organic compounds can be found in Mercer and Cohen (1990), Merck (2006), Pankow and Cherry (1996), and Mackay and others (2024). Physical properties of inorganic compounds can be found in Lindsay (1979).

2.3.1 Organic Compounds

Organic CoCs can be either naturally occurring or anthropogenic. In general, natural organic CoCs are likely to assimilate naturally; thus, assimilative capacity becomes an important consideration in remedial decision-making (Devlin et al., 2024). Synthesized (anthropogenic) organic CoCs tend to be more persistent.

Hydrocarbons: Typically, hydrocarbons are products of refining crude oil produced from sedimentary rock. Common petroleum products include fuels, lubricants, and chemical industry feed stock. Hydrocarbons are primarily composed of single carbon-carbon (C-C) and carbon-hydrogen (C-H) bonds and found coincident with oil and gas infrastructure.

Aromatic compounds: Are a subset of hydrocarbons that contain a six-carbon ring compounded with alternating single-double (conjugate) bonds. Aromatic compounds are commonly found in fuels. Primary aromatic CoCs in fuels include benzene, toluene, ethylbenzene, xylene, and naphthalene. Multiple-ring compounds such as naphthalene (two rings) and polynuclear aromatic hydrocarbons (PAHs) are commonly associated with high-boiling-point fuels (bunker) and wood-preserving NAPLs (creosote). Aromatics are commonly found at former manufactured-gas plants.

Energetic compounds: Compounds used in explosives are referred to as energetic compounds. Examples include trinitrotoluene (TNT), dinitrotoluene (DNT), Research Department explosive (RDX), and high-melting explosive (HMX). Many energetic compounds are composed of a benzene ring with substituted C-O and/or C-N bonds. Detonation leads to the release of large amounts of energy. Energetics are found in groundwater at bombing ranges, in war zones, and at weapons depots.

Halogenated compounds: Through imposed synthesis reactions, F, Cl, and Br are bonded to carbon to form hydrocarbons and aromatic compounds where C-H bounds are replaced with C-halide bonds. Organic syntheses lead to a broad range of CoCs. Both useful and potentially hazardous halogenated CoCs are listed in the next four groups of CoCs.

Chlorinated solvents: Widely employed compounds include carbon tetrachloride (CT), perchloroethene (PCE), and trichloroethene (TCE). Natural or imposed reductive dechlorination leads to an array of degradation products, some of which are also CoCs. A comprehensive review of production and uses of chlorinated compounds is presented in Pankow and Cherry (1996).

Chlorinated aromatics: Chlorinated benzene compounds used as dyes. Polychlorinated biphenyls (PCBs) are historically used as a heat-transfer liquid in electrical power transformers.

Pesticides and herbicides: A wide variety of chlorinated compounds have been used in agriculture. One of the most notorious is dichlorodiphenyltrichloroethane (DDT). To the positive, use of DDT prevented untold deaths due to malaria. At the same time, uses of DDT, prior to being banned in 1972, had broad undesirable environmental impacts (Carson, 1962).

Per- and polyfluoroalkyl substances (PFAS): Fluorinated alkanes have been widely used as firefighting foams, in food packaging, in chip manufacturing, and as a water repellant in carpets, furniture, and clothing. Given the stability associated with C-F bonds, PFAS have been widely referred to as *forever compounds*. Time will tell how PFAS might be assimilated and remediated under field conditions (Farhat et al., 2022).

2.3.2 Inorganic Compounds

Inorganic CoCs are derived from naturally occurring soils and rock. Additional information on inorganic CoCs in soils and groundwater can be found in Hem (1992) and Lindsay (1979).

Metals: Common metals of concern include lead (Pb), mercury (Hg), and copper (Cu). The oxidation states of metals depend on redox conditions. Redox, shorthand for reduction-oxidation, describes conditions governing the potential for a compound to be oxidized or reduced. Activities leading to elevated levels of metals include solid wastes associated with mining and industrial disposal practices.

Nonmetallic elements: Nonmetallic CoCs include arsenic (As) and selenium (Se). Both As and Se occur naturally and can be mobilized via anthropogenic activities that shift redox conditions, such as groundwater recharge and irrigation of crops.

Nitrogen and phosphate: In a world that must feed more than 8 billion people, nitrogen is necessary to enhance crop production. Common forms of nitrogen (N) in groundwater include nitrite (NO_2^-) and nitrate (NO_3^-). Nitrogen in groundwater is also associated with animal and human waste. Phosphate ($H_3PO_4^-$) is another common component of fertilizers. Phosphate has also been widely used in detergents. Phosphorous is in the same group in the periodic table as nitrogen. Broad releases of N and P can lead to adverse algal blooms and oxygen-depleted dead zones in surface water bodies.

Radioactive elements: Radioactive elements include naturally occurring compounds and compounds produced in nuclear fission facilities associated with power generation and nuclear weapons development. Rates of decay are described by half-lives. Natural compounds in groundwater (e.g., radon) are generally associated with decomposition of uranium-238, thorium-232-, and uranium-235 (Hem, 1992). Notably, cleanup efforts at sites impacted by anthropogenic radioactive elements, including Hanford Washington (USA), Chernobyl (Ukraine), and Fukushima Daiichi Reactors (Japan), are likely to be among the most difficult and expensive in the world.

2.4 Releases

To anticipate the current and future nature and extent of contaminants, resolving processes that introduce contaminants into subsurface settings is often key. Furthermore, insights from past releases provide a basis for preventing future releases. We need to be careful about judging the releases of past generations (e.g., our parents, grandparents, and great-grandparents; Figure 9) too harshly. Societal values are constantly in flux, and it is almost certain that future generations will adversely judge elements of today's practices.

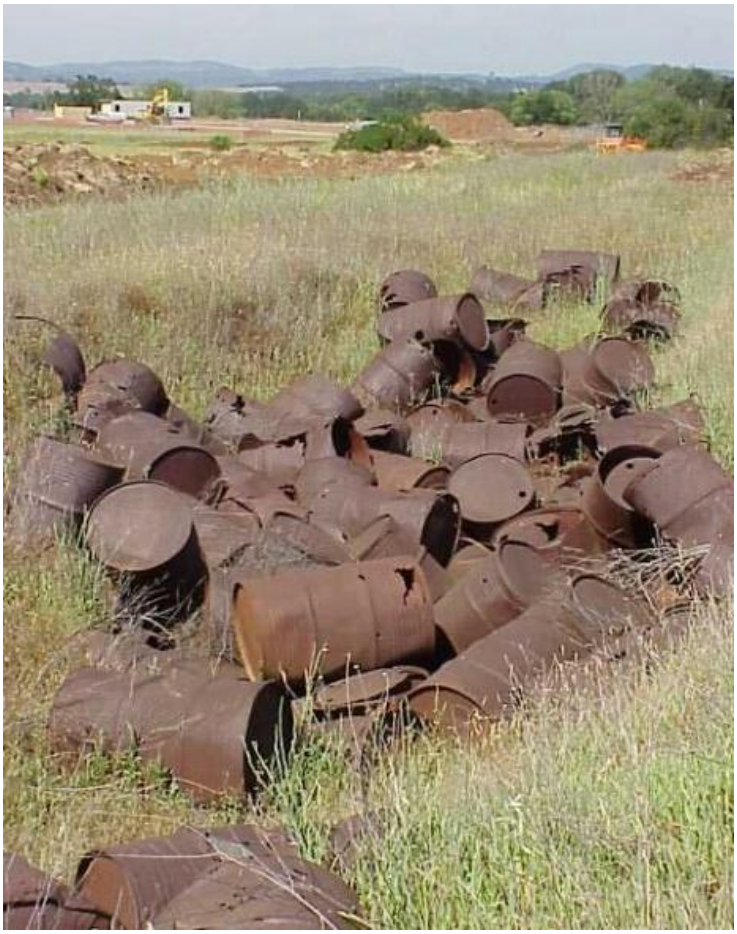

Figure 9 - Drums that contained chlorinated solvents (dense nonaqueous phase liquids (DNAPL)) in an unlined disposal trench with bullet-hole drainage perforations.

2.4.1 Point and Nonpoint Sources

Local releases from conveyance piping, storage tanks, and disposal pits are known as point sources. Removal or isolation of subsurface source zones is a common focus of remediation efforts. An example of a point source is leaky process water ponds (e.g., coal combustion residual [CCR] ponds). Although the US Environmental Protection Agency (EPA) ended the use of unlined ponds in 2014, as part of the Coal Combustion Residuals from Electric Utilities rule, legacy unlined CCR ponds remain a major source of aqueous inorganic contaminants.

Releases that occur over broad areas are referred to as nonpoint sources. Two common examples are agricultural fertilizers and road salt. Given a maximum contaminant level (MCL) of 10 mg/L nitrate as nitrogen, exceedances of drinking-water standards for nitrate are common in shallow groundwater in agricultural areas. Similarly, herbicides and pesticides can be an issue in agricultural areas.

2.4.2 Nonaqueous Phase Liquids (NAPLs)

Releases of NAPLs are a common source of subsurface contaminants and a central focus of this text. Examples of NAPLs include liquid fuels (e.g., gasoline, diesel, kerosene), chlorinated solvents, wood-treating oils, and petrochemical industry feedstocks. The following bullets list some key attributes of NAPLs.

- NAPLs are immiscible with water and gases, leading to multiple fluids being present in pore spaces.
- Given multiple immiscible fluids, NAPLs are commingled with an aqueous wetting phase and potentially a gas nonwetting phase wherein
  - interphase mass transfer occurs between all phases,
  - processes governing fluid flow are complex, and
  - the total mass of contaminant per volume of porous media is often large (e.g., a modest NAPL concentration of 10,000 mg of contaminant per kg of dry porous media equates to 1-percent contamination by dry weight of media.
- Given mass transfer constraints between phases, NAPLs can persist as subsurface sources of contamination for extended periods.
- Given the limited solubilities of NAPLs in water and low MCLs in drinking water, small amounts of NAPL can contaminate vast amounts of water. For example, 1 liter of trichloroethene can cause an exceedance of the MCL of 5 μg per L in 292 million liters of water.
- MCLs are often 4 to 5 orders of magnitude (OoM) lower than pure NAPL solubilities, leading to an often-impractical short-term cleanup goal of reducing aqueous concentrations in heterogeneous subsurface media by 4 to 5 OoMs.
- Large aqueous phase concentrations surrounding and downgradient of NAPLs can drive vast amounts of contaminant mass into low-k zones.

NAPLs are commonly split into liquids that are denser than water—dense nonaqueous phase liquids (DNAPLs)—and less dense than water—light nonaqueous phase liquids (LNAPLs). DNAPLs and LNAPLs commonly have the following differences.

- LNAPLs generally occur about the water table with morphologies that are driven by horizontal spreading of LNAPLs at and about the capillary fringe. A comprehensive review of LNAPLs can be found in Sale and others (2018).
- DNAPLs can be driven below the water table by negative buoyancy, where they preferentially enter large pore spaces in transmissive zones and are excluded from small pore spaces in low-*k* zones. The morphology of DNAPL zones typically involves sparse pools resting on low-permeability layers (Pankow & Cherry, 1996; Mumford et al., 2024).

Following NRC (2005), porous media that contain NAPLs are referred to as *source zones*. When present in groundwater, most common NAPLs dissolve very slowly to form dissolved COCs that then travel along with the flowing groundwater. Contaminated subsurface bodies beyond source zones are referred to as *plumes*. To the positive, natural source zone depletion (NSZD) processes (including dissolution, evaporation, and degradation) can consequentially deplete NAPLs over time.

2.4.3 Aqueous Phase Liquids

Many industrial processes and military operations produce vast amounts of process wastewater. Before the 1976 US Clean Water Act (CWA), wastewater was discharged directly to surface water bodies with limited treatment. After CWA enactment, wastewater was commonly routed into unlined process-water ponds. Seepage losses from process-water impoundments can be a source of subsurface contamination. In general, concentrations of aqueous contaminants are far lower with aqueous liquid releases versus NAPLs. On the other hand, large seepage losses from water impoundments can play a primary role in driving advective transport of contaminants through the subsurface, and overall mass of contaminant release can be large.

2.4.4 Leachate from Solid Wastes

All waste-containment facilities leak. Prior to the 1965 US Solid Waste Disposal Act (SWDA) and the 1976 US Resource Conservation and Recovery Act (RCRA), industrial and municipal solid waste was typically disposed of in unlined natural or man-made depressions, trenches, or pits. The term *solid* refers to the disposal of a material that is not entirely liquid. Solid industrial waste often includes barrels or drums of potential contaminants. Water interacting with solid waste leaches constituents in the form of leachate (often as aqueous phase liquids), which then flows to surface water or groundwater. After RCRA, municipal and hazardous waste containment facilities were required to have engineered liner systems; the role of these liners is to slow the rate of leachate transport from the waste-containment facility. Since 2014, municipal and

hazardous solid waste has been placed in lined waste-containment facilities. Unfortunately, all solid waste containment facilities are likely to be slow leachate releasers.

Mining wastes are another source of leachate in the form of acid rock drainage and metal leaching (INAP, 2024). Two main waste streams are generated from mining: tailings and waste rock. *Waste rock* is the rock removed to access economically valuable minerals. Often waste rock contains potentially acid-generating mineral phases (e.g., pyrite) that can lead to acid rock drainage if inadequately managed (i.e., inorganic aqueous releases of low pH and mineral laden leachate). *Tailings* are the waste solid residuum from the separation of valuable minerals from economically worthless minerals (*gangue*). After extraction and beneficiation, the residuals from mineral recovery are normally discharged as slurries composed of gangue ground to form submicrometer to sand-sized particles, chemicals, and process water. The resulting fine-grained tailings are slow to release water, yielding tremendous volumes of near-fluid waste material that must be managed. Water released from tailings may have high total dissolved solids (TDS) and, when tailings (eventually) become unsaturated, may be sources of acid rock drainage if not properly covered.

2.5 Partitioning Between Phases

In the 1970s and 1980s, broad recognition of contaminants in groundwater led to widespread efforts to restore groundwater in aquifers (transmissive zones) by pumping out a few pore volumes of contaminated groundwater. Spectacularly, many *pump and treat* remedies failed to restore aquifers. Doty and Travis (1991), EPA (1989), Mackay and Cherry (1989), Mercer and Cohen (1990), and Mercer and others (1990) advanced the simple premise that given contaminants in any phase (e.g., gas, NAPL, aqueous, solids) the same contaminants will be present in all adjacent phases; correspondingly, there is more to subsurface contamination than contaminated groundwater in transmissive zones. Partitioning between phases is rigorously advanced in Section 4.

2.6 Transport

Transport refers to processes that move contaminants through interconnected pores in subsurface media. Following the classical chemical engineering text *Transport Phenomena* by Bird and others (2002), advection and diffusion are the primary processes that cause contaminants to be transported. Advection and diffusion are briefly introduced in this section. Advection and diffusion are examined in detail in Section 3.

2.6.1 Advection

Advective transport involves migration of a fluid particle (gas or liquid) containing a contaminant. Analogously consider a river (liquid) carrying a raft (the contaminant) downstream. Advection is driven by gradients in the total head of a transporting fluid. Following Darcy's equation, a one-dimensional advective volumetric flux of fluid j (q_{ad_j} $L^3L^{-2}T^{-1}$) in a granular porous media is computed as shown in Equation (1).

$$q_{ad_j} = -\frac{kk_{r_j}\rho_j g}{\mu_j}\frac{dh_j}{dl} \quad (1)$$

where (parameter dimensions are dark green font with mass as M, length as L, time as T):

k = permeability (L^2), capacity of a porous media to conduct fluids

k_{r_j} = relative permeability for fluid j (dimensionless), a function of fluid saturation (dimensionless)

j = Subscript denoting a fluid (dimensionless)

ρ_j = density of fluid j (ML^{-3})

g = gravitational constant (LT^{-2})

h_j = head, potential energy driving flow of fluid j (L)

μ_j = viscosity of fluid j ($ML^{-1}T^{-1}$)

l = position (L) with positive fluxes occurring in the direction of decreasing head

Similarly, building on the Navier-Stokes equation, the one-dimensional volumetric fluid flux $q``_j$ ($L^3L^{-2}T^{-1}$) between two parallel plates, analogous to flow in a uniform fracture, is shown in Equation (2).

$$q``_{ad_j} = -\frac{b``^2\rho_j g}{12\mu_j}\frac{dh_j}{dl} \quad (2)$$

where (parameter dimensions are dark green font with mass as M, length as L, time as T):

$b``$ = distance between two plates or an equivalent fracture aperture

The seepage velocity v_j (LT^{-1}) in a porous media, where volumetric flux, q_j ($L^3L^{-2}T^{-1}$) is based on either granular or fractured porous media, is shown in Equation (3).

$$v_j = \frac{q_j}{\phi} \quad (3)$$

where (parameter dimensions are dark green font with mass as M, length as L, time as T):

ϕ = transmissive zone porosity, (volume of voids)/(total volume porous media) (dimensionless)

The one-dimensional mass flux of CoC i due to advection of fluid j is $J_{ad_{i,j}}$ ($ML^{-2}T^{-1}$) as shown in Equation (4).

$$J_{ad_{i,j}} = q_{ad_j}\rho_{i,j} \quad (4)$$

where (parameter dimensions are dark green font with mass as M, length as L, time as T):

i = subscript denoting a compound, e.g., a CoC (dimensionless)

$q_{i,j}$ = mass-based concentration of compound CoC i in fluid j (ML^{-3})

Typically, advection is the primary process driving contaminants through water-saturated transmissive zones.

2.6.2 Diffusion

Diffusion is the migration of a particle (e.g., molecule) due to the random motion of individual particles. Spatial differences in concentrations result in a net flux of CoCs in the direction of decreasing concentration. Diffusion occurs because molecules in fluids (including contaminants) are continuously in motion, constantly colliding with one another independent of external disturbances, as part of the natural pedesis (i.e., random Brownian motion) of particles in a fluid. Per Fick's first equation, the one-dimensional diffusive mass flux ($ML^{-2}T^{-1}$) for CoC i in fluid j due to diffusion is presented in Equation (5).

$$J_{D_{i,j}} = -D_{m_{i,j}} \frac{dq_{i,j}}{dl} \tag{5}$$

where (parameter dimensions are dark green font with mass as M, length as L, time as T):

$D_{m_{i,j}}$ = molecular diffusion coefficient (L^2T^{-1}) for CoC i in fluid j

Given solids in porous media (denoted by the subscript k) and assuming media fully saturated with fluid j,

1) porosity (ϕ_k) is incorporated into Fick's equation to correct for reduced cross-sectional transport areas given that flow does not occur through the solids and

2) tortuosity (τ_k) is incorporated to correct for the longer transport distances through porous media relative to direct point-to-point distances.

Equation (6) describes the diffusive mass flux of CoC i, in fluid j, in porous media k.

$$J_{D_{i,j,k}} = -\phi_k \tau_k D_{m_{i,j}} \frac{d\rho_{i,j}}{dl} = -D_{e_{i,j,k}} \frac{d\rho_{i,j}}{dl} \quad \ldots \quad D_{e_{i,j,k}} = \phi_k \tau_k D_{m_{i,j}} \tag{6}$$

where (parameter dimensions are dark green font with mass as M, length as L, time as T):

$\rho_{i,j}$ = mass based concentration for compound i in fluid j (ML^{-3})

$D_{e_{i,j,k}}$ = effective diffusion coefficient (L^2T^{-1}) for CoC i (L^2T^{-1}), in fluid j, in porous media k.

As a first approximation, following Bird and others (2002), advective and diffusive fluxes in a liquid can be summed to estimate total fluxes of CoC i, J_{Ti} ($ML^{-2}T^{-1}$) as shown in Equation (7).

$$J_{T_i} = J_{ad_{i,j}} + J_{D_{i,j}} \tag{7}$$

where (parameter dimensions are dark green font with mass as M, length as L, time as T):

$J_{ad_{i,j}}$ = advective flux of compound i due to advection of fluid j ($ML^{-2}T^{-1}$)

$J_{D_{i.j}}$ = diffusive flux of compound i ($ML^{-2}T^{-1}$) in fluid j

More careful evaluation is necessary for a more accurate result, particularly for transport in gases, advective and diffusive fluxes can be interdependent and simple summation of advective and diffusive fluxes can be invalid (McWhorter, 2021).

2.7 Reactions

Through time released contaminants commonly partition between phases, sorb to matrix solids including natural organic matter (NOM), and transform to new compounds. These processes are referred to as *reactions*. In many older releases, natural reactions, such as natural attenuation (NA) and natural source zone depletion (NSZD) play primary roles in assimilating released compounds and mitigating associated risks (Devlin et al., 2024). Given total contaminant losses due to reactions, equal to environmental loading, the extent of many plumes and LNAPL bodies are stable despite active releases and transport in NAPL bodies and/or plumes.

A glacier makes a useful analogy for the role of reactions in limiting contaminant migration (Figure 10). High-elevation precipitation typically adds ice to glaciers annually. Accumulated ice is transported downhill by gravity. At the downhill end, the glacier melts due to higher temperatures. Downhill migration ends when the net rate of ice addition is equal to the net rate of melting. Given increasing temperatures with climate change, many glaciers are shrinking due to reduced loading and/or faster melting. Building on this point, many source zones and plumes are shrinking due to reduced loading. Notable exceptions can occur if contaminants do not readily undergo reactions, or if substantial new releases occur.

Figure 10 - NAPL bodies and plumes can be analogous to glaciers in that there can be active transport within the bodies as the extent of the glacier is limited by natural losses. Natural losses in glaciers occur through melting. Natural losses in NAPL bodies and plumes occur through reactions.

2.8 Conceptual Models

A primary outcome from research, site investigations, remediation efforts, and modeling studies are schematics and text conceptualizing subsurface conditions and governing processes. Assembled text and schematics are called *conceptual models* (CMs) or, when relating to a specific site, *site conceptual models* (SCMs). Notably, we cannot literally see subsurface conditions. At best, we have access to sparse spatial and temporal data from monitoring wells, multiple level sampling systems, core samples, and sensors. SCMs allow us to assemble what we know into *best understandings*. Soberingly, per Bredehoeft (2003, 2005), all too often our CMs and SCMs have missed important characteristics and processes that we did not know about.

Figure 11 presents a general CM for NSZD processes in a petroleum LNAPL release in a Type 3 geologic type setting. Microbially mediated methanogenesis in the LNAPL body (yellow) converts petroleum compounds to CH_4 and CO_2. Released CH_4 and CO_2 are driven upward by advection and diffusion. Similarly, atmospheric O_2 is driven into the subsurface via advection and diffusion. At the position where CH_4 and O_2 meet, methanotrophs in the vadose zone convert methane into CO_2 and H_2O.

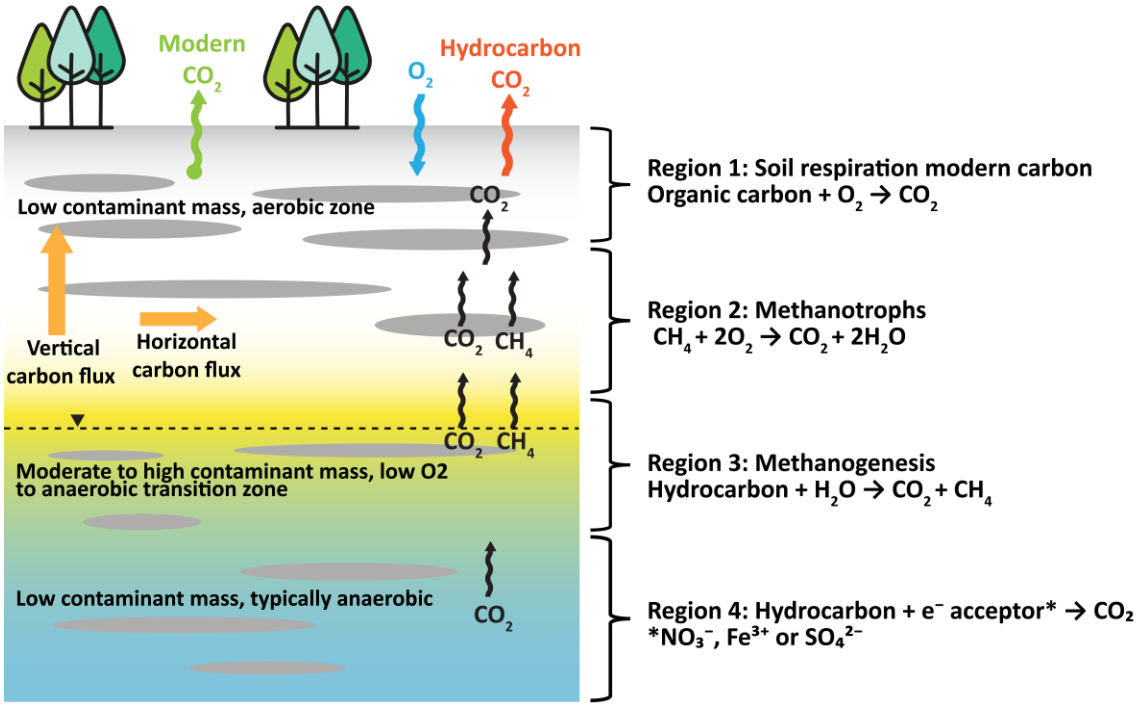

Figure 11 - A conceptual illustration of LNAPL NSZD following Amos and others (2005); Garg and others (2017); and Irianni-Renno and others (2015).

Figure 12 shows a SCM in plan and profile for a large mature PCE DNAPL release at an industrial site. Dissolution of DNAPL in the source zone leads to aqueous phase PCE being driven into low-*k* zones in the source zone via diffusion and slow advection. Advection has created downgradient aqueous phase PCE plumes in transmissive zones, leading to the potential for human exposure via groundwater. Partitioning of aqueous

phase PCE at the water table into unsaturated zone gas has created vapor plumes in the unsaturated zone, leading to the potential for human exposure via indoor air above both the source zone and plume. An adaptation of the 14C model is included in Figure 12 with an OoM color scale for levels of contamination and arrows anticipating fluxes between compartments. The 14C model supports consideration of all relevant compartments and transport processes and provides a basis for selecting remedies (Sale & Newell, 2011).

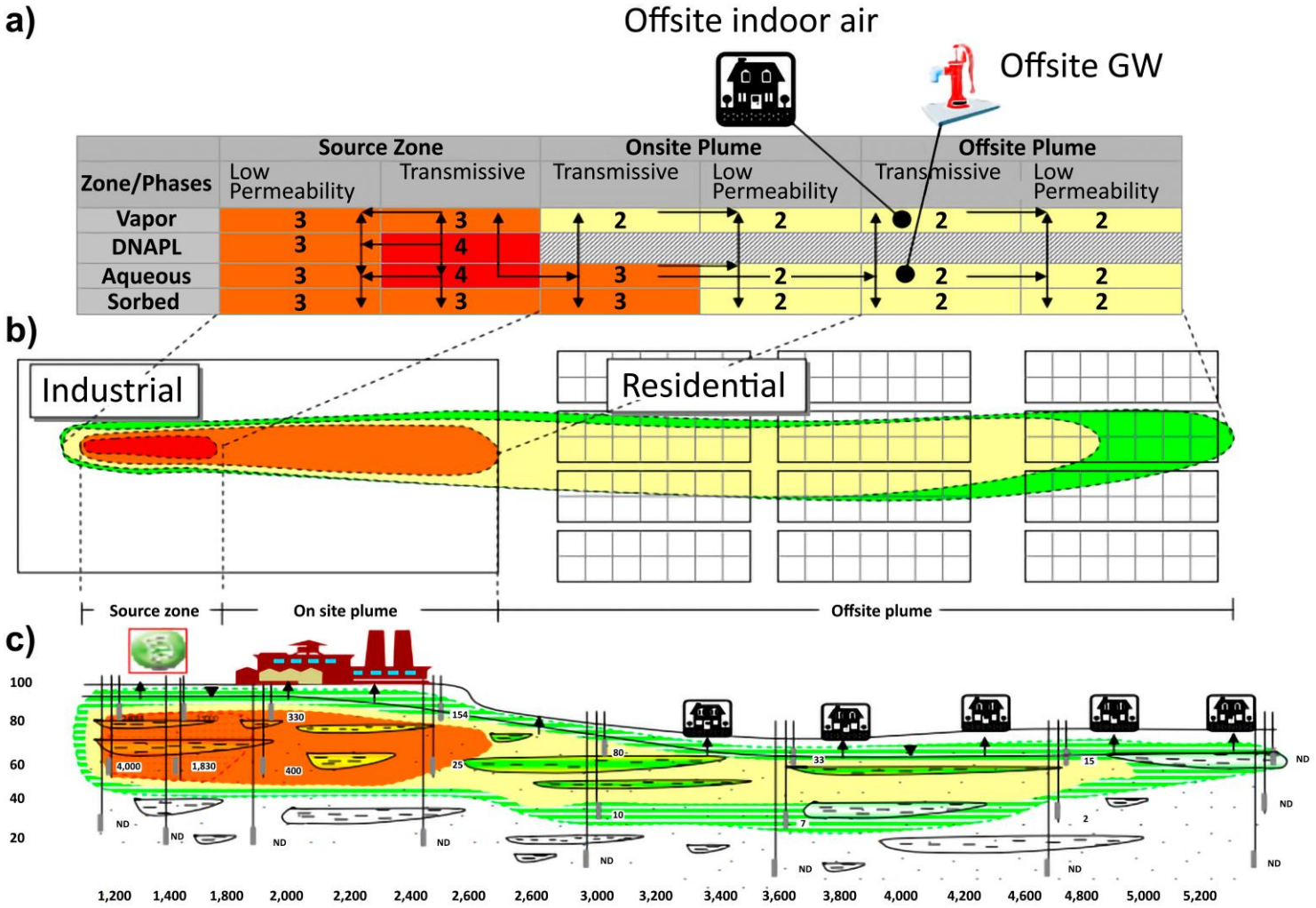

Figure 12 - a) 14C model of relevant compartments and transport processes in a mature PCE DNAPL release b) Plan-view and c) profile view of a SCM for PCE at a mature level of release impacting industrial and residential properties. Colors in the 14C conceptualize order of magnitude aqueous concentration of PCE (red 1000s ug/L, orange 100s ug/L, yellow 10s ug/L and green 1s of ug/L or less. Arrows depict fluxes between compartments.

2.9 Mathematics – The Language of Quantitative Conversations

For many, university-level mathematics courses mean tedious memorizing techniques such as integration by parts or use of transform variables (e.g., Boltzmann, Laplace, or Fourier) that are quickly forgotten. Mathematics can be like a foreign language that, used too little, lapses—in German, "alles ist vergessen."

You might be asking why we have included a subsection on mathematics. Herein, we use mathematics to concisely advance quantitative conversations regarding contaminant transport in natural porous media. In the spirit of Sir Issac Newton, we encourage all to see mathematics as an exploration of governing principles via quantitative conversations. Mathematics is a language. For many of us, seeing mathematics as a language takes a bit of practice and arrives at a "*Eureka!*" moment. Practice what you might have forgotten and be patient. If you already feel comfortable with the mathematics of contaminant hydrology, we still encourage a brief review of this section, particularly the next subsection, "Transport Variables as Vocabulary." Building on Fetter (1999), Section 2.9 provides a brief review of what you need to know.

2.9.1 Transport Variables as Vocabulary

Following the analogy of mathematics as a language, computational variables in this text are mathematical vocabulary terms for properties and processes that govern transport. After years of contemplation, the authors see many of the computational variables in this text as old friends and even best friends.

Computational variables have names, broadly accepted definitions, single-letter labels, and dimensions (e.g., porosity, the volume of voids per volume of porous media, ϕ, with units of L^3L^{-3}). Subscripts on letters are employed to convey additional information. As an example, the Greek letter ρ is used for parameters with units of mass per volume (ML^{-3}). Examples include ρ_w, ρ_{NAPL}, and ρ_b for densities of water, NAPL, and porous media, respectively. The Greek letter ρ is also used for mass-based concentrations (ML^{-3}), including ρ_{aq_i} and ρ_{g_i}, mass of compound i per volume aqueous phase (aq), and gas phase (g), respectively. For molar concentration, we use brackets and the variable C, [C] ($molesL^{-3}$).

In general, we follow nomenclature precedents set in the fields of chemical and petroleum reservoir engineering. We apologize for the inconsistencies between our nomenclature and the nomenclature used in other fields, soil science and geotechnical engineering among them. Variables employed in this text are presented as a notations list in Section 11. We invite all to jump in and build new vocabulary. Acronyms that appear in this book are listed in Box 1.

2.9.2 Derivatives

First-order derivatives express the rate of change of a dependent physical attribute (e.g., concentration) with respect to an independent variable (e.g., position or time). Figure

13 represents position as a function of time on a trip from home to school, with the amount of distance advanced along the path in a given amount of time varying because one's pace varies as a function of time. The derivative of the dependent variable distance (S) as a function of the independent variable time (t), dS/dt (LT^{-1}) is the rate of travel at time t, i.e., speed or velocity at time t.

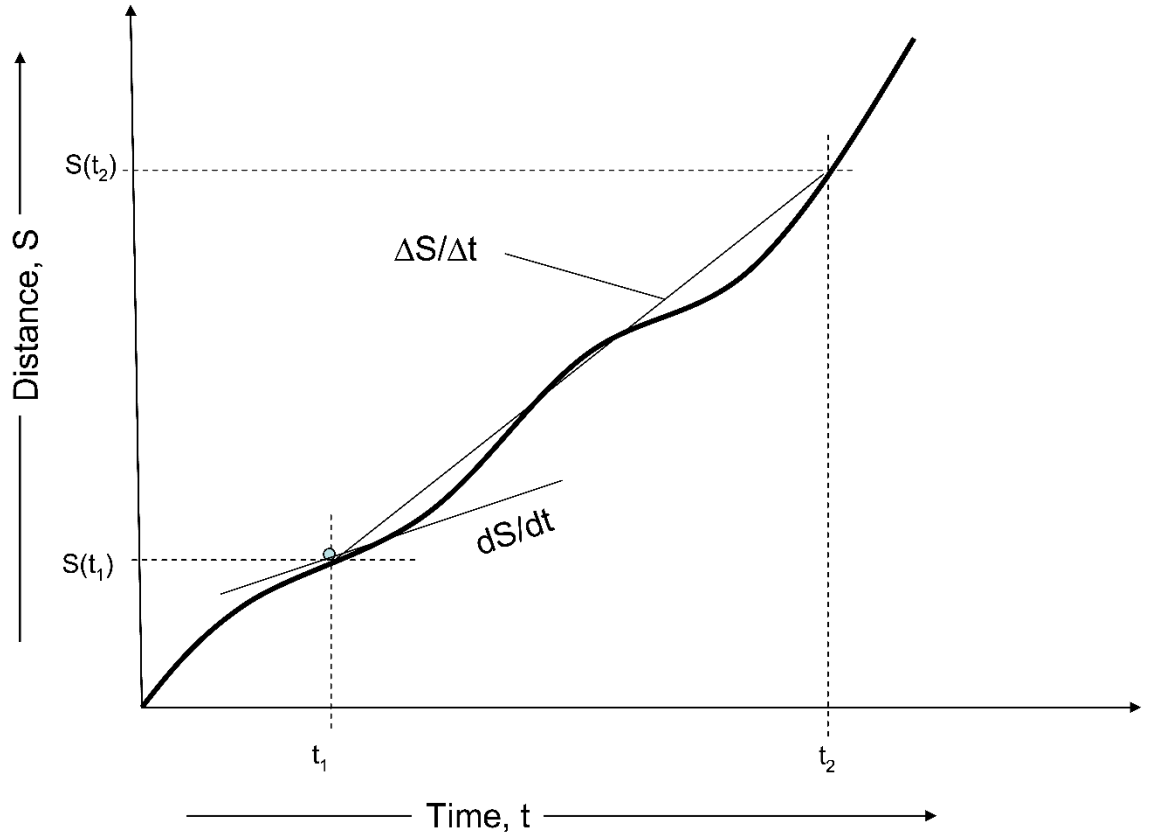

Figure 13 - First-order derivative of distance with respect to time.

Equation (8) provides the definition of a first derivative. Which in this case is the distance traveled over an infinitesimal amount of time.

$$\frac{dS}{dt} = lim_{t_2 \to t_1} \frac{S(t_2) - S(t_1)}{t_2 - t_1} \text{ and } \frac{dS}{dt} = lim_{\Delta t \to 0} \frac{\Delta S}{\Delta t} \quad (8)$$

Finite differences ΔS (change in distance) and Δt (change in time) can be used to approximate dS and dt, respectively. The accuracy of the approximation depends on the size of the discretizations of space and time as well as the dynamics of the function. For example, if the function is a straight line, any size discretization will provide an accurate derivative, while a squiggly line requires small discretization to capture an accurate derivative. Primary uses of first-order derivatives in transport include quantifying fluid fluxes—for example, Equations (1), (2), (5), and (6).

A second-order derivative of position with respect to time for the function presented in Figure 13 is shown in Equation (9).

$$\frac{d\left(\frac{dS}{dt}\right)}{dt} = \frac{d^2S}{dt^2} = \frac{d^2}{dt^2}S \tag{9}$$

Here the second-order derivative describes the rate of change of the rate of travel, or acceleration, at time t. Second-order derivatives are commonly encountered in mass balance-based governing equations that are discussed in Sections 2.9.3 through 2.9.6.

2.9.3 Integrals

Definite integrals sum physical attributes of systems over prescribed bounds of integration. As an example, Figure 14 presents total concentrations per dry weight of porous media (ω_{T_i}) for PCE and related degradation products as a function of vertical position in a low-k zone below a transmissive zone. The integral of ω_T from depth 0 m to 0.5 m, $\int_{0m}^{0.5m} \omega_{T_i}(z)dz$, provides the total mass of a given CoC (M_{T_i}).

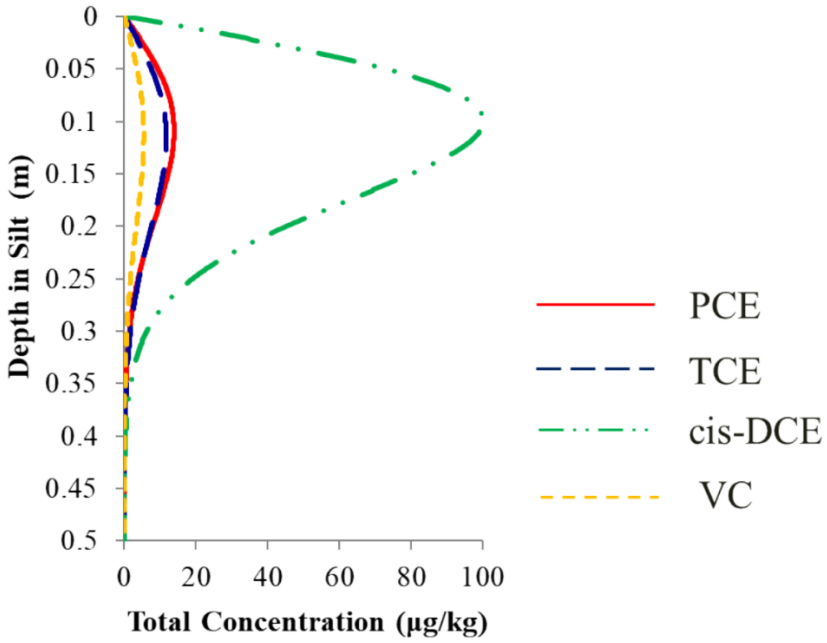

Figure 14 - Total concentration (MM^{-1}) of perchloroethylene (PCE) and related degradation products [trichloroethene (TCE), cis-dichloroethene (cis DCE), and vinyl chloride (VC)] as a function of vertical position in a uniform low-k zone (after Wahlberg, 2013).

Indefinite integrals lack upper and lower limits. Herein, indefinite integrals are developed through balances on representative elements of volume (REVs). Balance equations are employed in deriving computational solutions to problems of interest.

2.9.4 Types of Physical Properties

Physical properties of interest described via mathematics fit into three categories.

1. **Scalars** (zero-order tensors): A scalar is a quantity characterized by only magnitude. Examples of scalar quantities include pressure, concentration, density, viscosity, and temperature.

2. **Vectors** (first-order tensors): A vector has a magnitude and a direction (Figure 15a) Examples of vector quantities include volumetric fluid (Darcy) fluxes and contaminant fluxes.
3. **Tensors** (second-order tensor): In heterogeneous anisotropic media, permeability and diffusion coefficients are the product of two vectors yielding a 9-component (3×3) matrix. Hydraulic conductivity is a 3×3 tensor (15b). Herein, we will avoid the complexities of tensors by aligning the principal coordinates with the directions in which the parameters of interest were measured. Notably, aligning principal coordinates with the directions in which the parameters of interest were measured is not always possible.

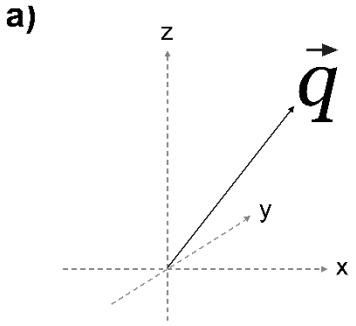

b)

$$\begin{bmatrix} q_x \\ q_y \\ q_z \end{bmatrix} = -K \begin{bmatrix} \frac{dh}{dx} \\ \frac{dh}{dy} \\ \frac{dh}{dz} \end{bmatrix} \quad -K = \begin{bmatrix} q_x \\ q_y \\ q_z \end{bmatrix} \begin{bmatrix} \frac{dh}{dx} & \frac{dh}{dy} & \frac{dh}{dz} \end{bmatrix} \quad K = - \begin{bmatrix} q_x \frac{dh}{dx} & q_x \frac{dh}{dy} & q_x \frac{dh}{dz} \\ q_y \frac{dh}{dx} & q_y \frac{dh}{dy} & q_y \frac{dh}{dz} \\ q_z \frac{dh}{dx} & q_z \frac{dh}{dy} & q_z \frac{dh}{dz} \end{bmatrix}$$

Figure 15 - Illustrations of a) a Darcy flux as a vector quantity and b) hydraulic conductivity as a 3x3 second order tensor.

2.9.5 Mass Balances and Governing Equations

At the core of most transport calculations are governing ordinary differential equations (ODEs) or partial differential equations (PDEs). Governing ODEs and PDEs are typically derived from mass balances on REVs wherein inflow to a representative elementary volume (REV) (e.g., contaminants, heat, electrical charge) minus outflow from an REV is equal to the change in the amount of the quantity within the REV with time. An REV with advective and diffusive inflows and outflows is presented in Figure 16.

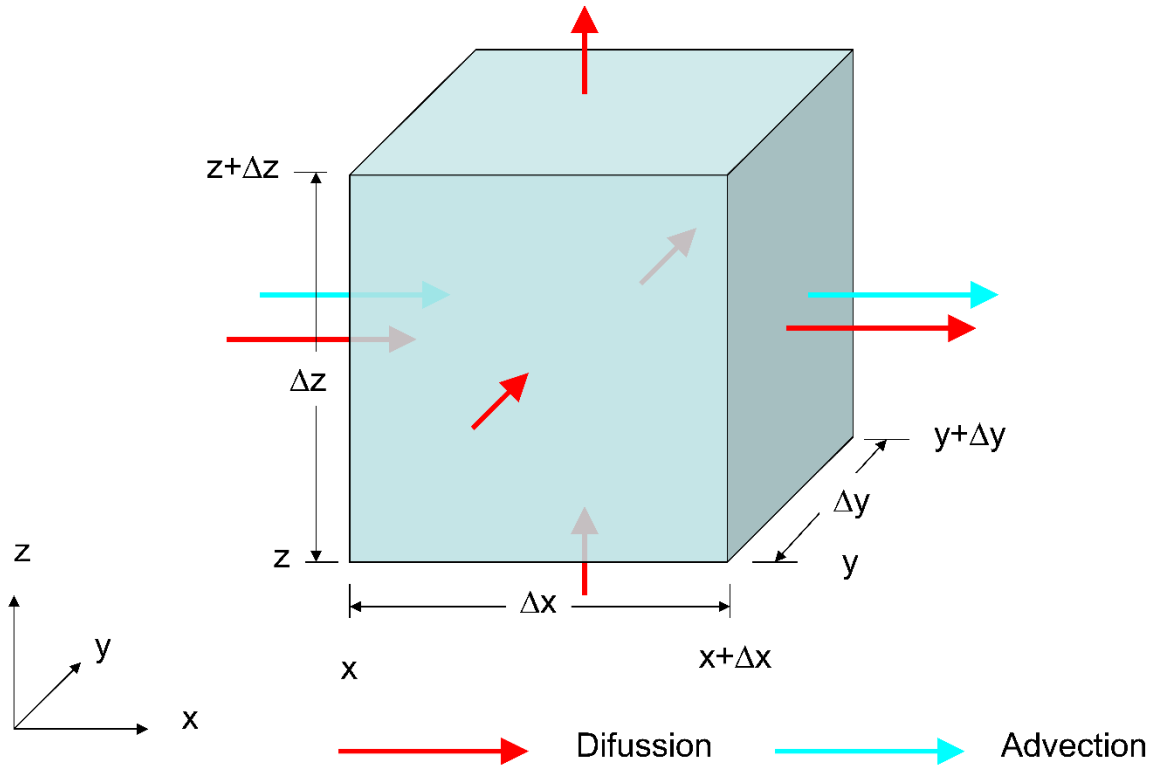

Figure 16 - Conceptualization of a representative elementary volume with the dimensions Δx, Δy, and Δz with one-dimensional flow in the x direction. As the deltas approach zero, Δx, Δy, and Δz converge to dx, dy, and dz, respectively.

ODEs have one dependent and one independent variable. An example of an ODE is the governing equation for first-order decay of a contaminant in an aqueous phase in a REV, as shown in Equation (10).

$$\frac{d\rho_{aq_i}}{dt} = -\lambda_i \rho_{aq_i} \tag{10}$$

where (parameter dimensions are dark green font with mass as M, length as L, time as T):

λ_i = first-order decay rate constant (T^{-1}) for compound i

This equation describes the rate of change (loss or creation) of an aqueous-phase contaminant in a REV due to a first-order reaction. ($\frac{d\rho_{aq}}{dt}$) is proportional to the aqueous concentration (ρ_{aq}) in the REV, by a constant (λ). First-order rate equations are commonly used in transport studies for resolving reaction kinetics for contaminants. Notably, first-order rate equations often fail to capture the complex thermodynamic and mass transfer processes that govern reactions.

PDEs have one dependent and two or more independent variables. The PDEs for contaminant transport through a saturated porous media are presented in Section 5.3.

2.9.6 Solutions

Building on old-school methods, exact analytical solutions describing aqueous concentrations, mass fluxes, total mass in place, and other relevant concerns are obtained by the following actions:

1. transforming PDEs into ODEs using transform variables (e.g., Boltzmann, Laplace, or Fourier),
2. separating variables and integrating results, and
3. applying spatial and or temporal boundary conditions to resolve constants of integration.

In this text, a handful of analytical solutions are advanced from first principles per the outlined steps. Derivations provide useful insights about the assumptions underpinning solutions and useful practice with basic math skills. For those with interest and time, notable resources for developing analytical transport solutions include Bird and others (2002) as well as Carslaw and Jaeger (1959). Furthermore, there is an ever-growing suite of modern mathematical resources, such as PTC Mathcad Prime↗, MATLAB PDE Solver, as well as numerous burgeoning AI tools that can help with obtaining exact analytical solutions from governing equations and boundary conditions.

When problems are too complex to find exact analytical solutions, we commonly turn to numerical methods. With these, derivatives are replaced with deltas based on temporal and spatial discretization of a domain in which the problem is being solved. As the speed of computing resources has grown, so too has our ability to use numerical methods to solve PDEs and ODEs, including select nonlinear problems. Introductions to numerical methods can be found in Anderson and Woessner (2002) and Thomas (1995).

A word of caution regarding numerical methods. Numerical methods provide approximate solutions to ODEs and PDEs that are valid only so long as appropriate spatial and temporal discretizations of domains are used (Chapman et al., 2012; Daus et al., 1985; Farhat et al., 2020). If processes governing transport (e.g., diffusion) occur at spatial scales or in temporal frames that are smaller than those used in numerical models, the models are likely to provide flawed results. Strengths and limitations of numerical methods are described in Section 5.

2.10 A Demonstrative Thought Experiment

As a prelude to content to come, we advance a thought experiment using heat stored in a heat battery (also known as a thermal energy storage system) analog to contaminant transport through natural heterogeneous subsurface media. We envision the following conditions:

- a semi-infinite plate heat sink composed of uniform thermally conductive solid metal plates (for heat storage) separated by gaps used as fluid convection zones; as shown in Figure 17;

- a uniform constant temperature T_0 throughout the domain for $t \leq 0$;
- driving fluid with an elevated temperature T_{on} at a constant rate through the gaps in the heat battery under laminar flow conditions for $0 < t \leq t'$; and
- returning the temperature of the influent fluid to T_0 for $t > t'$ while still driving fluid through the gaps to recover the stored heat.

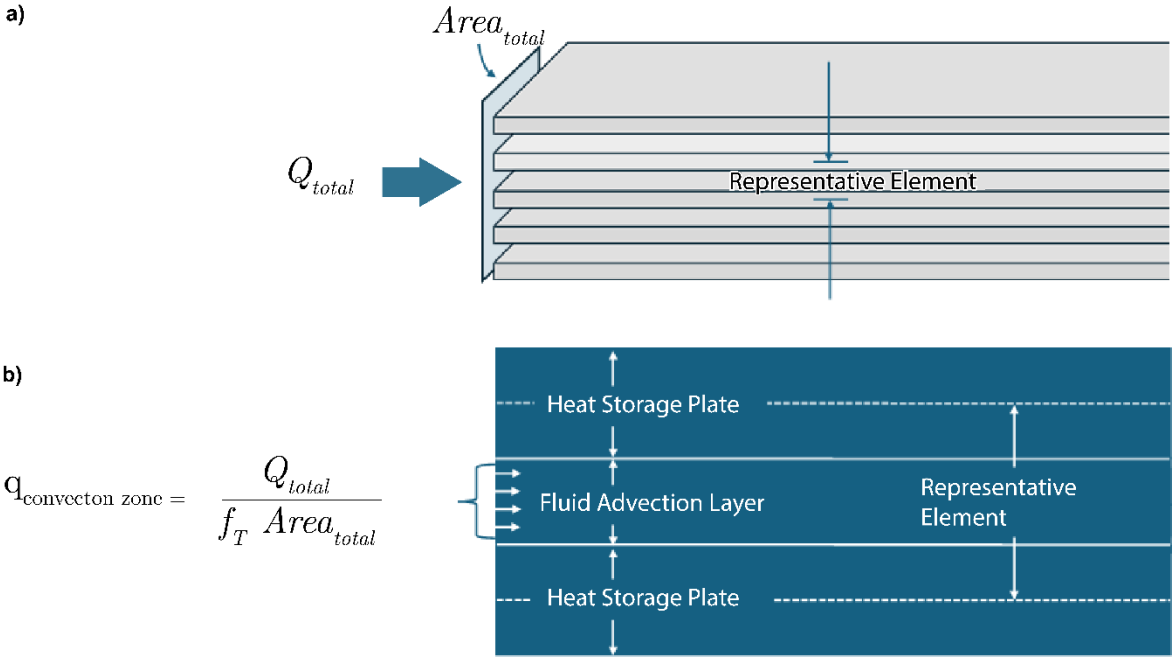

Figure 17 - An analogous plate heat exchanger: a) large-scale view of heat exchanger; b) close up of the representative element delineated in (a), with the convection zone flow rate equal to Q_{total} divided by both the total influent area of the heat exchanger $(Area_{total})$ and the fraction of the heat exchanger conducting flow (f_T).

Figure 18 shows that heat is driven through the gaps between plates principally by fluid advection (convection), but also by conduction and diffusion, while migrating into the plates by conduction. If transport in the gaps was by advection alone there would be a distinct vertical line between the red (relatively hot) and blue (relatively cold) colors within the gaps in Figure 18 as the plug of heat flowed forward. Heat is accumulated in the solid heat storage plates as heat is extracted from the driven fluid.

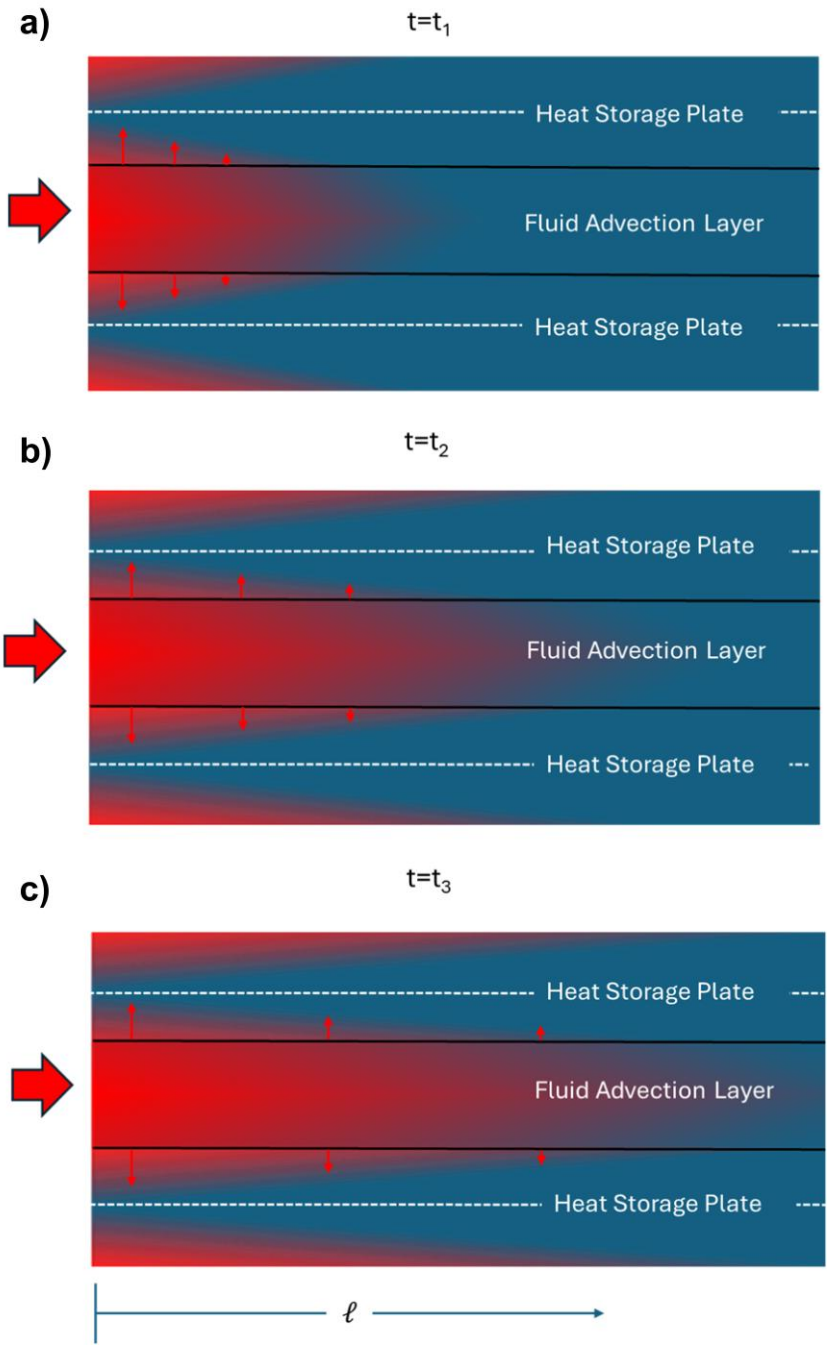

Figure 18 - Distribution of heat while the source temperature is elevated at $a)\ t = t_1;\ b)\ t = t_2;\ and\ c)\ t = t_3$, showing the advance of heat by advection and conduction in the fluid advection layer and by conduction in the storage plates. The large red arrow represents q_{fluid} at the elevated T_{on}. Small red arrows show heat conduction into the plates.

In the gaps, the position of the leading edge of the heat front while fluid of elevated temperature is being introduced, $l_{heating}$, at time t is expressed by Equation (11).

$$l_{heating}(t) = \frac{q_{fluid}\ t}{f_T} \qquad (11)$$

where (parameter dimensions are dark green font with mass as M, length as L, time as T):

l = distance to the front of the advective portion of the transported heat (L)

q_{fluid} = volumetric fluid flow rate divided by the total influent area (LT^{-1})

f_T = fraction of the domain that transmits flow (dimensionless)

The solid plates (analogs to low-*k* zones) accelerate flow through the fluid advection layer (analogs to transmissive zones that serve as preferential flow paths). Through time, heat in the gaps is conducted into the metal plates via conduction (analogous to diffusion from transmissive into low-*k* zones) into the cooler thermally conductive solid plates. The amount of heat stored in the metal plates at any point is a function of temporally varying temperature gradients at the boundaries between the gaps and the heat storage plates integrated over time.

Figure 19 illustrates the distribution of heat at a time, $t > t'$, when the inflow temperature is returned to T_0. The position of the cooling front $l_{cooling}$ at time t is Equation (12).

$$l_{cooling}(t) = \frac{q_{fluid}(t-t')}{f_t} \qquad \text{for } t > t' \qquad (12)$$

Throughout the cooling zone in the gaps, lower fluid temperatures drive release of heat from the solid plates into the fluid as heat flows from higher to lower temperature zones. The consequence of the release of heat from the solid plates is $T > T_0$ in the fluid within the gaps. Two conditions are worth note. 1) While the heat stored in the plates is being released into the fluid in the gaps, heat also continues to move further into the interior of the heat storage plates; and 2) theoretically, at any point an infinite amount of time will be needed to remove all the heat stored in the solid plates. This is because the rate at which heat is dissipated approaches, but never reaches, an asymptote as the fluid advection layer and heat storage plate temperatures approach the same temperature.

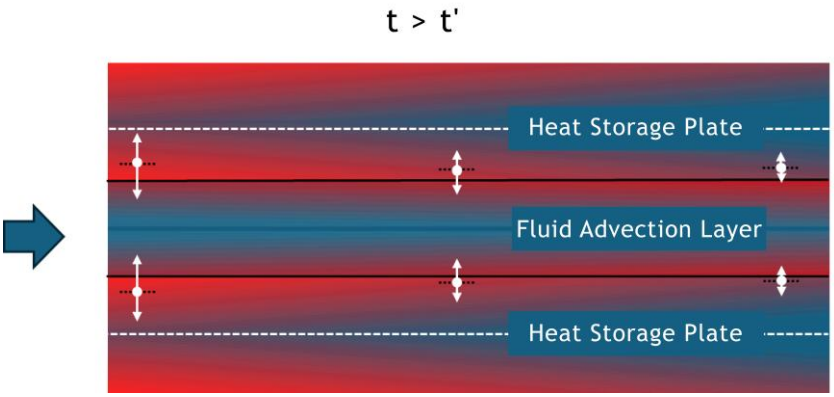

Figure 19 - Distribution of heat at a time after the influent fluid temperature is returned to T_0 at time t' when the cooling front has been able to migrate across the distance *l* included in the figure. The large blue arrow represents q_{fluid} at the initial temperature, T_o. Small white arrows show heat conduction into and out of the plates. The magnitude of heat conduction is greater at the entry end where more heat had been stored in the plates creating a larger temperature gradient.

Figure 20 plots normalized temperature versus time for a point in the center of the fluid flowing within the gaps in the heat battery. In Figure 20, (A) defines the time when the heating front arrives at l. (B) defines the time when the cooling front arrives at l. The striped area labeled C is proportional to the amount of heat stored in the solid plate in the heat exchanger. The striped area labeled D is proportional to the amount of remaining heat stored in the solid plate after the effects of the active source have passed and q_{fluid} with $T = T_0$ continues to flow through the system.

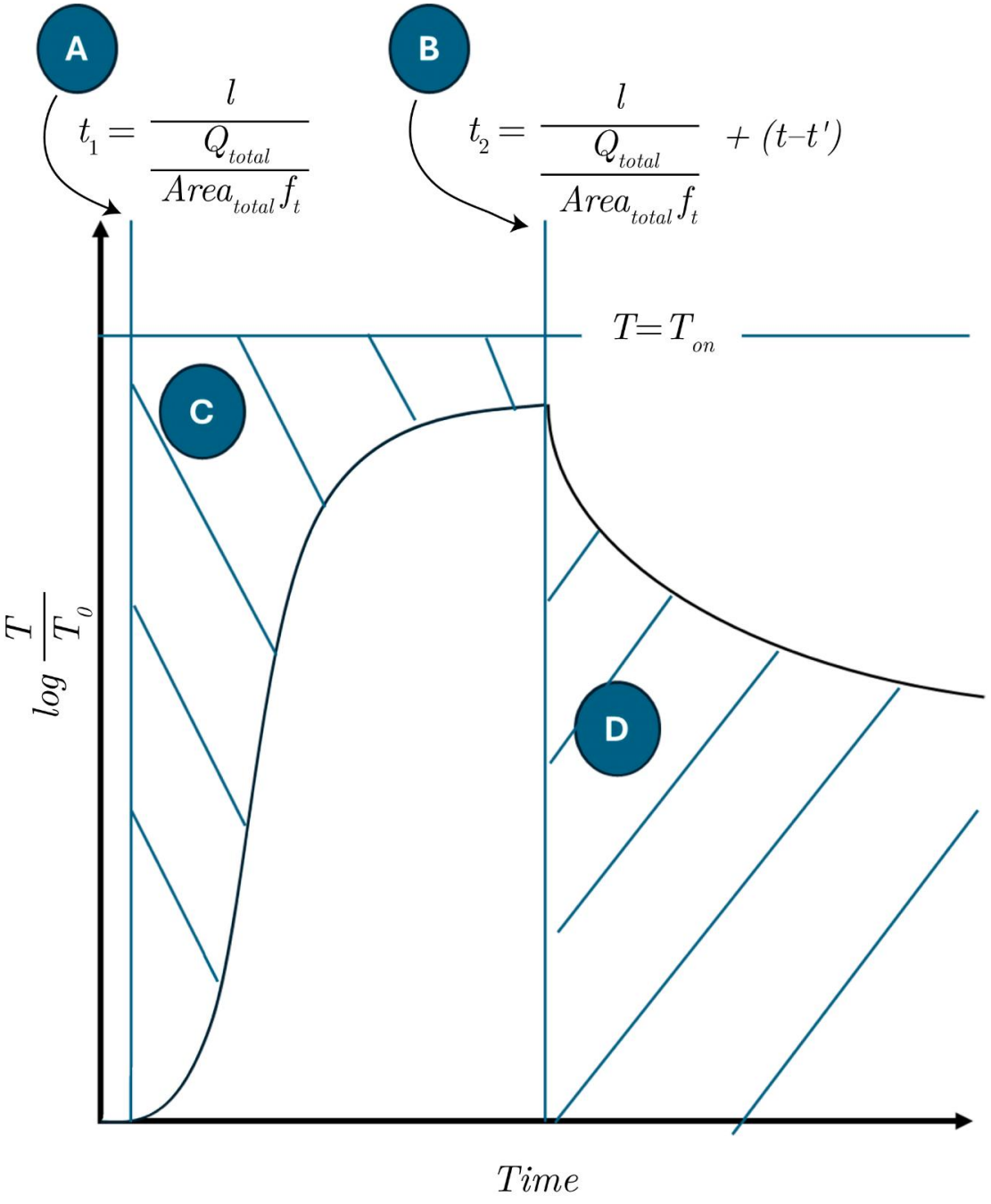

Figure 20 - Heat as measured using normalized temperature for a fixed downgradient position in the center of the fluid advection layer as a function of time. Items A through D are described in the text.

Thought questions for the reader.

1. Would it be practical to model the heat storage as a homogeneous domain without solid plates? The answer is no. Preferential flow in gaps and storage and release of heat to and from the solid plates are essential characteristics governing function.
2. Translating the concept of heat storage to contaminant transport in heterogeneous media (and accepting that all subsurface media are heterogeneous media), is it practical to model contaminant transport as a homogeneous domain and not include the low-*k* zones? Per the following sections and the supporting references, the answer is likely no. Missing preferred advection of contaminants through transmissive zones accompanied by storage and release of contaminants in low-*k* zones leads to, as per Theis (1967), misleading results.
3. Lastly, can we expect models predicated on stylistic renditions of transmissive and low-*k* zones to rigorously forecast contaminant concentrations and fluxes at field sites over large spans of time? As of 2025, the answer still is probably not. On the other hand, stylistic forecasts of contaminant transport in heterogeneous media provide essential foundations for managing subsurface releases of CoCs and efficient use of available resources. As the Rolling Stones sang in 1969, "You can't always get what you want, but if you try sometimes, you just might find … you get what you need.

2.11 Exercises Related to Section 2

After reading Section 2 the reader should be able to successfully complete the following exercises: Exercise 1; Exercise 2; Exercise 3; Exercise 4; Exercise 5; and Exercise 6.

3 Transport

Transport of contaminants through natural subsurface media is the product of two fundamental processes: advection and diffusion. Advective and diffusive transport can be modified by a diverse set of potential reactions addressed in Section 4. We envision transport in uniform bodies of either transmissive or low-permeability (low hydraulic conductivity, low-*k*) media. Mixing due to hydrodynamic dispersion is viewed as a weak process and addressed in the modeling discussions presented in Section 5. At the end of Section 3 readers should be able to complete Exercises 7 through 11 of Section 7.

3.1 Advection

CoCs are transported via advection in aqueous, gas, and nonaqueous fluids. Advective transport in gases, compressible fluids with potentially interdependent diffusive fluxes, is beyond the scope of this text. McWhorter (2021) provides information on transport in gases. Advective transport of NAPLs is discussed in Section 3.2.

3.1.1 Groundwater

Groundwater flow is driven by the hydrologic cycle as shown in Figure 8. Moving groundwater carries aqueous phase CoCs via a process referred to as advection. Advection of CoCs in groundwater creates contaminant plumes extending hundreds to thousands of meters beyond sources (e.g., Wiedemeier et al., 1999). Exposure to CoCs in plumes is a primary driver for CoC-related risks to human health and the environment. Equations for advective transport in media fully saturated by an aqueous phase, are presented in Table 1.

Table 1 - Primary equations for advective transport in media fully saturated by an aqueous phase.

Equation	Name	Concept and units	#
$q_{aq} = -\frac{k\rho_{aq}g}{\mu_{aq}}\frac{dh_{aq}}{dl}$	Aqueous flux in a granular porous media	Volumetric discharge water per unit area per time of an aqueous phase ($L^3L^{-2}T^{-1}$) for a granular porous media	(13)
$q``_{aq} = -\frac{b``^2}{12\mu_{aq}}\frac{dh_{aq}}{dl}$	Aqueous flux between parallel plates, as an analog to flow in a fracture	Volumetric discharge per unit area per time of an aqueous phase ($L^3L^{-2}T^{-1}$) for a fracture	(14)
$h_{aq} = \frac{1}{\rho_{aq}g}\frac{dP_{aq}}{dl} + \frac{dz}{dl}$	Hydraulic head	Potential energy (L) driving flow of an aqueous phase	(15)
$v_{ad} = \frac{q_{aq}}{\phi}$	Seepage velocity in a uniform zone	Rate of advective transport without sorption (LT^{-1})	(16)
$J_{ad_i} = q_{aq}\rho_{aq_i}$	Advective flux of CoC i	Flux of CoC i due to aqueous phase advective transport in a uniform, granular porous media ($ML^{-2}T^{-1}$)	(17)
$\dot{M}_{ad_i} = A_T J_{ad_i}$	Mass discharge of CoC i in a uniform porous media	Total mass of a CoC moving through a cross-sectional of area (A_T) of interest normal to flow (MT^{-1})	(18)

Given the flow of groundwater in fully saturated porous media, a more familiar form of Equation (13) (for many) is shown as Equation (19).

$$q_{aq} = -K\frac{dh}{dl} \quad \text{where: hydraulic conductivity } (\mathrm{LT}^{-1}),\ K = \frac{k\rho_{aq}g}{\mu_{aq}} \tag{19}$$

Through this book we use both permeability, k (L^2), and hydraulic conductivity, K (LT^{-1}), as physical properties constraining the flow of water. Permeability (k) has the advantage of being an intrinsic property of porous media independent of fluid saturations, fluid densities, and fluid viscosities. Problems involving multiple fluids in porous media or fluids other than water employ permeability. For simplicity, problems involving porous media fully saturated with an aqueous phase with a constant density near 1 gm/cm^3 employ hydraulic conductivity. The effects of dissolve-phase constituents in water on fluid density are not addressed herein. Information on the effects of dissolved phase constituents on transport can be found in Post and Simmons (2023) and Marinelli (2024). Figure 21 links to a video that documents spreading of a low-density aqueous phase above a higher density aqueous phase.

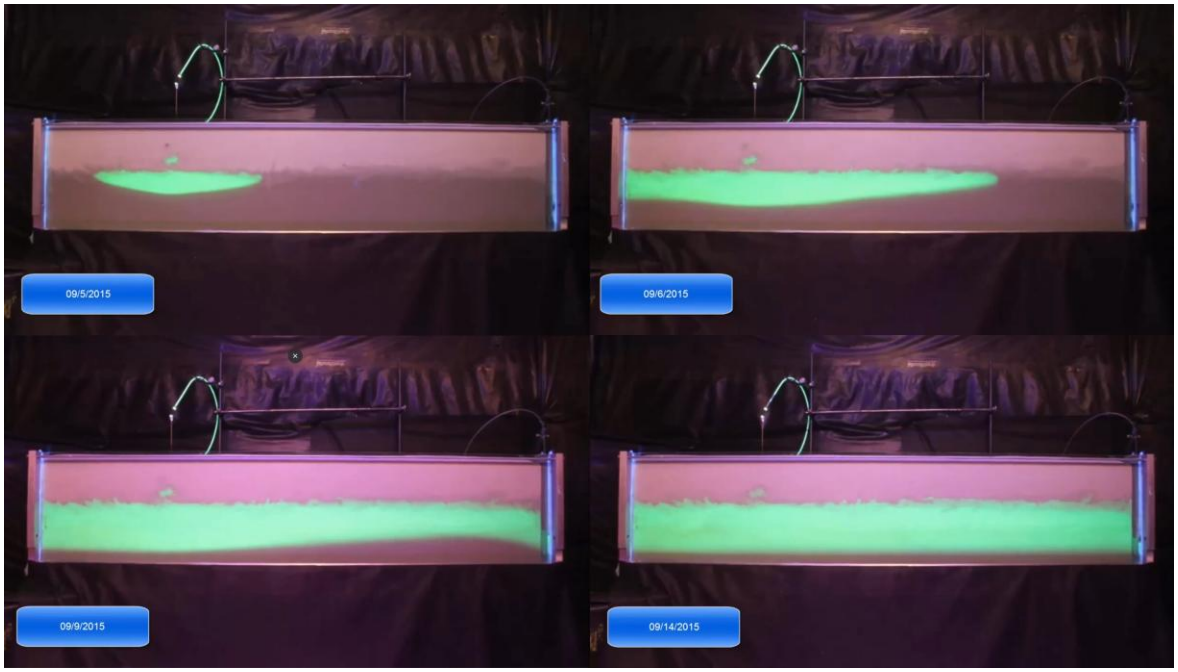

Figure 21 - Laboratory demonstration of capping a high TDS plume with fresh water: An animated version of this example is shown in this video. Created by Nolan Prat, Mitch Olsen, and Tom Sale of Colorado State University, USA and produced by Emma Schmit.

3.1.2 Visualizations of Advective Transport

Figure 22 illustrates advective transport of fluoresceine dye in a laboratory sand tank employing uniform sand (left panel) and heterogeneous sands (right panel). Similar volumetric tracer fluxes ($\frac{Q_{tracer}}{A_T}$) are used in both studies. The tracer arrives at the midpoint of the tank 3.6 times faster in the heterogeneous sand due to preferential flow in the more

transmissive zones. The arrival time suggests an effective transmissive zone fraction (f_T) of 0.28 (1/3.6) in the heterogeneous sand tank relative to the uniform sand.

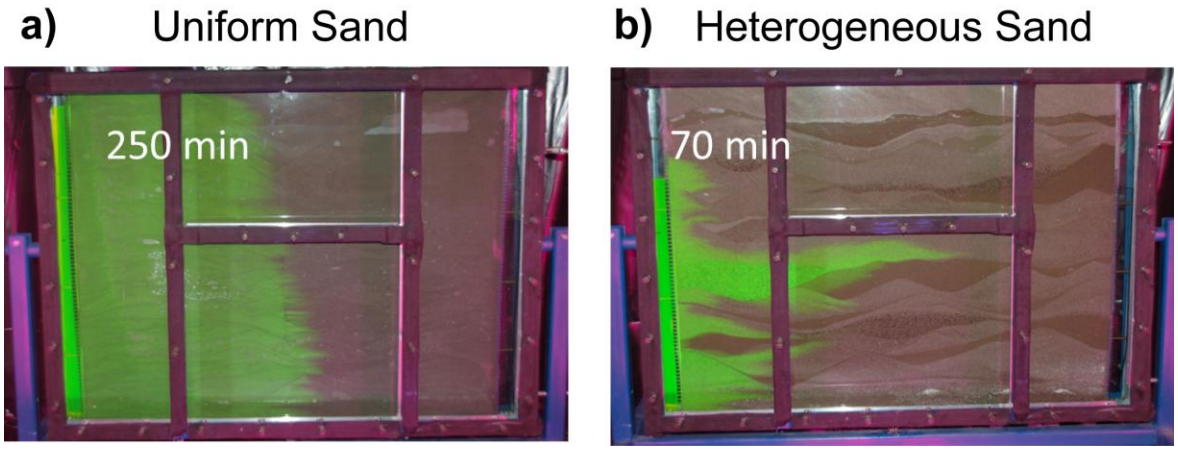

Figure 22 - Horizontal advective transport of fluorescein to the midpoint of 1090 by 800 mm sand tanks using identical total mass fluxes across a) uniform sand and b) heterogeneous sand. The arrival time is 3.6-times faster in the heterogeneous sand tank (Doner, 2008).

Given heterogeneous porous media (e.g., sand), the seepage velocity needed to estimate the arrival time of a given CoC is defined as shown in Equation (20).

$$v_{aq} = \frac{q_{aq}}{\phi f_T} \tag{20}$$

where (parameter dimensions are dark green font with mass as M, length as L, time as T):

v_{aq} = seepage velocity needed to estimate the arrival time of a given CoC in a permeable porous media (LT^{-1})

q_{aq} = aqueous flux ($L^3L^{-2}T^{-1}$)

ϕ = porosity (dimensionless)

f_T = fraction of the domain that transmits flow (dimensionless)

3.1.3 Advective Transport about Wells with Steady Pumping Rates

Flow nets provide a simple introduction to advective transport around pumping wells. For those unfamiliar with flow nets or wanting additional information, a detailed explanation is provided in Poeter and Hsieh (2020). Flow nets are assumed to have the following characteristics.

- Homogeneous and isotropic transmissive zones with steady-state flow.
- Flow in two dimensions with flow lines orthogonal to equipotential lines.
- "Plug flow" wherein there is no mixing along (longitudinal) or perpendicular to (transverse) stream tubes due to diffusion or hydrodynamic dispersion.
- No exchange of contaminants between transmissive and low-k zones via either diffusion or slow advection.
- The difference between equipotential line values (Δh) is constant.

A plan view flow net for flow around two pumping wells (wells 1 and 2) and one injection well (well 3) from Fitts (2002) is provided in Figure 23. Labeled on Figure 23 are curvilinear distances $W_{i,j}$ and $\Delta s_{i,j}$, which are assumed to be equal in all flow net elements i, j.

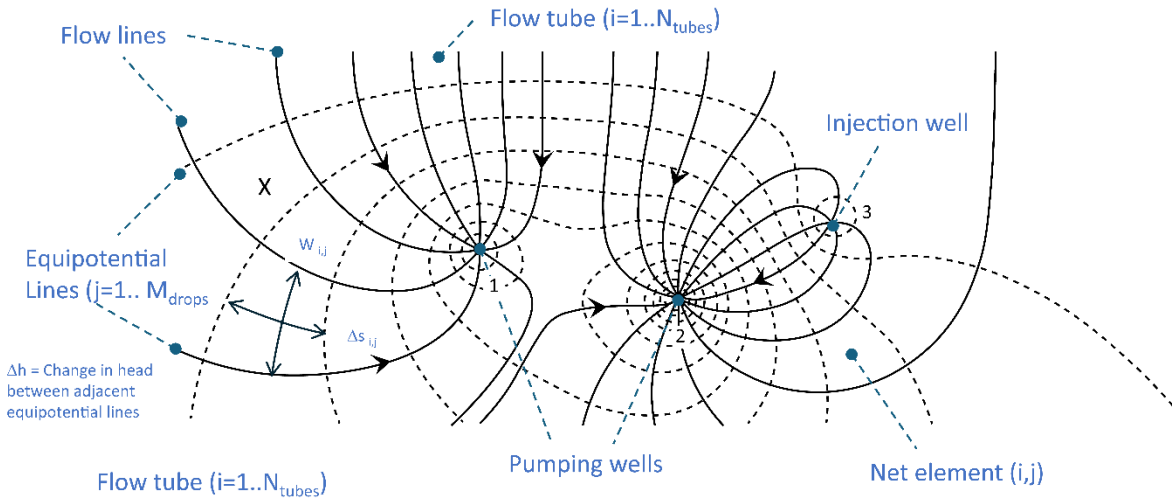

Figure 23 - Plan view flow net after Fitts (2002) where 1 and 2 are pumping wells and 3 is an injection well. Solid flow lines, forming stream tubes, are drawn orthogonally to dashed equipotential lines with uniform changes between contour intervals (Δh). X marks the location where a source is introduced.

Given no flow in the z direction (i.e., the direction perpendicular to the image, "into" the page), the governing equation for steady-state flow in Figure 23 is the two-dimensional form of the Laplace Equation (21).

$$\frac{\delta^2}{\delta x^2}h + \frac{\delta^2}{\delta y^2}h = 0 \tag{21}$$

Solving the Laplace equation given the assumptions, the volumetric discharge of groundwater, $Q_{Tube\ i}$ (L^3T^{-1}), through any stream tube (i) is as in Equation (22).

$$Q_{Tube\ i} = -KW_{i,j}b\frac{\Delta h}{\Delta s_{i,j}} \tag{22}$$

$W_{i,j}$ and $\Delta s_{i,j}$ are the curvilinear width and length of stream tube i, and element j, respectively. Given $W_{i,j} = \Delta s_{i,j}$ and $T = Kb$, Equation (22) simplifies to Equation (23).

$$Q_{Tube\ i} = -T\Delta h \tag{23}$$

The total discharge (L^3T^{-1}), to or from any well, is as in Equation (24).

$$Q_{Well} = -N_{tubes}T\Delta h \tag{24}$$

In Figure 23, pumping wells 1 and 2 and injection well 3 have 9, 14, and 6 flow tubes, respectively. An estimate of the travel time for a CoC through any stream tube is derived through the following steps shown in Equations (25), (26), (27), (28), (29), and (30).

1) For a single stream tube element (i), the average Darcy flux through element (i,j) is obtained by dividing the volumetric discharge through the tube as shown in Equation (22) by the cross-sectional area of flow $bW_{i,j}$ as in Equation (25).

$$q_{element_{i,j}} = \frac{Q_{Tube}}{bW_{i,j}} = \frac{-T\Delta h}{bW_{i,j}} \tag{25}$$

2) The average advective groundwater flux is converted to an average seepage velocity for flow net element i,j by dividing Equation (25) by ϕ and the transmissive fraction of the aquifer, f_T, resulting in Equation (26).

$$v_{ad_{i,j}} = \frac{-T\Delta h}{f_T bW_{i,j}\phi} \tag{26}$$

3) Given that travel time is equal to distance, $\Delta s_{i,j}$, divided by transport velocity, $v_{ad_{i,j}}$, the time to transverse a flow net element (i,j) is shown in Equation (27).

$$t_{elememt_{i,j}} = \frac{\Delta s_{i,j}}{v_{ad_{i,j}}} = \frac{\Delta s_{i,j}}{\frac{T\Delta h}{f_T bW_{i,j}\phi}} = \frac{\Delta s f_T bW_{i,j}\phi}{T\Delta h} = \frac{\Delta s^2 f_T b\phi}{T\Delta h} \tag{27}$$

Equation (27) tells us the travel time through a stream tube element is proportional to the square of the travel distance between equipotential lines, linearly (directly) proportional to $f_T b\phi$, and inversely proportional to $T\Delta h$.

4) The total time to move from a source element in the flow field to a well can be estimated as the sum of the travel times through all the stream tube elements of concern (e.g., from X to well 1 in Figure 23), as shown in Equation (28).

$$t_{source\ to\ well} = \sum_{i=1}^{N_{Elements}} \frac{\Delta s_i{}^2 f_T b\phi}{T\Delta h} = \frac{f_T b\phi}{T\Delta h} \sum_{i=1}^{N_{Elements}} \Delta s_i{}^2 \tag{28}$$

Notably, the accuracy of this equation improves as the number of stream tubes increases.

5) Following Einarson and Mackay (2001), estimates of the strength of a steady-state source in the capture zone of a well, $\dot{M}_{source}$ (MT^{-1}), absent degradation, can be calculated as the product of the concentration of the CoC in the pumped well, $\rho_{aq-well}$, and the well flow rate, Q_{well}, as in Equation (29).

$$\dot{M}_{source} = Q_{well}\,\rho_{aq-well} \tag{29}$$

Or, given a known $\dot{M}_{source}$, the aqueous concentration at the pumping well $\rho_{aq-well}$ (ML^{-3}) can be calculated as shown in Equation (30).

$$\rho_{aq-well} = \frac{\dot{M}_{source}}{Q_{well}} \tag{30}$$

Example calculations applying Equations (24) through (29) are provided in the calculation vignette shown in Figure 24.

Calculation Vignette
Advective Transport to a Well Field

Inputs

$$T = 100\frac{m^2}{\text{day}} \quad b = 30\,m \quad K = \frac{T}{b} = (3.858 \times 10^{-5})\frac{m}{s} \quad \Delta s = \begin{bmatrix} 70 \\ 50 \\ 30 \\ 20 \\ 10 \\ 5 \end{bmatrix} m$$

$$\Delta h = 1\,m \quad \phi = 0.3 \quad N_{\text{Elements}} = 6 \quad N_{\text{tubes}} = 9$$

What is the total flow rate to well 1 in Figure 23?

$$Q_{\text{Well}} = N_{\text{tubes}} \quad T \quad \Delta h = 900\frac{m^3}{\text{day}}$$

What is the travel time from X to Well 1 in Figure 23 given f_T varying from 0.1 to 1?

$$f_T = 0.1, 0.2, \ldots, 1 \qquad t_{\text{total}}(f_T) = \frac{f_T \quad b \quad \phi}{T \quad \Delta h} \sum_{i=1}^{N_{\text{elements}}} (\Delta s_i)^2$$

$$t_{\text{total}}(f_T) = \begin{bmatrix} 0.217 \\ 0.435 \\ 0.652 \\ 0.87 \\ 1.087 \\ 1.305 \\ 1.522 \\ 1.74 \\ 1.957 \\ 2.175 \end{bmatrix} \text{ yr} \qquad t_{\text{total}}(f_T) \text{ yr}$$

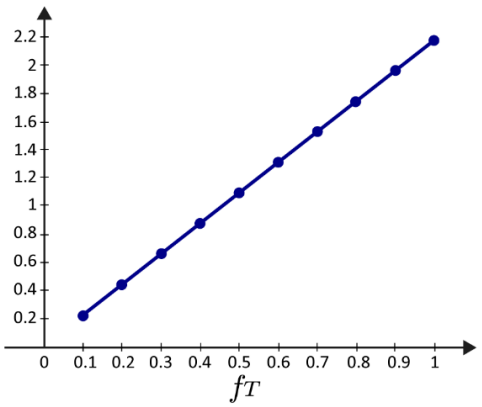

Given TCE concentrations in well 1 ranging from 0.005 to 50 mg, what are the associated strength of the source at X?

$$\rho_{\text{aq}} = \begin{bmatrix} 0.005 \\ 0.05 \\ 0.5 \\ 5 \\ 50 \end{bmatrix} \frac{\text{mg}}{\text{L}} \qquad \dot{M}(\rho_{\text{aq}}) = N_{\text{tubes}} \quad T \quad \Delta h \quad \rho_{\text{aq}}$$

$$\dot{M}(\rho_{\text{aq}}) = \begin{bmatrix} 1.6 \\ 1.6 \times 10 \\ 1.6 \times 10^2 \\ 1.6 \times 10^3 \\ 1.6 \times 10^4 \end{bmatrix} \frac{\text{kg}}{\text{yr}}$$

Figure 24 - Calculation vignette for advective transport in a well field as a function of the transmissive fraction of the aquifer illustrating that travel time decreases linearly with decreasing transmissive fractions.

3.1.4 Capture Zones Around a Pumping Well

Employing the Laplace Equation which is shown as Equation (21), applying assumptions used for developing flow nets, and following Todd (1980), capture zones of a pumped well can be delineated as shown in Figure 25. Resolving capture zones is a useful

endeavor in designing hydraulic containment systems for sources and wellhead protection zones for water supply wells. This section presents mathematical derivations for estimating 1) the distance from the pumped well to the downgradient stagnation point, x_s, and 2) the upgradient width of the capture zone, w_c.

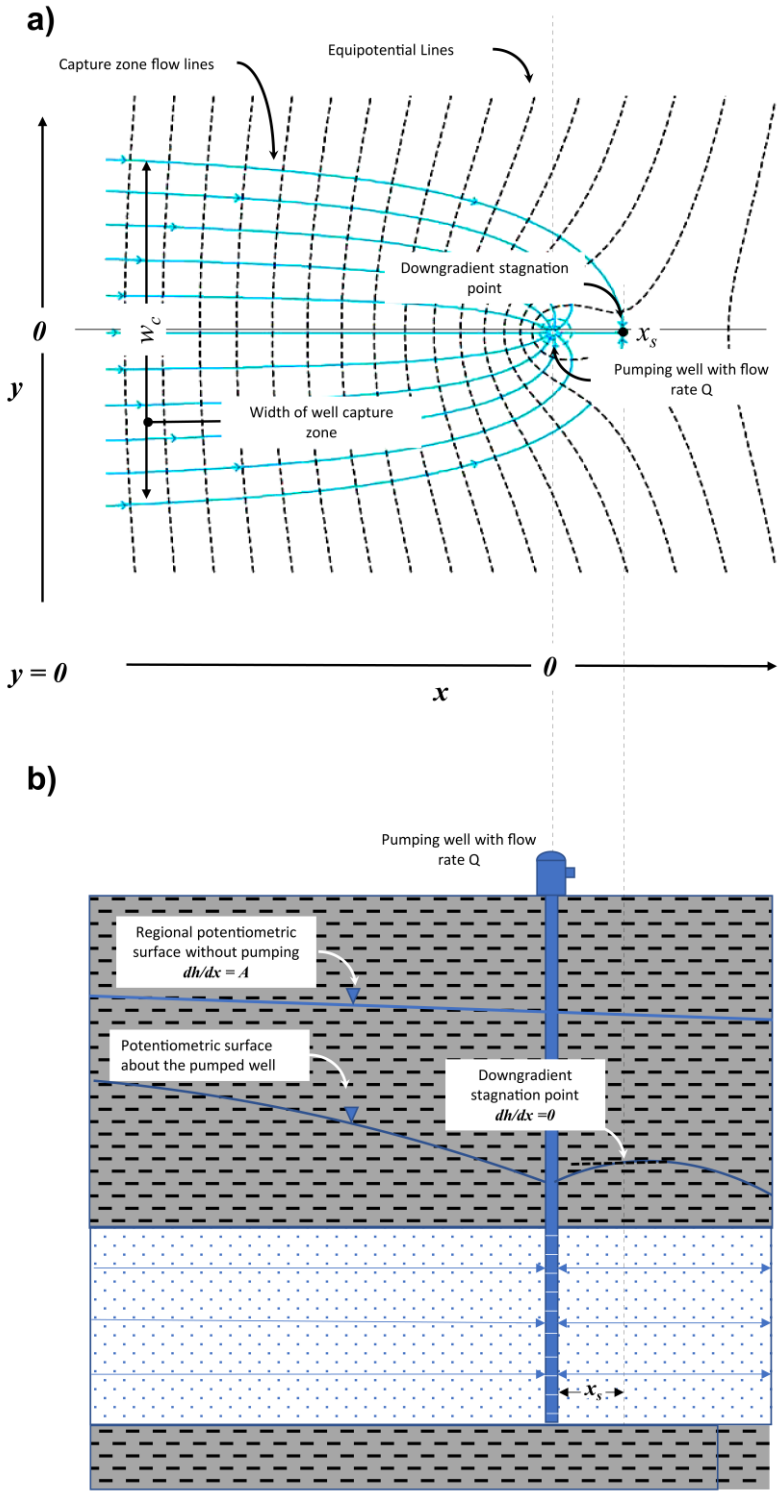

Figure 25 - Delineation of the capture zone of a pumping well under steady-state conditions given a uniform regional ground water flow field with a hydraulic gradient of A in the x-direction: a) plan view, and b) corresponding cross section. After Todd, (1980).

First, employing the principle of superposition, the solution for the hydraulic head around a pumping well can be obtained by summing solutions for a uniform sloping water table and steady-state pumping around a well. The solution for a uniform sloping water table is as shown in Equation (31).

$$h(x,y) = Ax + By + C \tag{31}$$

where:

A = the slope of the water table in the x direction (LL^{-1})

B = the slope of the water table in the y direction (LL^{-1})

C = a constant equal to a known head $h\ at\ x = 0, y = 0$.

Following the Thiem solution (Theim, 1906) for steady flow to a well as in shown in Equation (32).

$$h(r) = -\frac{Q_{well}}{2\pi T} ln(\frac{r}{r_o}) + h_{ss} \tag{32}$$

where (parameter dimensions are dark green font with mass as M, length as L, time as T):

r = radial distance from the well (L)

r_o = radial distance for a known steady-state head, h_{ss} (L)

h_{ss} = steady-state head at the distance r_o from the well (L)

Assigning $r = \sqrt{x^2 + y^2}$ as shown in Equation (33).

$$h(x,y) = \frac{Q_{well}}{2\pi T} ln \sqrt{\frac{x^2 + y^2}{x_o^2 + y_o^2}} + h_{ss} \tag{33}$$

Given that both these equations are linear solutions with common boundary conditions (no drawdown at infinite distances), they can be superposed (summed) to obtain a solution for water levels around a pumped well in a uniform flow field, as long as the x, y values have the same origin [i.e., the well location must be used as the origin in both Equations (31) and (33)]. Given that Equation (33) uses x, y as 0,0 at the well location, the x, y origin used to determine of C in Equation (31) should be the well location. The superposed solution is shown as Equation (34).

$$h(x,y) = Ax + By + C - \frac{Q_{well}}{2\pi T} ln \sqrt{\frac{x^2 + y^2}{x_o^2 + y_o^2}} \tag{34}$$

A solution for the distance to the downgradient stagnation point (the point dividing captured and not-captured groundwater) can be obtained by assuming there is no regional flow in the y direction ($B = 0$), by taking the derivative of Equation (34) with respect to x, and assigning the gradient at x to zero, as shown in Equation (35).

$$\frac{d}{dx}h(x,y) = A + \frac{Q_{well}}{2\pi T x_s} = 0 \tag{35}$$

Solving for the horizontal distance from the well to the stagnation point, results in Equation (36).

$$x_s = -\frac{Q_{well}}{2\pi T A} \tag{36}$$

A solution for the upgradient width of the capture zone, w_c, can be developed by again assuming there is no regional flow in the y direction ($B = 0$) and applying Darcy's equation to the upgradient flow to the well, as shown in Equation (37). We note that the A of Equation (37) is not an area, but the gradient in the x direction.

$$Q_{well} = -K(Area)\frac{d}{dx}h = -Kbw_c\frac{d}{dx}h = Tw_cA \tag{37}$$

Solving for w_c is shown in Equation (38).

$$w_c = \frac{Q_{well}}{TA} \tag{38}$$

This approach to delineation of a capture zone around a pumped well assumes spatially homogeneous, isotropic conditions at the REV scale, steady-state flow, and f_T=1. Example calculations applying Equations (34) through (38) are provided in the calculation vignette shown in Figure 26.

Calculation Vignette
Capture Zone of a Steady State Pumping Well

Inputs

$$T = 300\frac{m^2}{\text{day}} \quad A = \frac{1\ m}{100\ m} \quad B = \frac{0\ m}{100\ m} \quad C = 100\ m \quad Q = 1000\frac{m^3}{\text{day}}$$

$$x_o = 100\ m \quad y_o = 100\ m \quad C_2 = 100\ m$$

Assumes the well is at 0,0 and 0.1m is added to the range variables to avoid calculating infinite drawdown at the well

Solutions

$$h(x, y, A) = A\ x + B\ y + \frac{Q}{2\ \pi\ T} \ln\left(\frac{\sqrt{x^2 + y^2}}{\sqrt{x_o^2 + y_o^2}}\right) + C_2$$

$$AA(A) = \begin{cases} \text{for } i = 1 \ldots 80 \\ \quad \begin{cases} \text{for } j = 1 \ldots 40 \\ \quad \begin{cases} x \leftarrow -410.1\ m + i\ 10\ m \\ y \leftarrow -210.1\ m + j\ 10\ m \\ AA_{i,j} \leftarrow h(x, y, A) \end{cases} \end{cases} \\ AA \end{cases}$$

No Regional Gradient A=0

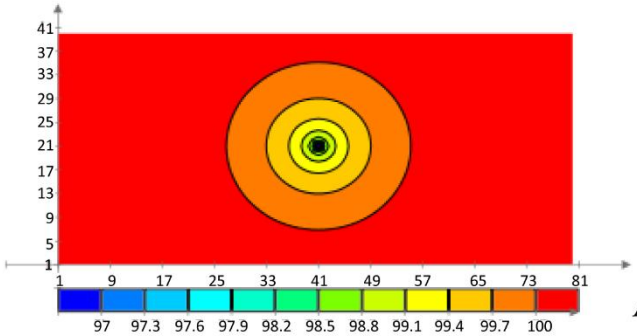

$AA(0)$

Regional in x = 1/100 A=0.01

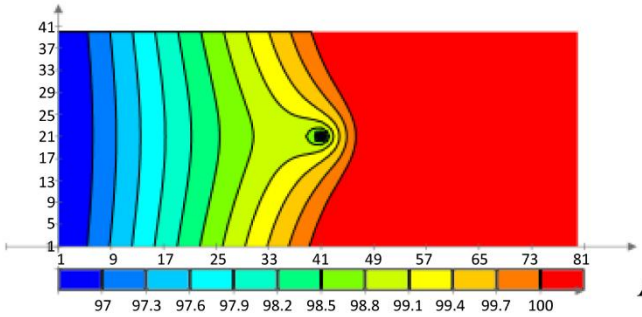

$AA(0.01)$

$$x_s = \frac{Q}{2\ \pi\ T\ A} = 53\ m \qquad w_c = \frac{Q}{T\ A} = 333\ m$$

Figure 26 - Calculation vignette for capture zone about a steady state pumping well.

3.1.5 Exercises related to Section 3.1

After completing Section 3.1, the reader should be able to undertake the following exercises: Exercise 7, Exercise 8, Exercise 9, Exercise 10, and Exercise 11.

3.2 Multiple Immiscible Fluids

In many instances, two or even three immiscible fluids coexist in pores in porous media. An example is vadose zone porous media with water wetting the porous media grains and gas as a nonwetting fluid. A more complex example is water as a wetting fluid, gas as a nonwetting fluid, and petroleum liquids as an intermediate wetting fluid (between gas and water). Classic examples of three-phase systems include petroleum oil-gas reservoirs (e.g., Corey, 1994) and, more recently, shallow petroleum spills around the water table (e.g., Sale et al., 2018). The presence of multiple fluids in pore space adds significant complexity to our study of transport processes. However, given the broad relevance of understanding the processes governing multiple fluid phases in porous media across remediation, agriculture, geoenvironmental engineering, and petroleum reservoir engineering, the rewards for understanding the behavior of multiple immiscible fluids in porous media are considerable. Building on Corey (1994), the following describes multiple immiscible fluid distributions and flow under steady-state conditions. More comprehensive information can be found in Corey (1994) as well as in Mumford and others (2024). At the end of Section 3.2, the reader should be able to complete the Exercises 12 through 19.

3.2.1 Hydrostatic Pore-Scale Fluid Distributions

Principles governing the behavior of wetting fluids (including intermediate wetting fluids) and nonwetting fluids are fundamentally different. As such, knowing whether a fluid is wetting or nonwetting is essential. As a first-order approximation, the following principles apply.

- Attraction: Like compounds are attracted and polar aqueous solutions (e.g., water) are attracted to polar mineral solids.
- Repulsion: Similarly, dislike compounds are repelled, and polar liquids repel nonpolar gases (e.g. N_2, O_2, CO_2, and CH_4).
- Intermediate wetting fluids: Where present, intermediate wetting fluids are commonly more polar than gases and less polar than aqueous solutions.

Figure 27 presents photographs adapted from classic laboratory tank studies of nonaqueous phase PCE in systems of glass beads, water, and atmospheric air (Schwille, 1984; Schwille & Pankow, 1988). Schwille (1984) is widely credited for early recognition of chlorinated solvents as DNAPL CoCs. The order of wetting follows the general principles in the preceding bulleted list and as shown in Figure 27. When two fluids are present, water acts as the wetting fluid, wetting the glass beads, while PCE is the nonwetting fluid. This distribution is analogous to a porous media containing pore air and pore water. When three fluids are present, water wets the glass beads, gas is the nonwetting fluid, and PCE is an intermediate wetting fluid. The intermediate wetting fluid occurs between nonwetting gases in large pores and water wetting the solids.

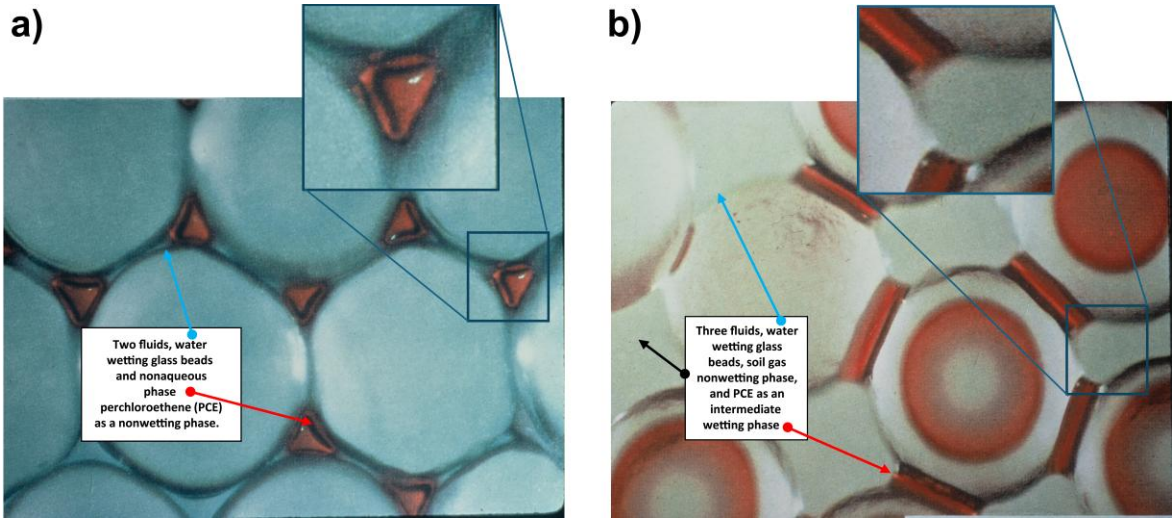

Figure 27 - Multiple fluid phase in porous media: a) two fluid phases, and b) three fluid phases. When two fluids are present, water acts as the wetting fluid, wetting the glass beads, while PCE is the nonwetting fluid. This distribution is analogous to a porous media containing pore air and pore water. When three fluids are present, water wets the glass beads, gas is the nonwetting fluid, and PCE is an intermediate wetting fluid. The intermediate wetting fluid occurs between nonwetting gases in large pores and water wetting the solids. (Adapted from Schwille, 1984).

A key attribute illustrated in Figure 27 is that the interfaces between the immiscible fluids are curved surfaces wherein

- nonwetting fluids have convex outward surfaces pushing outward into wetting fluids and
- intermediate wetting fluids have convex outward surfaces pushing outward into wetting fluids.

The outward deflections of interfaces reflect pore-scale differences in fluid pressures, as shown in Equation (39).

$$P_{nw} > P_{iw} > P_w \tag{39}$$

where:

P_{nw} = pressures in the nonwetting phase ($ML^{-1}T^{-2}$)

P_{iw} = pressures in the intermediate wetting phase ($ML^{-1}T^{-2}$)

P_w = pressures in the wetting phase ($ML^{-1}T^{-2}$)

The difference between the nonwetting and wetting fluid pressures is capillary pressure, P_c, as shown in Equation (40).

$$P_c = P_{nw} - P_w \tag{40}$$

where (parameter dimensions are dark green font with mass as M, length as L, time as T):

P_c = capillary pressure ($ML^{-1}T^{-2}$)

Capillary pressure is a critical parameter governing the distribution and movement of fluids in systems with multiple immiscible fluid phases. In the developments that follow, P_c governs:

- fluid saturations,
- the capacity of a porous media to conduct a fluid,
- forces driving fluid flow, and
- the ability of a nonwetting fluid to invade a media fully saturated with a wetting fluid.

The fluids in Figure 27 are not moving. Capillary pressures are balanced by other forces such that (following Newton's first law), the sums of the forces at fluid interfaces are zero. Capillary forces are balanced by interfacial forces that occur at the interfaces between the fluid phases, as shown in Figure 28. In a uniform fluid, such as water, molecules are attracted to each other through cohesive forces (e.g., van der Waals forces). However, at the interface between dissimilar fluids, molecular interactions differ—molecules are typically less attracted to or may even repel one another. As a result, molecules at the interface experience a net inward pull from cohesive forces, conceptually represented by white arrows in Figure 28. Interfacial forces (σ) have the units of force per length (e.g., dyne/cm). Solid–liquid and liquid–liquid interfacial forces are referred to as *interfacial tensions*. Liquid–gas and solid–gas interfacial forces are referred to as *surface tensions*.

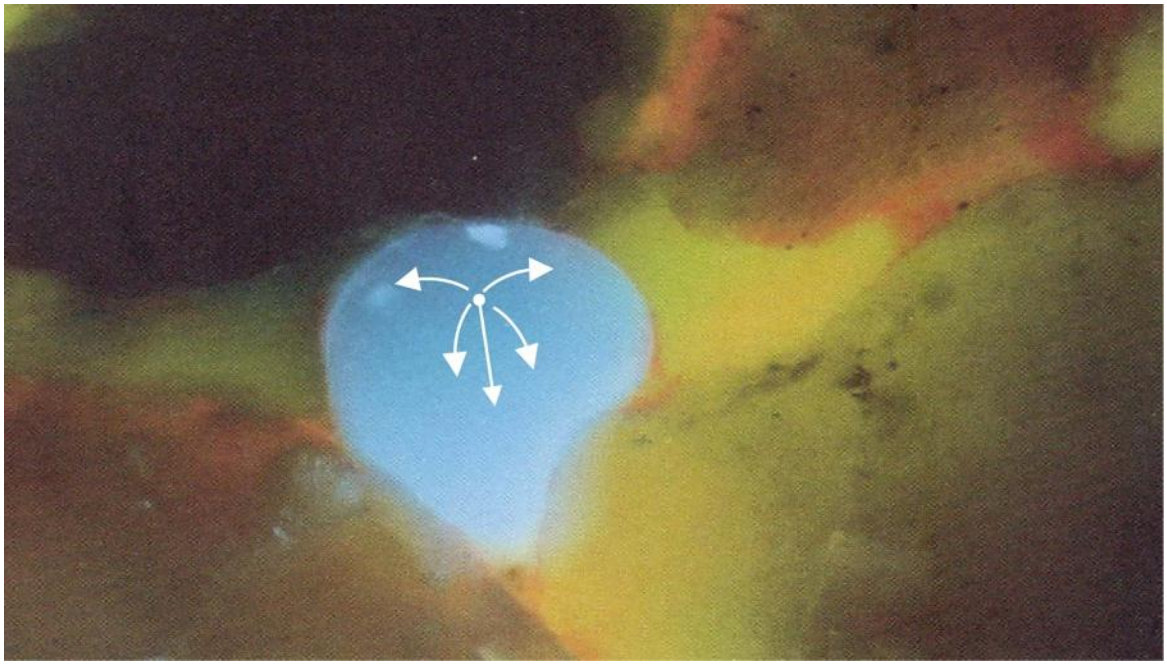

Figure 28 - Illustration of internal cohesion forces leading to interfacial tension between a nonwetting and wetting phase in granular porous media. Base image from Wilson and others (1990).

Figure 29 provides an illustrative example of capillary pressure balanced by interfacial forces under static conditions in a capillary tube.

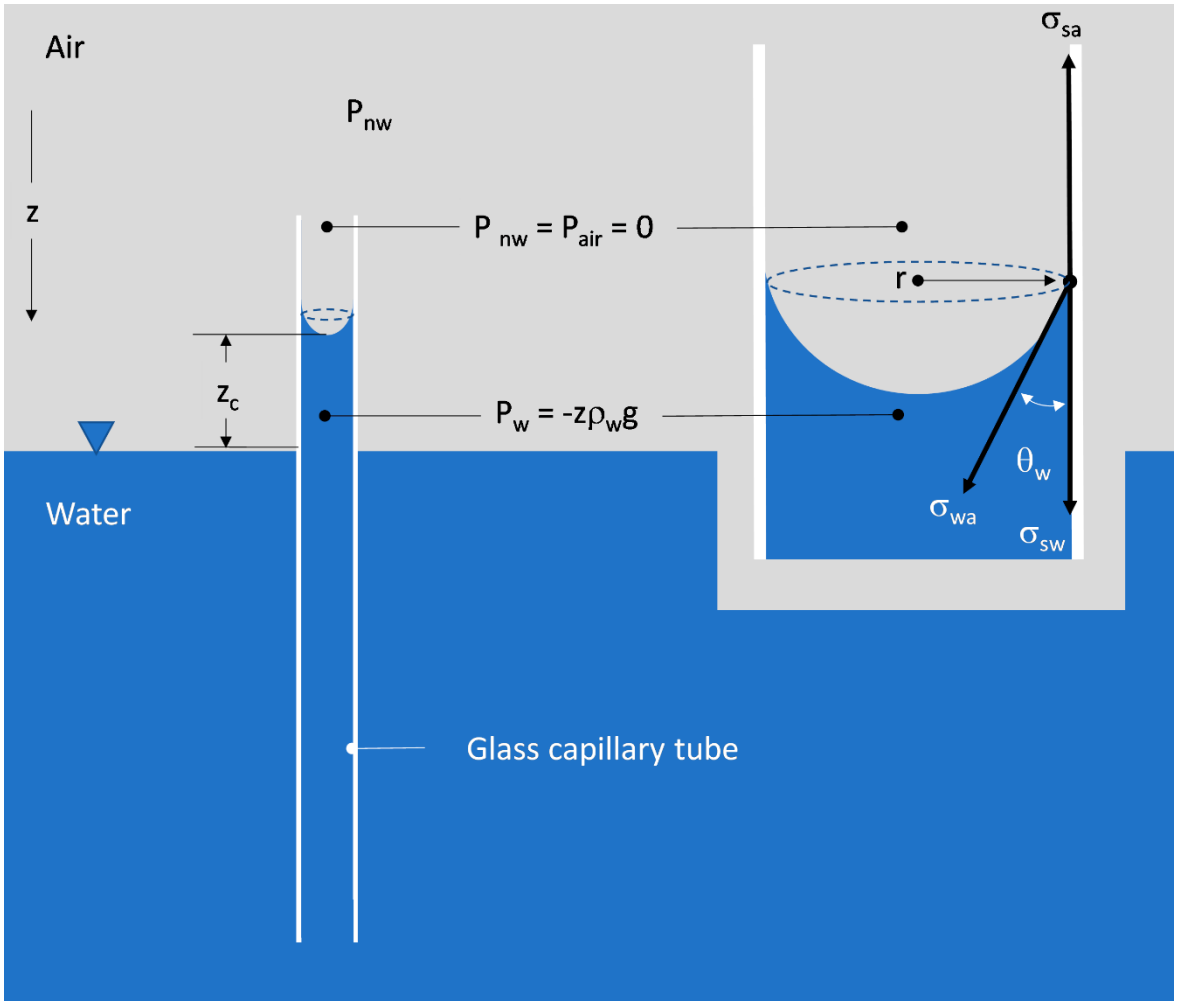

Figure 29 - Capillary rise in a capillary tube (small glass tube) inserted into water. An enlarged image of the water surface in the capillary tube is shown as the inset. The parameters and their relationships are described in Equations (41) through (44).

First, the interfacial forces acting along the perimeter of the water-air meniscus are summed as shown in Equation (41).

$$\sigma_{sw} - \sigma_{sa} - \sigma_{wa}\, cos(\theta_w) = 0 \text{ rearranging, } \sigma_{sw} - \sigma_{sa} = \sigma_{wa}\, cos(\theta_w) \qquad (41)$$

where (parameter dimensions are dark green font with mass as M, length as L, time as T):

θ_w = wetting angle between the air-water and water-solid interfaces (radians)

σ_{sw} = solid-water interfacial tension (MLT^{-2})

σ_{sa} = solid-air surface tension (MLT^{-2})

σ_{wa} = water-air surface tension (MLT^{-2})

Second, the total upward interfacial force, F_i, is obtained by multiplying the circumference of the wetted perimeter of the tube by the net upward force of Equation (41), as shown in Equation (42).

$$F_i = 2\pi r\, \sigma_{wa}\, cos(\theta_w) \qquad (42)$$

where (parameter dimensions are dark green font with mass as M, length as L, time as T):

F_i = the net upward force (MLT^{-2})

Third, the balancing force associated with capillary forces, F_c, is the product of the area of the air–water interface and the capillary pressure as shown in Equation (43).

$$F_c = P_c Area = P_c \pi r^2 = (P_{nw} - P_w)\pi r^2 = (0 - (-z_c \rho_w g)\pi r^2 = z_c \rho_w g \pi r^2 \quad (43)$$

where (parameter dimensions are dark green font with mass as M, length as L, time as T):

F_c = the balancing force associated with capillary forces (MLT^{-2})

ρ_w = water density (ML^{-3})

z_c = height of capillary rise (L)

Finally, equating F_c and F_i, $[P_c \pi r^2 = 2\pi r \sigma_{wa} \cos(\theta_w)]$ yields Equation (44).

$P_c = \frac{2\sigma_{wa}\cos(\theta_w)}{r}$ and dividing both sides by $\rho_w g$, knowing that $z_c = \frac{P_c}{\rho_w g}$ yields

$$z_c = \frac{2\sigma_{wa}\cos(\theta_w)}{r\rho_w g} \quad (44)$$

Following the outlined steps, the solution for capillary rise between two parallel plates (analogous to a fracture) is shown in Equation (45).

$$P_c = \frac{2\sigma_{wa}\cos(\theta_w)}{b``} \text{ or dividing both sides by } \rho_w g \; z_c = \frac{2\sigma_{wa}\cos(\theta_w)}{b``\rho_w g} \quad (45)$$

where (parameter dimensions are dark green font with mass as M, length as L, time as T):

$b``$ = the distance between two plates: analogous to the aperture size of a fracture (L)

Equations (44) and (45) tell us that capillary pressure and the height of capillary rise are inversely proportional to the radius of the capillary tube or the distance between two plates. Notably, capillary pressure can be expressed as pressure or as fluid height (pressure head) for a specific fluid density.

Extrapolating the solution to porous media, z_c (the height of the fully saturated capillary fringe) in sand is commonly a few centimeters, whereas z_c in clay can be 10 m or more (McWhorter & Nelson, 1980). Furthermore, low-*k* zones in the vadose zone can be fully saturated with water, while adjacent transmissive zones are unsaturated. This variable saturation can be a complicating factor for advection and diffusion of CoCs in gases in the vadose zone.

The height of capillary rise in a tube, or the height of the capillary fringe in porous media, provides a basis for introducing the concept of a threshold nonwetting phase pressure for invasion of a nonwetting phase into media fully saturated by a wetting phase. This pressure is referred to as displacement pressure (P_d). Mathematically, the necessary P_c for a nonwetting phase to invade a porous media that is saturated with wetting fluid is

$P_c > P_d$. Given $P_d = P_c$ at the top of the water column in the capillary shown in Figure 29, the air displacement pressure for water in the capillary tube is as shown in Equation (46).

$$P_d = P_c = -z_c g \rho_w = \frac{2\sigma_{wa}\, cos(\theta_w)}{r} \tag{46}$$

A key implication of this equation is that the nonwetting phase liquids (e.g., NAPL in a two-phase system) selectively invade larger pores or fractures (transmissive zones) but are precluded from smaller pores or fractures in low-*k* zones. Exclusion of nonwetting phase NAPLs commonly leads to sparse dendritic distributions of DNAPL in water-saturated media, as shown in Figure 30. Vertically oriented zones of continuous DNAPL are referred to as "*fingers*" and laterally extensive DNAPL bodies perched on low-*k* zones are referred to as pools. Illustrations of occurrences of multiple fluid phases in granular porous media are presented in Figure 31, Figure 32, and Figure 33. Each of these figures is accompanied by a video link in which the phenomenon is better displayed because the transient conditions are revealed.

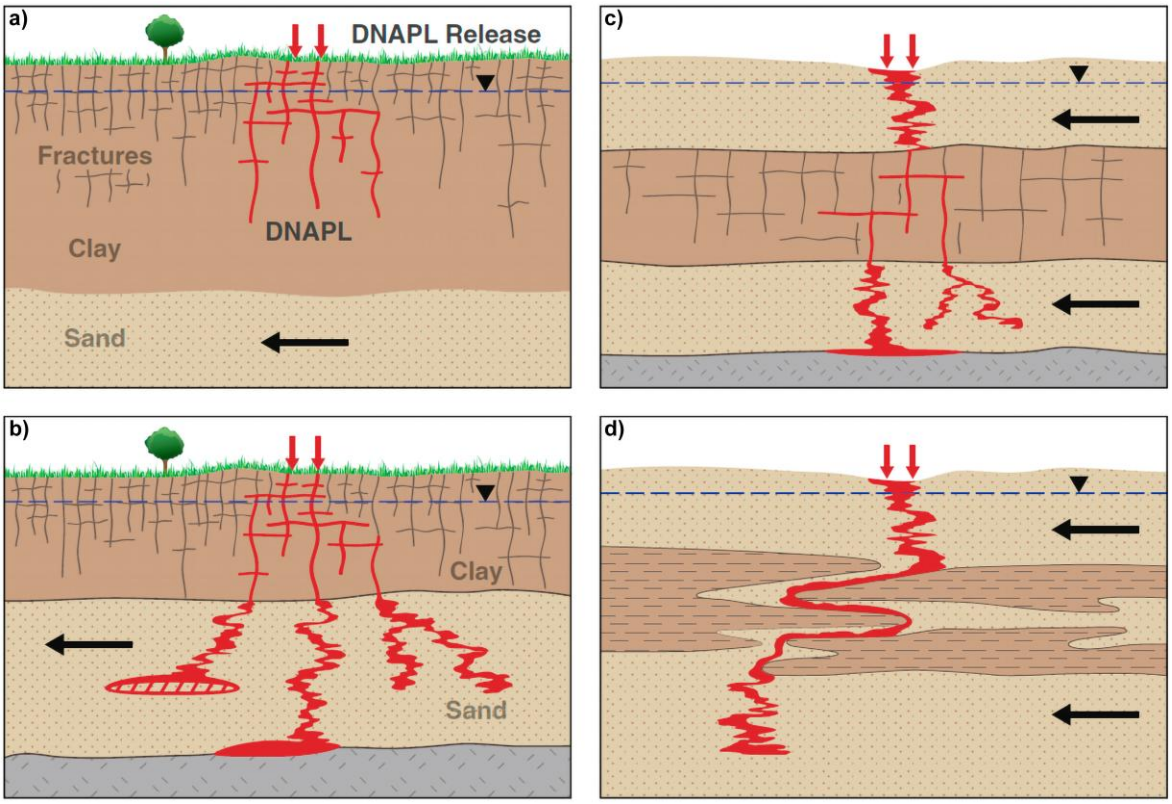

Figure 30 - DNAPL architecture in systems of transmissive (tan) and low-*k* (brown) zones shortly after a DNAPL release:
a) fine-grained, fractured media near the surface with fractures terminating within the fined-grained layer;
b) fine-grained, fractured media near the surface with fractures fully penetrating fractures extending to a coarse-grained layer overlying bedrock;
c) coarse-grained material near the surface underlain by fine-grained material with fully penetrating fractures extending to another coarse-grained layer overlying bedrock; and
d) coarse-grained material near the surface underlain by interfingered fine- and coarse-grained material overlying more coarse-grained material
(after Feenstra et al., 1996).

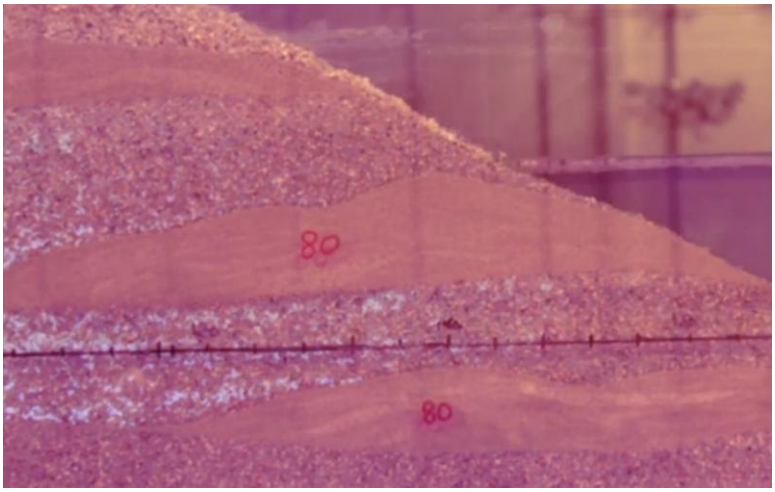

Figure 31 - Multiphase Flow in Heterogeneous Porous Media: an animated version of this is shown in this video.

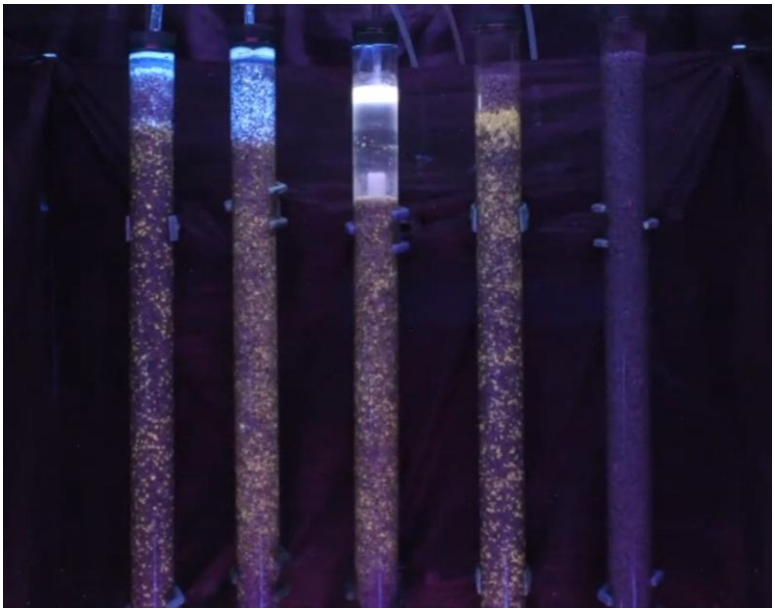

Figure 32 - Ebullition Driven LNAPL Stripping: an animated version of this is shown in this video.

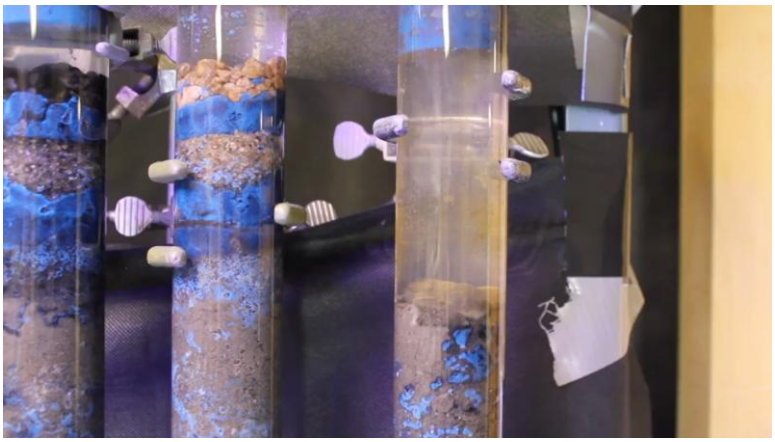

Figure 33 - Ebullition Bubbles: an animated version of this is shown in this video.

Given a continuous fluid phase (i) under static conditions, fluid pressures are a function of vertical position, z, as shown in Equation (47).

$$P_i(z) = \rho_i g z \tag{47}$$

Many readers will have experienced pressure as a function of depth by swimming to the bottom of a pool of water. Figure 34 depicts a two-phase porous media-water system with water as the wetting phase and gas as the nonwetting phase. Starting with Figure 34a, at the water table the pressure in the water (wetting phase) (P_w) is equal to the nonwetting atmospheric soil gas pressure (P_{nw}). By definition, gas pressure in the vadose zone is zero-gauge pressure because it is equal to atmospheric pressure and the gauge measures pressures relative to the ambient atmospheric pressure. Moving below the water table, P_w increases linearly at a slope of $\rho_w g$ with depth. Moving above the water table, where water is present as a continuous wetting phase under negative pressure, P_w decreases (i.e., becomes more negative) linearly at a slope of $\rho_w g$ with height above the water table.

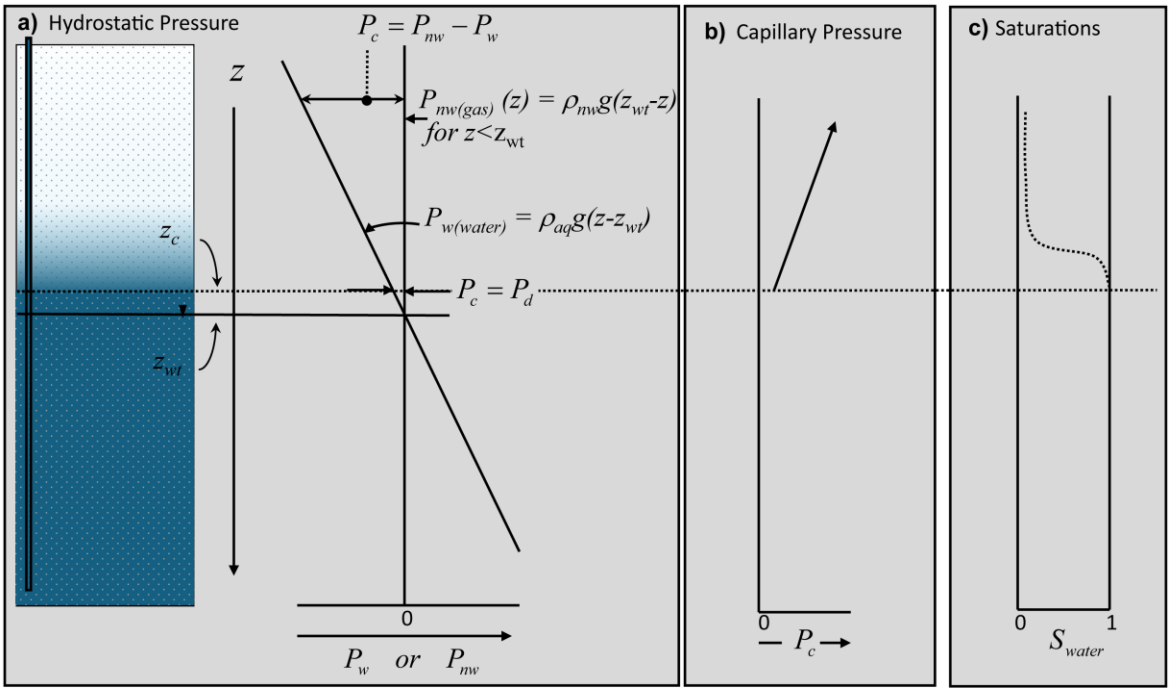

Figure 34 - Pressure in water and gas as a function of depth (z increases in the downward direction) with corresponding capillary pressures and water saturations (assuming uniform porous media).

Figure 34b shows that for $P_c > P_d$ or equivalently, for $z < z_{cap\_fringe}$, capillary pressure as a function of depth is shown in Equation (48) and for $P_c > P_d$ or equivalently, $z < z_{cap\_fringe}$.

$$P_c(z) = P_{nw}(z) - P_w(z) = \rho_{nw} g z - \rho_w g z = \Delta\rho g z \tag{48}$$

$$P_c(z) = \rho_w g(z_{cap\_fringe} - z) \tag{49}$$

A schematic illustration of both wetting and nonwetting phases within a porous media pore are shown in Figure 35. Increasing capillary pressure is like blowing up a balloon in a water-filled box with a drain on top. Greater capillary pressure displaces water, reducing wetting phase saturation and, correspondingly, increasing nonwetting phase saturations. The relationship between capillary pressure and fluid saturations is dependent on the morphology of the porous media. Key factors include the shape of porous media particles, the degree of sorting, and the size of the pores.

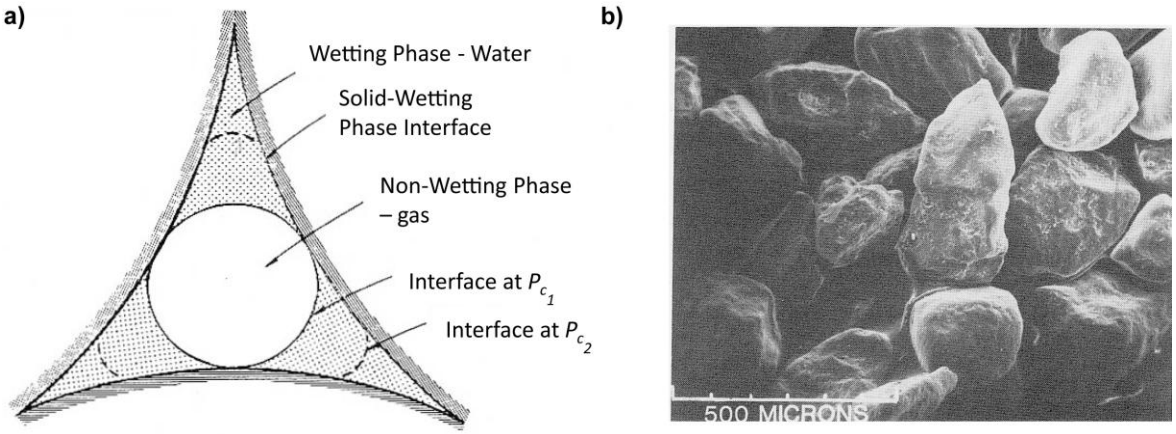

Figure 35 - a) Saturation of an idealized pore as a function of capillary pressure with $P_{c_2} > P_{c_1}$ (after Corey,1994). b) Scanning electron microscope photograph of granular porous media from Wilson and others (1990).

3.2.2 Capillary Pressure Curves

Data describing two-phase fluid saturations as a function of capillary pressure are referred to as capillary pressure curves. Figure 36 presents a conceptual capillary pressure curve where the following occur with each item listed here associated with the number in Figure 36.

1) Starting with a media fully saturated with a wetting fluid (water), capillary pressure is increased without significant drainage up to a capillary pressure equal to P_d.
2) At $P_c > P_d$ pores begin to drain (be filled with air) as P_c increases, following the drainage curve.
3) With further increases in P_c, the drainage slows and asymptotically approaches an irreducible wetting phase termed residual saturation (S_r).
4) Moving to imbibition (i.e., uptake of water), reduction of P_c leads to rewetting of the media by the wetting fluid on a new curve.
5) Ultimately, at S_m the nonwetting phases become a discontinuous set of discrete ganglia and blobs that cannot be displaced (Wilson et al., 1990). The nonwetting blob in Figure 28 is an example of a discrete blob.
6) When drainage begins again, a different drainage curve forms starting at the P_c associated with the S_m and following a different path with a roughly similar shape and offset from the first drainage curve. Given cyclic drainage and imbibition, a series of *scanning loops* form between the *drainage* and imbibition curves, wherein fluid

saturations depend on the history of drainage and imbibition. One set of such loops are labeled as scanning curves in Figure 36.

The hysteretic nature of drainage and imbibition complicates rigorous quantitative analyses of multiple-phase fluid distributions and flow. Rigorous analysis of P_c as a function of fluid saturations requires a historical knowledge of wetting and drying cycles leading to the label *hysteretic*. Similarly, as introduced in Section 3.3, storage and release of CoC to and from low-*k* zones is a hysteretic process.

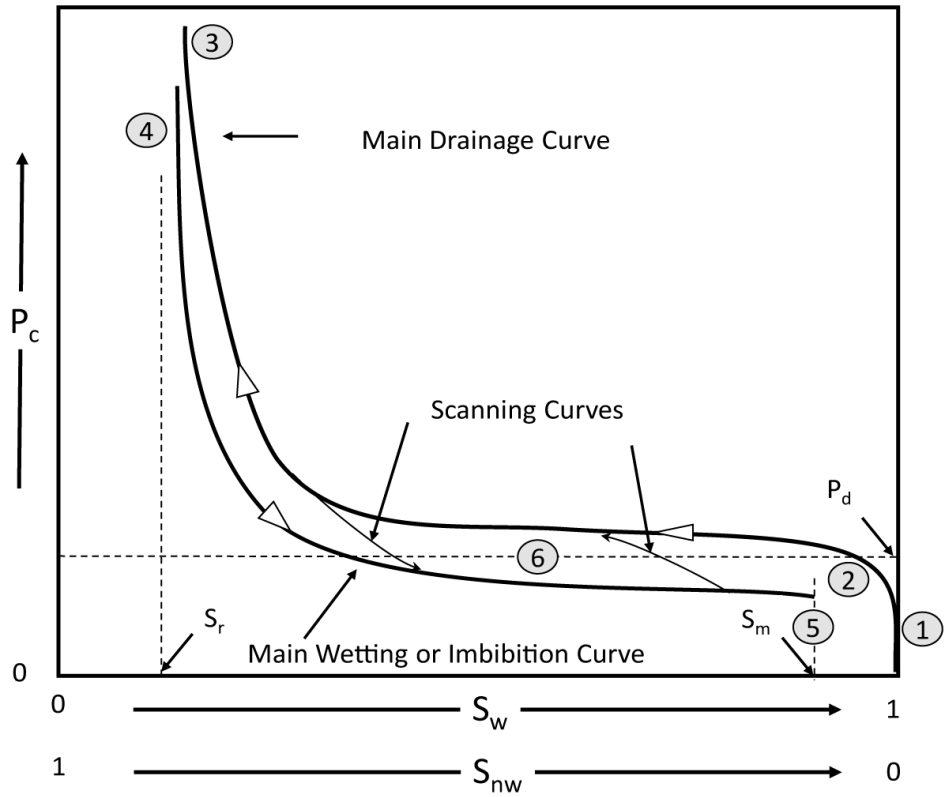

Figure 36 - Capillary pressure curves illustrating hysteresis with drainage and imbibition. The items numbered one through six are described in the text. (after Corey, 1994).

Brooks and Corey (1964) present an empirical (curve-fitting) model for effective wetting phase saturation (S_e) as a function of P_c, as shown in Equation (50).

$$S_e(P_c) = \left(\frac{P_d}{P_c}\right)^{\lambda} \tag{50}$$

where (parameter dimensions are dark green font with mass as M, length as L, time as T):

P_d = displacement pressure ($ML^{-1}T^{-2}$)

λ = fitting parameter (dimensionless)

S_e = Effective saturation (dimensionless)

P_d is displacement pressure and λ is a fitting parameter, and S_e for the main drainage curve is defined as in Equation (51).

$$S_e = \frac{S_w - S_r}{1 - S_r} \tag{51}$$

S_e for the main wetting curve is defined as in Equation (52).

$$S_e = \frac{S_w - S_r}{S_m - S_r} \tag{52}$$

The effective saturation term normalizes the wetting phase saturations to the effective range of wetting phase saturation such that effective saturations range from 0 to 1 for the main wetting, main drainage, and scanning curves. For the main drainage curve, substituting Equation (51) into Equation (50) yields Equation (53).

$$S_{wd}(P_c) = \left(\frac{P_d}{P_c}\right)^{\lambda} (1 - S_r) + S_r \tag{53}$$

For the main drainage and scanning curves, substituting Equation (52) into Equation (50) yields Equation (54).

$$S_{wi}(P_c) = \left(\frac{P_d}{P_c}\right)^{\lambda} (S_m - S_r) + S_r \tag{54}$$

Example calculations using the Brooks-Corey equation are provided in calculation vignette shown in Figure 37. Published in 1964, the Brooks and Corey equation has proven to be exceedingly useful, being widely applied in petroleum reservoir engineering, agronomic soil-water engineering, geotechnical engineering, and subsurface remediation.

Calculation Vignette
Brooks-Corey Equations

Inputs

$$\rho_w = 1.0\frac{kg}{L} \qquad S_r = 0.1 \qquad S_m = 0.95 \qquad \lambda_d = 2 \qquad \lambda_i = 3$$

$$P_d = 10\ cm\ g\ \rho_w = 981\ Pa \qquad P_c = P_d\ 1000\ Pa \ldots 10000\ Pa$$

Drainage Phase Solution

$$S_{wd}(P_c) = \left(\frac{P_d}{P_c}\right)^{\lambda_d} ((1 - S_r) + S_r)$$

Imbibition Phase Solution

$$S_{wi}(P_c) = \left(\frac{P_d}{P_c}\right)^{\lambda_i} ((S_m - S_r) + S_r)$$

Capillary Pressure Curve

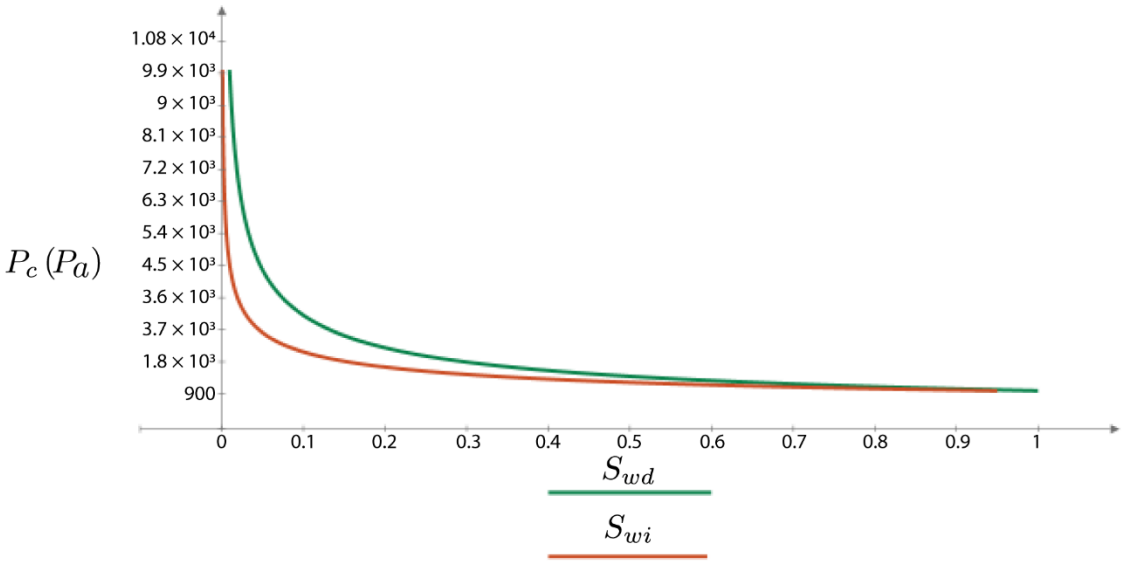

Figure 37 - Calculation vignette for the Brooks-Corey equations.

Another common model for S_e as a function P_e is advanced in van Genuchten (1980), referred to as the van Genuchten equation. Unfortunately, the van Genuchten equation does not consider P_d and correspondingly misses the important principle of exclusion of nonwetting fluids (e.g., NAPLs and gases) from media when $P_c < P_d$. Notably, both Brooks and Corey and van Genuchten equations are empirical models that are fit to data by modifying empirical model parameters. Neither equation is predicated directly on physics.

3.2.3 Steady-State Flow of Immiscible Fluids

Three key assumptions for steady-state flow of immiscible fluids are (Corey, 1994):

1. Darcy's equation is valid for the fluid phase of interest,

2. the fluids are immiscible with $P_c = P_{nw} - P_w$, and
3. all fluids can be treated as incompressible.

Darcy's equation for the volumetric flux ($L^3L^{-2}T^{-1}$) of fluid j is presented in Equation (55).

$$q_j = -\frac{kk_{r_j}\rho_j g}{\mu_j}\nabla h_j \text{ or } q_j = -\frac{kk_{r_j}\rho_j g}{\mu_j}\left(\frac{d}{dx}h_j + \frac{d}{dy}h_j + \frac{d}{dz}h_j\right) \text{ and } h_j = \frac{P_j}{\rho_j g} + z_j \qquad (55)$$

where (parameter dimensions are dark green font with mass as M, length as L, time as T):

qj = volumetric flux of fluid j ($L^3L^{-2}T^{-1}$)

P_j = pressure in fluid j ($ML^{-1}T^{-2}$)

∇h_j represents the gradient of h in each of the three coordinate directions

Given that k_{r_j} and P_j are functions of the effective saturation of fluid j, then the flux as a function of saturation is shown in Equation (56).

$$q_j(S_{e_j}) = -\frac{kk_{r_j}(S_{e_j})\rho_j g}{\mu_j}\nabla\left(\frac{P_j(S_{e_j})}{\rho_j g} + z_j\right) \qquad (56)$$

Employing the Brooks-Corey equation for effective saturations for either nonwetting (nw) or wetting (w) phases, per the methods of Burdine (1952), then the permeability of each phase is as shown in Equation (57) where S_{e_j} can be based on solutions for either drainage Equation (51) or imbibition Equation (52).

$$k_{rnw}\left(S_{e_j}\right) = \left(1 - S_{e_j}\right)^2\left(1 - S_{e_j}^{\frac{\lambda+2}{\lambda}}\right) \text{ and } k_{rw}(S_{e_j}) = S_{e_j}^{\frac{2+3\lambda}{\lambda}} \qquad (57)$$

Substituting in the Brooks-Corey equation for effective saturation, $S_{ew}(P_c) = \left(\frac{P_d}{P_c}\right)^{\lambda}$, results in expressions for permeability as shown in Equation (58).

$$k_{rnw}\left(S_e(P_c)\right) = \left(1 - \left(\frac{P_d}{P_c}\right)^{\lambda}\right)^2\left(1 - \left(\frac{P_d}{P_c}\right)^{\lambda+2}\right) \text{ and } k_{rw}(S_e(P_c)) = \left(\frac{P_d}{P_c}\right)^{2+3\lambda} \qquad (58)$$

Example calculations for estimating relative permeabilities as a function of wetting-phase saturations between S_m and S_r are shown in Figure 38. Notably, as more than one fluid is present, relative permeabilities are always less than 1. When wetting fluid saturations are 0.6, relative permeability values for wetting and non-wetting phases approach 0.1 indicating the capacity of the media to conduct wetting and non-wetting fluids is reduced by an order of magnitude. Decreasing wetting and nonwetting saturations above or below a wetting phase saturation of 0.6 reduces relative permeabilities by multiple orders of magnitude.

Calculation Vignette
Relative Permeability

Inputs

$$S_r = 0.1 \qquad S_m = 0.95 \qquad \lambda = 3 \qquad S_w = S_r, S_r + 0.01 \ldots S_m \qquad \rho_w = 1\frac{kg}{L}$$

Relative Permeability to the Wetting Phase

$$k_{rw}(S_w) = \left(1 - \left(\frac{S_w - S_r}{1 - S_r}\right)\right)^2 \left(1 - \left(\frac{S_w - S_r}{1 - S_r}\right)^{\frac{\lambda+2}{\lambda}}\right)$$

Relative Permeability to the Non-Wetting Phase

$$k_{rnw}(S_w) = \left(\frac{S_w - S_r}{S_m - S_r}\right)^{\frac{2+3\cdot\lambda}{\lambda}}$$

Wetting and Non Wetting Phase Relative Relative Permeabilities

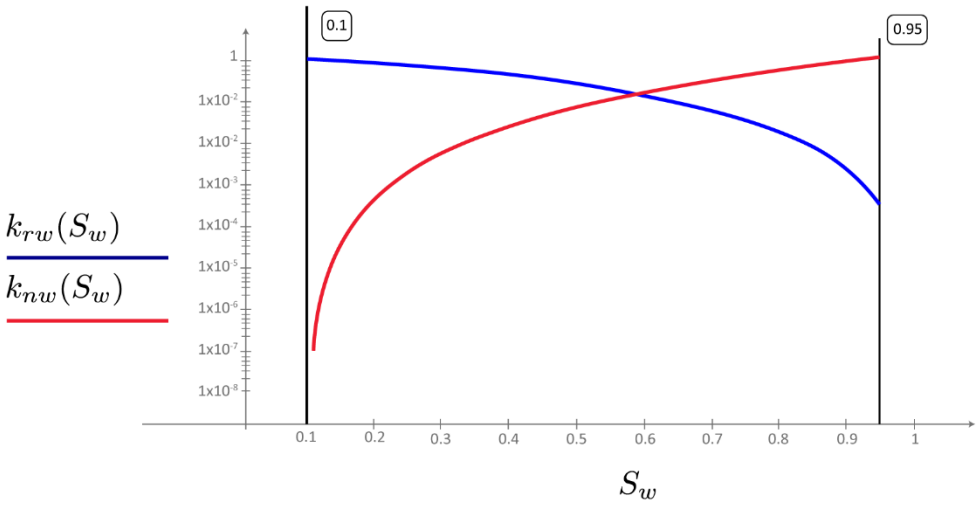

Figure 38 - Calculation vignette presenting estimates of relative permeabilities of wetting and nonwetting phases as a function of wetting-phase saturations.

Moving to a field-scale example problem, calculations shown in Figure 39 use the concepts advanced in this section to explore the significance of heterogeneity for a two-layer system. Calculations applying the Brooks-Corey equation for effective wetting-phase fluid saturations and relative permeabilities are presented. The calculations show that 1) heterogeneity matters and 2) sharp jumps in effective wetting-phase fluid saturations and relative permeability occur at the contact between the fine and coarse sand layers. Ubiquitous natural heterogeneities in natural porous media lead to complex distributions of fluid saturations and relative permeability in natural settings.

Calculation Vignette
Occurrences of Water and Air in Two Layers of Sand

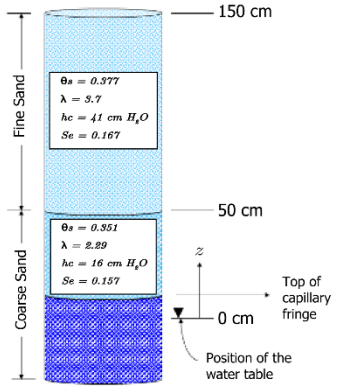

Inputs

$$pw = 1 \ \frac{kg}{L}$$

$\phi_{\text{fine}} = 0.377$ $S_{r_{\text{fine}}} = 0.167$

$\lambda_{\text{fine}} = 3.7$ $h_{\text{dfine}} = 41 \ cm$

$z_{\text{fine}} = 50 \ cm, 50.2 \ cm \ldots 150 \ cm$

$\phi_{\text{coarse}} = 0.351$ $S_{r_{\text{coarse}}} = 0.157$

$\lambda_{\text{coarse}} = 2.29$ $h_{d_{\text{coarse}}} = 16 \ cm$

$z_{\text{coarse}} = 16 \ cm, 16.2 \ cm \ldots 50 \ cm$

$S_{\text{cap}}(z) = 1$ $kcap_{rw}(z) = 1$

$z_{\text{cap}} = 0.1 \ cm, 1 \ cm \ldots 16 \ cm$

Calculations

$$S_e(h_d, h_c, \lambda) = \left(\frac{h_d}{h_c}\right)^{\lambda} \quad h_c(z) = \frac{\rho_w \ g \ z}{\rho_w \ g} \quad k_{rw}(h_d, h_c, \lambda) = S_e(h_d, h_c, \lambda)^{\frac{2+3\lambda}{\lambda}}$$

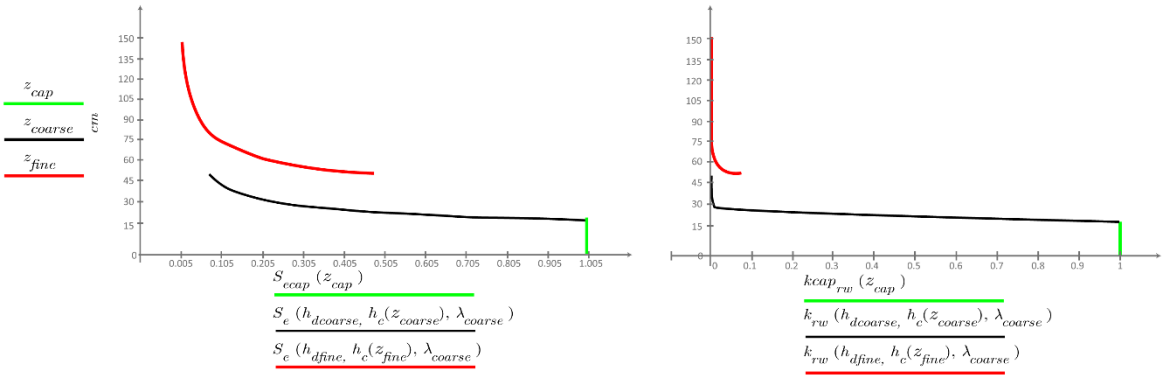

Figure 39 - Calculation vignette exploring the occurrence of water and air in two layers of sand above a water table with the fine sand overlying the coarse sand.

Moving to the common problem of petroleum liquids released to soil and groundwater, Figure 40 presents a laboratory photo of LNAPL in a well and in an adjacent sand impacted by an LNAPL release.

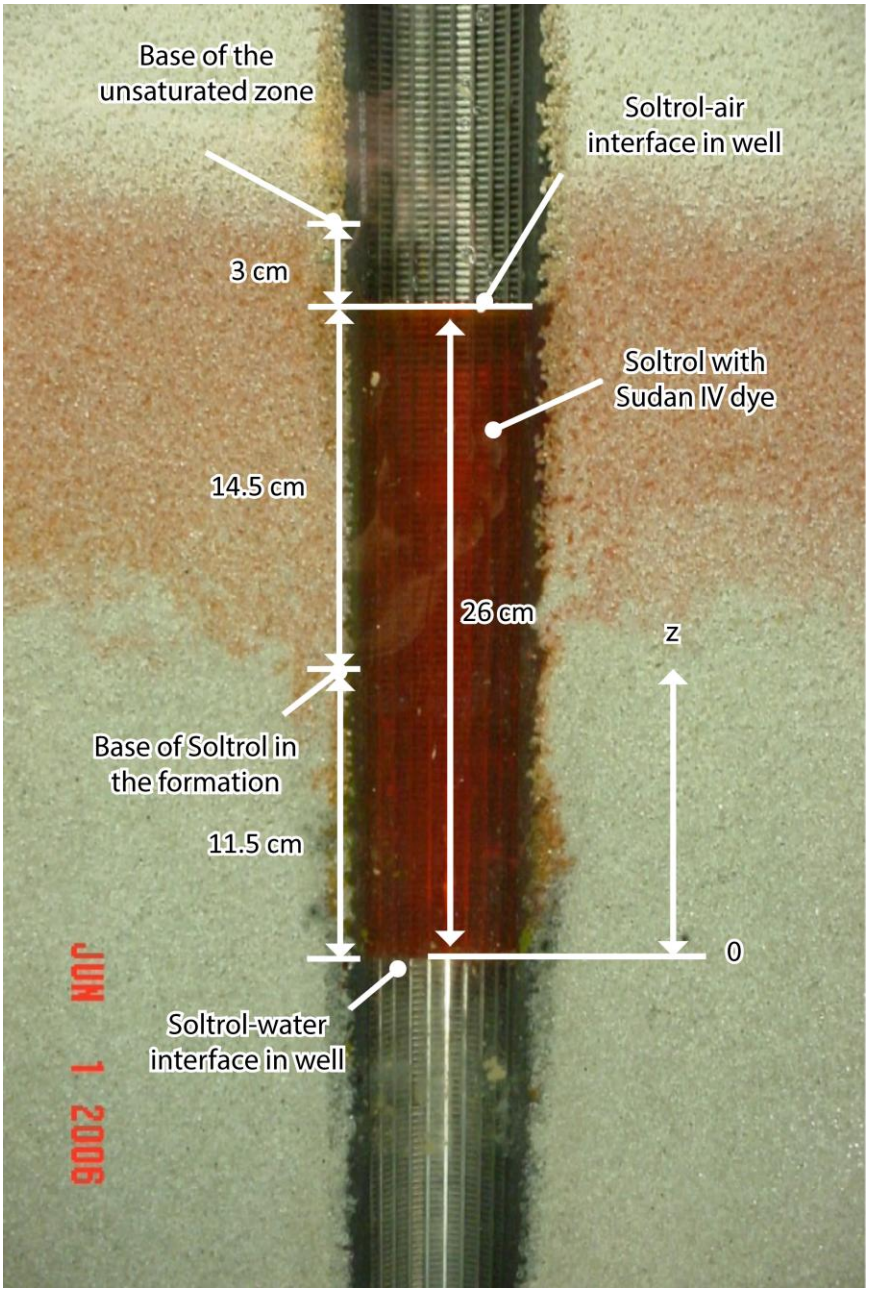

Figure 40 - Cross section of a 5-cm OD wire-wrap well screen in a uniform water wet sand with Soltrol (a laboratory grade LNAPL) in the formation that has entered the well. Soltrol density is 0.75 gm/cm^3, water density is 1 gm/cm^3, Brooks-Corey parameter λ is 2.2 and S_r for water is 0.1.

Building on Farr and others (1990) $P_{water} = P_{LNAPL}$ at the water–LNAPL interface in the well. With increased vertical position z above the water–LNAPL interface in the well, the difference in pressure between LNAPL in the well and water in the formation (i.e., capillary pressure) is as shown in Equation (59). At the LNAPL–air interface in the well, $P_{LNAPL} = P_{air} = 0$. With increasing z above the LNAPL–air interface in the well, the difference in pressure between air and LNAPL in the formation (i.e., capillary pressure is as shown in Equation (60).

$$P_{c_{LNAPL-Water}} = z(\rho_{water} - \rho_{LNAPL})g = z\Delta\rho g \text{ for z} \geq 0 \quad (59)$$

$$P_{c_{air-LNAPL}} = z(\rho_{LNAPL} - \rho_{air})g \approx z\rho_{LNAPL}g \text{ for } z \geq 26 \text{ cm} \quad (60)$$

Employing equations (59) and (60), the setup for a calculation vignette related to LNAPL transmissivity is shown in Figure 41. The calculations shown in the solution vignette of Figure 42 explores fluid pressure, capillary pressure, and relative permeability as a function of vertical position. Using the results shown in Figure 42, the bulk capacity of the continuous LNAPL body to conduct LNAPL (*LNAPL transmissivity*) is estimated. LNAPL transmissivity is a common metric used to resolve the feasibility of hydraulic recovery of LNAPL (Sale et al., 2018).

Calculation Vignette
LNAPL Transmissivity

Inputs

$$\rho_w = 1\frac{kg}{L}, \quad \mu_{\text{water}} = \frac{1}{100} \text{ poise}, \quad \rho_{\text{LNAPL}} = 0.75\frac{kg}{L}, \quad \mu_{\text{LNAPL}} = \frac{5}{100} \text{ poise}, \quad K_{\text{sand}} = 10^{-3}\frac{cm}{sec}$$

$$z_{\text{water}} = 0\ cm, 0.1\ cm \ldots 50\ cm, \quad z_{\text{LNAPL}} = 11.5\ cm, 11.6\ cm \ldots 50\ cm, \quad z_{\text{air}} = 29\ cm, 29.1\ cm \ldots 50\ cm$$

$$\lambda = 2.2 \qquad S_r = 0.1$$

Setup Calculations

$$\rho_{z0} = \rho_{\text{LNAPL}}\ \ g\ \ 26\ cm = (1.91 \times 10^3)\ Pa \qquad P_{\text{air}}(z) = 0\ Pa \qquad P_{\text{LNAPL}}(z) = -z\ \ \rho_{\text{LNAPL}}\ \ g + \rho_0$$

$$P_{\text{water}}(z) = \rho_w\ \ g\ \ -z + \rho_0 \qquad P_{c_{\text{LNAPL, water}}}(z) = P_{\text{LNAPL}}(z) - P_{\text{water}}(z)$$

$$Pd_{\text{LNAPL, water}} = 11.5\ \ cm\ \ (\rho_{\text{w}} - \rho_{\text{LNAPL}})\ \ g = 281.94\ Pa \qquad P_{c_{\text{air, LNAPL}}}(z) = P_{\text{air}}(z) - P_{\text{LNAPL}}(z)$$

$$Pd_{air,LNAPL}(z) = 3\ \ cm\ \ \rho_{\text{LNAPL}}\ \ g = 220.65\ Pa$$

$$S_e(P_c, Pd) = \left(\frac{Pd}{P_c}\right)^{\lambda} \qquad S(P_c, Pd) = S_e(P_c, Pd)\ \ (1 - S_r) + S_r$$

$$k_{\text{T LNAPL}}(P_c, Pd) = \left(1 - \left(\frac{Pd}{P_c}\right)^{\lambda}\right)^2 \left\{1 - \left(\left(\frac{Pd}{P_c}\right)^{\lambda}\right)^{\frac{2+\lambda}{\lambda}}\right\} \qquad k_{\text{r water}}(P_c, Pd) = \left(\frac{Pd}{P_c}\right)^{\frac{2+3\ \lambda}{\lambda}}$$

Figure 41 - Calculation vignette showing the setup for LNAPL transmissivity calculations of Figure 42.

Solution - Fluid Pressure vs. Depth (z)

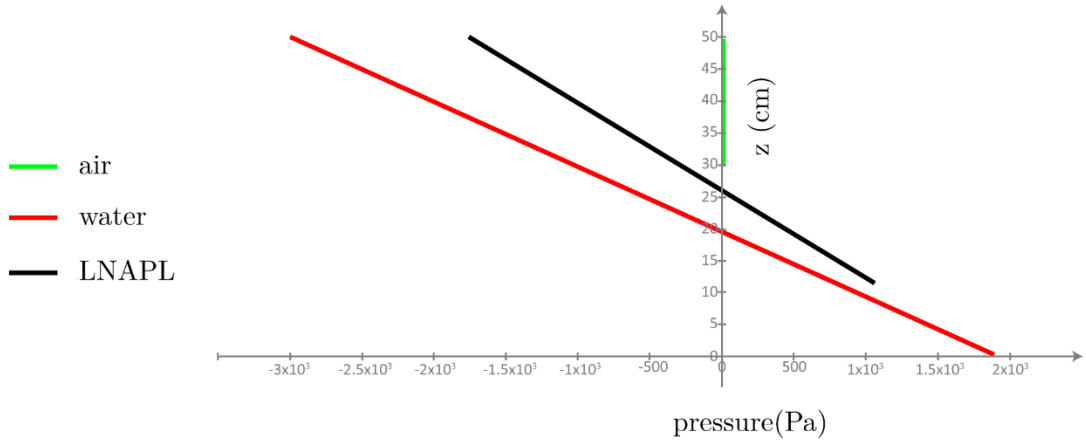

Solution - Capillary Pressure (Pc) vs. Depth

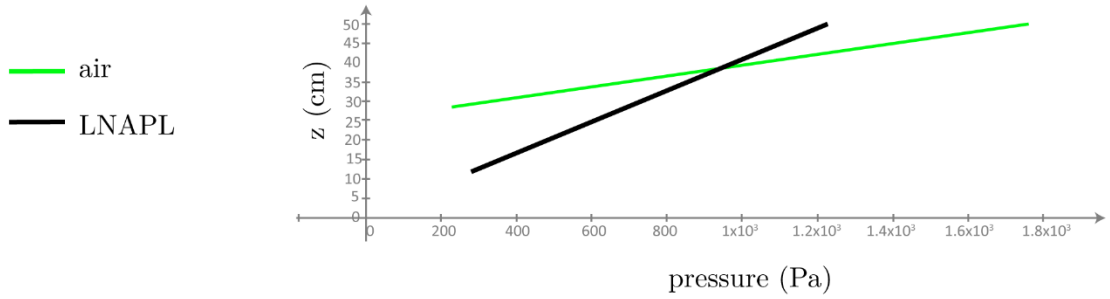

Solution - Relative Permeability (kr) to LNAPL and Water vs. Depth (z)

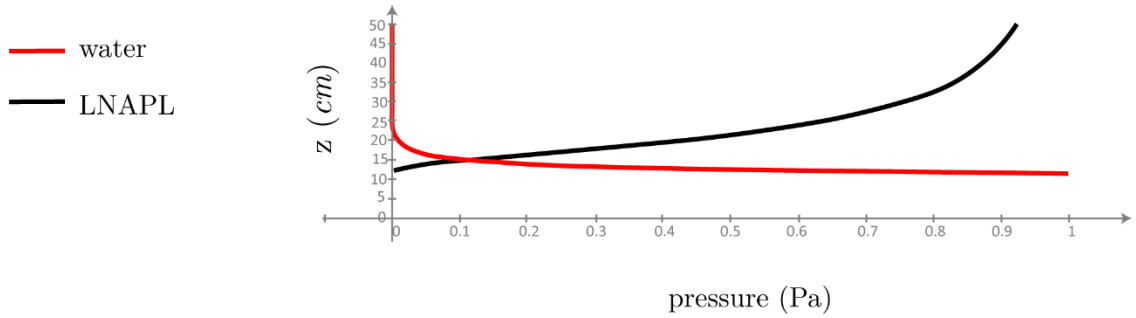

Figure 42 - Calculation vignette continued from the setup shown in Figure 41, showing the solutions for fluid pressures, capillary pressure, and relative permeability to LNAPL and to water as a function of depth.

Table 2 - Calculation vignette continued from the setup shown in Figure 41, showing the solutions integrated LNAPL properties based on the calculation vignettes shown in Figure 41 and Figure 42.

Mean relative to LNAPL	$kr_{LNAPLmean} = \frac{\int_{11.5\text{ cm}}^{29\text{ cm}} k_{rLNAPL}\,(Pc_{LNAPL\_water}(z), Pd_{LNAPL\_water})dz}{29.5\text{ cm} - 11.5\text{ cm}} = 0.4$
Mean LNAPL K	$K_{LNAPLmean} = kr_{LNAPLmean}\,K_{sand}\,\frac{\mu_{water}}{\mu_{LNAPL}} = 8x10^{-5}\frac{\text{cm}}{\text{s}}$
Mean Transmissivity to LNAPL	$T_{LNAPL} = K_{LNAPLmean}\,(29.5\text{ cm} - 11.5\text{ cm}) = 0.012\frac{\text{m}^2}{\text{day}}$

Returning to the differential form of Darcy's equation (Equation (55)), flow of immiscible fluids is driven by head gradients wherein head is a function of capillary pressures, fluid pressure, and vertical position. Given the definition of capillary pressure $P_c = P_{nw} - P_w$, expressions for P_w and P_{nw} are shown in Equations (61) and (62).

$$P_w = P_{nw} - P_c \tag{61}$$

$$P_{nw} = P_c + P_w \tag{62}$$

Substituting Equation (61) and Equation (62) into Equation (56) yields expressions for flux of each phase as a function of saturation as shown in Equations (63) and (64).

$$q_w(S_e) = -\frac{kk_{r_w}(S_e)\rho_w g}{\mu_w}\nabla\left(\frac{(P_{nw} - P_c)}{\rho_w g} + z_w\right) \tag{63}$$

$$q_{nw}(S_e) = -\frac{kk_{r_{nw}}(S_e)\rho_{nw} g}{\mu_{nw}}\nabla\left(\frac{(P_w - P_c)}{\rho_{nw} g} + z_{nw}\right) \tag{64}$$

An application of Equations (63) and (64) is using waterfloods to drive recovery of crude oil and/or natural gas from production wells in petroleum reservoirs. Applying the principles of waterflooding to remediation, Figure 43 illustrates recovery of creosote-based DNAPL from a braided-stream-channel-deposit aquifer using a waterflood and horizontal drains. This is described in detail by Sale and Applegate (1997). Site-wide application of the waterflood produced 1.8 million gallons (≈ 6800 cubic meters) of a high viscosity DNAPL. Initial testing through full-scale application of the creosote waterflood cost US$15M in the mid-1990s. The design and implementation was based on conceptual understandings of flow of immiscible fluids in porous media and the observational method advanced by Peck (1969). As described in Section 1, this method involves thoughtfully assembled *site conceptual models,* anticipating a range of plausible alternatives, monitoring to evaluate actual outcomes, developing contingencies for consequential alternatives, and implementing contingencies as needed. Derivation of an analytical solution for waterflood DNAPL recovery is presented in Box 2↴. We encourage readers to work through the derivation to gain practice and further insight into the principles presented in this section.

Initial condition of creosote based DNAPL perched above a fine-grained bedrock capillary barrier with horizontal drains in the overlying alluvium.

Pumping the lower drain leads to truncation of the DNAPL flow path by the water with a viscosity 1/54 th that of the DNAPL.

Pumping the upper drain leads to mounding of DNAPL below the upper drain and increased formation transmissivity to DNAPL due the increased DNAPL saturations and thickness of the DNAPL flow path

Recovery of high viscosity DNAPL is optimized by concurrently pumping water (upper drain) and DNAPL (lower drain), with recharge of produced water via parallel drain, to optimize the formation capacity to conduct DNAPL and pressures driving flow.

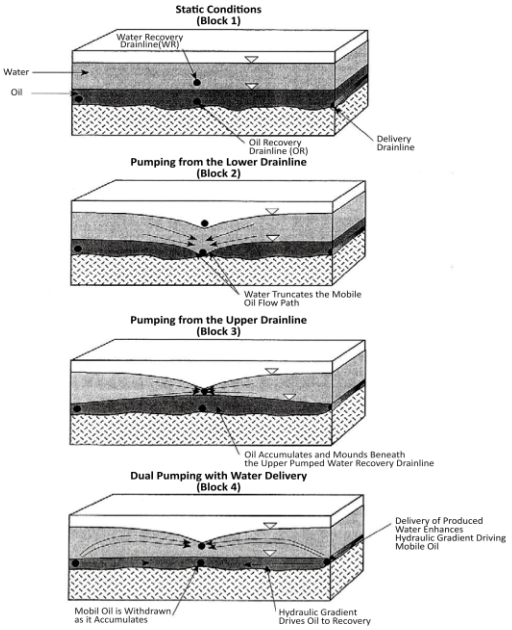

Figure 43 - Dual drain waterflood DNAPL recovery (adapted from Sale & Applegate, 1997)

Supporting illustrations of NAPL transport in systems with multiple fluid phases are presented in Figure 44, Figure 45, and Figure 46.

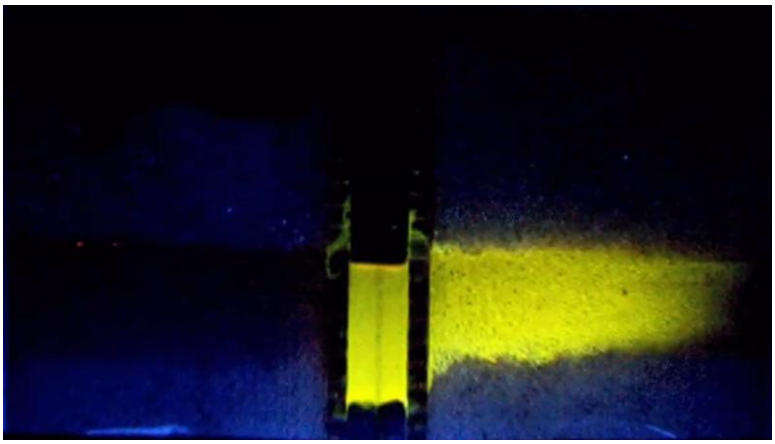

Figure 44 - Fluorescing Tracer in LNAPL: an animated version of this is shown in this video.

Figure 45 - Downward Migration of DNAPL: an animated version of this is shown in this video.

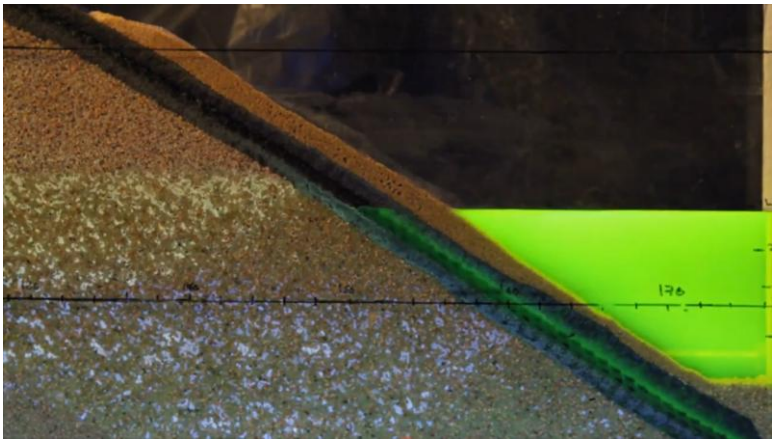

Figure 46 - Oleophilic Bio-Barrier Sand Tanks Study: an animated version of this is shown in this video.

3.2.4 Exercises Related to Section 3.2

Having studied Section 3.2, the reader should be able to complete the following exercises: Exercise 12, Exercise 13, Exercise 14, Exercise 15, Exercise 16, Exercise 17, and Exercise 18.

3.3 Diffusion

Diffusion is a fundamental transport process resulting from kinetic energy (i.e., motion that increases with increasing temperature) of small particles (e.g., atoms or molecules) in fluids with net movement in response to local concentration gradients. A conceptual illustration of diffusion is shown in Figure 47. With respect to contaminant transport in subsurface media, diffusion leads to storage and release of contaminants to and from low-*k* zones in aquifers (Figure 1). Historically, diffusion in water-saturated media was dismissed by many as inconsequential for CoCs in groundwater because it generally occurs over small distances (e.g., centimeters to meters). While aqueous phase diffusion occurs over short distances, it also acts over vast interfacial areas between

transmissive and low-*k* zones and, as such, can be of great consequence. At the conclusion of this section the reader should be able to complete Exercises 19 through 28 of Section 7.

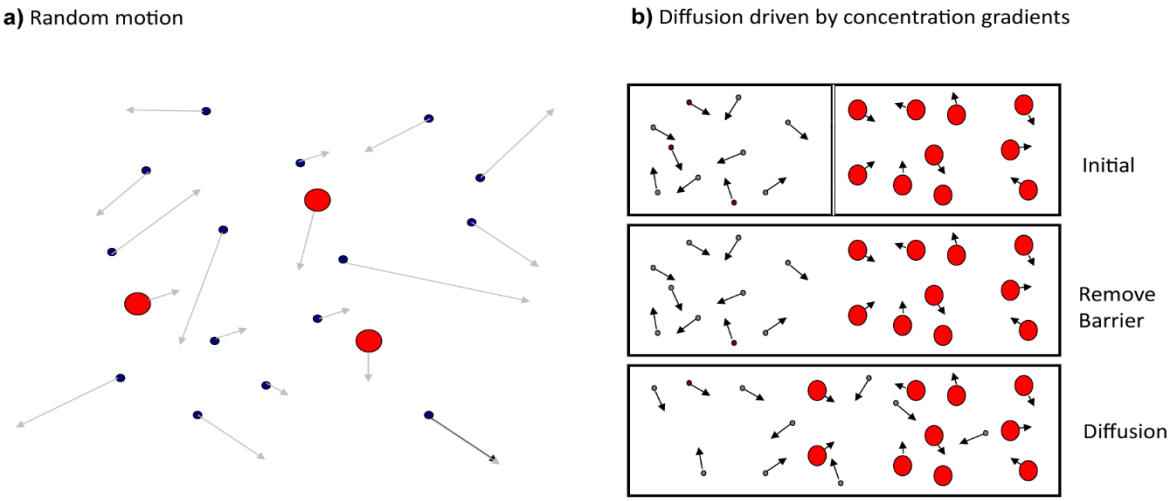

Figure 47 - a) Random motion of small particles in a fluid due to temperature-related motion with the lower-mass atoms moving faster. b) Diffusion driven by a gradient of concentration until eventually the concentration becomes uniform throughout the domain.

The role of diffusion in contaminant transport has received historical and evolving attention in journal articles from Foster (1975) to You and others (2020). Other introductions to diffusion can be found in Pankow and Cherry (1996), Sale and others (2013), as well as McWhorter (2021).

A primary factor driving recognition of diffusion in groundwater-centered contaminant transport has been the persistence of contaminants in groundwater plumes after removal of upgradient source zones. Plume persistence is attributed to releases of contaminants stored in low-*k* zones (Figure 1). Building on McWhorter (1996), we provide a brief introduction to the mechanics of diffusion and an idealized problem involving aqueous phase storage and release of contaminants in a low-*k* zone. The idealized problem advances a conceptual understanding of diffusion in water-saturated heterogeneous media and builds a foundation for further developments in Section 5.

3.3.1 Mechanics of Diffusion

An early account of diffusion is provided by Brown (1827), a Scottish botanist who closely studied the behavior of pollen grains suspended in water. As described by Clark (1971), Brown observed that the particles moved in a continuous, erratic, and seemingly random pattern under a microscope. After repeated observations, he concluded that the motion was not caused by water currents or evaporation. This phenomenon later became known as Brownian motion.

More rigorously, in 1905, Albert Einstein, at age 26, published *On the Motion of Small Particles Suspended in a Stationary Liquid According to the Molecular Kinetic Theory of Heat*. In this work, Einstein proposed that the irregular movement of suspended particles results

from collisions with the invisible, rapidly moving molecules of the liquid—an idea rooted in kinetic theory (Einstein, 1905; Clark, 1971). At the time, the existence of atoms and molecules in solution was still debated, and Einstein's theoretical explanation of diffusion played a significant role in advancing molecular theory and ultimately contributed to his receipt of the 1921 Nobel Prize.

Given a fluid (gas or liquid) composed of multiple molecules, all molecules on average have the same mean kinetic energy. A binary system with only particles A and B, for which particles A and B have different masses, can be described by Equation (65).

$$\frac{1}{2}m_A\bar{v}_A^2 = \frac{1}{2}m_B\bar{v}_B^2 \text{ and correspondingly } \bar{v}_A = \bar{v}_B\sqrt{\frac{M_B}{M_A}} \text{ and } \bar{v}_B = \bar{v}_A\sqrt{\frac{M_A}{M_B}} \quad (65)$$

where (parameter dimensions are dark green font with mass as M, length as L, time as T):

m_A = the mass of the particles (M) of A

m_B = the mass of the particles (M) of B

$\bar{v}_A$ = the mean velocity (LT^{-1}) of particles A

$\bar{v}_B$ = the mean velocity (LT^{-1}) of particles B

Kinetic energy velocities are greatest for particles with the smallest mass and smaller for particles with larger masses.

Following Fick (1855), estimates of diffusive flux ($ML^{-2}T^{-1}$) of compound i across a plane normal to a concentration gradient, in a uniform fluid j, can be obtained using Fick's First Equation, as shown in Equation (66).

$$J_{i,j} = -D_{m_{i,j}}\frac{d\rho_{i,j}}{dl} \quad (66)$$

where (parameter dimensions are dark green font with mass as M, length as L, time as T):

$J_{i,j}$ = diffusive flux of compound i in fluid j ($ML^{-2}T^{-1}$)

$D_{m_{i,j}}$ = molecular diffusion coefficient (L^2T^{-1}) for compound i in fluid j in a free solution at a specific temperature

Given diffusion in a porous media, (a) the true diffusion path becomes longer than the point-to-point distance that would be traversed in an open body of fluid j (i.e., a free solution) due to tortuosity of the pore openings, and (b) solids limit the available cross-sectional area through which transport occurs. Following Shackelford (1991), an effective diffusion coefficient for compound i in fluid j in porous media can be estimated by knowing the fluid saturation of j, the effective porosity, tortuosity, and diffusion coefficient of compound i in a free solution of fluid j as shown in Equation (67).

$$D_{e_{i,j}} = S_j\phi\tau D_{m_{i,j}} \quad (67)$$

where (parameter dimensions are dark green font with mass as M, length as L, time as T):

τ = tortuosity (dimensionless)

Following Millington and Quirk (1961), a first-order estimate of τ in a wetting fluid j is provided by Equation (68).

$$\tau_j = \phi^{1/3} S_j^{7/3} \tag{68}$$

It would be preferable to measure τ of the porous media rather than using Equation (68).

Replacing the free solution molecular diffusion coefficient with the effective diffusion coefficient in Equation (66), per (67) and (68), yields the following solution for diffusive fluxes in porous media—Equation (69).

$$J_{D_{i,j}} = -\phi^{4/3} S_j^{10/3} D_{m_{i,j}} \frac{d\rho_{i,j}}{dx} \tag{69}$$

Given this equation, diffusive fluxes are dependent on porosity, saturation, the molecular diffusion coefficient (where the molecular diffusion coefficient is governed by the mass of molecules, temperature, and density of the fluid) and concentration gradients. Interestingly, per Equation (69), diffusive fluxes are not a function of permeability. Somewhat nonintuitively, Equation (69) shows that diffusive fluxes are larger in high-porosity media (e.g. silts and clays, which are low-*k* zones) as compared to moderate- to low-porosity media (sands and gravels, transmissive zones). As a first-order approximation, transport in transmissive zones is often dominated by advection, and transport in low-*k* zones is often dominated by diffusion.

A governing equation for diffusive transport is obtained by performing a mass balance on a REV. Here we consider diffusion in the aqueous phase. McWhorter (2021) discusses gas phase diffusion. Assuming the fluid of interest is water, with density $\rho_{i,j} = \rho_{aq_i}$ then the net diffusion in and out of the REV is shown in Equation (70).

$$J_{D_{in}} - J_{D_{out}} = \phi R \frac{d\rho_{aq_i}}{dt} \tag{70}$$

where (parameter dimensions are dark green font with mass as M, length as L, time as T):

R = ratio of sorbed plus aqueous mass to aqueous contaminant mass (dimensionless)

Inserting Fick's First (Equation (66)) into Equation (70) yields:

$$\begin{aligned} &\left(- D_{e_{i,aq_x}} \frac{d\rho_{aq_i}}{dx}\bigg|_x - D_{e_{i,aq_y}} \frac{d\rho_{aq_i}}{dy}\bigg|_y - D_{e_{i,aq_z}} \frac{d\rho_{aq_i}}{dz}\bigg|_z \right) \\ &\quad - \left(- D_{e_{i,aq_x}} \frac{d\rho_{aq_i}}{dx}\bigg|_{x+\Delta x} - D_{e_{i,aq_y}} \frac{d\rho_{aq_i}}{dy}\bigg|_{y+\Delta y} - D_{e_{i,aq_z}} \frac{d\rho_{aq_i}}{dz}\bigg|_{z+\Delta z} \right) \\ &\quad = \phi R_i \frac{d\rho_{aq_i}}{dt} \end{aligned} \tag{71}$$

The right-hand side describes the change in mass of compound i in an REV with respect to time. Given R=1, there would be no sorbed CoCs. Given R=2, there would be equal masses of aqueous and sorbed contaminants. An expanded discussion of sorption is provided in Section 4.3. Taking the limits of Equation (71) as Δx, Δy, and Δz go to zero transforms Equation (71) to Equation (72).

$$D_{e_{i,aq_x}} \frac{d^2\rho_{aq_i}}{dx^2} + D_{e_{i,aq_y}} \frac{d^2\rho_{aq_i}}{dy^2} + D_{e_{i,aq_z}} \frac{d^2\rho_{aq_i}}{dz^2} = \phi R_i \frac{d\rho_{aq_i}}{dt} \tag{72}$$

Equation (72) is Fick's Second Equation applied to porous media. Equation (72) has the form of the heat equation. As introduced in Section 2, there are three fundamental PDEs: the Laplace equation (introduced with flow nets), the heat equation (introduced above), and the wave equations (not used in this text). We find it a pleasant surprise that all the complexities of contaminant transport in porous media boil down to two fundamental PDEs and a few ODEs with problem-specific initial and/or boundary conditions. In Equation (72), ρ_{aq_i} is the dependent variable, x, y, z, and t are independent variables, and $D_{e_{i,aq_x}}$, $D_{e_{i,aq_y}}$, $D_{e_{i,j_z}}$, ϕ, and R_i are scalar coefficients. As a matter of simplification, in the following equations, we: 1) consider water (aqueous phase) as the fluid of interest; 2) consider only one fluid and CoC, thus drop notation i and j for compounds and fluids of interest; and 3) assume effective diffusion coefficients are not dependent on direction, thus dropping $x, y\ and\ z$ notation on effective diffusion coefficients.

3.3.2 Storage and Release of Contaminants in a Low-*k* Zone

Figure 48 presents an idealized scenario for a two-layer system where a DNAPL pool is in a transmissive zone perched above a low-permeability layer. It is envisioned that the displacement pressure P_d of the low-k zone is greater than the capillary pressure P_c associated with the overlying DNAPL pool ($[\rho_{DNAPL} - \rho_w]gb_{pool}$). NAPLs perched above, and precluded from low-k zones, is a common condition in DNAPL and LNAPL source zones. Given the concurrent presence of both water (wetting) and DNAPL (non-wetting), relative permeabilities to water in pools are small (i.e., 0.1 or lower). Low relative permeabilities result in low water-seepage velocities through NAPL bodies, leading to concentrations of NAPL constituents at NAPL-water interface near or at effective solubilities (Sale, 1998).

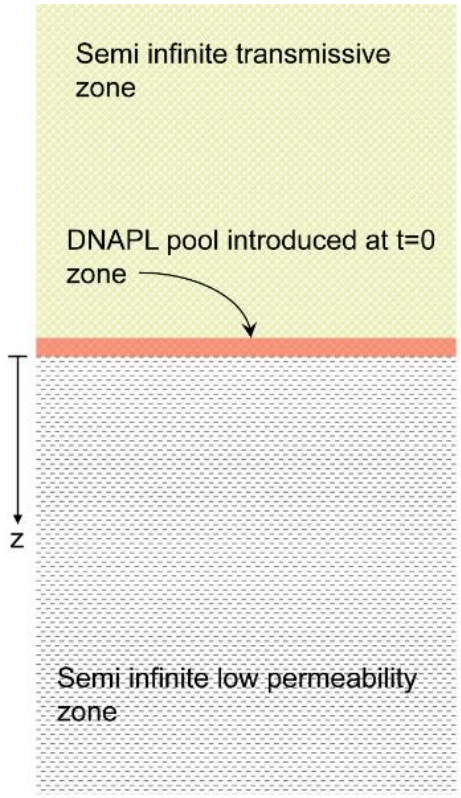

Figure 48 - DNAPL in a transmissive zone perched above a low-permeability layer. DNAPL is precluded from entry into the low-*k* zone by a displacement pressure that is greater than the capillary pressure at the base of the pool.

Assuming an areally extensive pool in the transmissive zone, concentration gradients in the x and y directions are assumed to be zero and Equation (72) simplifies to Equation (73).

$$\alpha \frac{d^2 \rho_{aq}}{dz^2} = \frac{d\rho_{aq}}{dt} \tag{73}$$

In Equation (73), α is defined as shown in Equation (74).

$$\alpha = \frac{D_e}{\phi R_i} \tag{74}$$

As shown in Figure 48, the condition at the boundary between transmissive and low-*k* zones (bottom of the DNAPL pool) is that of aqueous concentrations equal to the effective NAPL solubility of ρ_o for all times greater than time zero ($\rho_{aq}(0,t) = \rho_o$). The initial condition in Figure 48 is an aqueous concentration of zero for all z>0 at time zero ($\rho_{aq}(z,0) = 0$). The solution for Equation (73) given the noted boundary and initial conditions is as shown in Equation (75).

$$\rho_{aq}(z,R,t) = \rho_{o_{aq}} erfc\left(\frac{1}{2}\frac{z}{\sqrt{\frac{D_e}{\phi R}t}}\right) \tag{75}$$

A derivation for (72) is presented in Box 3↴. The complementary error function (erfc) does not have a closed-form solution. Values for erfc can be obtained from iterative numerical integration schemes and/or truncated Taylor Series approximations. An analogous solution for mass transfer from the DNAPL pool into flowing groundwater in the transmissive zone is presented in Section 4.4.2.

An example calculation vignette shown in Figure 49 applies Equation (75) to a scenario of pure trichloroethene (TCE) DNAPL (ρ_o=1,100 mg/L) introduced at $t = 0$ years in a pool perched above a low-*k* zone with ϕ =0.4. Progressing through time, diffusion into the low-*k* zone leads to increasing concentrations of aqueous phase TCE with depth into the low-*k* zone. Results are plotted on a linear scale to illustrate vertical concentrations driving inward diffusion with ρ_o =1,100 mg/L for $t > 0$. Results are also plotted on a log scale over six orders of magnitude ranging from solubility (ρ_o) down to the maximum contaminant level (MCL) of 0.005 mg/L (5 µg/L) for PCE.

Calculation Vignette
Concentration for Diffusion into a Low-k Zone while Source is Active

Inputs

$$\phi = 0.4 \quad S_w = 1 \quad D_m = 7.5 \times 10^{-10}\frac{m^2}{s} \quad \rho_s = 1100\frac{mg}{L} \quad z = 0\ m,\ 0.01\,m \ldots 5\ m$$

Setup Calculations

$$D_e = \phi^{\frac{4}{3}}\ S_w^{\frac{10}{3}}\ D_m = \left(2.21\times10^{-10}\right)\ \frac{m^2}{s} \qquad \rho_{aq}(z,R,t) = \rho_0\ \operatorname{erfc}\left(\frac{1}{2}\ \frac{z}{\sqrt{D_e\ t}}\right)$$

Solutions - Concentration (ρ_{aq}) vs. Depth (z) into a Low k Zone at 0.3, 3, and 30 Years Without Sorption (R = 1)

Linear Scale

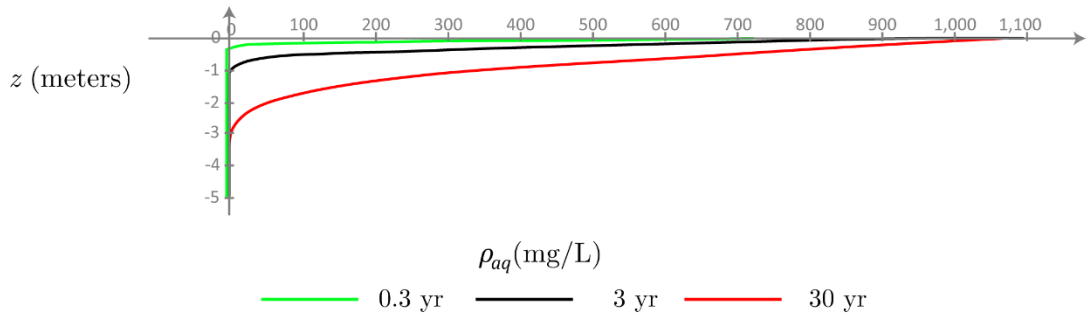

Log Scale

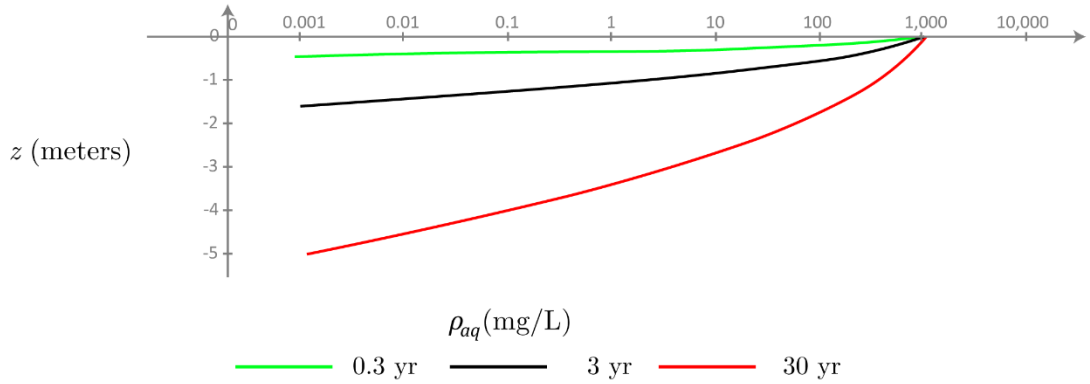

Figure 49 - Calculation vignette showing aqueous concentrations of trichloroethene (TCE) in a low-k zone below a pool of TCE DNAPL introduced at $t = 0$ years. a) linear aqueous phase concentration scale. b) log aqueous phase concentration scale.

The total contaminant concentration, sorbed and aqueous phases, per volume porous media can be obtained by multiplying both sides of Equation (75) by ϕR as shown in Equation (76).

$$\rho_T(z,R,t) = \phi R \rho_{o_{aq}} erfc\left(\frac{z}{\sqrt{4\alpha t}}\right) = \phi R \rho_{o_{aq}} erfc\left(\frac{1}{2}\frac{z}{\sqrt{\frac{D_e}{\phi R}t}}\right) \quad (76)$$

Integrating Equation (76) across the impacted depth provides a basis for estimating total mass of TCE per unit area (ML^{-2}), as in Equation (77).

$$M_{TCE}(R,t) = \int_0^z \rho_{o_{aq}} erfc\left(\frac{1}{2}\frac{A}{\sqrt{\frac{D_e}{\phi R}t}}\right) dA \quad (77)$$

where:

A = variable of integration

Estimates of total mass of TCE per square meter after 30 years based on Equation (77) are obtained using Mathcad™ numerical integration tools and shown as a calculation vignette in Figure 50. Notably, increasing R values (sorption) increases the total mass stored in the low-*k* zones. Increased mass in low-*k* zones with larger R values reflects sorption increasing aqueous concentrations, thus increasing the gradient driving diffusion into the low-*k* zone.

Calculation Vignette
Total Mass Diffusion into a Low-k Zone while Source is Active

Inputs

$$\phi = 0.4 \quad S_w = 1, \quad D_m = 7.5 \times 10^{-10}\frac{m^2}{s} \quad \rho_0 = 1100\frac{mg}{L} \quad z = 0\ m, 0.01\ m \ldots 5\ m$$

Setup Calculations

$$D_e = \phi^{\frac{4}{3}}\ S_w^{\frac{10}{3}}\ D_m = \left(2.21{\times}10^{-10}\right)\ \frac{m^2}{s} \qquad \rho_T(z,R,t) = \phi\ \ R\ \ \rho_0\ \ \operatorname{erfc}\left(\frac{1}{2}\ \ \frac{z}{\sqrt{D_e\ \ t}}\right)$$

$$\phi\ \ R$$

$$M_{TCE}(R,t) = \int_{0{\cdot}m}^{5\ m} \rho_T(z,R,t)\ dz$$

Solutions - Total mass of TCE per volume porous media (ρ_T) vs depth (z) at 30 years for retardation factors of 1,5, and 10.

Linear Scale

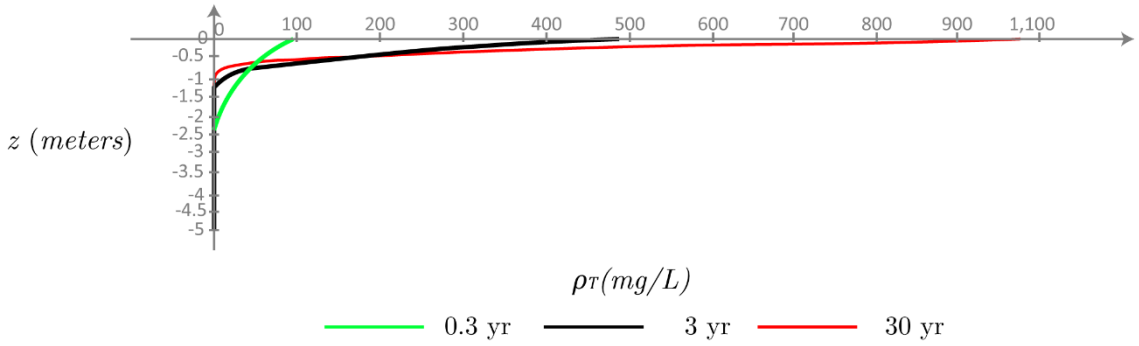

Solutions - Total mass of TCE per unit area of aquifer at 30 years for a range of R values

$$\textbf{For}\ \ R = 1 \qquad M_{TCE}(1, 30\ \text{yr}) = 0.359\frac{kg}{m^2}$$

$$\textbf{For}\ \ R = 5 \qquad M_{TCE}(5, 30\ \text{yr}) = 0.803\frac{kg}{m^2}$$

$$\textbf{For}\ \ R = 10 \qquad M_{TCE}(10, 30\ \text{yr}) = 1.136\frac{kg}{m^2}$$

Figure 50 - Calculation vignette for total mass of TCE per square meter after 30 years based on Equation (77) obtained using Mathcad™ numerical integration tools. Notably, increased R values (sorption) increase the total mass stored in the low-*k* zones because larger R values increases aqueous concentrations, thus increasing the gradient driving diffusion into the low-*k* zone.

With time, NAPL pools are fully depleted via diffusion into low-*k* zones and dissolution into groundwater in the transmissive zone. The topic of NAPL dissolution into groundwater in transmissive zones is addressed in Section 4.5.2. A solution for aqueous concentrations in the low-*k* zone, after depletion of the pool, is obtained by superposing the solution for inward diffusion with the pool present (Equation (75)) and the same solution (Equation (75)) with the opposite (-) sign at time $t`$. Superposition of sources is conceptualized in Figure 51. Since the superposed solutions have identical boundary conditions, and the governing PDEs are linear, the necessary conditions for superposition are met.

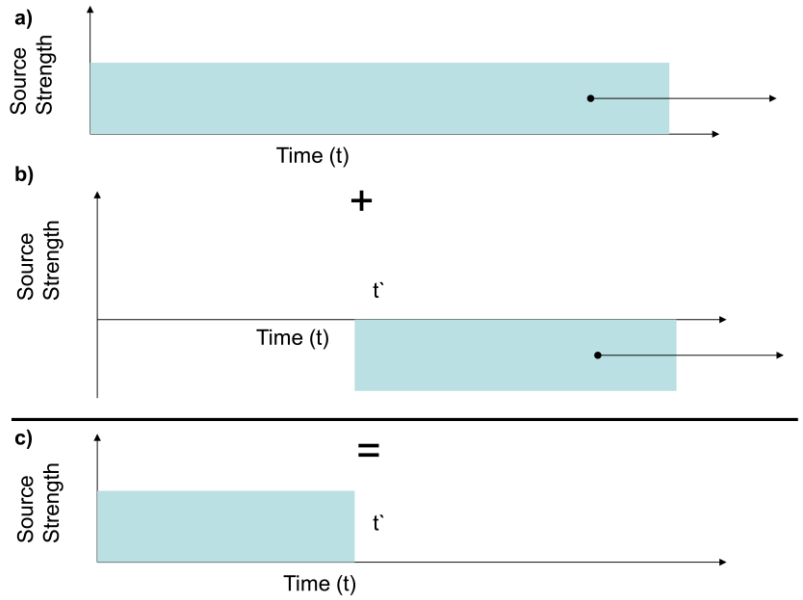

Figure 51 - Superposition of equal and opposite sources at time t` to assess diffusive transport in a low-*k* zone after depletion of the source (pool) at z=0. a) Continuous source. b) Negative source strength delayed to begin at time t'. c) Sum of sources (a) and (b).

Equation (78) shows the solution for aqueous concentration in a low-*k* zone for $t > t`$ via superposition:

$$\rho`_{aq}(z,R,t,t`) = \rho_{o_{aq}} erfc\left(\frac{1}{2}\frac{z}{\sqrt{\frac{D_e}{\phi R}t}}\right) - \rho_{o_{aq}} erfc\left(\frac{1}{2}\frac{z}{\sqrt{\frac{D_e}{\phi R}(t-t`)}}\right)$$
$$= \rho_{o_{aq}}\left(erfc\left(\frac{1}{2}\frac{z}{\sqrt{\frac{D_e}{\phi R}t}}\right) - erfc\left(\frac{1}{2}\frac{z}{\sqrt{\frac{D_e}{\phi R}(t-t`)}}\right)\right) \quad (78)$$

Figure 52 provides a calculation vignette that uses Equation (78) to estimate aqueous concentrations in the low-*k* zone, given a NAPL source present for 30 years, followed by instantaneous removal, with no retardation. Aqueous concentrations are shown at 30.1, 35, and 50 years (i.e., 0.1, 5, and 20 years after source removal). Once the

source is removed, the aqueous phase TCE concentration at $z = 0$ becomes zero and shallow contaminants in the low-*k* zones are driven by diffusion into the overlying transmissive zone. The depth at which contaminants continue to diffuse into the low-k zone evolves from 0.14 to 0.61 to 0.91 m at 30.1, 35, and 50 years, respectively. Critically, below the noted depths and times, contaminants continue to move deeper into the low-*k* zone despite the source having been removed. Storage and release of contaminants in low-*k* zones is a hysteretic process wherein contaminants are released far more slowly than they are stored. Hysteretic storage and release of contaminants to and from low-k zones is addressed in detail in Section 5.

Calculation Vignette
Aqueous Concentrations with Depth after Source Removal

Inputs

$$\phi = 0.4 \quad S_w = 1 \quad D_m = 7.5\times10^{-10}\,\frac{m^2}{s} \quad \rho_0 = 1100\,\frac{mg}{L} \quad z = 0\ m,\ 0.01\,m, \ldots,\ 4\ m \quad R = 1$$

Setup Calculations (τ = time that source is removed)

$$D_e = \phi^{\frac{4}{3}}\ S_w^{\frac{10}{3}}\ D_m = (2.21\times10^{-10})\,\frac{m^2}{s} \quad \rho_{\text{aqpf}}(z,R,t,\tau) = \rho_0\left(\text{erfc}\left(\frac{1}{2}\ \frac{z}{\sqrt{D_e\ \ t\ \ \phi\ \ R}}\right) - \text{erfc}\left(\frac{1}{2}\ \frac{z}{\sqrt{D_e\ \ (\tau - t)\ \ \phi\ \ R}}\right)\right)$$

Solutions - Aqueous Concentrations (ρ_{aq}) **vs. depth** (z) **at 30.1, 40 and 60 Years Given Source Removal at 30 years**

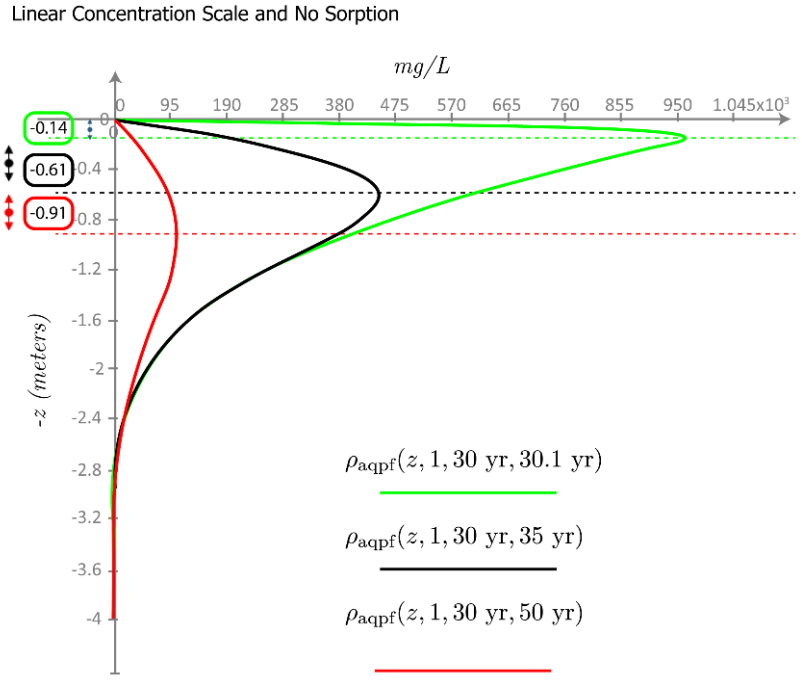

Figure 52 - Calculation vignette for aqueous concentrations of TCE in a low-k zone after removal of a TCE DNAPL pool at 30 years. Once the source is removed, the aqueous phase TCE concentration at z=0 becomes zero and shallow contaminants in the low-k zones are driven by diffusion into the overlying transmissive zone. The horizontal dotted lines show the depth above which contaminants are diffusing upward out of the low-k zone, at 30.1, 35, and 50 years. Below those depths, contaminants continue to diffuse into the low-k zone. Concurrent inward and outward diffusion is a primary factor leading to asymmetrical breakthrough curves with long tails for CoCs in transmissive zones.

Finally, we consider how quickly contaminants are stored in and released from low-*k* zones. More precisely, what is the flux of contaminants at the transmissive low-*k* zone contact through time? This question can be evaluated using Fick's First Equation where the gradient of concentration driving storage or release of contaminants is evaluated at z=0. The mass flux at the contact between layers for $0 < t < t`$ is shown in Equation (79).

$$J_{D_i}(R,t) = -D_e\rho_{o_{aq}}\sqrt{\frac{R\phi}{\pi D_e t}} = -\rho_{o_{aq}}\sqrt{\frac{D_e R\phi}{\pi t}} \quad \text{for} \quad 0 < t < t` \tag{79}$$

The mass flux at the contact between layers for $t > t`$ is shown in Equation (80).

$$J_{D_i}(R,t,t`) = -D_e\rho_{o_{aq}}\left(\sqrt{\frac{R\phi}{\pi D_e t}} - \sqrt{\frac{R\phi}{\pi D_e (t-t`)}}\right) = -\rho_{o_{aq}}\left(\sqrt{\frac{D_e R\phi}{\pi t}} - \sqrt{\frac{D_e R\phi}{\pi (t-t`)}}\right) \tag{80}$$

TCE fluxes into a low-*k* zone for 5 years while a pool persists and TCE fluxes out of a low-*k* zone after the TCE pool is depleted are shown as a calculation vignette in Figure 53. R-values from 1 to 10 are considered. Fluxes decay with time as a function of the inverse of the square root of time. Increased sorption (i.e., larger R-values) increases fluxes into and out of the low-*k* zone.

Calculation Vignette
Flux into and out of a Low-k Zone as a Function of Time

Inputs

$$\phi = 0.4 \quad S_w = 1 \quad D_m = 7.5 \times 10^{-10}\frac{m^2}{s} \quad \rho_0 = 1100\frac{mg}{L} \quad t = 0.01\ yr,\ 0.101\ yr \ldots 10\ yr, \quad \tau = 5\ yr$$

Setup Calculations (τ = time that source is removed)

$$D_e = \phi^{\frac{4}{3}} \quad S_w^{\frac{10}{3}} \quad D_m = \left(2.21\times10^{-10}\right)\ \frac{m^2}{s}$$

$$J_{on}(R,t) = \rho_0 \ \sqrt{\frac{D_e \ \ R \ \ \phi}{\pi \ \ t}} \qquad J_{off}(R,t,\tau) = \rho_0 \ \left(\sqrt{\frac{D_e \ \ R \ \ \phi}{\pi \ \ t}} - \sqrt{\frac{D_e \ \ R \ \ \phi}{\pi \ \ (t-\tau)}}\right)$$

Solutions - Flux Into and Out of a Low-k Zones given source on from 0-5 years for a retardation of 1, 5, and 10

$$XXX(R,t,\tau) := \begin{cases} \text{if } t < \tau \\ \quad XXX - J_{on}(R,t) \\ \text{else if } t > \tau \\ \quad XXX - J_{off}(R,t,\tau) \\ XXX \end{cases}$$

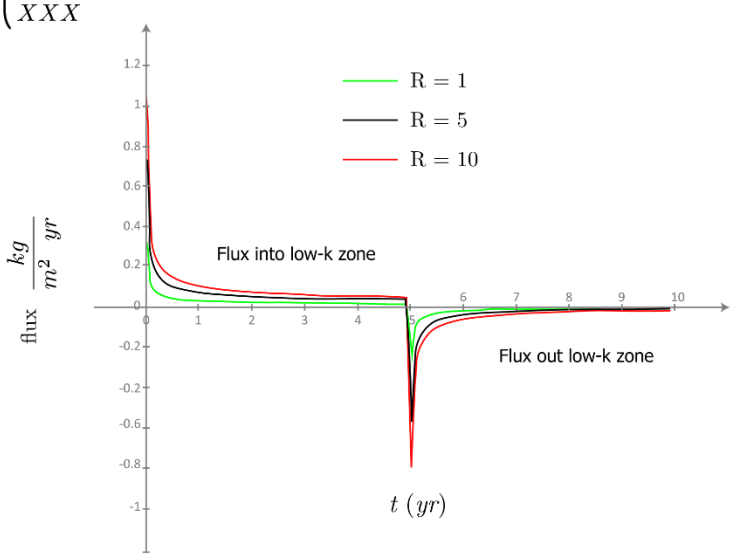

Figure 53 - Calculation vignette for TCE fluxes into a low-*k* zone for 5 years while a DNAPL pool persists on top of a low-*k* layer and TCE fluxes out of the low-*k* zone after the TCE pool is depleted. Calculated using Equations (79) and (80).

3.3.3 Diffusion Examples

Two demonstrative examples are provided. The first example is a laboratory sand tank study conducted by Donor (2008). Figure 54 shows the sand tank (107 cm wide, 84 cm tall, and 2.9-cm deep) at different times. Figure 55 presents a video of the sand tank study including the images shown in Figure 54. The dark layers are bentonite clay (low-*k*) and the light layers are quartz sand (transmissive). The source is fluorescein in tap water, fluorescing green under UV light. Fluorescein was in the influent water from day 1 to 23 and absent from day 24 to 134. Time on the clock in the images reflect days (e.g. 00:00:03:04

= 3.07 days). Inward diffusion into the low-*k* zones is visible when the source is active. Once the source is removed, the transmissive zones flush clear, except for halos around the low-*k* zones. Halos around the low-*k* zones reflect releases from low-*k* zones after the upgradient source was removed.

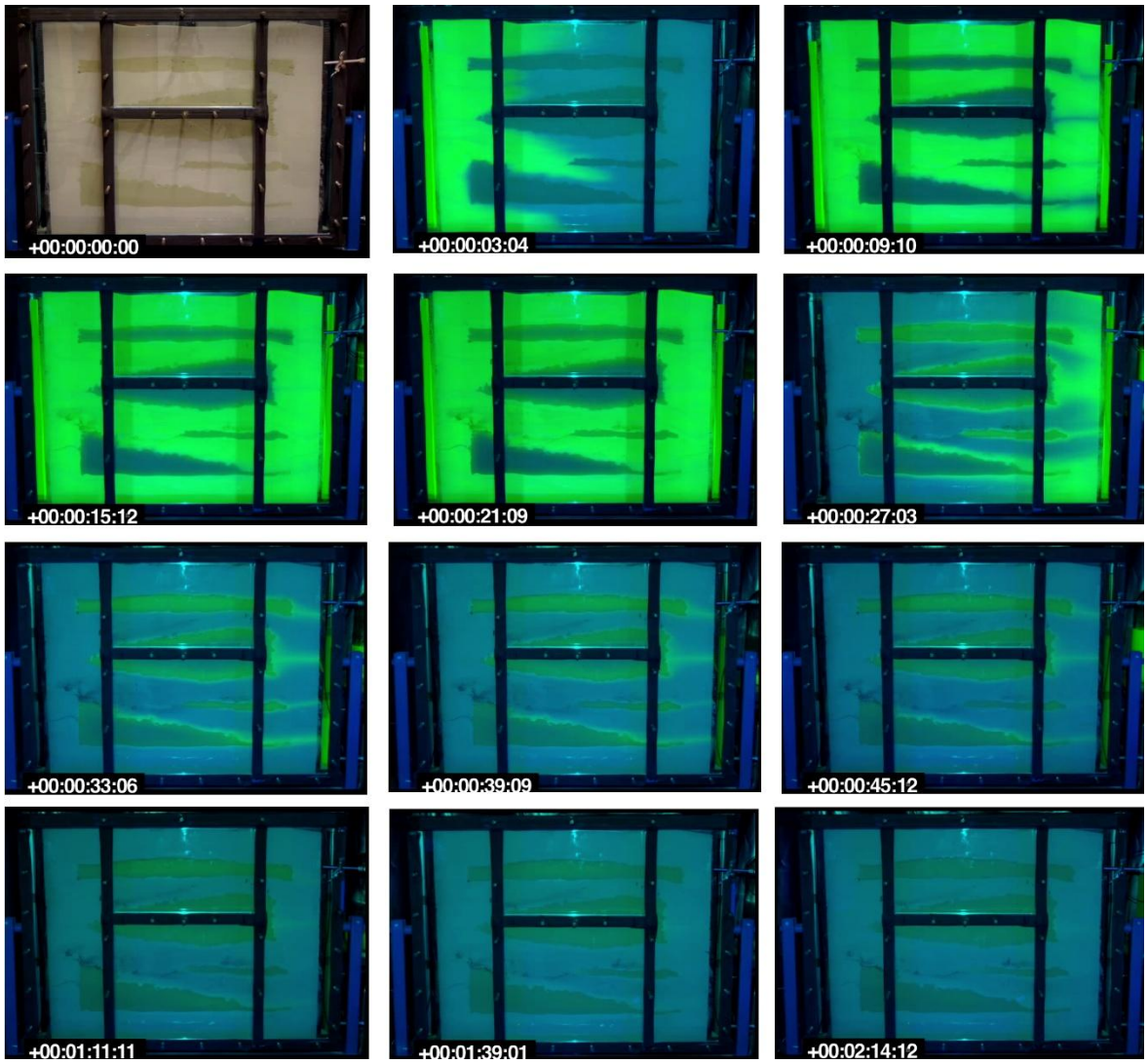

Figure 54 - Results of a sand-tank experiment with low-*k* and transmissive zones. The tank is 107 cm wide, 84 cm tall, and 2.9-cm deep, with dark-tan layers of bentonite clay (low-*k* zones) and light-tan layers of quartz sand (transmissive zones). Time on the clock in the lower left of each image reflect days such that 00:00:03:04 is 3.07 days, and 00:02:14:12 is 134.2 days. The source is introduced at time zero and terminated at 24 days. The transmissive zones are flushed shortly after the source is terminated while contaminants diffuse out of the low-*k* zones long after termination. Notably the interior portions of the low-*k* zones increase in concentration after the source is terminated as diffusion continues into the interior of the low-*k* zones while contaminants diffuse out of their periphery (modified from Doner, 2008).

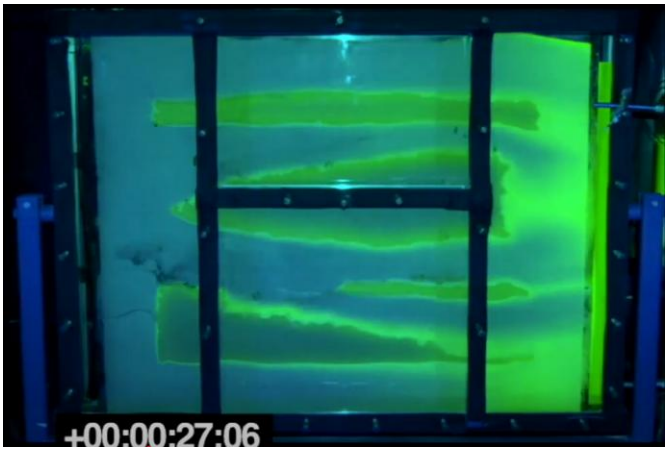

Figure 55 - Back Diffusion: an animated version of the sand tank study portrayed by still frames in Figure 54 is shown in this video.

The second example comes from a US Department of Defense (DOD) munitions depot in the western USA (Sale et al, 2010). Figure 56 presents a plan-view map of 1,3,5 trinitrobenzene (1,3,5-TNB) in plumes 30 years after source ponds were decommissioned. Groundwater flows from north to south in braided stream channel deposits overlying black shale with high natural organic carbon content.

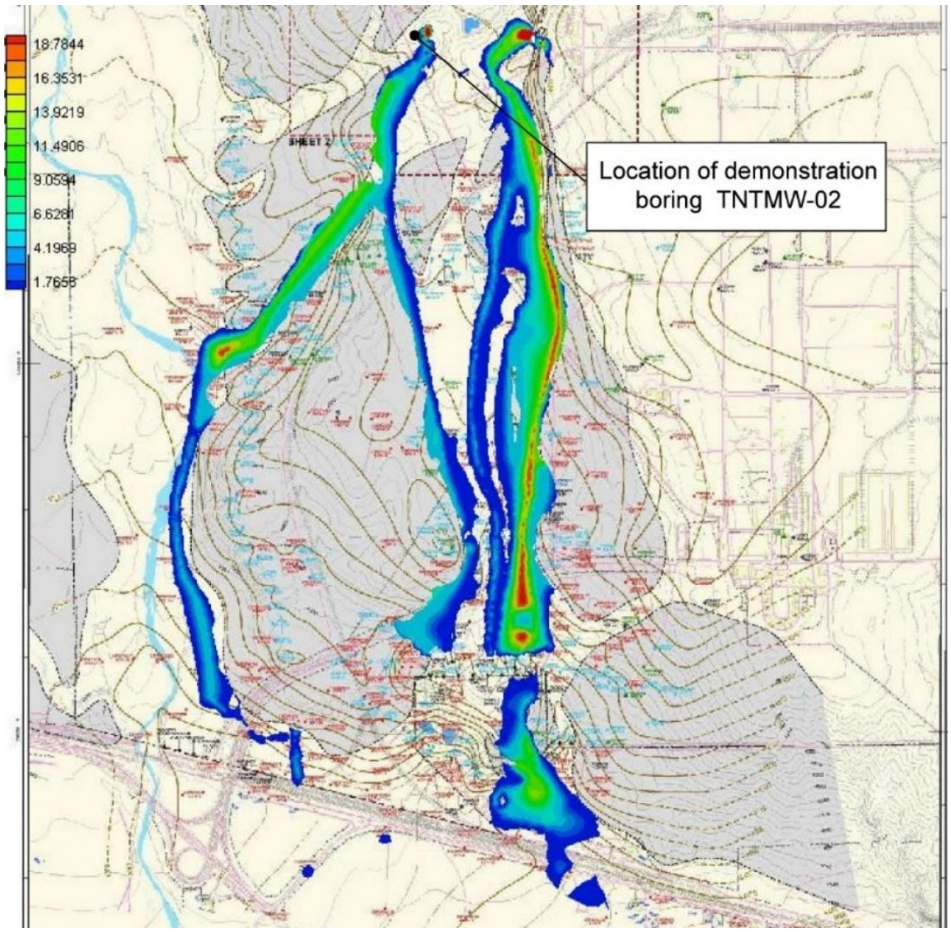

Figure 56 - Plumes emanating from former ponds 30 years after the ponds were used to dispose of wastewater from demilitarization of artillery rounds containing 1,3,5 trinitrobenzene (1,3,5-TNB) and Royal Demolition Explosive (RDX). Concentration scale is in ug/L.

Figure 57 provides vertical profiles of total 1,3,5-TNB and RDX concentrations as a function of depth through the alluvium and into the low-*k* shale. Large concentrations of CoCs in the low-*k* shale and low-*k* zone inclusions in the alluvium are thought be a primary source of the plume shown in Figure 56, nearly 30 years after the upgradient sources (ponds) were removed.

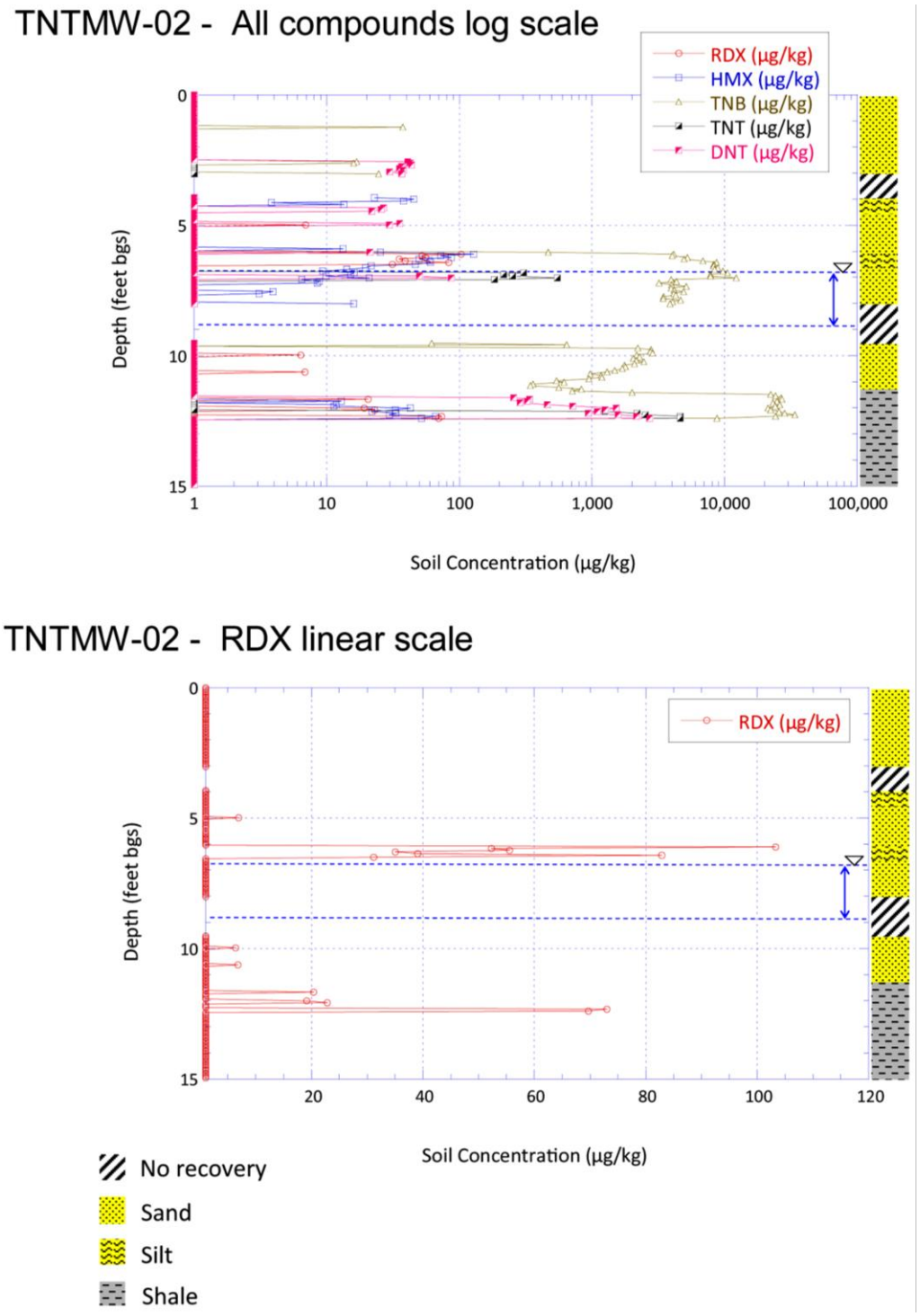

Figure 57 - Concentrations of energetic compounds as a function of depth and type of porous media. Borings located at the demonstration location shown in Figure 56. Maximum concentrations of CoCs are encountered in low-*k* zones.

Figure 57 illustrates an all-too-common situation wherein CoCs stored in low-*k* zones are governing concentrations in transmissive zones. As Allen-King and others (2021) and Shapiro (2019) noted, matrix diffusion can be viewed as either a "blessing or a curse" in groundwater contamination management. A quote from Allen-King and others (2021) follows.

> *"The retention and release of contaminants in flow-limited regions of aquifers can be viewed as either a 'blessing' or a 'curse' in managing groundwater at contamination sites. Diffusion of contaminants into the void space of low-permeability zones delays the arrival and reduces peak contaminant concentrations in groundwater advected downgradient. Sorption onto solid surfaces in these zones will retain contaminant mass over long time frames, thus further reducing downgradient contaminant migration. The processes of diffusion and sorption, however, also serve as significant impediments to achieving groundwater remediation objectives." (p. 11)*

3.3.4 Exercises Related to Section 3.3

After reading Section 3.3, the reader should be able to complete the following exercises: Exercise 19↴, Exercise 20↴, Exercise 21↴, Exercise 22↴, Exercise 23↴, Exercise 24↴, Exercise 25↴, Exercise 26↴, and Exercise 27↴.

4 Reactions

In this section we explore the roles that reactions play in modifying the distribution and transport of contaminants in natural subsurface media, in all phases, in source zones, and in plumes. Considered reactions include (a) phase changes, (b) sorption–desorption to and from matrix solids, and (c) transformations of contaminants into new compounds. Storage and release of contaminants into/from low-permeability zones *(low-k zones*), in conjunction with reactions, is addressed by the modeling discussions in Section 5.

Over the prior century, models for subsurface contamination often failed to fully appreciate subsurface reactions. Students in the prior century often received little input on subsurface reactions leading to consequential misconceptions. Historical examples of flawed conceptualizations include missing (a) NAPLs as persistent sources of aqueous phase contaminants (e.g., Anderson et al., 1992), (b) sorbed phases as contaminant sinks and sources (e.g. Allen-King et al., 2002), and (c) reactions leading to stable aqueous phase plumes (e.g., Hadley & Armstrong, 1991).

A primary factor driving our appreciation of reactions has been field data documenting assimilation of contaminants in plumes and source zones via biologically and geochemically mediated transformations. As biologic and chemical processes are often interdependent, they are lumped together as *biogeochemical* processes. Following Wiedemeier and others (1999), natural losses of contaminants in plumes are referred to as natural attenuation (NA). Following the Interstate Technology and Regulatory Council (2009), natural losses of NAPLs in source zones is referred to as natural source zone depletion (NSZD).

As with CoCs in air and surface water, natural assimilation of subsurface contaminants can play a primary role in mitigating risks associated with anthropogenic contaminants. Septic systems provide a vivid example. Homes in rural areas discharge hundreds of gallons of household wastewater into shallow leach fields daily. According to the EPA, "More than one in five households in the United States depends on individual onsite or small community cluster systems (septic systems) to treat their wastewater" (https://www.epa.gov/septic/about-septic-systems↗). Additional information regarding septic systems is presented by Robertson (2021). Another example is natural assimilation of subsurface petroleum liquids (referred to as NSZD) at gas stations, fuel terminals, and refineries . Given plausible areas underlain by petroleum liquids and NSZD rates on the order of tens of thousands of liters/hectare/year (Kulkarni et al., 2022), it seems likely that NSZD has done far more to deplete releases of petroleum liquids than active remedies have (Sale et al., 2018).

As of the 2020s, the heyday of large-scale recovery of NAPLs, treatment of NAPL source zones (e.g., heating, oxidants, and reductants), and isolation of NAPL source zones (e.g., walls or permeable reactive barriers) has passed in the USA. We note that the same is

not true for other CoCs, such as PFAS and those from coal combustion residuals. However, it seems our attention is shifting away from immediate moves to remedial intervention, particularly for NAPLs, to 1) remediating where it is responsible to do so, relying on NA and NSZD to address what remains after decades of active remediation, 2) finding ways to enhance NA and NSZD, and 3) exploring the potential for using subsurface media to assimilate trace contaminants in drinking-water supplies (e.g., in conjunction with subsurface water storage projects).

This section begins with data from field sites, which we use to explore reactions in plumes and source zones. Second, we advance a foundational review of college chemistry. Third, we consider the implications of depositional settings on contaminant reactions. Finally, we present the fundamentals of reactions, including contaminant partitioning between phases, sorption, and transformation reactions. The topic of reactions is a vast interdisciplinary space. Our goals in this section are to 1) set a foundation of knowledge needed to advance modern contaminant hydrology and 2) provide paths forward for those who want to know more. Important resources for learning more include Bird and others (2002), Lindsay (1979), Pankow (1991), Rittmann (2023), Schwarzenbach and others (2017), and Wiedemeier and others (1999). At the completion of Section 4 the reader should be able to complete the Exercises 28 and 29 in Section 7.

4.1 Observations from Field Sites

Building on observations from field sites, Figure 58 conceptually illustrates vertically averaged groundwater mass concentrations $\left(\overline{\rho_{aq}}\right)$ in plumes emanating from instantaneous, pulse, and steady sources, with and without reactions. Figure 58 is a common historical plan view illustration of plumes based on vertically integrated water quality data from monitoring wells. Concentrations of samples collected from monitoring wells are weighted by preferential flow through transmissive zones. Attributes of conceptual models A–C introduce the implications of sorption, phase changes, and transformation reactions. These conceptual models are explored in the following subsections.

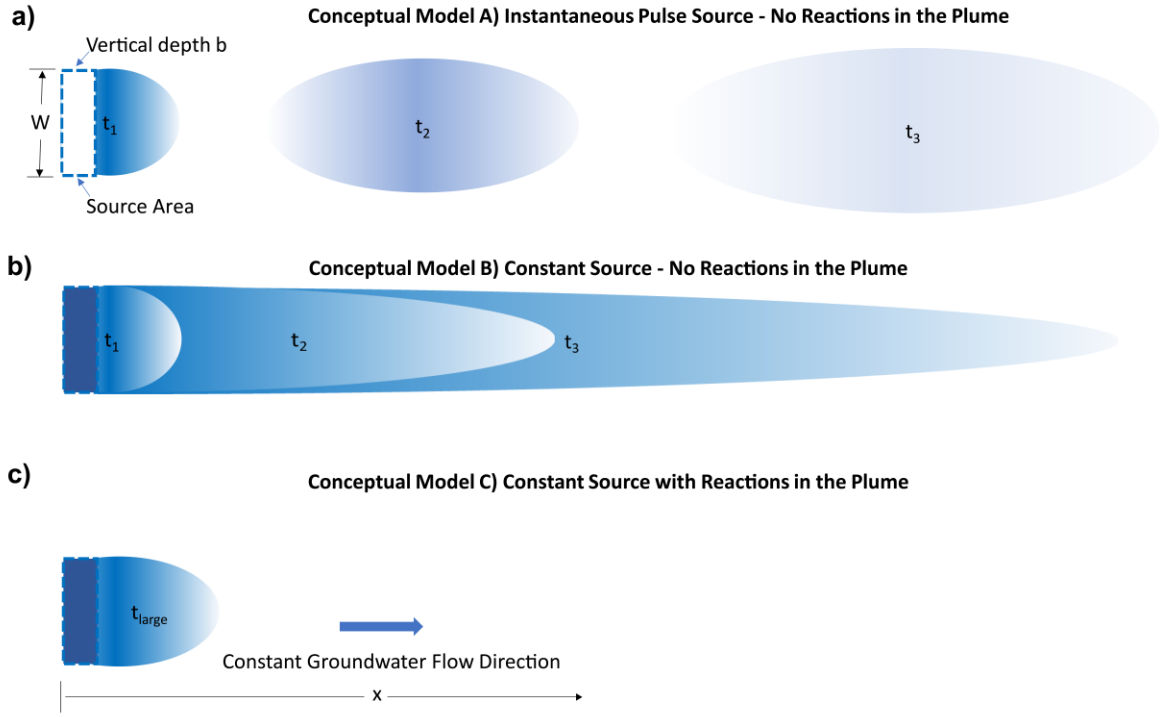

Figure 58 - Plan views of idealized plumes emanating from a fully penetrating source based on conceptual monitoring well data from field sites, with deeper blue indicating higher concentration. a) A plume at three times after introduction of an instantaneous source without reactions in the plume; b) A plume at three times after introduction of a constant source without reactions in the plume and the coloring of earlier times overlying those of later times. c) A plume long after introduction of a constant source with reactions in the plume. Data from monitoring wells could look the same for the early time plumes of conceptual models A and B and the late-time plume of model C.

4.1.1 Conceptual Model A, Pulse Source—No Reactions

In conceptual model A, a fixed mass (M) of an inert contaminant is instantaneously introduced along a vertical plain with width W and vertical height b at time t_0. At times t_1, t_2, and t_3, the plume detaches from the source area and the center of mass of the plume moves via advection (groundwater flow) as described by Equation (81).

$$x_{center_{t_i}} = v_{aq} t_i \text{ for i=1,2,3...} \tag{81}$$

At all times, given no losses due to phase changes, sorption, or transformations, the total contaminant mass in the plume is equal to the initial mass released as in Equation (82).

$$M_R = M_{t_1} = M_{t_2} = M_{t_3} \ldots \tag{82}$$

Similarly, at all times, the volume integral of the aqueous concentrations of compound i, multiplied by the porosity and multiplied by the volume of the plume is equal to the initial mass released, as shown in Equation (83).

$$M_R = \iiint \rho_{aq} \phi \, dxdydz \tag{83}$$

Longitudinal (in the direction of flow) spreading of the plume with time is envisioned as occurring due to differences of seepage velocities in the porous media

traversed by the plume. In truth, storage and release of contaminants to and from low-*k* zones will lead to apparent longitudinal spreading and retardation of the plumes. Following Guilbeault and others (2005), little *transverse* (perpendicular to flow) spreading is envisioned based on laminar flow of fluids in porous media and presumed groundwater flow in a constant direction.

Ideal aspects of conceptual model A (Figure 58a) make it uncommon. An analog of conceptual model A is provided by the Waterloo–Stanford experiment conducted at Canadian Forces Base Borden, Ontario, Canada (Roberts et al., 1986) as shown in Figure 59. The Borden aquifer is a relatively uniform beach sand. An instantaneous experimental release of contaminants was employed, including carbon tetrachloride (CTET), perchloroethene, (PCE), and chloride (CL). Figure 59a shows CTET, PCE, and CL plumes detaching from the source with the center of mass moving downgradient with groundwater flow through time. Figure 59b shows the PCE and CTET plumes at 633 days, and the CL plume at 647 days. CL, typically a nonsorbing contaminant, shows transport with little sorption. Transport of PCE and CTET, with greater propensities to sorb to solids, is retarded. Sorption reactions, not considered in conceptual model A, are illuminated in Figure 59 by sorption-driven chromatographic separation of the PCE, CTET, and CL plumes with PCE exhibiting the most sorption.

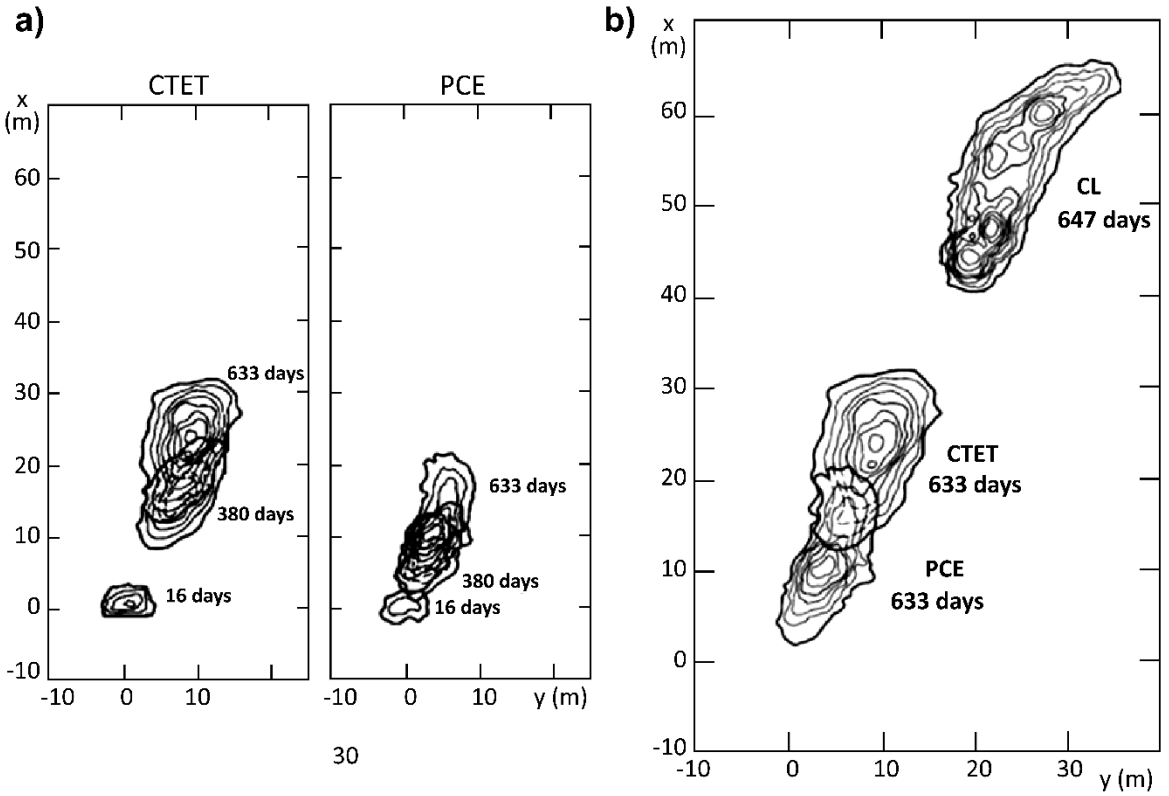

Figure 59 - Figures from the Waterloo–Stanford experiment conducted at Canadian Forces Base Borden, Ontario, Canada. a) CTET and PCE plumes detaching from the source location. b) PCE and CTET plumes at 633 days and CL plume at 647 days. Both (a) and (b) were adapted from Roberts and others (1986).

4.1.2 Conceptual Model B, Constant Source—No Reactions

Conceptual model B envisions a contaminant source with a constant mass discharge rate $\dot{M_{Source}}$ (M/T). Subsurface NAPL bodies (including LNAPLs and DNAPLs) commonly produce sources with largely steady mass discharge rates over extended periods of time. Constant sources from NAPLs at field sites illuminate phase-change reactions in which contaminants in a nonaqueous phase partition into an aqueous phase. The longevity of NAPL source zones is a function of the amount of NAPL released, groundwater flow rates, aqueous solubility of the NAPL, transverse diffusion coefficients, and the morphology of the NAPL body (Sale & McWhorter, 2001). Often, NAPL source zones provide persistent sources to plumes for decades. Leaking ponds and tanks, chemical conveyance ditches, and leaking pipelines can also provide near-constant releases. Fortunately, given evolving best practices, almost all types of sources have become less common over the past half century.

With time, conceptual model B plumes expand downgradient. Assuming no reaction in plumes, the plume mass is as shown in Equation (84) which equals the amount of mass input from the source over the time that it is present.

$$M_{plume} = \int_{t_0}^{t_i} \dot{M_{Source}}\, dt = \iiint \rho_{aq} \phi \, dxdydz \,|_t \tag{84}$$

Examples of conceptual model B plumes can be found in alluvial basins of Arizona, USA, in Tucson (Air Force Plant 44) and Phoenix (52nd Street Superfund Site). Releases of chlorinated solvent DNAPL at these sites have created plumes extending over many kilometers. Oxic conditions and low natural organic carbon concentrations lead to conditions where sorption and transformation reactions have limited effects on the movement of chlorinated solvents. Conceptual model B plumes are commonly captured by water-supply wells (domestic or municipal) or, in humid climates, discharge to surface water bodies (Einarson & Mackay, 2001).

4.1.3 Conceptual Model C, Constant Source—Transformation Reactions in Plumes

In conceptual model C, the source releases a contaminant at a constant rate $\dot{M_{Source}}$ and transformation reactions occur in the plume. Transformation-driven losses of contaminants in plumes are common (Wiedemeier et al., 1999). In most cases, losses are driven by biogeochemical processes. Contaminants are mineralized or transformed to new CoCs. Pathways proposed in Eykholt (1999) for degradation of PCE are presented in Figure 60. Additional information on reductive dechlorination pathways is presented in Arnold (2000). In the case of radioactive isotopes, radioactive decay can lead to similar losses in plumes.

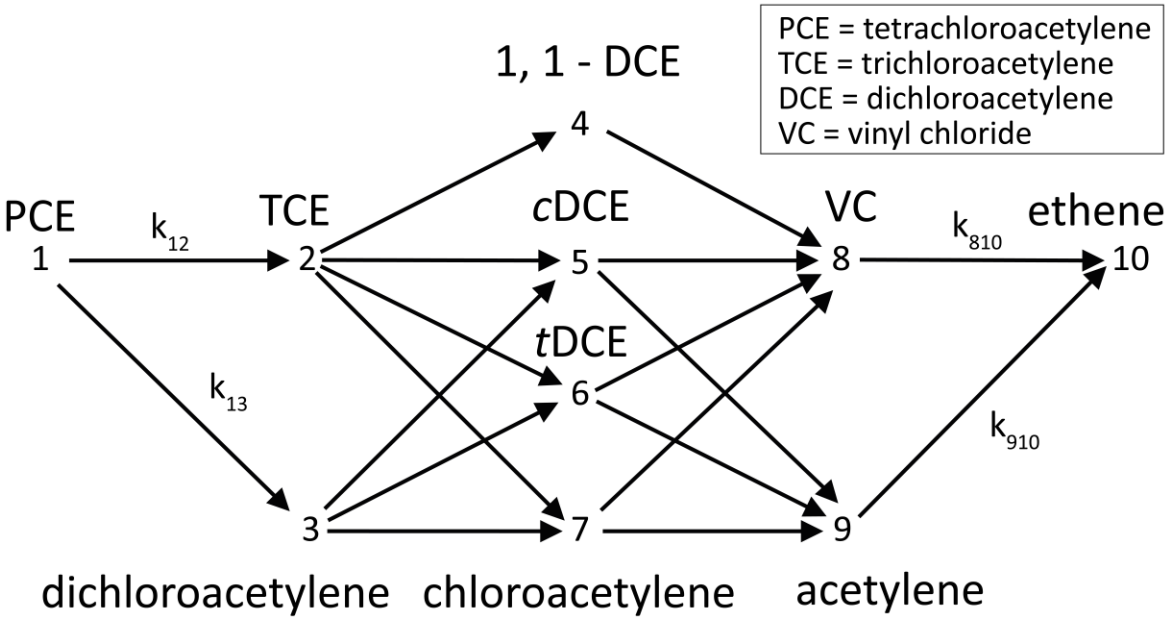

Figure 60 - Pathways for reductive dechlorination of PCE following Eykholt (1999). The node number is associated with the chemical component written next to it, while c stands for cis and t stands for trans.

The key attribute of conceptual model C is that in time, as a plume expands, total loss of contaminant mass from the plume ($R_{\dot{plume}}$ M/T) approaches the contaminant discharge from the source and the plume stabilizes as indicated in Equation (85).

$$R_{\dot{plume}} \cong M_{\dot{Source}} \text{ ... at large time} \tag{85}$$

The time it takes a plume to stabilize is a function of multiple factors, including the strength of the source $M_{\dot{Source}}$ and rates of contaminant degradation $R_{\dot{plume}}$. Observations of stable plumes at field sites illuminate NA transformation reactions. Critically, transformation reactions can play a primary role in mitigating risks to drinking-water supplies and other receptors.

Early documentation of transformation reactions in plumes at field sites is presented in "'Where's the Benzene?' – Examining California Ground-Water Quality Surveys" (Hadley & Armstrong, 1991). A quote from the abstract follows.

"In a state mandated program 7,167 wells serving water-supply systems throughout California were tested for a broad panel of organic contaminants. Of the wells tested, 812 (11.3%) had detectable concentrations of at least one of the contaminants tested for. Detectable concentrations of benzene were reported for only 10 wells" (p. 35).

The authors attributed the limited presence of benzene in drinking water to benzene being "*destroyed near its source by biodegradation.*" In 1991, and for a decade or more after, many viewed the observations of Hadley and Armstrong (1991) regarding natural attenuation of benzene in plumes with skepticism. It seems skeptics were seeing the world through the lens of conceptual model B all the while that NA transformation reactions had produced stable plumes per conceptual model C. Today, following numerous publications,

including Wiedemeier and others (1999) and Devlin and others (2024), the relevance of conceptual model C and transformation reactions in plumes has become widely embraced given *degradable contaminants* and favorable biogeochemical conditions.

Additional lines of evidence for reactions at field sites include the following list, which is likely incomplete. An exercise for the reader is to think about additional field-based lines of evidence for reactions.

Compound-specific isotope analysis (CSIA) – Building on Hunkeler and others (1999), biogeochemical transformations of organic compounds lead to increased ratios of heavier stable isotopes of carbon, hydrogen, chlorine, and other elements in organic CoCs. Shifts in ratios of stable isotopes in space and time provide a basis for realizing transformation reactions at field sites. Furthermore, CSIA may sometimes be used to resolve often elusive reaction rates.

Microbial ecology – Following Betts and others (2018), diverse microbial communities in soil have been metabolizing buried organic compounds for billions of years. Microbial activity in soil plays a primary role in the natural carbon cycle. It is no surprise that adaptation of microbial communities to degrade anthropogenic releases of organic compounds is just another part of the natural carbon cycle. Adaption of microbial communities at field sites to anthropogenic contaminants and large microbial numbers in release zones provide vivid lines of evidence for transformation reactions at field sites (e.g. Irianni-Renno et al., 2015).

Heat – Natural oxidation of petroleum hydrocarbons in source zones produces heat (e.g., Karimi Askarani et al., 2018). Temperatures in petroleum LNAPL bodies can be 1 to 6 °C warmer than background locations. Quantification of heat generated in petroleum source zones leads to estimated NSZD losses of tens of thousands of liters per hectare per year (Karimi Askarani et al., 2018).

Disappearance of NAPLs – Given that surface releases have been addressed, NSZD processes, including natural dissolution, reduce the remaining NAPL through time. As an example, Figure 61 documents full depletion of an LNAPL release through dissolutions and volatilization in a sand tank experiment. Ongoing depletion of NAPL bodies illuminates both phase changes from nonaqueous to aqueous phases and transformation reactions.

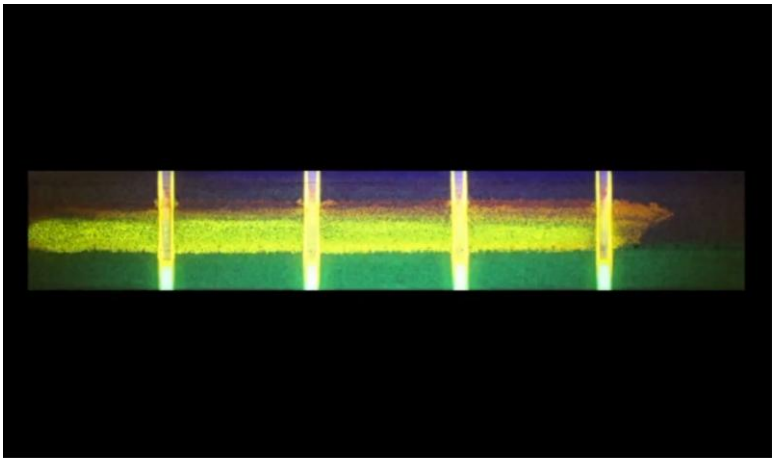

Figure 61 - The life and death of an LNAPL pool in a sand tank results from vaporization and dissolution as shown in this video.

4.2 Chemistry Principles

Section 4.2 provides a brief review of chemistry principles pertaining to the behavior of contaminants (primarily organic) in natural subsurface settings. This section covers college chemistry familiar to many and could be skipped by readers who are already familiar with this material. For others, revisiting key principles governing the behavior of CoCs in natural systems can be essential. Notably, applying what we gain from college chemistry courses to natural systems can be an intriguing and rewarding journey.

4.2.1 Bonding Overview

Atoms in molecules are held together by bonds. Building on Bohr's atomic orbital diagrams in Figure 62, atoms in the first two columns tend to shed electrons in their outer shell (under natural environmental conditions) by donating these so-called *valence electrons* to form cations (H^+, Li^+, Na^+, Mg^{+2}, and others). Similarly, elements in the seventh column (halogens) tend to fill their outer shell (under natural environmental conditions) by accepting an electron to form anions (F^-, Cl^-, and others). Elements in the eighth column (noble gases—He, Ne, and Ar) have filled outer shells and correspondingly are largely inert, not forming bonds with other atoms. Select elements empty or fill their outer shell (e.g., S^{+6} or S^{-2}) as a function of oxidation-reduction (redox) conditions poised by other phases, including solid matrix minerals.

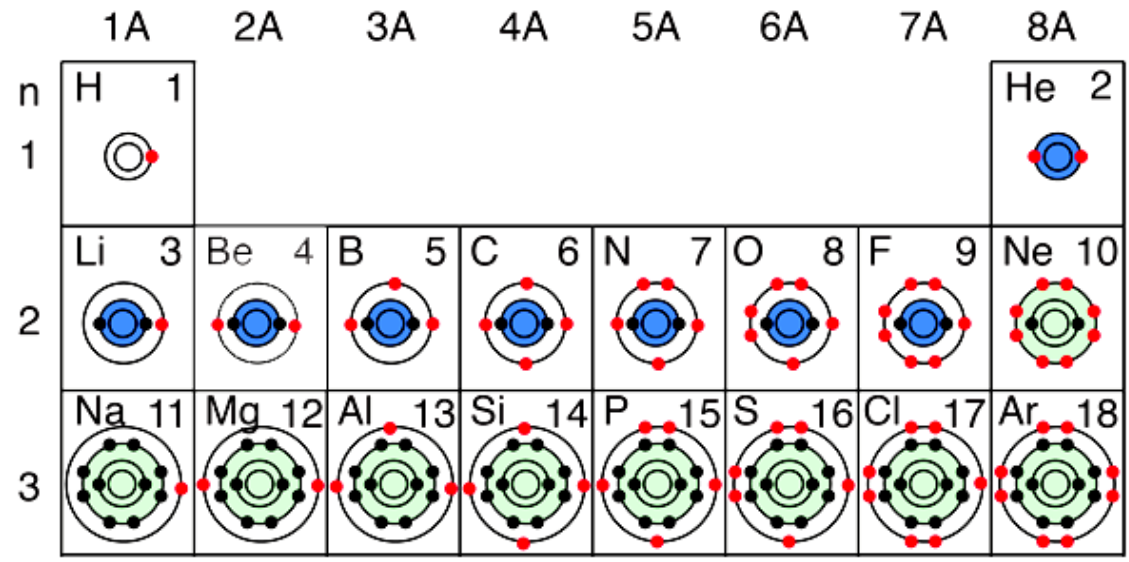

Figure 62 - Bohr atomic orbital diagrams depicting electrons in outer orbitals.

To understand how atoms bond, we first look at Linus Pauling's scale of electronegativity. Electronegativity is the tendency for an element to attract shared electrons when a chemical bond is formed. Fluorine is the most electronegative element, with an electronegativity, X, of 4.0, followed by oxygen (3.5), chlorine (3.0), nitrogen (3.0), bromine (2.8), iodine (2.5), sulfur (2.5), carbon (2.5), and hydrogen (2.2). When the difference in electronegativity between two bonding atoms is less than 0.5, such as carbon and hydrogen ($\Delta X=0.3$), the electrons are equally shared, and the bond is *nonpolar covalent*. With a ΔX between 0.5 and 1.7, a bond is *polar covalent*, such as the oxygen-hydrogen bond ($\Delta X=1.3$). When the ΔX exceeds 1.7, such as in hydrogen-fluorine bonds, the bond becomes *ionic*. In neutral water, H-F dissociates into H^+ and F^- with the more electronegative fluorine taking both of the bonding electrons.

4.2.2 Ionic Bonding

Ionic bonds are weaker than covalent bonds. An example of a chemical held together by ionic bonds that dissociates into ions upon dissolution in water is the salt calcium sulfate as shown in Equation (86). The denotation (s) indicates solid from and (aq) indicates dissolved in water.

$$CaSO_4\,(s) \leftrightarrows Ca^{+2}\,(aq) + SO_4^{-2}\,(aq) \qquad (86)$$

Following Lindsay (1979), the degree to which $CaSO_4$ (s) dissociates to Ca^{+2} (aq) and SO_4^{-2} (aq) under equilibrium conditions can be estimated using dissociation constants experimentally measured under standard conditions (K^o), along with the molar ratios of product to reactants. For example, given $CaSO_4$ (s) in the form of gypsum, the dissociation constant is defined by Equation (87), where the brackets [] indicate molar concentrations

$$K^o = \frac{[Ca^{+2}][SO_4^{-2}]}{[\mathrm{CaSO4\ (s)}]} = 10^{-4.41} \quad (87)$$

Given gypsum as an infinite solid, it can be assumed that $[\mathrm{CaSO_4\ (s)}]$=1 under standard conditions as in Equation (88).

$$[Ca^{+2}] = [SO_4^{-2}] = \sqrt{10^{-4.41}} = 6.2\mathrm{x}10^{-3}\ \mathrm{moles/L} \quad (88)$$

Ionic bonding is also relevant to natural and engineered ion-exchange processes. Many clays (hydrous aluminum sheet silicates) have surfaces that are negatively charged. Negatively charged surfaces can exchange cations (cation exchange capacity) with a general order of preference being dictated by aqueous concentrations and the size of the charged cations. Conversely, anions tend to be repelled by negatively charged surfaces. Given negatively charged surfaces, anions tend to be *conservative tracers* with limited propensity for exchange-driven retardation.

4.2.3 Covalent Bonding

Carbon is the central element in organic chemicals and, ultimately, of life. Given methane–which is composed of one carbon atom (moderate electronegativity) and four hydrogen atoms (weak electronegativity)–the four hydrogen-atom electrons spend most of their time in proximity to the carbon atom along with carbon's four valence electrons. Methane is the most reduced natural form of carbon. In the case of carbon dioxide, carbon electrons spend most of their time associated with the more electronegative oxygen atoms. Carbon dioxide is the most oxidized form of carbon under natural conditions.

Moving to the right of carbon in Figure 62, nitrogen, oxygen, fluorine, and chlorine (in the following row) are all progressively more electronegative than carbon. Carbon–halogen bonds are very relevant in environmental organic contaminants (Gamlin et al., 2024). Halogen elements include fluorine, chlorine, bromine, and iodine. Given greater electronegativity with smaller atomic sizes, the order of the strength of carbon halide bonds is carbon–fluorine>carbon–chlorine>carbon–bromine.

Various processes can lead to the breaking of covalent bonds. Simple bond cleavage (*dissociation*) is common in high-temperature processes such as incineration. Elimination and substitution reactions such as hydrolysis can lead to covalent bond breaking without electron transfer. In contrast, under natural conditions, reduction–oxidization (redox) reactions involve transfer of electrons from one atom or molecule to another.

As we move on to principles that are often important to organic molecules, it is useful to present the general nomenclature for common organic compounds as shown in Figure 63.

	Family												
	Alkane	Alkene	Alkyne	Arene	Haloalkane	Alcohol	Ether	Amine	Aldehyde	Ketone	Carboxylic Acid	Ester	Amide
Specific Example	CH3CH3	$CH_2=CH_2$	HC≡CH		CH_3CH_2Cl	CH_3CH_2OH	CH_3OCH_3	CH_3NH_2	$CH_3\overset{O}{\overset{\|}{C}}H$	$CH_3\overset{O}{\overset{\|}{C}}CH_3$	$CH_3\overset{O}{\overset{\|}{C}}OH$	$CH_3\overset{O}{\overset{\|}{C}}OCH_3$	$CH_3\overset{O}{\overset{\|}{C}}NH_2$
IUPAC Name	Ethane	Ethene or Ethylene)	Ethyne or Acetylene	Benzene	Chloro-ethane	Ethanol	Methoxy-methane	Methan-amine	Ethanal	Propanone	Ethanoic acid	Methyl ethanoate	Ethanamide
Common Name	Ethane	Ethylene	Acetylene	Benzene	Ethyl chloride	Ethyl alcohol	Dimethyl ether	Methyl-amine	Acetal-dehyde	Acetone	Acetic acid	Methyl acetate	Acetamide
General Formula	RH	$RCH=CH_2$ $RCH=CHR$ $R_2C=CHR$ $R_2C=CR_2$	$RC\equiv CH$ $RC\equiv CR$	ArH	RX	ROH	ROR	RNH_2 R_2NH R_3N	$R\overset{O}{\overset{\|}{C}}HO$	$R\overset{O}{\overset{\|}{C}}OR$	$R\overset{O}{\overset{\|}{C}}OOH$	$R\overset{O}{\overset{\|}{C}}OR$	$R\overset{O}{\overset{\|}{C}}ONH_2$ $R\overset{O}{\overset{\|}{C}}ONHR$ $R\overset{O}{\overset{\|}{C}}ONR_2$
Functional Group	C – H and C – C bounds		– C ≡ O –	Aromatic ring									

Figure 63 - General nomenclature for common organic compounds.

Redox reactions are important pathways for natural and engineered breakdown of organic contaminants in the environment. As an example, consider reductive dechlorination of PCE (C_2Cl_4) to TCE (C_2HCl_3) in which a C-Cl bond is replaced by a C-H bond as shown in Equation (89).

$$C_2Cl_4 + H^+ + 2e^- \leftrightarrows C_2HCl_3 + Cl^- \quad (89)$$

Given an equilibrium constant of $K^0 = 10^{21.68}$ (Wiedemeier et al., 1996) based on activities of products over reactants, the result is shown in Equation (90).

$$\frac{[C_2HCl_3]\,[Cl^-]}{[C_2C_{14}]\,[H^+][e^-]^2} = 10^{21.68} \quad (90)$$

Rearranging Equation (90) to solve for the ratio of log[TCE]/[PCE], given pH=-log$[H^+]$ and pe=-log$[e^-]$, we have Equation (91).

$$\log\frac{[C2HCl3]}{[C2Cl4]} = 21.68 - \log[Cl\text{-}] + \log[H+] + 2\log[e\text{-}] = 21.68 - \log[Cl\text{-}] - pH - 2pe \quad (91)$$

Notably the ratio of TCE to PCE under equilibrium conditions is a function of the *master variables* pH and pe, as well as chloride concentrations. Assuming equimolar concentrations of PCE and TCE, and a fixed chloride concentration (10^{-3} moles/L), standard conditions, and equilibrium conditions, molar concentrations of PCE and TCE will be equal when Equation (92) describes the conditions.

$$pH + 2pe = 24.68 \quad (92)$$

Figure 64 plots pe-pH conditions in which equimolar concentration of PCE and TCE will be present given equilibrium at standard conditions. Also shown in Figure 64 are pe-pH equilibrium conditions for TCE-DCE and DCE-VC. Spaces between the equilibrium lines indicate conditions where PCE, TCE, DCE, and VC tend to be stable at specified ratios. Conversely, outside of their stability fields, PCE, TCE, DCE, and VC have the potential (i.e., thermodynamic driving force) to degrade. If, or how fast, they will degrade, however, depends on the kinetics of the reaction (free energy of activation, referred to in Section 4.2.5). The electron activity, pe, can be converted into a more intuitive redox potential Eh as in Equation (93) and at a standard temperature of 25 °C, as in Equation (94).

$$pe = \frac{F}{2.3RT} Eh \quad (93)$$

$$E_h = 0.059\ pe \quad (94)$$

where (parameter dimensions are dark green font with mass as M, length as L, time as T, current as I, temperature as Θ):

F = Faraday's constant (TI mole^{-1}) typically coulomb per mole

R = gas constant (ML^{2}T^{-2}Θ^{-1}mole^{-1}) typically J/mole degree K

T = temperature (Θ) typically degrees Kelvin

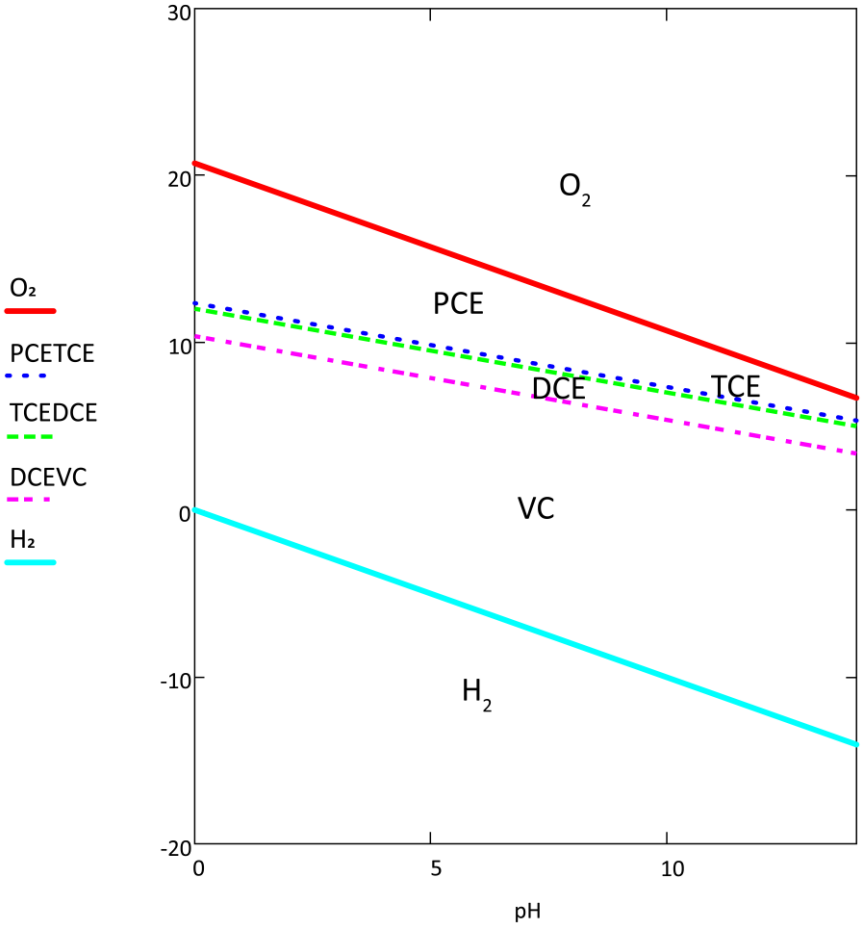

Figure 64 - Equimolar pe-pH stability field diagram for chlorinated ethenes with stability lines for water and common iron compounds assuming [Cl$^-$]=10^{-3} moles/L. Supporting calculations are presented in Box 4.

Importantly pe-pH stability field diagrams provide a point of embarkation for assessing the stability of CoCs under pe-pH conditions poised by natural or added electron donors or acceptors. Rigorous development of pe-pH stability field diagrams is presented in Hem (1985), Pankow (1991), and Stumm and Morgan (1995).

As a first-order approximation, oxidation states of carbon atoms in molecules can be developed by summing values for all bonds where C-H bonds are -1, C-C bonds are 0,

and C-N, -O, -F, -S, and -Cl bonds are +1 (Hendrickson et al., 1970). then dividing by the number of carbon atoms. Reduced contaminants (e.g., hydrocarbons) tend to degrade given natural or imposed oxidizing conditions, and oxidized contaminants (e.g., chlorinated solvents) tend to degrade given natural or imposed reducing conditions.

The following text and Table 3 organize ethene-based (two carbons bonded by a double bond), ethane-based (two carbons bonded by a single bond), and methane-based (one carbon) compounds by the average oxidation state of the carbon atoms.

Ethene-based compounds include the following.

- PCE (+2) – perchloroethene or tetrachloroethene (C_2Cl_4). The prefix "*per*" means fully chlorinated.
- TCE (+1) – trichloroethene (C_2HCl_3)
- DCE (0) – dichloroethene ($C_2H_2Cl_2$)
- VC (-1) – vinyl chloride (C_2H_3Cl)
- Ethene (-2) – (C_2H_4)

Ethane-based compounds include the following.

- PCA (+3) – perchloroethane (C_2Cl_6)
- TCA (0) – trichloroethane ($C_2H_3Cl_3$)
- DCA (-1) – dichloroethane ($C_2H_4Cl_2$)
- Ethane (-3) – ethane(C_2H_6)

Methane-based compounds include the following.

- CT (+4) – carbon tetrachloride (CCl_4)
- CF (+2) – chloroform ($CHCl_3$)
- MC (0) – methylene chloride (CH_2Cl_2)
- M (-4) – methane (CH_4)
-

Table 3 - Oxidation states of carbon in common halogenated ethene-ethane- and methane-based CoCs

	Ethene	Ethane	Methane
4			CT
3		PCA	
2	PCE		CF
1	TCE		
0	DCE	TCA	MC
-1	VC	DCA	
-2	Ethene		CM
-3		Ethene	
-4			Methane

Oxidized ↑ ↓ Reduced

4.2.4 Polarity and Polar versus Nonpolar Bonding

The degree to which charge is asymmetrically distributed around molecules is referred to as *polarity*. Polarity is caused by an electric dipole moment, which has magnitude and is directional (i.e., a vector). This is important to consider. If electric dipole moments in a molecule are symmetrical, they cancel each other out and the molecule is nonpolar despite having polar covalent bonds as per Pauling's scale of electronegativity. This explains, for instance, why 1,4-dioxane and the common soil gas CO_2 are nonpolar.

Polarity plays an important role in intermolecular bonding, such as hydrogen bonding between water molecules or the adsorption of polar organic chemicals (e.g., MTBE) to solid natural organic matter (NOM) or activated carbon. Polarity governs the arrangement of fluids and gases in pore spaces. Polar bonding such as hydrogen bonding is weaker than ionic bonding but stronger than nonpolar bonding.

Sorption – To varying degrees, solids contain NOM. NOM includes both polar and nonpolar functional groups from decaying organic materials, organic detritus from natural fires, and microbial biomass (e.g., Allen-King et al., 2002). Nonpolar compounds sorb to NOM like solutes being attracted to like solids—*like-likes-like*—and vice versa for polar compounds.

Fluids in pores – Polarity governs the distribution of fluids in pore spaces. Polar water molecules are typically most attracted to polar mineral surfaces. As such, water is typically a wetting fluid in direct contact with mineral surfaces. Common soil gases, including O_2, CO_2, N_2, and CH_4, are nonpolar. Nonpolar soil gases are repelled by polar water present on (i.e., wetting) solid grains. Correspondingly, these nonpolar gases are commonly the non-wetting fluid occupying the large pore spaces. In general, NAPLs are composed of organic compounds that are less polar than water and more polar than soil gases. As such, NAPLs commonly occur as an intermediate wetting phase present between water-wet minerals and nonwetting gas.

4.2.5 Thermodynamics

The potential for a reaction to proceed (reactants→products) is governed by thermodynamics. Typically, students are introduced to thermodynamics via courses in physical chemistry and/or engineering thermodynamics. Building on Figure 65, relevant tenets of thermodynamics include the following.

1. The Gibbs energy of formation (G_f, joules/mole) can be estimated for all molecules using published values (e.g., Wiedemeier et al., 1996).
2. The change in free energies of formation between product and reactants can be used to calculate changes in G_f values for reactions, ΔG_r.
3. Given ΔG_r values <0 (G_f products$<G_f$ reactants), a spontaneous forward reaction (reactants→products) will occur.

4. Conversely, given ΔG_r values >0 (G_f products>G_f reactants), a forward reaction will not occur. Given a positive ΔG_r value, a forward reaction would require an external energy input sufficient to create a negative ΔG_r.
5. The initial step in a reaction (breaking bonds or moving a molecule out of a phase) leads to a system with an increased G_f.
6. The increase in G_f associated with the initial reaction step is referred to as the "*reaction's free energy of activation*" (ΔG_a).
7. Sources of energy for activation of reactions in natural systems include the kinetic energy of molecules (motion and related collisions) and internal energy in molecules (bond vibration, flexing, rotation).
8. In general, larger activation energies lead to slower reaction rates.
9. Biological systems use reaction-specific enzymes to reduce activation energies and enhance reaction rates without being consumed in the reaction (*catalysis*).

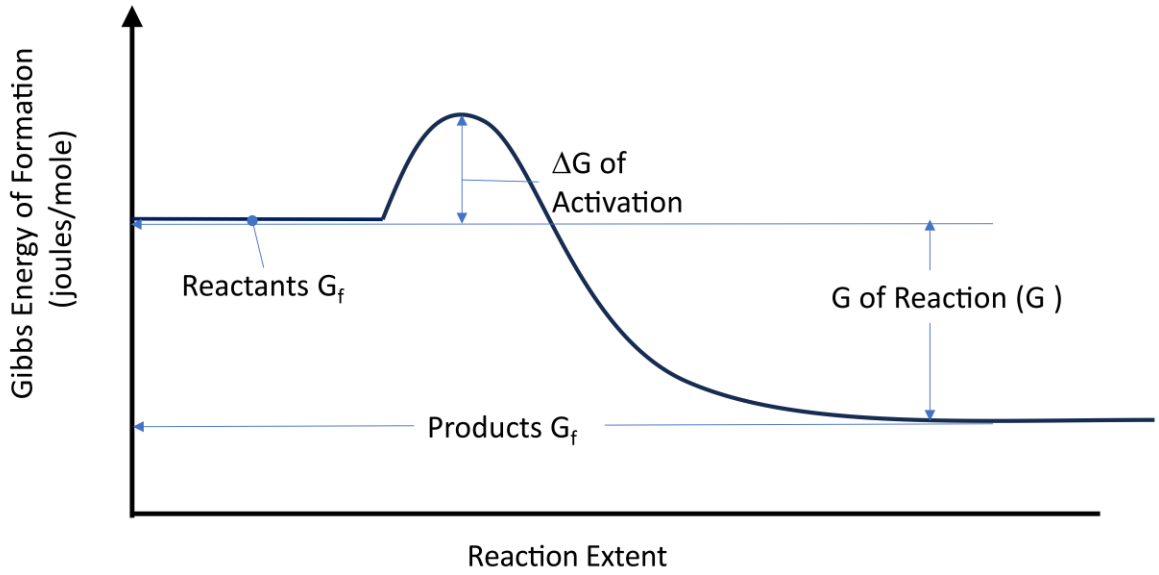

Figure 65 - Changes in Gibbs free energy in a reaction.

Useful thermodynamic identities include those shown in Equations (95) to (98).

$$\Delta G_r = G_{f_p} - G_{f_r} \tag{95}$$

$$\Delta G_r^o = -RTlnK^o \tag{96}$$

$$\Delta G_r = RTlnQ_r \tag{97}$$

$$\Delta G_r = -nFE \tag{98}$$

where (parameter dimensions are dark green font with mass as M, length as L, time as T, current as I):

^{o} = standard conditions (dimensionless)

Q_r = reaction quotient (ratio) of molar concentrations of product to reactants (dimensionless)

n = moles of number of electrons transferred in the reaction (dimensionless)

E = potential (often called voltage) ($ML^2T^{-3}I^{-1}$)

4.3 Site Attributes Governing Reactions

4.3.1 Conditions Imposed by Depositional Settings

The propensity of reactions to occur is dependent on settings that are the product of depositional and post-depositional processes. Sediments deposited in quiescent environments (e.g., swamps, low gradient fluvial deposits, and silts–clays inclusions in sands) can have low permeability, high levels of NOM, and reduced minerals, including reactive metal sulfides. Examples include swamps, low-energy deltas, and coastal estuaries.

Sediments deposited in quiescent environments often impose reducing conditions that favor reductive dechlorination (e.g., PCE→TCE→DCE...) and/or stabilization of inorganic CoCs via precipitation reactions (e.g., those involving Se). Conversely, thermodynamic arguments can be advanced that reduced CoCs (e.g., VC) will be less prone to transformation reactions in depositional systems with reducing conditions.

In contrast, sediments deposited in high-energy environments often have high permeabilities, low levels of NOM, and oxidized reactive minerals, including redox-poising ferric iron oxides. Examples of high-energy depositional environments include sand dunes, streams with large hydraulic gradients, and cinder beds associated with extrusive basalts.

Sediments deposited in high-energy environments often impose oxidizing conditions that favor oxidative transformations of reduced CoCs (e.g., VC). Conversely, thermodynamic arguments can be advanced that oxidized CoCs (e.g., PCE) will be less prone to transformation reactions in depositional environments with oxidizing conditions (Wiedemeier et al., 1999). These two observations by the authors support the preceding statements.

1. PCE and TCE co-released with hydrocarbons (e.g., at petroleum refineries) are readily attenuated due to reducing conditions imposed by hydrocarbons.
2. Plumes of VC can be stable under reducing conditions, while VC plumes are readily attenuated under oxidizing conditions.

Regarding sorption, 1) quiescent depositional environments with elevated NOM are likely to have elevated fractions of sorbed contaminants, and 2) high-energy depositional environments with low NOM are less likely to have elevated fractions of sorbed contaminants.

Hydrogeologic systems can include oxidized high-energy transmissive zones with inclusions of reduced low-energy low-*k* zones. Examples of settings with mixed bodies of oxidized and reduced media include:

- a transmissive sand with interbeds of low-*k* silt,
- a transmissive sand overlying a low-*k* aquitard, and
- transmissive fractures in shales or clays with low-*k* matrix blocks.

In these settings, oxidized PCE or TCE can be stable in transmissive zones while PCE and TCE are reductively dechlorinated in low-*k* zones (e.g., Kiaalhosseini et al., 2025; Muskus & Falta, 2018; Wahlberg, 2013).

4.3.2 Microbial Ecology

In the twenty-first century, emerging molecular and biological tools have led to wide recognition that subsurface media contain diverse microbial communities (Rittmann, 2023; Taggert & Key, 2024). For billions of years, microbial communities have been adapting to exploit energy that can be obtained through thermodynamically favored transformations of naturally occurring organic and inorganic compounds (e.g., Betts et al., 2018). Impressively, following Wang and others (2014), it can be argued that biomass below ground (such as microbes and roots) is on par with above-ground biomass (such as trees, grasses, and animals). Following Leopold (1949), *"Land, then, is not merely soils; it is a fountain of energy flowing through a circuit of soils, plants, and animals"* (p. 181). An emerging theme (e.g., Thornton et al., 2020) is that, in time, microbial communities in subsurface media evolve to novelly transform anthropogenic CoCs. Future editions of this book will spend more time on the topic of microbially mediated transformation reactions.

4.4 Partitioning Between Phases

Per Figure 3 and Figure 66, porous media can include, aqueous, NAPL, gas, and sorbed phases. Introduction of an organic CoC to porous media leads to partitioning of the CoC into all phases that are present. Management of sites impacted by organic releases typically requires a quantitative appreciation of all phases in which CoCs are present.

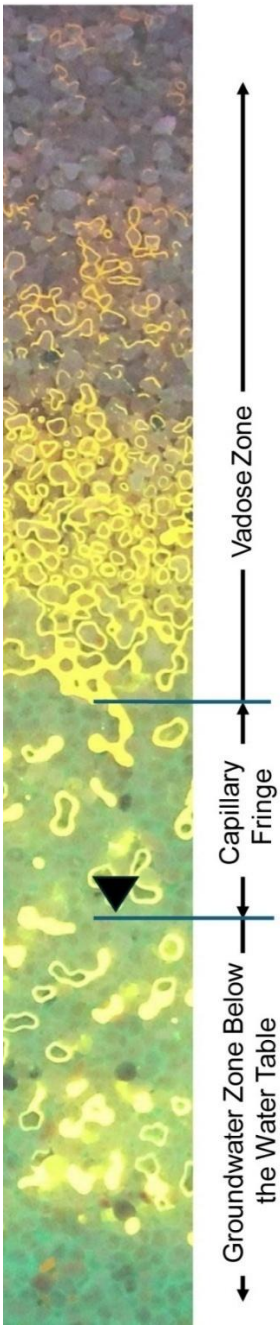

Figure 66 - Water-wet sands with intermediate and nonwetting phase diesel fuel (NAPL) dyed with fluoresceine, under UV light, around the water table (Modified after Skinner, 2013).

Following Schwarzenbach and others (1993), the process of moving a CoC from one phase to another involves an initial activation energy associated with overcoming attractions between the CoC and adjacent molecules in the first phase and forming a cavity in the second phase. Subsequently, the CoC is surrounded by the molecules of the second phase and a lower Gibbs free energy is realized. In the cases of (a) dissolution of organic CoCs in a NAPL into an aqueous phase (water) and (b) evaporation of water into

atmospheric air, the processes are endothermic. Reversal of (a) and (b) are exothermic processes.

4.4.1 Equilibrium Conditions

An equilibrium condition exists when the net flux of a CoC between phases is zero. For example, Pankow and Cherry (1996) report calculated and measured aqueous solubilities (at equilibrium) for PCE ($\rho_{aq_{s_{PCE}}}$), in water of 237 and 200 mg/L, respectively. Small differences in measured aqueous solubility values found in other references (e.g., Cohen & Mercer, 1993) are common. Differences in reported measured aqueous solubility values are due in part to net fluxes between phases approaching zero asymptotically with time. Ideally, true aqueous phase solubility values are reached at infinite time. The following presents solutions for equilibrium conditions. Complete derivations of solutions for equilibrium distributions of contaminants in all phases are presented in Box 5.

Raoult's law

Following Raoult's law and Figure 67, the effective aqueous solubility of a CoC ($\rho_{aq_{e_i}}$), given a multiple component NAPL, can be estimated using the mole fraction of the CoC in the NAPL, as shown in Equation (99).

$$\rho_{aq_{e_i}} = \rho_{aq_{s_i}} \chi_i \tag{99}$$

where:

χ_i = mole fraction of compound i in a NAPL

Similarly, applying the ideal gas law and Raoult's law, the molar concentration of a volatile compound i in gas adjacent to a NAPL can be estimated as shown in Equation (100).

$$P_i V = n_i RT \rightarrow P_{v_i} \chi_i V = n_i RT \rightarrow \frac{P_i \chi_i}{RT} = \frac{n_i}{V} = [C_{g_i}] \tag{100}$$

where (parameter dimensions are dark green font with mass as M, length as L, time as T):

P_i = partial pressure of CoC i ($ML^{-1}T^{-2}$)

V = gas volume (L^3)

C_{g_i} = equilibrium molar concentration of compound i (moles L^{-3})

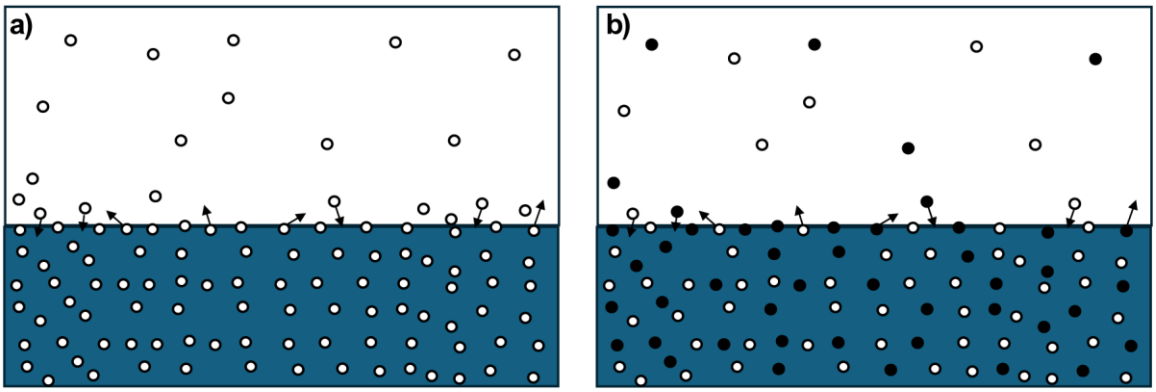

Figure 67 - Conceptualization of Raoult's law given a NAPL (blue) in equilibrium with a fluid (white). At equilibrium, the transfer of molecules in and out of the NAPL to and from the fluid is equal. When the NAPL is comprised of multiple components the concentration of each component in the fluid depends on the mole fraction of the component in the NAPL. a) A single component NAPL. b) A multiple component NAPL.

Gas↔NAPL

Based on the ideal gas law, the mass-based concentration of a CoC in a gas ρ_{g_i} adjacent to NAPL at equilibrium is shown by Equation (101).

$$\rho_{g_i} = \frac{\gamma_i P_{gas_i}^{NAPL} \chi_{NAPL_i} MW_i}{RT} \tag{101}$$

where (parameter dimensions are dark green font with mass as M, length as L, time as T):

γ_i = activity coefficient for compound i (dimensionless)

$P_{gas_i}^{NAPL}$ = partial pressure of compound i in a gas adjacent to a NAPL ($ML^{-1}T^{-2}$)

MW_i = molecular weight for compound i (M)

For dilute solutions, activity coefficients are commonly assumed to be equal to one.

Gas↔Aqueous

Employing Henry's equation, the mass-based concentration of a CoC in a gas adjacent to a contaminated aqueous phase at equilibrium is expressed as Equation (102).

$$\rho_{gas_i} = K_{HD_i} \rho_{aq_i} \tag{102}$$

where (parameter dimensions are dark green font with mass as M, length as L, time as T):

$K_{HD_i} = \frac{K_{H_i}}{RT}$

K_{H_i} = Henry's coefficient for compound i (MT^{-2} mole)

Aqueous ↔ NAPL

Based on Raoult's law, the mass-based concentration of a CoC in an aqueous phase adjacent to a NAPL at equilibrium is as in Equation (103).

$$\rho_{aq_i} = \gamma_i \rho_{aq_i}^{NAPL} \chi_{NAPL_i} \tag{103}$$

Sorbed ⟷ Aqueous

Employing a linear relationship between sorbed and aqueous concentrations, the relationship between sorbed mass and aqueous concentration is shown in Equation (104).

$$\omega_{s_i} = f_{oc} K_{oc_i} \rho_{aq_i} \tag{104}$$

where (parameter dimensions are dark green font with mass as M, length as L, time as T):

ω_{s_i} = mass of sorbed compound i per dry weight of porous media (dimensionless)

f_{oc} = organic carbon porous media fraction based on weight (dimensionless)

K_{oc_i} = octanol water-partitioning coefficient for compound i (L^3M^{-1})

Further consideration of sorption is presented in Section 4.6.

Total contaminant mass per mass dry porous media

Going further with partitioning between phases, emphasis is given to considering all potential contaminant phases. Historically, failing to address all contaminant phases has led to unfavorable surprises and often remediation failures. An analogy is chipping ice from the top of an iceberg per Figure 68. Every time you knock ice off the iceberg it floats higher yet despite the perceived accomplishment, in reality, there is little progress. Herein, emphasis is given to holistic consideration of subsurface contamination.

Figure 68 - An analogy to failing to address all contaminant phases resulting in little perceptible progress and project failures, is chipping away at the part of a problem one can see, all the while the biggest part of the problem is not immediately apparent (schematic created by Chat GPT 5o).I

Following McWhorter (1996) and Mercer and Cohen (1990), the total mass of contaminant i per mass dry porous media (e.g., mg of CoC/kg dry media) is described by Equation (105).

$$\omega_{T_i} = \omega_{g_i} + \omega_{NAPL_i} + \omega_{aq_i} + \omega_{s_i} \tag{105}$$

The gas-phase mass of contaminant i per mass dry porous media (e.g., mg of CoC-in-gas/kg dry media) is shown in Equation (106).

$$\omega_{g_i} = \frac{\rho_{gas_i}(\phi - \phi S_w - \phi S_{NAPL})}{\rho_b} \tag{106}$$

The aqueous phase mass of contaminant i per mass dry porous media (e.g., mg of CoC-in-water/kg dry media) is as in Equation (107).

$$\omega_{aq_i} = \frac{\rho_{aq_i}\phi S_w}{\rho_b} \tag{107}$$

The NAPL mass of contaminant i per mass dry porous media (e.g., mg of CoC-in-NAPL/kg dry media) is shown in Equation (108) and ω_{s_i} was defined in Equation (104).

$$\omega_{NAPL_i} = \frac{\rho_{NAPL_i}\phi S_{NAPL}\chi_{NAPL_i}}{\rho_b} \tag{108}$$

Substituting ω values for each phase into Equation (105) yields Equation (109).

$$\omega_{T_i} = \frac{\rho_{gas_i}(\phi - \phi S_w - \phi S_{NAPL})}{\rho_b} + \frac{\rho_{NAPL_i}\phi S_{NAPL}\chi_{NAPL_i}}{\rho_b} + \frac{\rho_{aq_i}\phi S_w}{\rho_b} + f_{oc}K_{oc_i}\rho_{aq_i} \tag{109}$$

Substituting in expressions for ρ_{gas_i} and χ_{NAPL_i} yields Equation (110).

$$\omega_{T_i} = \rho_{aq_i}\phi\left(\frac{K_{HD}(1 - S_w - S_{NAPL})}{\rho_b} + \frac{\rho_{NAPL_i}S_{NAPL}}{\rho_b\gamma_i\rho_{aq_i}^{Pure}} + \frac{S_w}{\rho_b} + \frac{f_{oc}K_{oc_i}}{\phi}\right) \tag{110}$$

Total and aqueous contaminant mass per volume of porous media

Alternatively, the total mass of contamination can be normalized to the volume of porous media. Total contaminant mass per volume porous media can be used to track the relative differences between contaminant mass in transmissive versus low-k zones. The solution for total contaminant mass per unit volume porous media (ML^{-3}) is obtained by multiplying both sides of Equation (105) by the bulk density of the porous media, as shown in Equation (111).

$$\rho_{PMT_i} = \omega_{T_i}\rho_b = \rho_{aq_i}\phi\left(K_{HD}(1 - S_w - S_{NAPL}) + \frac{\rho_{NAPL_i}S_{NAPL}}{\gamma_i\rho_{aq_i}^{Pure}} + S_w + \frac{f_{oc}K_{oc_i}\rho_b}{\phi}\right) \tag{111}$$

Special cases

Maximum total concentration without NAPL: A common question is, given a value of ω_{Total_i} is it likely that a NAPL is present? Setting $S_{NAPL} = 0$ in Equation (110), we solve for the threshold concentration that is indicative of NAPL in Equation (112).

$$\omega_{NAPL-Threshold\ i} = \frac{\rho_{gas_i}(\phi - \phi S_w)}{\rho_b} + \frac{\rho_{aq_i}\phi S_w}{\rho_b} + f_{oc}K_{oc}\rho_{aq_i} \tag{112}$$

Aqueous phase retardation coefficient for S_w=1: Given an aqueous phase CoC, transport can be retarded by the CoC partitioning to solid phases. The ratio of the total mass of CoC i per volume porous media to aqueous phase mass per volume porous media is defined as the aqueous phase retardation coefficient and given $S_W = 1$, it is as shown in Equation (113) and in a slightly different form in Equation (114).

$$R_{aq}\big|_{S_w=1} = \frac{\rho_{PMT_i}}{\phi \rho_{aq_i}} \tag{113}$$

$$R_{aq}\big|_{S_w=1} = 1 + \frac{f_{oc} K_{oc_i} \rho_b}{\phi} \tag{114}$$

Given $R_{aq}\big|_{S_w=1} = 1$, all the contaminant mass is in the aqueous phase and the advective advancement of an aqueous plume will be equal to the seepage velocity. Given $R_{aq}\big|_{Sw=1} = 2$, equal parts of the total contaminant mass will be in the aqueous and sorbed phases and the rate of advancement of an aqueous plume will be half the seepage velocity.

Gas phase retardation coefficient for S_{NAPL}= 0: Given a gas phase CoC, transport can be retarded by the CoC partitioning into aqueous and solid phases. The ratio of the total mass of CoC i per volume porous media to the gas phase mass per volume porous media is defined as the gas phase retardation coefficient and given $S_{NAPL} = 0$ is shown in Equation (115) and in a slightly different form in Equation (116).

$$R_g\big|_{SNAPL=0} = \frac{\rho_{PMTotal_i}}{\phi \rho_{g_i}} \tag{115}$$

$$R_g\big|_{SNAPL=0} = \frac{S_w}{K_{HD} S_g} + 1 + \frac{\rho_b K_d}{\phi S_g K_{HD}} \tag{116}$$

Given $R_g\big|_{SNAPL=0} = 1$, all the contaminant mass is in the gas phase. Given $R_{aq}\big|_{Sw=1}$ =2, equal parts of the total contaminant mass will be in the gas phase and in the aqueous+sorbed phases.

4.4.2 Nonequilibrium

Nonequilibrium conditions exist when net fluxes between phases are nonzero. Nonequilibrium conditions are either steady-state or transient.

Steady-state nonequilibriun

As an instructive example, we consider steady-state mass transfer from a DNAPL pool at the base of a transmissive zone into an overlying flowing aqueous phase. The steady nonequilibrium is a persistent flow of matter between the DNAPL pool and its surroundings. We encourage readers to review the derivation for diffusion into a low-*k* zone that is presented in Box 3. The derivation for mass transfer from a DNAPL pool into an overlying flowing aqueous phase is essentially identical to the solution for diffusion into a low-*k* zone. The derivation provides a solid refresher on college-level mathematics and an advanced appreciation of governing processes.

We begin with a general 3D transient PDE for advective diffusive transport, as in Equation (117) and make the bulleted assumptions following Equation (117).

$$-q_x \frac{\delta \rho_{aq_i}}{\delta x} + D_{e_x} \frac{\delta^2 \rho_{aq_i}}{\delta x^2} + D_{e_y} \frac{\delta^2 \rho_{aq_i}}{\delta y^2} + D_{e_z} \frac{\delta^2 \rho_{aq_i}}{\delta z^2} + \lambda_i \rho_{aq_i} + \frac{G_m}{\phi} - \frac{R_m}{\phi} = \frac{\delta}{\delta t}\left(\rho_{aq_i} R_{aq} \phi\right) \quad (117)$$

- Steady-state conditions prevail, $\frac{\delta}{\delta t}\left(\rho_{aq_i} R_{aq} \phi\right) = 0$.
- The pool width is infinite, therefore, $\frac{\delta^2 \rho_{aq_i}}{\delta y^2} = 0$.
- There is no consequential diffusion or dispersion in the x direction, $D_{e_y} \frac{\delta^2 \rho_{aq_i}}{\delta y^2} = 0$.
- There are no transformation reactions, $\lambda_i = 0$.
- There are no contaminant sources, $G_m = 0$.
- There are no contaminant sinks, $R_m = 0$.

As with the PDE for diffusion into a low-*k* zone, Section 3.3.2, the transport equation simplifies to a PDE with the form of the heat equation, as shown in Equation (118).

$$q_x \frac{\delta \rho_{aq_i}}{\delta x} = D_{e_z} \frac{\delta^2 \rho_{aq_i}}{\delta z^2} \rightarrow \frac{\delta \rho_{aq_i}}{\delta x_1} = \frac{D_{e_z}}{q_x} \frac{\delta^2 \rho_{aq_i}}{\delta x_2{}^2} \rightarrow \frac{\delta \rho_{aq_i}}{\delta x_1} = \alpha \frac{\delta^2 \rho_{aq_i}}{\delta x_2{}^2} \quad \text{where } \alpha = \frac{D_{e_z}}{q_x} \quad (118)$$

Relevant boundary conditions are in presented in Equations (119) to (121):

$$\rho_{aq_i}(0, z) = 0 \quad (119)$$

$$\rho_{aq_i}(x, 0) = \rho_{aq_{o_i}} \text{ for } x \leq L \text{ (pool length)} \quad (120)$$

$$\rho_{aq_i}(x_1, \infty) = 0 \quad (121)$$

The solution is shown in Equation (122).

$$\rho_{aq_i}(x, z) = \rho_{aq_{o_i}} \left(1 - erf\left(\frac{z}{2\sqrt{\frac{D_{ez_i} x}{v_w}}}\right)\right) \quad (122)$$

The form of Equation (122) is identical to the solution for diffusion into a low-*k* zone of Box 3 and Equation (75) of Section 3.3.2, because $1 - \text{erf}\,(x) = erfc(x)$.

Figure 69 applies Equation (122) to a 5-m-long PCE DNAPL pool. Per Equation (122), steady-state aqueous concentrations above a DNAPL pool are a function of the aqueous solubility of the DNAPL constituent of interest, the position z above the pool, the effective diffusion coefficient in the z direction, and the position x for $x \leq L$.

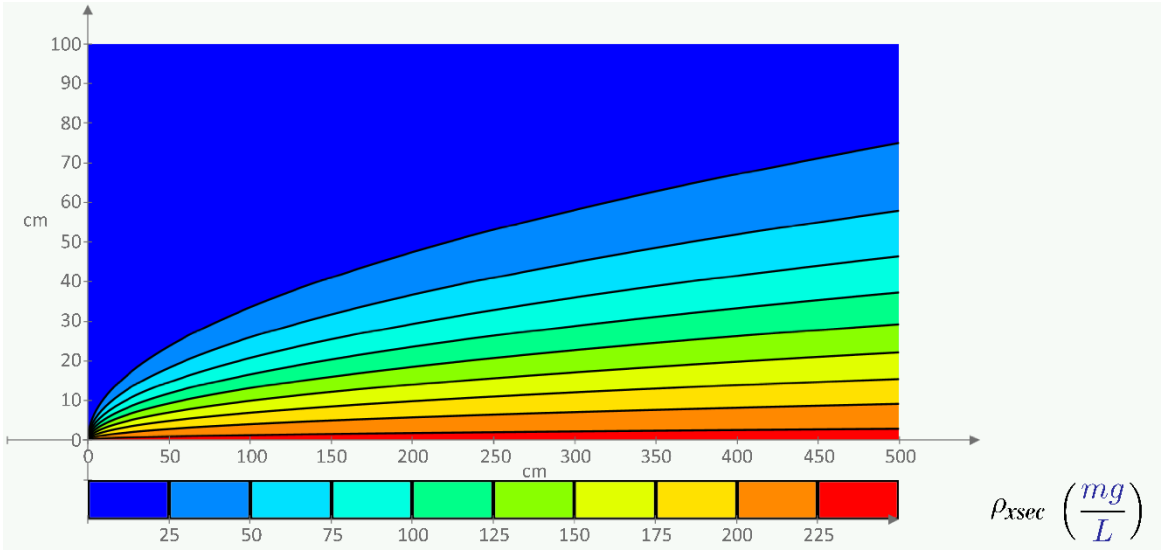

Figure 69 - Concentrations of PCE above a DNAPL pool (v_w =100m/yr, D_{ez} =6.8x10^{-10} m^2/sec, and ρ_{aq_o} =150 mg/L).

A solution for the flux of contaminants from the DNAPL pool to the aqueous phase at the top of the DNAPL pool is obtained by inserting Equation (122) into Fick's First Law and evaluating the concentration gradient at z=0, $\frac{\delta \rho_{aq_s}}{\delta z}|_{z=0}$, as presented in Equation (123).

$$J(x)|_{z=0} = -\phi D_{ez} \frac{\delta \rho_{aq_i}}{\delta z}|_{z=0} =$$

$$-\phi D_{ez} \frac{\delta\left[\rho_{aq_{o_i}}\left(1-\text{erf}\left(\frac{z}{2\sqrt{\frac{D_{ez}x}{v_w}}}\right)\right)\right]}{\delta z}|_{z=0} = \rho_{aq_{o_i}}\ \phi\sqrt{\frac{v_w D_{ez}}{x\pi}} \tag{123}$$

Equation (123) was obtained using the MathCad Prime™ symbolic evaluation tool. Figure 70 presents the mass flux from the top of the pool over its length from $x = 0\ m$ to $x = 5\ m$. The greatest flux occurs at the leading edge of the pool where the concentration gradient is largest. Dissolution mass fluxes are directly proportional to ρ_{aq_o} and ϕ and proportional to the square root of v_w, D_{ez}, and $\frac{1}{x}$.

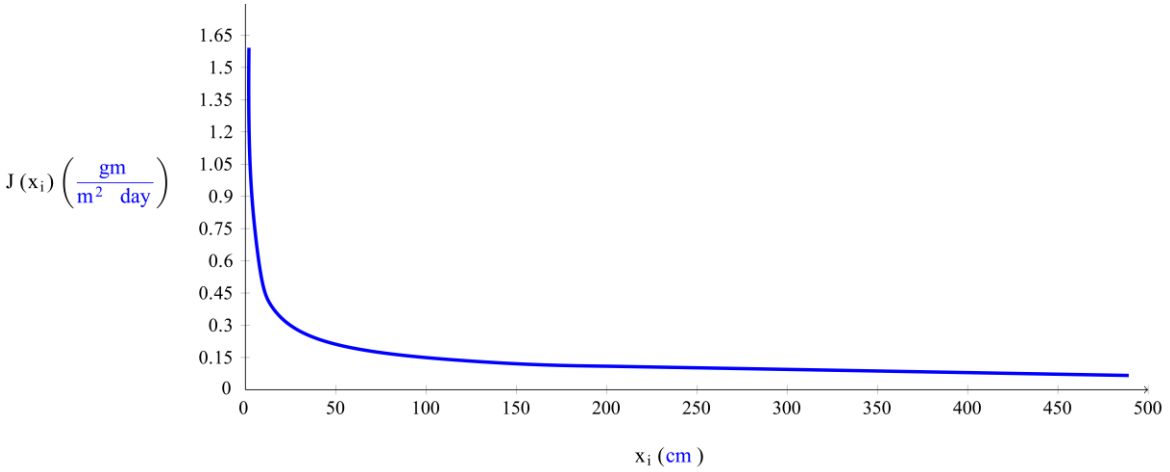

Figure 70 - Dissolution-driven mass flux above a PCE pool as a function of position (v_w =100m/yr, D_{ez} =6.8x10^{-10} m^2/sec, ρ_{aq_o} =150 mg/L, and ϕ =0.3).

A solution for total mass released from the top of the pool is obtained by integrating $J(x)$ over the length of the pool and width of interest such as one unit width because the pool is infinitely wide thus the total mass flux us infinite, as shown in Equation (124).

$$\dot{M}_{pool} = \int_0^L \int_0^{W_i} \phi \rho_{aq_{o_i}} \sqrt{\frac{v_w D_T}{\pi x}} dx dy = \phi W \rho_{aq_{o_i}} \sqrt{\frac{L v_w D_{ez_i}}{\pi}} \tag{124}$$

Equation (124) reveals that $\dot{M}_{pool}$ increases (a) linearly with effective solubility and (b) as the square root of the pool length, seepage velocity, and effective diffusion coefficient.

Lastly, consideration is given to aqueous concentrations in a monitoring well above the pool. Building on conditions considered in Figure 70, we consider a monitoring well located at x =5 m with a screened interval from z =0 to 3 m. The average concentration in the well is obtained by integrating the solution over the screen interval at x=5 and dividing by the length of the screened interval, as shown in Equation (125).

$$\overline{\rho_{aqwell_i}} = \frac{\int_{0m}^{3m} \rho_{aq_{o_i}} \left(1 - erf\left(\frac{z}{2\sqrt{\frac{D_{ez} x}{v_w}}}\right)\right) dz}{3m} \tag{125}$$

Figure 71 presents the average concentration in the well $\overline{\rho_{aqwell_{PCE}}}$ as a function of seepage velocities ranging from 0 to 100 m/year. Calculations were made using the MathCad Prime™ numerical integration tool. At low seepage velocities, $\rho_{aqwell_{PCE}}$ approaches the effective solubility of PCE. With increasing seepage velocities, $\overline{\rho_{aqwell_{PCE}}}$ asymptotically approaches zero. Low seepage velocities equate to high concentrations in the well above the pool (a negative) and low loading to the downgradient plume (a positive). Conversely, high seepage velocities equate to low concentrations in the well above the pool (a positive) and large loading to the downgradient plume (a negative).

Monitoring wells are useful for resolving concentration-based risks to human health related to exposure to groundwater, however concentrations in monitoring wells, by themselves, can be misleading with respect to loading to plumes.

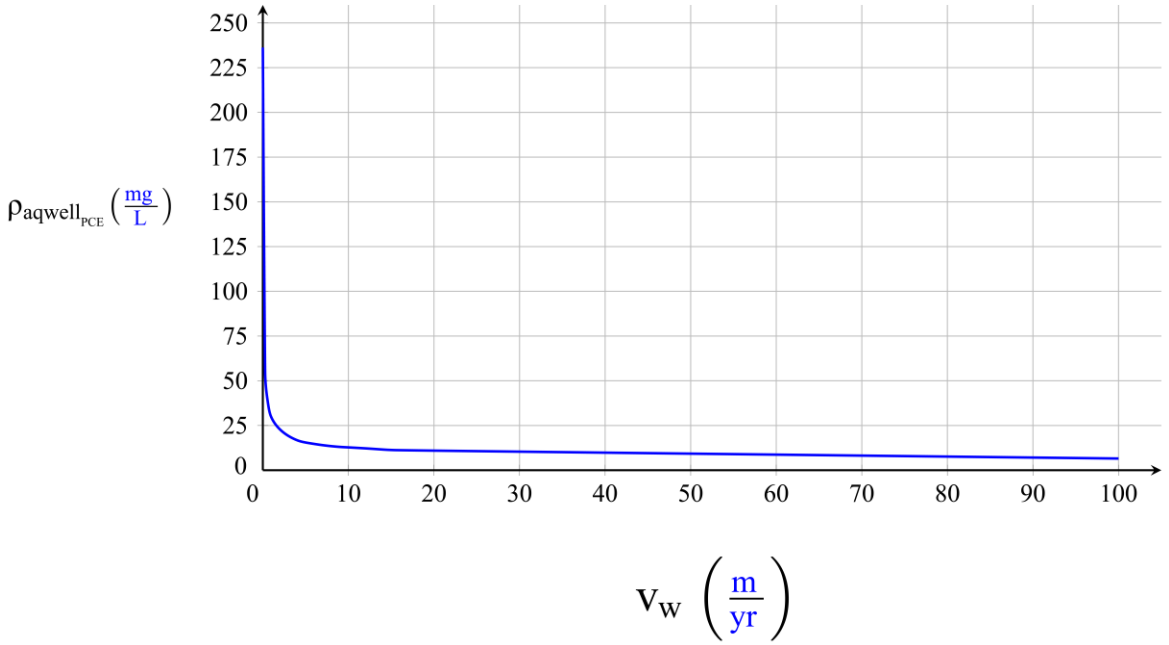

Figure 71 - Aqueous concentration in a monitoring well at x = 5 m, screened from 0 to 3 m above a PCE pool as a function of the horizontal groundwater seepage velocity (with D_{ez} =6.8x10^{-10} m^2/sec, ρ_{aq_o} =150 mg/L, and ϕ =0.3).

Transient nonequilibriun

Given a finite release, NAPL bodies are like water puddles on asphalt on a sunny day. In time they will shrink in size and depth and, eventually, be fully depleted (Sale, 1998). As a first approximation, one can assume idealized NAPL pool dimensions and NAPL saturations to obtain an initial mass of NAPL. The gradual disappearance of the pool can be quantified by applying a succession of steady-state losses from the pool over time, estimated using and accommodating the step-wise calculated losses by shortening the length of the pool before calculating loss for the next step through time (Sale, 1998). NAPLs with greater effective solubilities and systems with larger groundwater velocities will be depleted faster. Following solubilities, and holding all other factors constant, the longevity of single component NAPL bodies is high-molecular-weight hydrocarbon>PCE>TCE>MTBE (methyl-tert-butyl-ether).

Pragmatically, building on Sale (1998), estimating the longevity of NAPL bodies is complicated by numerous factors, including:

- NAPLs being drawn by capillary forces to the leading edge of NAPL bodies where mass transfer rates are the greatest;
- impracticability of characterizing the dimensions and masses of CoCs in NAPL bodies;

- biogeochemical transformation reactions increasing concentration gradients around NAPL bodies thus increasing overall rates of dissolution; and
- complexities associated with multiple-component NAPL bodies, including evolving effective aqueous solubilities of NAPL components.

4.5 Sorption

Sorption is a process wherein CoCs are attracted to and held by matrix solids. Sorption involves either *adsorption*—CoCs being held on solid surfaces—or absorption—CoCs moving into solids. A diverse set of physical processes govern CoCs being bound to solids. Examples include the following.

- Adsorption is a two-dimensional phenomenon. A few examples are given in this bullet list.
  - Nonpolar organics being attracted to nonpolar NOM that was naturally part of the aquifer solids (like-likes-like). The NOM is sometimes referred by the measurement name Fraction Organic Carbon ("foc"). It remains as a stable phase, providing a surface that enhances sorption of nonpolar contaminants from groundwater. The foc of unconsolidated aquifer material can range from almost zero to a few percent with 0.1% often used as a typical value. There are many sources of NOM. Even in sandy aquifers, NOM can originate from soil organic matter (humic and fulvic acids) produced by decaying plants and animals at the surface that have leached into the aquifer; trapped bits of plant debris; and microbes within the aquifer.
  - Cations being attracted to negatively charged surfaces in sheet silicates (opposites attract).
  - Covalent bonding of CoCs to the surface of clays.
- Absorption is a three-dimensional phenomenon. A few examples are given in this bullet list.
  - Diffusion into porous solids.
  - Steric entrapment in solids.

Sorption leads to 1) transport of CoCs being retarded, 2) sources of CoC that can sustain aqueous CoC concentrations after depletion of sources, 3) reduced aqueous concentrations in low-*k* zones that can increase diffusion of CoC into low-*k* zones, and 4) chemical demand for treatment reagents (e.g., oxidants) exceeding demands posed by aqueous-phase CoCs. Comprehensive reviews of sorption are presented in Allen-King and others (2002) and Schwarzenbach and others (1993). Two example sorption data sets are presented in Box 6↴.

4.5.1 Linear Sorption

As a first approximation, and perhaps most pragmatically, one can assume a constant, reversible, and instantaneous linear relationship between masses of sorbed and aqueous phases, as shown in Equation (126).

$$K_{d_i} = \frac{\omega_{s_i}}{\rho_{aq_i}} \tag{126}$$

where (parameter dimensions are dark green font with mass as M, length as L, time as T):

K_{d_i} = the linear partitioning coefficient for compound i (L^3M^{-1})

K_{d_i} can be estimated using Equation (127).

$$K_{d_i} = f_{oc} K_{oc_i} \tag{127}$$

where (parameter dimensions are dark green font with mass as M, length as L, time as T):

f_{oc} = the fraction of organic carbon (MM^{-1})

K_{oc} = organic carbon partitioning coefficient (obtained experimentally and reported in physical property references—e.g., Merck, 2006) (L^3M^{-1})

Building on Equation (114)(115), the widely used retardation coefficient can be estimated as in Equation (128).

$$R_{aq}\big|_{Sw=1} = 1 + \frac{K_{d_i}\rho_b}{\phi} \tag{128}$$

Alternatively K_{d_i} can be measured by 1) preparing closed sample vials with known masses of homogeneous porous media and aqueous solutions of known volume with concentrations ranging over the range of interest, 2) allowing sufficient time for aqueous and sorbed phases to equilibrate, 3) using losses from the aqueous phase to resolve sorbed phase mass, 4) plotting aqueous phase concentrations ρ_{aq_i} versus sorbed phase concentrations ω_{s_i}, 5) performing data, and 6) using the slope of the regressed data to resolve K_{d_i}. Figure 72 presents a conceptual plot of ρ_{aq_i} versus ω_{s_i}.

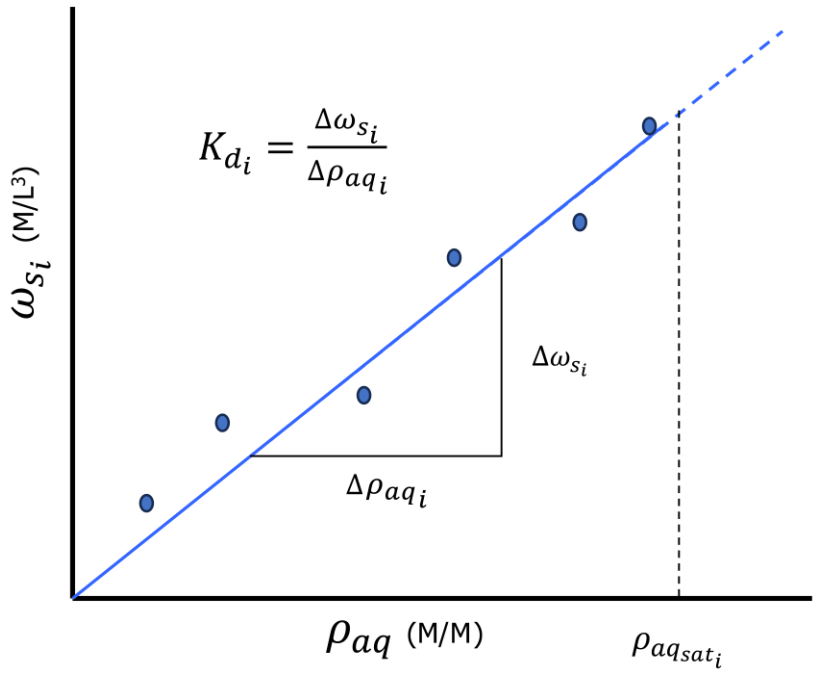

Figure 72 - Conceptual plot of ω_{s_i} versus ρ_{aq_i}.

Factors that can bias measured K_{d_i} values include:

- large periods of time being needed to reach equilibrium between aqueous and sorbed phases;
- losses in aqueous phase contaminants to processes other than sorption including biogeochemical reactions and losses of CoCs through septa in vials; and
- nonuniform distributions of sorptive media (e.g., char from fires) in porous media samples.

Another potential source of bias is hysteretic sorption wherein releases of CoC from solids is slow as compared to the initial uptake (Chen et al., 2002; Kan et al., 1998).

4.5.2 Nonlinear Sorption

Sometimes, relationships between ρ_{aq_i} and ω_{s_i} are nonlinear. Nonlinear relationships can occur where the sorbed compounds (sorbents) approach or exceed the number of sorption sites. Scenarios where sorbents can exceed sites include large aqueous concentrations, low f_{oc}, and low K_{oc}.

Following Allen-King and others (2002), Freundlich and Langmuir empirical models for nonlinear sorption are presented here. Selection of a preferred model is commonly predicated on using the model that provides the best fit. Limitations to nonlinear sorption models include increased numbers of fitting parameters and mathematical complexities introduced by ρ_{aq_i} being a nonlinear function of ω_{s_i}.

Freundlich

The Freundlich empirical nonlinear sorption model is defined as in Equation (129).

$$\omega_{s_i} = K_{f_i} {\rho_{aq_i}}^n \tag{129}$$

where (parameter dimensions are dark green font with mass as M, length as L, time as T):

K_{f_i} = the Freundlich constant (L^3M)

n = dimensionless Freundlich exponent

Freundlich isotherms are commonly used to model the sorption of PFAS on activated carbon.

Langmuir

The Langmuir empirical nonlinear sorption model is defined as in Equation (130).

$$\omega_{s_i} = \frac{\Gamma_{max} K_L \rho_{aq_i}}{1 + K_L \rho_{aq_i}} \tag{130}$$

where (parameter dimensions are dark green font with mass as M, length as L, time as T):

Γ_{max} = total number of sorption sites per mass of sorbent (M^{-1})

K_L = Langmuir constant, assuming a constant sorbate affinity for all surface sites (L^3M^{-1})

4.6 Transformation Reactions

Transformation reactions convert CoCs into new compounds. Transformation reactions lead to assimilation of CoCs in space and time or creation of new CoCs.

In many cases, new compounds pose limited risk. A notable exception is the formation of VC from chlorinated ethenes. Ideally, CoCs are fully mineralized to carbon dioxide, water, and inorganic ions, in which case the new compounds pose little risk. Consider conversion of decane ($C_{10}H_{22}$) and oxygen to water and carbon dioxide, as shown in Equation (131).

$$2C_{10}H_{22} + 32O_2 \rightarrow 20\ CO_2 + 22H_2O \tag{131}$$

Given combustion of decane, the reaction occurs rapidly, effectively as a single step. In the case of biogeochemical processes oxidation of decane (Figure 73), the net reaction is conceptualized as a cascade of reactions. Sequentially C-H bonds are replaced by C-O bonds. Rates of reactions are governed by transport and/or the kinetics of microbially mediated processes. Further information regarding biogeochemical conversions of petroleum liquids to CO_2 and H_2O can be in Irianni-Renno and others (2015) and Askarani and others (2024).

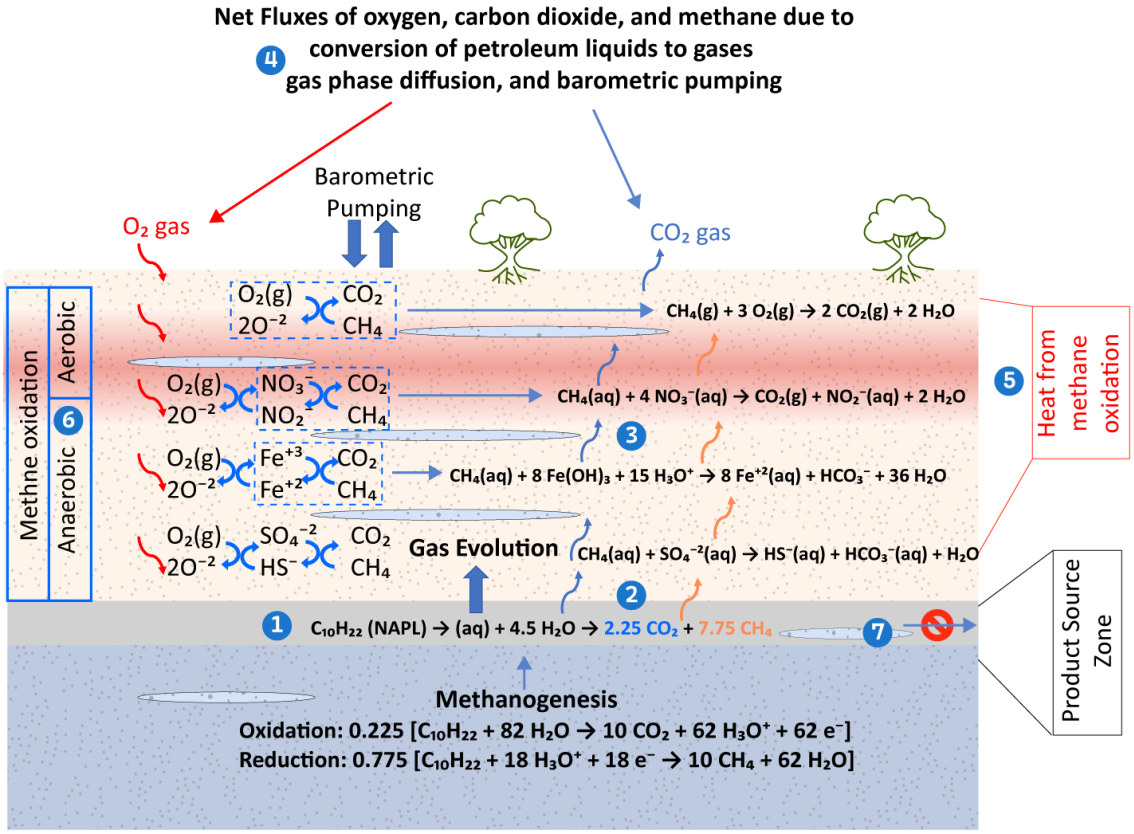

Figure 73 - Conceptual model for mineralization of decane in a product zone around the water table.

Radioactive decay provides another example of transformations. As an example, radioactive decay of ^{238}U occurs as a series of steps ($^{235}U \rightarrow ^{234}Th \rightarrow ^{234}Pa \rightarrow ...$) with emissions of alpha particles, beta particles, and gamma rays leading to losses of electrons, protons, and neutrons; and new compounds with reduced molecular weights. Half-lives of reaction steps range from billions of years to seconds. Radon-226, a stable intermediate ($t_{1/2}$=1,600 years), is a common issue for indoor air (EPA, 2016).

The reactions provided in Equation (131) as well as radioactive decay of ^{238}U are irreversible under natural conditions. Potentially reversible transformation reactions include precipitation-dissolution of Se and As minerals. Per Figure 74, zero, first, and pseudo first-order models can be used to quantify rates of losses of CoCs. Networks of reactions can be modeled as networks of irreversible pseudo first-order reactions following Eykholt (1999) and Figure 60.

	Zero-Order	First-Order	Pseudo First-Order
	A ➔ ...	A ➔ ...	A+B... ➔...
Data Plots	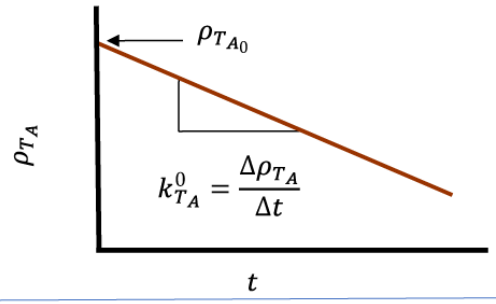	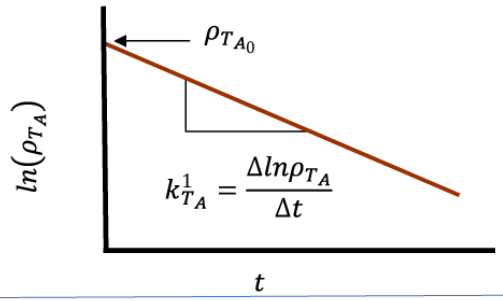	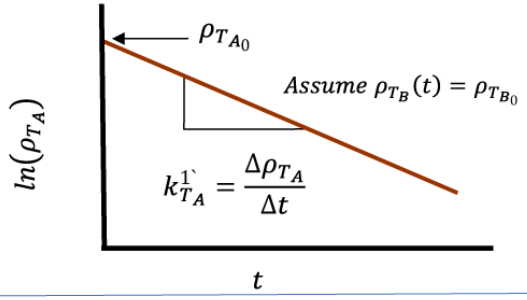
Governing Equation	$M^{\dot{0}}_{T_A} = \frac{d\rho_{T_A}}{dt} = -k^0_{T_A}(\rho_{T_A}) = -k^0_{T_A}$	$M^{\dot{1}}_{T_A} = \frac{d\rho_{T_A}}{dt} = -k^1_{T_A}(\rho_{T_A})$	$M^{\dot{1`}}_{T_A} = \frac{d\rho_{T_A}}{dt} = -k^{1`}_{T_A}(\rho_{T_A})(\rho_{T_B})$
Boundary Condition	$\rho_{T_A}(0) = \rho_{T_{A_0}}$	$\rho_{T_A}(t_{1/2}) = \frac{0.5\rho_{T_A}}{\rho_{T_A}}$	$\rho_{T_A}(t_{1/2}) = \frac{0.5\rho_{T_A}}{\rho_{T_A}}$
Conc. v. t	$\rho_{T_A}(t) = \rho_{T_{A_0}} - k^0_{T_A}t$	$\rho_{T_A}(t) = \rho_{T_{A_0}} e^{-0.693 t_{1/2A} t}$ $\quad t_{1/2_A} = \frac{-k^1_{T_A}}{\ln(2)}$	$\rho_{T_A} = \rho_{T_{A_0}} e^{-0.693 t`_{1/2A} t}$ $\quad t`_{1/2_A} = \frac{-k^{1`}_{T_A}}{\ln(2)}$
Mass v. t	$M^{0\dot{}}_{T_A}(t) = \frac{d}{dt}(\rho_{T_A} - k^0_{T_A}t) = -k^0_{T_A}$	$M^{\dot{}}_{T_a} = \frac{d}{dt}(\rho_{T_A} e^{-0.693 t_{1/2A} t}) = -0.693 t_{1/2A} \rho_{T_A} e^{-0.693 t}$	$M^{\dot{}}_{T_a} = \frac{d}{dt}(\rho_{T_A} e^{-0.693 t_{1/2A} t}) = -0.693 t_{1/2A} \rho_{T_A} e^{-0.693 t}$

Figure 74 - Zero, first-order, and pseudo first-order models for transformation reactions. Superscript 0, 1, and 1` denote zero-, first-, and pseudo first-order models for transformation reactions, respectively. ρ_{T_A} is the total mass compound A for all contaminant phases per volume porous media. Rate constants k are specific to the order of the model and the basis in which concentrations are expressed.

4.6.1 Zero Order

The premise of the zero-order model is that losses are a constant $k^0_{T_A}$ ($ML^{-3}T^{-1}$) in time, independent of the amount of the compound of concern remaining. We propose that petroleum NSZD rates are zero order. A zero-order model for petroleum NSZD is predicated on the narrow range of reported NSZD rates (1,000 to 10,000 L/hectare/yr) based on vadose zone gas fluxes and generated heat (Kulkarni et al., 2022; McCoy et al., 2015) for sites with varying amounts and types of LNAPL. Collaborative results are presented in Karimi Askarani and Sale (2025) wherein daily NSZD rates are near constant for periods of hundreds to thousands of days at petroleum sites based on generated heat from eight locations.

4.6.2 First Order

The premise of a first-order rate model is that losses are solely proportional to the amount of the CoC of concern present by a rate constant $k^1_{T_A}$ (T^{-1}). Strictly speaking, a first-order model is applicable to single-reactant reactions such as decay of a radioactive isotope.

4.6.3 Pseudo First Order

Most transformation reactions involve two reactants. Mechanistic reactions between two reactants are facilitated by collisions between the reactants. Rates of reactions are a function of the frequency of collisions, which is dependent on concentrations and the kinetic energy (temperature) of the reactants, activation energies for reactions, and the status of microbial communities (microbial enzymes as catalysts) mediating reactions.

To facilitate computation viability, the pseudo first-order model assumes that one of the reactants is present in a constant amount independent of time. Given a fixed amount of the second reactant, the reaction rate constant is dependent on the concentration of the first reactant, and the pseudo first rate constant is $k^{1`}_{T_A}$ (1/T).

As an example, consider PCE being reduced by zero valent iron (ZVI) in a constructed ZVI permeable reactive barrier (Figure 75), as described in Equation (132). (note the horizontal line in the middle represents the summation of the two half-reactions are being combined to form the overall balanced redox reaction).

$$C_2Cl_{4(aq)} + 8H^+ + 12e^- \rightarrow 2CH_{4(aq)} + 4Cl^-_{(aq)} \text{ (reduction of PCE)}$$

$$6Fe^0_{(s)} \rightarrow 6Fe^{+2}_{(aq)} + 12e^- \text{ (oxidation of ZVI)}$$

$$C_2Cl_{4(aq)} + 8H^+ + 6Fe^0 \rightarrow 2CH_{4(aq)} + 4Cl^-_{(aq)} + 6Fe^{+2}_{(aq)} \quad (132)$$

In truth, the reaction presented in Equation (132) is far more complicated. The reaction is the result of multiple steps. Additional information regarding ZVI treatment of chlorinated solvents can be found in Tratnyek and others (2014).

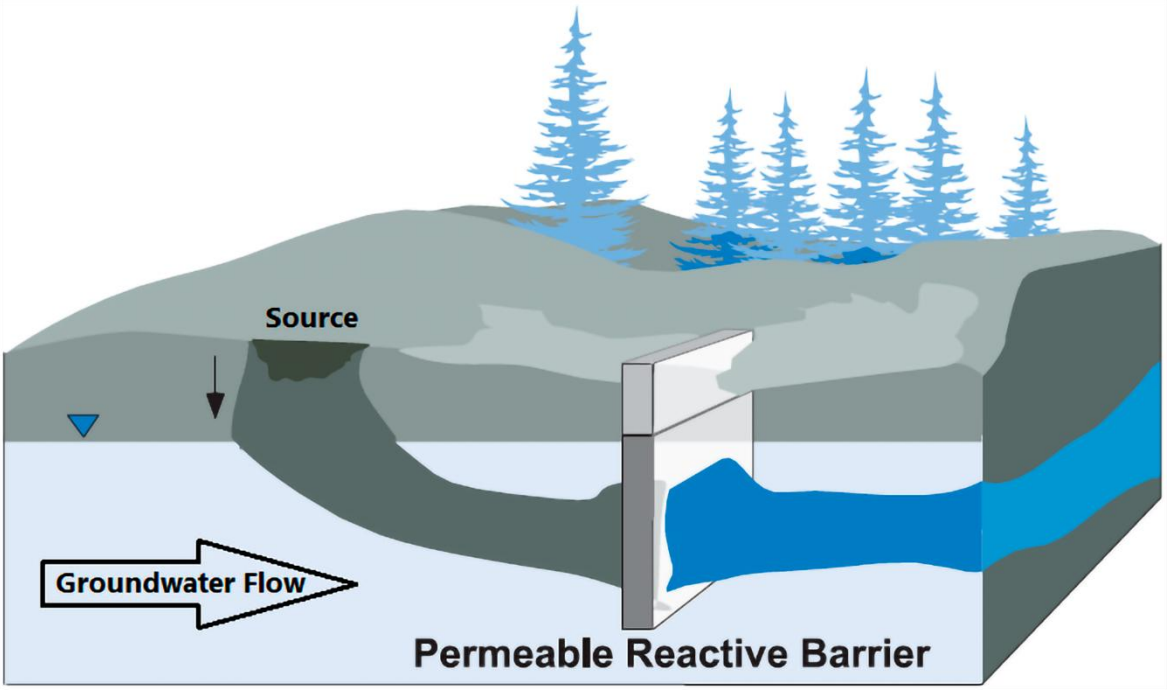

Figure 75 - Concept of a permeable reactive barrier (PRB) with a simplified version of the reactions described by Equation (132). In a simplified version of the chemistry, Water entering the barrier on the left contains the products on the left-hand-side of Equation (132) and water exiting on the other side of the barrier has the products shown on right-hand-side of Equation (132) (modified from Gillham & O'Hannesin, 1994).

4.6.4 Second Order

Another approach to modeling transformation reactions, not included in Figure 74, is second-order models per Equation (133).

$$\dot{M}^2_{T_A} = \frac{d\rho_{T_A}}{dt} = -k^2_{T_A}\left(\rho_{T_A}\right)\left(\rho_{T_B}\right) \qquad (133)$$

Equation (133) states that the rate at which contaminant A is transformed is a function of a second-order rate constant, the concentration of A, and the concentration of B. Pragmatic applications of second-order rate models in subsurface media can be challenging. For one thing, forecasting transport of two compounds may be required. As such, rates are a function of transport. Advancement of second-order models for transformation of contaminants is beyond the scope of this text. A useful reference for second-order reactions, where transport constrains rates, is Chen and others (2016).

4.7 Exercises Related to Section 4

At the completion of Section 4 the reader should be able to complete Exercise 28 Exercise 29.

5 Contaminant Transport Modeling

Here we integrate and apply material from the preceding sections through an introduction to contaminant transport modeling. We consider the use of mathematical methods and relevant field data to quantitively forecast contaminant concentrations and/or contaminant fluxes, in time and space, at relevant scales, in support of sound decisions for managing subsurface releases. Our vision of contaminant transport modeling involves concurrent consideration of multiple governing processes in heterogeneous media—for example, concurrent consideration of advection, diffusion, and reactions in both transmissive and low-*k* zones. Topics in this section include the following.

- why we model,
- the art of modeling,
- governing equations,
- mathematical approaches,
- transport modeling using heterogeneous advective-diffusive-reactive (HADiffR) models, and
- key takeaways from modeling systems of transmissive and low-*k* zones.

References for those wanting to know more are provided throughout this Section. At the end of this section the reader should be able to complete Exercises 30 through 39 in Section 7.

5.1 Why We Model

Having a clear vision of what one is trying to achieve is central to modeling. In the words of Yogi Berra, *"If you don't know where you are going, you might not get there,"* or *"you will end up somewhere else."*

5.1.1 Academic research

Three fundamental themes in academic research are 1) collecting data relevant to a specific topic, 2) developing or employing mathematical methods, and 3) testing the validity of conceptualized processes and/or computational methods using independent data sets.

Agreement between independent data sets and models often leads to a sense of confirmation of beliefs or hypotheses. Given confirmation, we feel more comfortable believing that what we thought was true is true. Notably, human nature is to have a bias toward seeing confirmation in results.

The alternative to confirmation is potentially disconcerting disproof, or contradictions to hypotheses. As suggested by Dr. Art Corey (1919–2018), professor at Colorado State University, students and researchers are often disappointed by disproof of hypotheses. Meanwhile, they may be on the verge of discovering something important they

did not know. In research, few rewards are greater than taking the first step into spaces unseen by others and turning the lights on for the first time. To quote John Milton (1608–74), from *Paradise Lost*, "*So easy it seemed once found, which yet unfound most would have thought impossible…" (lines 500–1).*

Notably, disproof of results from contaminant transport models have been a keystone to some of the greatest breakthroughs in subsurface contaminant hydrology. Examples include realizing assimilative transformation reactions leading to stable aqueous plumes (e.g., Wiedemeier et al., 1999), realizing that NSZD leads to stable NAPL bodies (e.g., Mahler et al., 2012), and that storage and release of CoCs to and from low-*k* zones leads to asymmetrical breakthrough curves with long tails (e.g., Chapman & Parker, 2005).

5.1.2 Modeling to Develop Quantitative CSMs (Conceptual Site Models)

We cannot see directly into the subsurface. Thus, we are forced to use sparse temporal and spatial field data, our understanding of depositional environments, and experience with specific CoCs to develop CSMs. CSMs typically begin with cross-sectional or 3D block sketches of a site, as shown in Figure 76. Primary CSM elements in Figure 76 include the following:

- an upgradient chlorinated solvent source zone being flushed and contained by a low-permeability wall and a pumping well,
- treated water being returned to the aquifer via a surface recharge pond,
- clean water flooding beneath homes, forming a barrier that mitigates vapor intrusion to indoor air in homes,
- chlorinated solvents in low-*k*-zones, sustaining chlorinated solvents in transmissive zones, and
- assimilation processes, reducing contaminant loading to surface water

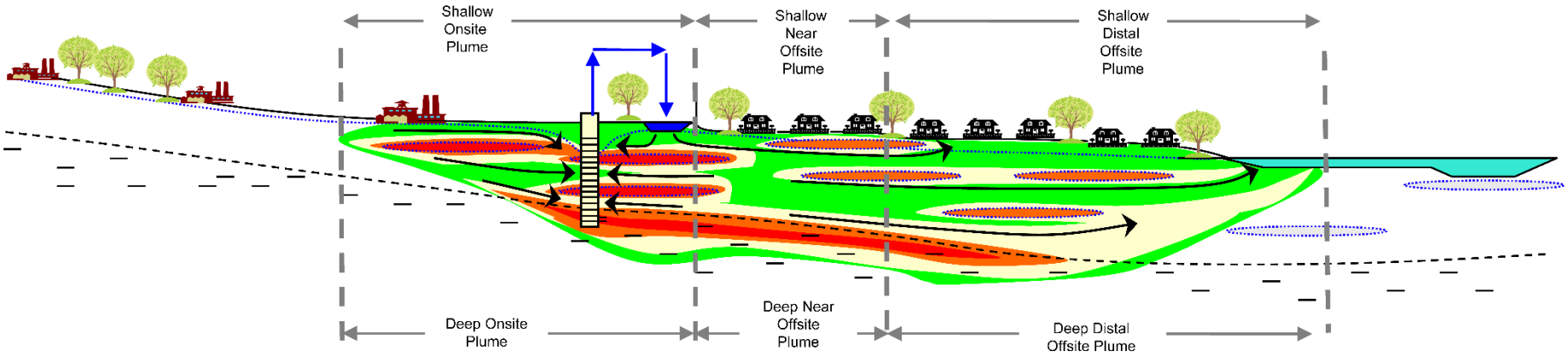

Figure 76 - Example of a Conceptual Site Model (CSM). Aqueous concentrations decrease by orders of magnitude with colors from red, to orange, to tan, to green, with white being below detection level. The water table is a blue dotted line. Dotted black lines surround fine-grained materials. The dashed black line indicates the contact between shallow coarse-grained material and deep fine-grained material. Black arrows represent general direction of groundwater flow. Some notable components of the conceptual model include: an upgradient chlorinated solvent source zone is flushed and contained by a low permeability wall and a pumping well, treated water is returned to the aquifer via a surface recharge pond, clean water from the pond flows beneath homes and forms a barrier that mitigates vapor intrusion to indoor air, chlorinated solvents in low-k zones sustain chlorinated solvents in transmissive zones, and assimilation processes reduce contaminant loading to the surface water on the right side of the diagram (modified from Sale & Newell, 2011).

CSMs often include complementary contaminant transport models. Transport models add quantitative elements to CSMs, including:

- formal tabulations of site attributes in the form of input parameters;
- a basis for evaluating future spatial distributions of CoCs, fluxes of fluids, and fluxes of contaminants in space and time that can be used to assess risk; and
- a basis for evaluating and designing remedies, for example, estimating pumping rates from wells, understanding the general timing of reductions in risk, and understanding the broad benefits of low-permeability walls

5.1.3 Modeling to Standardize Approaches to Decision-Making

Consistent application of mandates advanced in environmental regulations can be daunting. To the positive, mandates requiring use of specific models for similar problems can provide a degree of consistency as to what responsible parties need to do. An underlying assumption in mandating use of specific models is that the models are predicated on sound site characterizations and mathematical approximations of relevant transport processes.

5.1.4 Modeling to Forecast Future Conditions

Much like forecasting weather in the short- and long-term, we are often driven to forecast the distributions and fluxes of CoCs in the short- and long-term. As an example, nuclear waste repositories in the USA are mandated to consider transport over a period of 10,000 years based on half-lives of radioactive isotopes of concern (US Nuclear Regulatory Commission, 2000).

Short-term forecasts tend to be easy and long-term forecasts, more difficult. As an example, wondering what the weather will be like in the next hour, one can look out the window, employ experience with similar conditions, and make a fair guess. Errors in projections over short periods are likely to be less significant than errors that can accumulate over longer periods. Continuing with weather, it is common for 10-day forecasts to be far more flawed than next-day weather forecasts and detailed weather forecasts beyond 10 days to be justifiably viewed with a high degree of skepticism.

With respect to process-based mathematical contaminant transport models, factors constraining the accuracy of longer-term forecasts include the following.

- **Flawed CSMs** – We are frequently surprised when we compare contaminant transport model predictions with actual outcomes (Bredehoeft, 2003, 2005). A common source of surprise is the use of incomplete CSMs. All too often we do not know what we do not know until we see forecasts diverging from measured outcomes.
- **Assumptions** – Pragmatically, mathematical models are predicated on simplifying assumptions. First-principle of science and math derivations of transport solutions, as advanced in this text, are among the best ways to appreciate assumptions. With

time, errors introduced through assumptions can grow. Examples of simplifying assumptions include the following items.

- Methods used to model governing processes including linear isotherms for sorption and pseudo first-order-rate models for transformation reactions.
- Systems with complex spatial and temporal boundary conditions can require use of numerical methods wherein derivatives are approximated by deltas (e.g., $\frac{dh}{dx} \rightarrow \frac{\Delta h}{\Delta x}$ as $\Delta x \rightarrow 0$) and model domains are discretized in space and time. Absent sufficient discretization of space or time, numerical methods can produce flawed results. Chapman and others (2012) describe a need to use up to 10,000 nodes to capture 2D advective diffusive transport in a 1 m by 1 m tank study with continuous transmissive sand and inclusions of low-*k* clay. Per Chapman and others (2012), a simple way to test the rigor of numerical methods is to iteratively reduce spatial and temporal discretizations until results converge to constant values. The dependence of results on spatial discretization is demonstrated in Farhat and others (2020).

- **Adequacy of site characterization data** – Embracing heterogeneity leads to a potential need to resolve spatial distributions of porous media properties and contaminants in all phases; including permeability, solid-phase sorbents, redox conditions, and microbial ecologies. Absent sufficient understandings of the modeled domain, including the architecture of heterogeneities, it becomes difficult to reach high levels of confidence in long-term quantitative forecasts.
- **Overparameterization** – Having multiple model inputs can lead to a scenario referred to as overparameterization where (a) models can be fit to field data using substantially different sets of input parameter values and (b) different calibrations provide consequentially different forecasts. As a simple example, high water levels can be obtained in groundwater flow models (e.g., MODFLOW) by using either high recharge rates or low transmissivities (Hughes et al., 2017). Forecasts based on elevated recharge versus low transmissivities can be substantially different. A more complex example is integrated hydrologic models (e.g., MIKE SHE) that can holistically consider stochastic precipitation, runoff infiltration, groundwater flow, and surface water flow coupled with stochastic representation of transport parameter values (Abbot et al., 1986).

5.2 The Art of Using Models

A widely acknowledged scientific conundrum is that *all models are wrong, but some are useful* (e.g., Box (1976) and Skogen et al., 2021). We would add that many models can be essential, given the alternative of intuitive guessing. However, modeling requires thoughtful framing of problems, sound appreciation of methods, and recognition of limitations. The art of modeling (in our case, transport modeling) is a matter of soberly

recognizing the limitations of models all the while embracing insights that can be gained. Like writing a paper on a difficult topic, one needs to take great care in advancing truths that are defensible while remaining honest with respect to often intriguing but speculative possibilities.

An early step in modeling is resolving the questions or objectives to be addressed. Some questions are comparatively easy, such as estimating water-production rates from wells or drains used in hydraulic containment systems. In contrast, rigorously forecasting distributions of contaminant concentrations, absent containment features or rapid rates of degradation, at large distances, and times, can be difficult.

Models commonly need to be calibrated and/or tested using relevant data—in most cases, relevant field data. Calibration involves using the spatial distribution of a measurable quantity such as hydraulic head or aqueous solute concentrations to find a *best fit* set of input parameter values that are consistent with site attributes. A notable problem with embracing heterogeneous aquifers is that water quality from purged monitoring wells is likely to reflect in-well blending of water with likely nonuniform solute concentrations weighted to transmissive zones. Heterogeneous distributions of PCE in the Borden Aquifer are presented in Figure 77. The blending of solute concentrations in monitoring wells, completed in heterogeneous aquifers, is rarely considered when using monitoring well data to support conventional contaminant transport models. One always needs to reflect on the validity of data used in calibrating and/or verifying models.

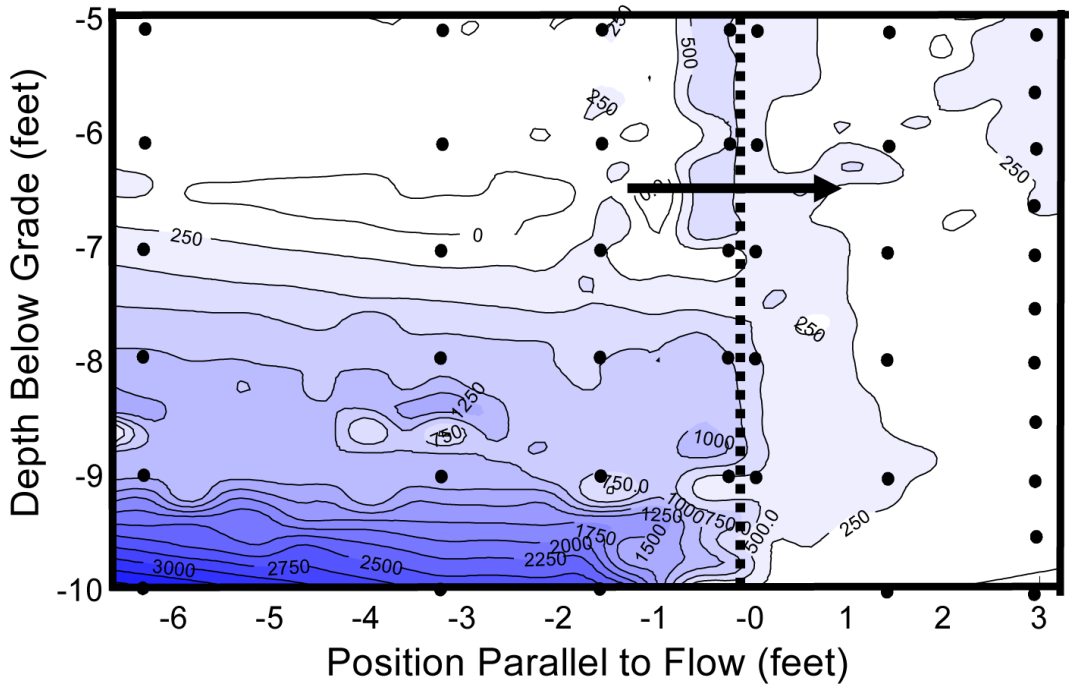

Figure 77 - Unpublished data from Canadian Forces Base Borden, Ontario, Canada. Prototype field demonstration of an electrolytic permeable reactive barrier (PRB) indicated by dotted vertical line (Gilbert, D. & Sale, T.C., 2002). Aqueous phase PCE concentrations (μg/L) in cross-section with a slight vertical exaggeration, based on samples collected from multiple-level point-sampling devices located at solid black circles. Black arrow indicates direction of groundwater flow. Porous media are Great-Lakes, North-American, transmissive, littoral, beach sands underlain by low-*k* lacustrine silts and clays.

Model testing involves using additional relevant data sets to verify that model forecasts are reasonable. Testing data sets can be historical data that were not used for calibration. Alternatively, post-modeling audits can be conducted by collecting additional data after the modeling project is complete to assess the accuracy of predictions. A sobering observation is that it is not uncommon for post modeling audits to observe significant variations from predictions (Anderson & Woessner, 2002; Bredehoeft, 2003, 2005).

Mathematical formulations used to address transport in heterogeneous domains, including storage and release of contaminants in low-*k* zones, need to be tested. Historically hydrodynamic dispersion, modeled as a Fickian process, has been used to account for nonuniform distributions of permeability (e.g., Bear, 1972; Fetter, 1999; Freeze & Cherry, 1979). Unfortunately, as outlined in Gillham, Sudicky and others (1984) and Payne and others (2008), models relying on hydrodynamic dispersion to account for heterogeneities miss:

- focused flow through preferential flow paths,
- often consequential long tailing concentrations of contaminants in monitoring wells associated with release of stable contaminants from low-*k* zones to transmissive zones, and
- assimilation of contaminants in low-permeability zones.

Publications addressing limitations of using hydrodynamic dispersion to account for heterogeneities include Sudicky and others (1985), Harvey and Gorelick (2000), Anderson and Woessner (2002), Sale and others (2008), Payne and others (2008), Hadley and Newell (2014), and Cherry (2023).

Lastly, as with any measured quantities, model inputs have uncertainties. Uncertainties arise from methods used to estimate values (e.g., aquifer tests, tracer tests) as well as difficulties in quantifying spatial and temporal variations in inputs. Exercising all inputs governing results through plausible ranges provides a basis for identifying plausible outcomes. Unfortunately, exercising inputs through plausible ranges often leads to results with such broad outcomes as to be of uncertain value.

The observational approach advanced by Peck (1969) is a laudable approach to managing uncertainties. The observational method has been used by geotechnical engineers for over 75 years as an approach for addressing uncertainties inherent with subsurface conditions and earthen materials. Although observational methods are not unique to geotechnical engineering, "*the observational method*" has a specific and restricted meaning as established by Peck (1969). In brief, application of the observational method in remediation includes the following steps (adapted from Peck, 1969):

1. site investigation sufficient to establish a general SCM, but not necessarily in detail;
2. assessment of the most probable conditions (extent, transport, and fate of contaminants) and the most unfavorable conceivable deviations from these conditions;

3. establishment of the remedial design based on a working hypothesis of behavior anticipated under the most probable conditions;
4. selection of parameters and locations to be observed as remediation proceeds and calculation of anticipated values based on the working hypothesis;
5. selection in advance of contingency plans for foreseeable significant deviation of the observational findings from those predicted based on the working hypothesis;
6. measurement of parameters to be observed and evaluation of actual conditions; and
7. modification of the plans for remediation considering the observational results.

Using models in conjunction with the observational approach provides bases for the following outcomes:

- resolving likely future conditions and plausible consequential variations;
- establishing relevant monitoring to resolve plausible consequential variations from anticipated outcomes; and
- aiding the development of contingency plans for plausible consequential variations.

5.3 Governing Equations

Governing equations with temporal and spatial boundary conditions are the foundation of analytical and numerical transport models. Categories of governing equations considered for transport modeling include (a) groundwater flow, (b) solute transport via advection, and (c) solute transport via advection and diffusion. Additional terms can be added to governing equations to address reactions including solute sorption and transformations. Fluid or solute sources-sinks are introduced via additional terms in governing equations or temporal and/or spatial boundary conditions. Not addressed herein are governing equations for problems involving multiple fluid phases, flow in fractured media, and transport via soil gases. The purpose of our advancing governing equations is to (a) engage the reader in mathematics as a language for quantitative advancement of governing principles, (b) support recognition of imposed simplifying assumptions, and (c) provide a foundation for analytical and numerical modeling schemes.

5.3.1 Groundwater Flow for Fully Saturated Media Under Confined Conditions

Following Anderson and Woessner (2002) and McWhorter and Sunada (1977) a general governing equation for confined flow, of a fully saturating incompressible fluid with constant density, in porous media, given measured values of k_x, k_y, and k_z colinear to the x, y, and z axes is as shown in Equation (134).

$$\frac{\delta}{\delta x}\left(k_x \frac{\rho_i g}{\mu_i}\frac{\delta h_i}{\delta x}\right) + \frac{\delta}{\delta y}\left(k_y \frac{\rho_i g}{\mu_i}\frac{\delta h_i}{\delta y}\right) + \frac{\delta}{\delta z}\left(k_z \frac{\rho_i g}{\mu_i}\frac{\delta h_i}{\delta z}\right) = S_s \frac{\delta h_i}{\delta t} \qquad (134)$$

Assuming water is the fluid of interest and ignoring temperature effects on the density and viscosity of water, $k\frac{\rho g}{\mu}$ can be replaced by hydraulic conductivity (K), as in Equation (135).

$$\frac{\delta}{\delta x}\left(K_x\frac{\delta h}{\delta x}\right)+\frac{\delta}{\delta y}\left(K_y\frac{\delta h}{\delta y}\right)+\frac{\delta}{\delta z}\left(K_z\frac{\delta h}{\delta z}\right)=S_s\frac{\delta h}{\delta t} \tag{135}$$

Transgressing toward classroom aquifers, assuming that directional hydraulic conductivity values are not a function of position (a homogeneous domain), allows hydraulic conductivity to be pulled out of the spatial derivative, as shown in Equation (136).

$$K_x\frac{\delta h^2}{\delta x^2}+K_y\frac{\delta h^2}{\delta y^2}+K_z\frac{\delta h^2}{\delta z^2}=S_s\frac{\delta h}{\delta t} \tag{136}$$

Transgressing further toward classroom aquifers, assuming that hydraulic conductivity values are not a function of direction (i.e., an isotropic domain), allows directional hydraulic conductivity values to be replaced by a single hydraulic conductivity value, as in Equation (137)

$$K\left(\frac{\delta h^2}{\delta x^2}+\frac{\delta h^2}{\delta y^2}+\frac{\delta h^2}{\delta z^2}\right)=K\nabla^2 h=S_s\frac{\delta h}{\delta t} \tag{137}$$

Given steady-state conditions, steady groundwater flow in a homogeneous, isotropic material can be represented as shown in Equation (138).

$$\nabla^2 h=0 \tag{138}$$

5.3.2 Advective-Reactive Solute Transport

Given Darcy velocities from a groundwater flow model ($v_{w_x}, v_{w_y}, v_{w_z}$), the solution for transport of a dilute solute, solely by advection, in a homogeneous isotropic porous media, ignoring solute concentration effects on fluid density is shown in Equation (139).

$$-\frac{\delta\left(v_{w_x}\rho_{aq}\right)}{\delta x}-\frac{\delta\left(v_{w_y}\rho_{aq}\right)}{\delta y}-\frac{\delta\left(v_{w_z}\rho_{aq}\right)}{\delta z}=\frac{\delta\rho_{aq}}{\delta t} \tag{139}$$

Employing a first-order rate model for loss of contaminants via transformation reactions and a constant ratio for the distribution of sorbed and aqueous contaminants as captured by a retardation coefficient (R) for sorption reactions. The model is as shown in Equation (140).

$$-\frac{\delta\left(v_{w_x}\rho_{aq}\right)}{\delta x}-\frac{\delta\left(v_{w_y}\rho_{aq}\right)}{\delta y}-\frac{\delta\left(v_{w_y}\rho_{aq}\right)}{\delta y}-\lambda\rho_{aq}=R\frac{\delta\rho_{aq}}{\delta t} \tag{140}$$

5.3.3 Advective-Diffusive-Reactive Solute Transport

Starting with an anisotropic, heterogeneous media with seepage velocities and effective diffusion coefficients, D_e, measured in the x, y, and z directions, a mathematical description of transport is shown in Equation (141).

$$-\frac{\delta\left(v_{w_x}\rho_{aq}\right)}{\delta x}-\frac{\delta\left(v_{w_y}\rho_{aq}\right)}{\delta y}-\frac{\delta\left(v_{w_y}\rho_{aq}\right)}{\delta y}+\frac{\delta}{\delta x}\left(D_{e_x}\frac{\delta\rho_{aq}}{\delta x}\right)+\frac{\delta}{\delta y}\left(D_{e_y}\frac{\delta\rho_{aq}}{\delta y}\right)\frac{\delta}{\delta z}\left(D_{e_z}\frac{\delta\rho_{aq}}{\delta y}\right)=\frac{\delta\rho_{aq}}{\delta t} \quad (141)$$

Assuming a homogeneous porous media with respect to seepage velocities and diffusion coefficients, the velocities can be pulled out of the spatial derivatives as in Equation (142).

$$-v_{w_x}\frac{\delta\rho_{aq}}{\delta x}--v_{w_y}\frac{\delta\rho_{aq}}{\delta y}--v_{w_z}\frac{\delta\rho_{aq}}{\delta z}+D_{e_x}\frac{\delta^2\rho_{aq}}{\delta x^2}+D_{e_y}\frac{\delta^2\rho_{aq}}{\delta y^2}+D_{e_z}\frac{\delta^2\rho_{aq}}{\delta x^2}=\frac{\delta\rho_{aq}}{\delta t} \quad (142)$$

And, again employing a first rate model for loss of contaminants via transformation reactions and a constant ratio of sorbed and aqueous contaminants captured by R for sorption reactions, then transport is described as shown in Equation (143).

$$-v_{w_x}\frac{\delta\rho_{aq}}{\delta x}-v_{w_y}\frac{\delta\rho_{aq}}{\delta y}-v_{w_z}\frac{\delta\rho_{aq}}{\delta z}+D_{e_x}\frac{\delta^2\rho_{aq}}{\delta x^2}+D_{e_y}\frac{\delta^2\rho_{aq}}{\delta y^2}+D_{e_z}\frac{\delta^2\rho_{aq}}{\delta x^2}-\lambda\rho_{aq}=R\frac{\delta\rho_{aq}}{\delta t} \quad (143)$$

Assuming groundwater flow is only in the x direction, then transport is described as in Equation (144).

$$-v_{w_x}\frac{\delta\rho_{aq}}{\delta x}+D_{e_x}\frac{\delta^2\rho_{aq}}{\delta x^2}+D_{e_y}\frac{\delta^2\rho_{aq}}{\delta y^2}+D_{e_z}\frac{\delta^2\rho_{aq}}{\delta x^2}-\lambda\rho_{aq}=R\frac{\delta\rho_{aq}}{\delta t} \quad (144)$$

Notably, groundwater flow directions can change temporally with changing seasons and/or in response to dynamic pumping of wells. Furthermore, groundwater flow directions change spatially as groundwater in transmissive zones moves around low zone inclusions. The assumption that groundwater flow is only in one direction is rarely the case.

Historically D_e values have commonly been inflated in zones with active groundwater flow to account for hydrodynamic dispersion (e.g., Cherry, 1979; Fetter 1999). Given water as the fluid of interest and *i* as the CoC of concern, an example of inflating D_e is given in Equation (145) where α (L) values are directional dispersity coefficients that align with the primary axes and are dependent on the size (scale) of the domain of interest.

$$D_{e_{(x,y,z),i}}=\alpha_{(x,y,z),i}v_{w_x}+S_w\phi\tau_{(x,y,z)}D_{m_i} \quad (145)$$

Regarding longitudinal α values (α_L), we advance our opinion that typically, concentrations at the leading and trailing ends of plumes in transmissive zones are primarily governed by storage and release of contaminants in low-*k* zones via diffusion and slow advection. As such, longitudinal dispersion (direction of groundwater flow) is not a critical parameter.

Regarding transverse α values (α_T), we agree with Cherry (2023) that transverse mixing is best seen as a weak process. For example, using laboratory scale transverse α values on the order 1 cm or less. Primary arguments for small transverse α values include the following.

- Description of plumes based on point versus monitoring well based aqueous concentration measurement show limited transverse mixing at large downgradient distances. Limited transverse mixing is supported by Guilbeault and others (2005), van der Kamp and others (1994), and their supporting references. Limited transverse mixing is also supported by Figure 44. We argue that dilute concentrations seen in conventional monitoring wells in plumes are more reflective of in-well mixing of heterogeneous aqueous concentrations in plumes weighted to transmissive zones than hydrodynamic dispersion in aquifers.
- Large mixing due to dispersion imposed in models dilutes aqueous concentrations in transmissive zones in ways that erroneously limit concentration gradients, driving storage of contaminants in low-*k* zones in plumes. In our opinion, widespread documentation of consequential CoC concentrations in low-*k* zone in plumes (i.e., Boggs et al., 1992; Chapman & Parker, 2005; Parker et al., 2008) supports dispersive mixing in plumes as being a weak process.
- Mechanistically, the basis for large transverse mixing process is unclear. Payne and others (2008) argue that hydrodynamic dispersion is mechanistically analogous to a Fibonacci series. Given this perspective Payne and others (2008) argue that, per our perspectives and those of Cherry (2023), transverse mixing is best seen as a weak process.

Our perspective on dispersity values is one perspective in a space with many perspectives. We encourage those wanting to know more to consider Zech and others (2023), Zech and others (2019), Zech and others (2015), and supporting references.

As an alternative to having a single PDE for the modeled domain and invoking dispersion to account for heterogeneities, separate PDEs can be employed for transmissive and low-*k* zones. Separate PDEs are linked by equating either aqueous concentrations and/or fluxes at transmissive low-*k* zone boundaries. PDEs and computational approaches, given separate PDEs for transmissive and low-*k* zones, are developed in detail in Section 5.5.

5.3.4 Scaling REV-Based Governing Equations up to Field-Scale Problems

Sections 5.3.1 to 5.3.4 are predicated on balances performed on representative elements of volume (REVs) as introduced in Section 2.8.5 and Figure 15. REVs need to be large enough that they can be treated as uniform media with respect to dependent variables (h and ρ_{aq}) and constants (including $\phi, v_w, D_e, R, \lambda$). Dependent variable values (h or ρ_{aq}) are treated as point values applying to the centroid of the REV.

In granular media, the dimensions of an REV need to exceed the size of individual grains. As a generalization, the dimensions of an REV in a uniform porous media are likely to be on the order of 10s of grains in all dimensions. Given grain sizes on the order of 1 μm (clay) to 1 mm (fine sand) REVs are on the order of 10^{-9} to 1 cm^3. Given fractured media, REVs are likely to be much larger. In the case of sparse fractures, it can be impractical to resolve a useful REV volume. Concurrently, REVs need to be small relative to the scale at which dependent variables and physical properties governing coefficients are measured.

Classically, in fluid mechanics, we employ viscosity μ_i as a phenomenological proportionality constant to move from molecular to REV scales. For groundwater, we use hydraulic conductivity (K) to move from REV to laboratory scales and transmissivity (T) to move from laboratory to field scales. Phenomenological models are predicated on the impracticability of resolving small-scale attributes at a large scale. Phenomenological constants are based on ratios of observed fluxes divided by driving gradients ($i.e., K = -\frac{q}{dh/dl}$).

For uniform classroom aquifers, governing PDEs with initial and boundary conditions can be solved for systems with simple initial and boundary conditions. In general, the scale at which portions of subsurface bodies might be treated as homogeneous is on the order of cubic centimeters to cubic meters. Examples include laboratory scale columns and tanks with uniform porous media and some eolian sand deposits. Beyond laboratory scales, natural occurring porous media are, in our experience, not uniform.

For groundwater flow, use of transmissivity to get to field scale problems arguably can work. Theis (1967) states, "*the simple and useful model for problems of wellfield development*" (p. 146). In support of Theis, Figure 78 presents a geologic cross-section of a heterogeneous section of the Denver Basin aquifer, Colorado, USA. The depositional environment is mass-wasting associated with uplift of the modern Rocky Mountains, USA. Figure 79 displays observed and modeled water levels in four wells in a nine-well wellfield with dynamic pumping over 6 years. Modeled water levels are predicated on 1) using transmissivity to address field scale processes and 2) superposition in time and space of the Theis solution for water levels around a pumping well (Theis, 1935). Close agreement between observed and modeled water levels supports the use of transmissivity as a scaling factor for groundwater flow at a wellfield scale. Figure 80 presents dynamic pumping water levels in an, Aquifer Storage and Recovery wellfield in the Denver Basin, USA over an operational period of 5 years using the methods of Lewis and others (2016).

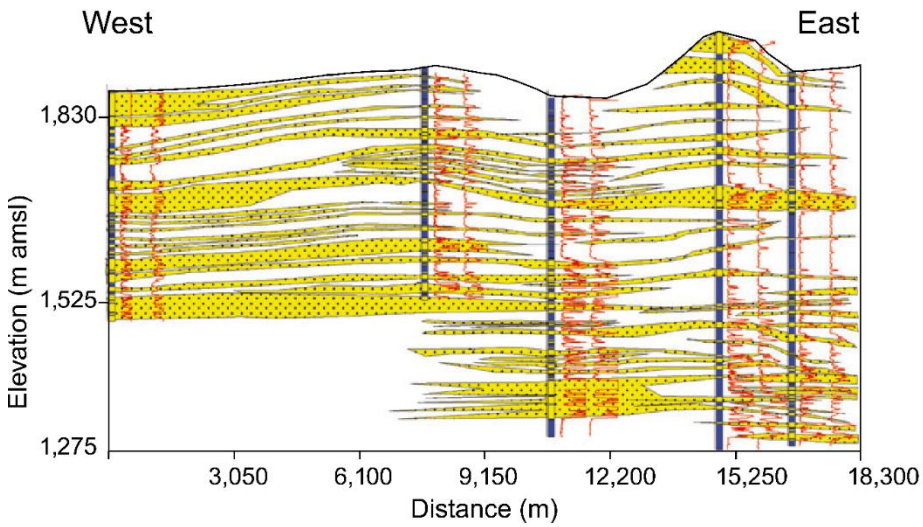

Figure 78 - Stylistic occurrences of transmissive sandstones (white) and low-*k* siltstones and shales in a Denver basin aquifer wellfield, Colorado, USA (after Lewis et al., 2016). Stratigraphy is based on resistivity and natural gamma geophysical logs (orange lines).

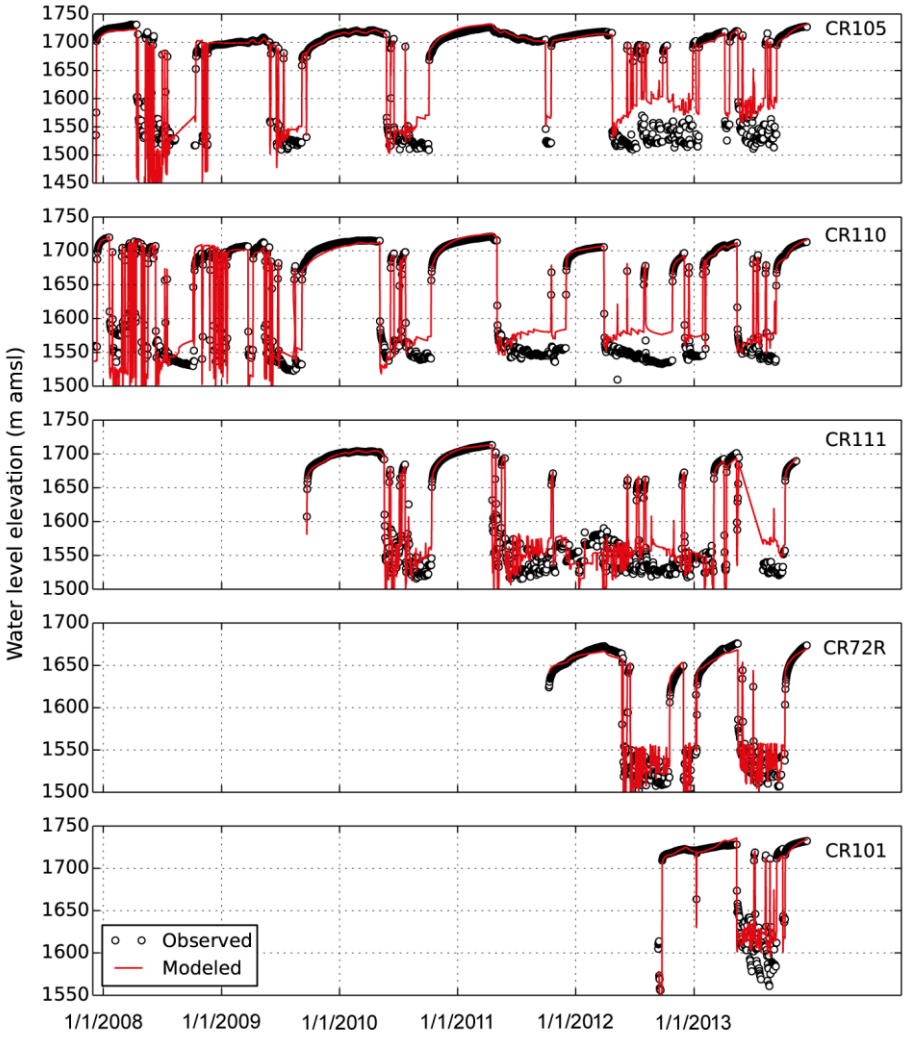

Figure 79 - Observed and modeled water levels in five wells in a nine-well Denver Basin aquifer wellfield, from Lewis and others (2016).

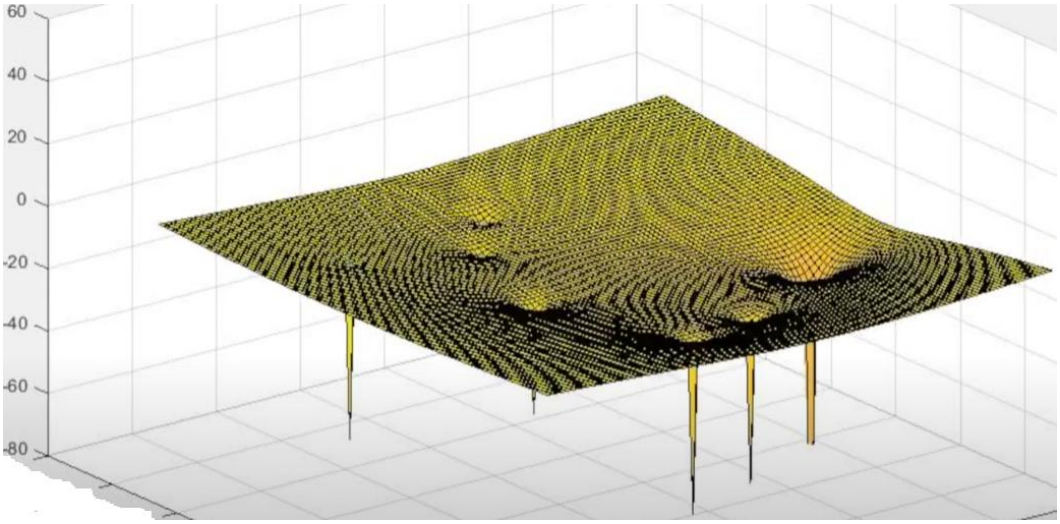

Figure 80 - An animated version of the ASR wellfield water levels in the Denver Basin, Colorado, USA are shown in this video.

For contaminant transport modeling, dispersion has been widely employed to address field-scale transport in heterogeneous media. Per Cherry (2023), use of dispersion to address the transport is, "*at best, misleading and at worst simply wrong*". We agree with Cherry's observations. Adding to Cherry's observations we offer the thought that the absence of storage in and release of contaminants from low-*k* zones in models invokes the knowledge that advection-dispersion paradigms have irreconcilable shortcomings.

5.4 Modeling Methods

Modeling contaminant transport can be approached using empirical, analytical, and numerical methods. Each approach has merits and limitations.

5.4.1 Empirical Methods

Per Merriam-Webster's Unabridged Dictionary, Merriam-Webster (n.d.), "empirical" refers to "*originating in or relying or based on factual information, observation, or direct sense experience usually as opposed to theoretical knowledge*." Empirical approaches include curve fitting, regression analysis, and machine learning. As empirical models are based on data, they have the potential to reflect what we know about governing processes as well as aspects of problems that may be transparent to us.

As an example of an empirical method, Sale (2001) advances decline curve techniques for forecasting LNAPL recovery using dual pump recovery wells as shown in Figure 81a. Decline curve methods are widely used in upstream petroleum production to forecast production from oil and gas wells (Fetkovich et al., 1996). Figure 81b shows cumulative production versus time indicating declining recovery rates attributable to depletion of recoverable LNAPL. Extension of the curve by hand or regression provides a simple means to anticipate future production.

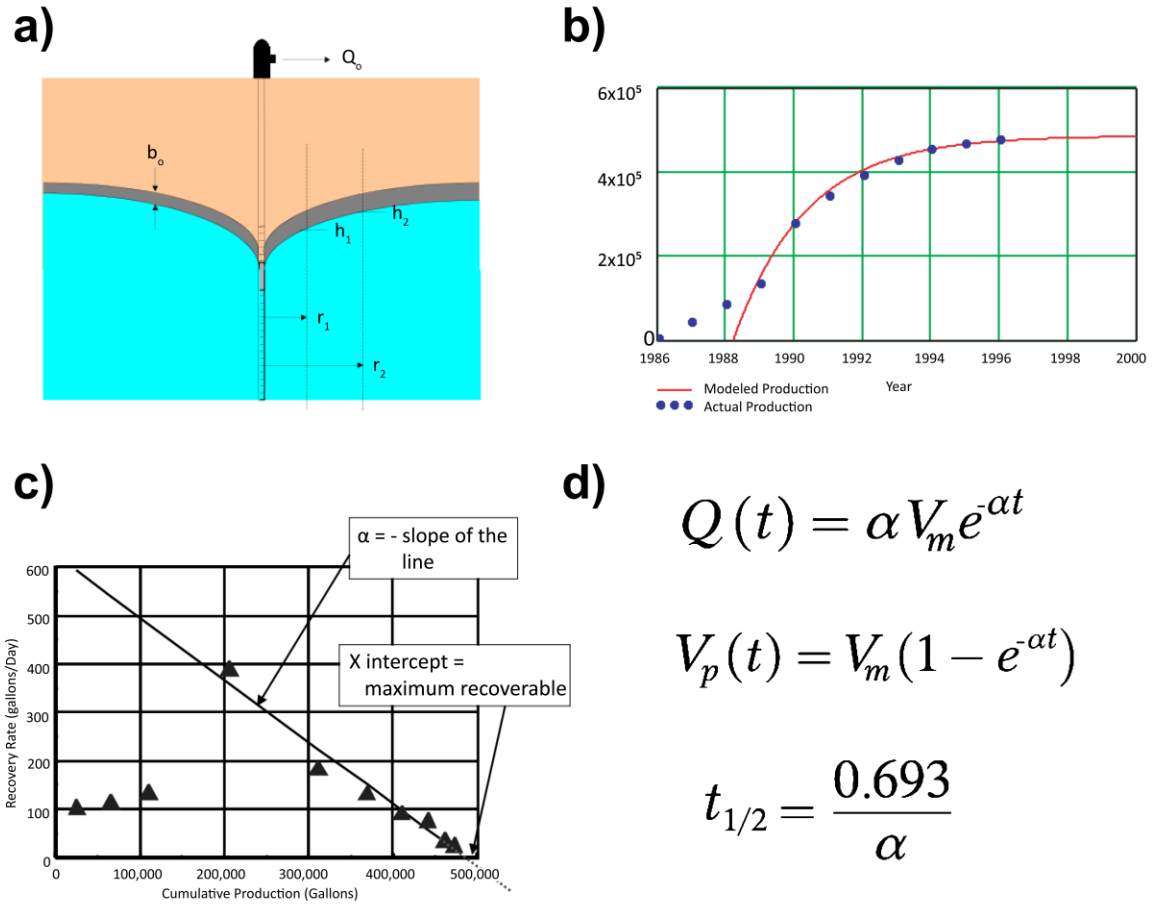

Figure 81 - Decline curve analysis for LNAPL production from a dual pump LNAPL recovery well. a) Schematic cross section showing well with a shallow pump to collect LNAPL (gray) and a deep pump to create a drawdown cone in the underlying water (blue) to enhance flow of LNAPL to the well. b) Cumulative volume of NAPL recovered declines with time. c) Recovery rate decreases with the x-intercept indicating the maximum recoverable volume (V_m). d) Expressions for the production rate (Q) and the cumulative volume produced (V_p) with time as well as the half-life of the production project (after Sale, 2001).

More rigorously, following oil and gas production decline forecasting methods, Figure 81c shows recovery rate versus cumulative production. Linear regression of the data over the period of production decline provides the x intercept which is an estimate of maximum recoverable LNAPL (V_m). The slope of the line provides a first-rate constant (α) that can be used to estimate LNAPL recovery rates ($Q(t)$), cumulative production as a function of time ($V_p(t)$), and the time it takes for production rates to fall by half ($t_{1/2}$) as shown in Figure 81d.

Appealing aspects of empirical approaches include:

- computational simplicity, and
- so long as governing processes are constant, the data reflects all that is governing outcomes, even if we do not know all the governing processes.

Limitations to empirical approaches include:

- high quality data is needed for the model outcomes to be correct;
- sufficient, potentially large, temporal data sets may be needed to accurately forecast future conditions;

- spatial and/or temporal changes in governing conditions can be missed; and
- results are generally not transferable to other sites.

5.4.2 Analytical Methods

Analytical solutions begin with a mass or volume balance performed on a REV, as advanced in Section 2.9.5 and the preceding introduction to governing equations. Balances are predicated on inflow minus outflow being equated to a change in a stored quantity with time. Balances provide governing equations in the form of ODEs or PDEs. Applying initial and boundary conditions leads to exact closed form solutions. As an example, a solution for one-dimensional diffusion into an infinite low-*k* zone is presented in Section 3.3.2. Appealing aspects of analytical solutions include:

- often (but not always) analytical solutions are computationally simple;
- as advanced by Morel-Seytoux (1932–2022), a professor at Colorado State University, USA, analytical solutions speak to us regarding governing processes, building our intuition as to how things work;
- solutions for common sets of governing equations and boundary conditions can be found in existing publications, including Carslaw and Jaeger (1959); and
- results for specific spatial and/or temporal points are resolved without having to computationally march through time and/or space.

Limitations to analytical approaches include:

- obtaining analytical solutions for complex heterogeneous settings can be difficult or impossible; and
- spatial and/or temporal changes in governing conditions may not be accounted for.

5.4.3 Numerical Methods

Common numerical methods employed in flow and transport models are finite difference and finite element. Other numerical methods include integrated finite differences, boundary integral methods, and analytical element methods (Anderson & Woessner, 2002; Strack, 2017). Finite difference methods discretize (subdivide) space into 2D grids or 3D boxes. Finite element methods discretize space into 2D or 3D elements. Similarly, time is divided into increments. Results for specific spatial and/or temporal points are resolved by computationally marching through time and space.

Following Chapman and others (2012), examples of spatial discretization of an approximately 1 m by 1 m sand tank study using transport models HydroGeoSphere, FEFLOW, and MODFLOW/MT3DMS are presented in Figure 82.

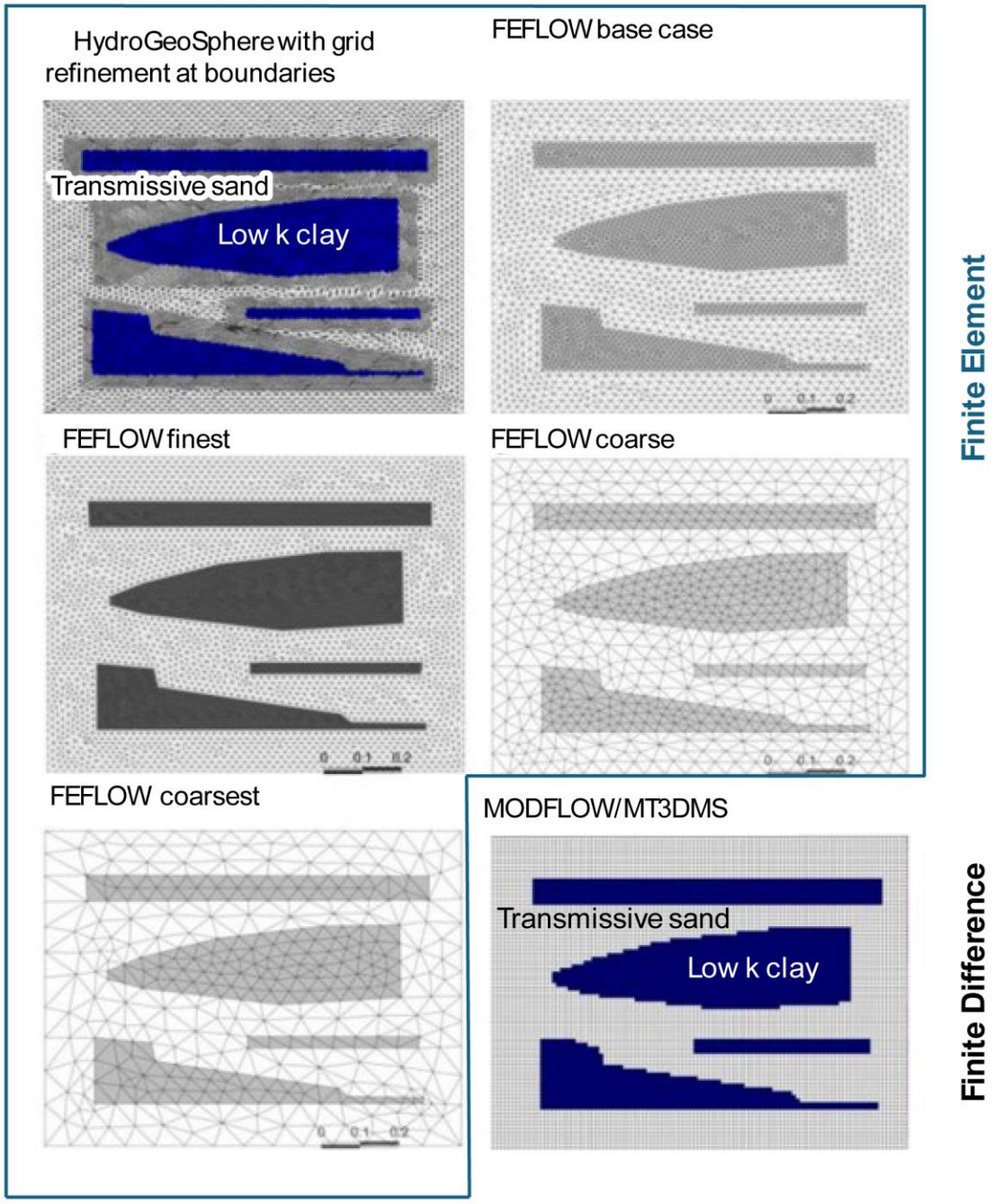

Figure 82 - Spatial discretization of a 1 m^2 sand tank study after Chapman and others (2012).

Potential advantages to finite element methods, over common finite difference methods, include capturing the shapes of irregular boundaries more effectively, avoiding the need to carry high-resolution grids across the entire domain of interest, and reduced numerical dispersion in transport problems.

Many are introduced to numerical methods in upper-level graduate courses—in the authors' experience, up to four upper-level graduate courses. Our goal here is to introduce finite differences as a basis for appreciating the merits and limitations of numerical methods. Those wanting to know more about finite difference approaches should look to

Anderson and Woessner (2002) and Thomas (1995). As a word of caution, using models with insufficient appreciation of the complexities of numerical methods can lead to egregious errors.

Groundwater flow as an example

As an introduction to finite numerical difference methods, brief consideration is given to one-dimensional modeling of groundwater flow in a confined aquifer following McWhorter and Sunada (1977).

1. Using the mathematical definition of a derivative, spatial and temporal derivatives are approximated using increments Δx and Δt for the first derivatives in Equation (146).

$$\lim_{\Delta x \to 0} \frac{\Delta h}{\Delta x} \xrightarrow{yields} \frac{\delta}{\delta x} h \qquad \lim_{\Delta t \to 0} \frac{\Delta h}{\Delta t} \xrightarrow{yields} \frac{\delta}{\delta t} h \tag{146}$$

2. Using differences to form approximate solutions to governing equations, consider a confined aquifer in cross-section as shown in Figure 83. To keep track of finite difference grids ranging from 1 to "NR", "i" is used as a counter. Time is addressed by marching through time in temporal discretization of Δt. Head values have grid number subscripts "i" and time step superscripts "n". For a set of three adjacent cells their positions are indicated by *i-1*, *i*, and *i+1*.

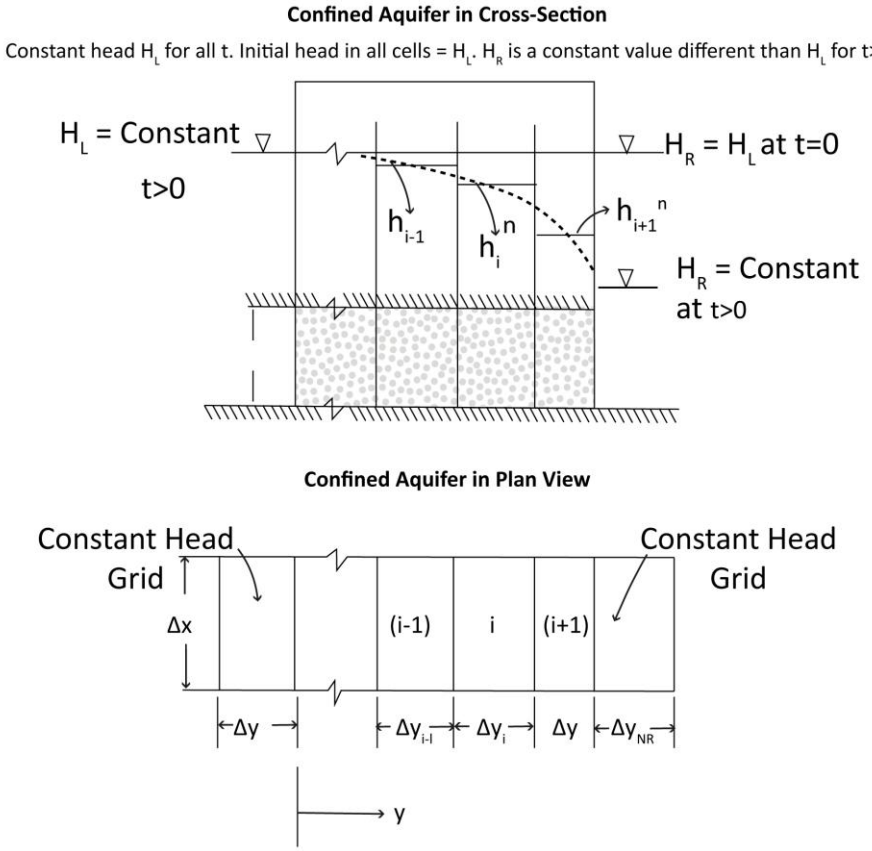

Figure 83 - Application of the finite difference method to 1D confined flow of groundwater. Head values have grid number subscripts "i" and time step superscripts "n". For a set of three adjacent cells their positions are indicated by *i-1*, *i*, and *i+1*. after McWhorter and Sunada (1977).

For simplicity, K, b, Δx, and Δy are constant for each grid cell. Using T (transmissivity) for Kb and S for the storage coefficient, equating inflow minus outflow to the change in water stored in the cell yields Equation (147).

$$\left(-T\frac{h_i^n - h_{i-1}^n}{\Delta y}\right) - \left(-T\frac{h_{i+1}^n - h_i^n}{\Delta y}\right) = S\Delta y(\frac{h_i^{t+\Delta t} - h_i^t}{\Delta t}) \quad (147)$$

Setting $n = t$ in Equation (147) yields an *explicit finite difference scheme*. Beginning with known initial heads, all terms on the right-hand-side are known, and head at the future time can be solved as in Equation (148).

$$h_i^{t+\Delta t} = \frac{T\Delta t}{S(\Delta y)^2}\left(h_{i+1}^t + h_{i-1}^t\right) + h_i^t\left[1 - \frac{2T\Delta t}{S(\Delta y)^2}\right] \quad (148)$$

Using explicit solutions, marching through time calculations are a matter of arithmetic. A shortcoming for explicit solutions is that the stability of the solution is dependent on the solution constants and the discretization of space and time. For this case of 1D flow in a homogeneous domain with uniform discretization of time and space, the criterion for a stable solution is shown in Equation (149).

$$\frac{T\Delta t}{S(\Delta y)^2} < \frac{1}{2} \quad (149)$$

Failing to meet the stability criteria can lead to dramatic, erroneous oscillations in results. It is important to recognize that meeting the stability criteria does not guarantee accuracy. Care is needed with iteratively testing temporal and spatial discretization to verify convergence of results to values with acceptable accuracies and without erroneous oscillations. Given concerns with the stability of solutions and accuracy, uses of explicit solutions are less common.

Alternatively, unconditionally stable solutions can be obtained using *implicit finite difference* schemes wherein n in Equation (148) is set to $t + \Delta t$. Implicit solutions are stable independent of solution constants and discretization of space and time. Again, it is important to recognize that solution stability does not guarantee solution accuracy. The only way to confirm accuracy is to rerun the model with smaller time steps and also rerun with smaller spatial discretization and obtain essentially the same result. Rerunning with smaller time steps is fairly easy while reducing discretization usually involves more effort. By using $n = t + \Delta t$ and rearranging so that known terms are on the right-hand-side yields Equation (150).

$$h_{i+1}^{t+\Delta t} - \left(2 - \frac{S(\Delta y)^2}{T\Delta t}\right)h_i^{t+\Delta t} + h_{i-1}^{t+\Delta t} = \frac{S(\Delta y)^2}{T\Delta t}h_i^t \quad (150)$$

Using a matrix and a vector for the head solution, heads at future times are obtained by writing an equation for each grid element and solving a set of n equations with n for unknown future head values, as shown in matrix form by Equation (151).

$$\begin{bmatrix} 2-\frac{S`(\Delta y)^2}{T\Delta t} & 1 & 0 & 0 & 0 & 0 \\ 1 & 2-\frac{S`(\Delta y)^2}{T\Delta t} & 1 & 0 & 0 & 0 \\ 0 & 1 & 2-\frac{S`(\Delta y)^2}{T\Delta t} & 1 & 0 & 0 \\ 0 & 0 & 1 & \dots & 1 & 0 \\ 0 & 0 & 0 & 1 & 2-\frac{S`(\Delta y)^2}{T\Delta t} & 1 \\ 0 & 0 & 0 & 0 & 1 & 2-\frac{S`(\Delta y)^2}{T\Delta t} \end{bmatrix} \begin{bmatrix} h_1 \\ h_2 \\ h_3 \\ \dots \\ h_{n-1} \\ h_n \end{bmatrix}^{t+\Delta t} = \frac{S`(\Delta y)^2}{T\Delta t} \begin{bmatrix} h_1 \\ h_2 \\ h_3 \\ \dots \\ h_{n-1} \\ h_n \end{bmatrix}^{t} \quad (151)$$

Solving for the unknown future head values of Equation (151) yields Equation (152).

$$\begin{bmatrix} h_1 \\ h_2 \\ h_3 \\ \dots \\ h_{n-1} \\ h_n \end{bmatrix}^{t+\Delta t} = \begin{bmatrix} 2-\frac{S`(\Delta y)^2}{T\Delta t} & 1 & 0 & 0 & 0 & 0 \\ 1 & 2-\frac{S`(\Delta y)^2}{T\Delta t} & 1 & 0 & 0 & 0 \\ 0 & 1 & 2-\frac{S`(\Delta y)^2}{T\Delta t} & 1 & 0 & 0 \\ 0 & 0 & 1 & \dots & 1 & 0 \\ 0 & 0 & 0 & 1 & 2-\frac{S`(\Delta y)^2}{T\Delta t} & 1 \\ 0 & 0 & 0 & 0 & 1 & 2-\frac{S`(\Delta y)^2}{T\Delta t} \end{bmatrix}^{-1} \frac{S`(\Delta y)^2}{T\Delta t} \begin{bmatrix} h_1 \\ h_2 \\ h_3 \\ \dots \\ h_{n-1} \\ h_n \end{bmatrix}^{t} \quad (152)$$

The primary computational chore in solving the equations is inverting the diagonally dominant *n* by *n* matrix where *n* is the number of grid cell in the solution domain. Numerical model codes take advantage of the diagonal dominance of the matrix to advance efficient computational schemes to invert the matrix. Increasing dimensionality of the problem to 2D or 3D, leads to additional non-zero diagonals in the matrix. Given a 3D model, with a grid that is 10 by 10 by 10 cells (i.e., a total of 1,000 model cells), and the matrix needing inversion is 1,000 by 1,000 with a total of 10^6 terms.

Problems more complex than the example from McWhorter and Sunada (1977) typically include:

- each node being assigned unique properties for governing constants;
- finer spatial discretization in some areas to better resolve portions of the domain where dependent variables exhibit abrupt spatial changes;
- smaller time increments during some of the model time frame to capture dynamic events and expanded increments for other periods to reduce computational requirements;
- individual nodes being designated as constant head or constant flux boundaries;
- inclusion of temporally varying sources and sinks to account for spatial and temporal varying recharge and groundwater extraction; and
- expansion to two and three dimensions.

Solutes

Finite element and finite difference numerical methods for solute transport follow similar themes as groundwater flow methods. Some notable unique aspects of numerical solute transport modeling include the following items.

- Numerical method results can exhibit solute spreading greater than the input parameter values would produce due to *numerical dispersion* which results from the parameters of the discretized solution. It can be difficult to employ numerical models for transport without large-scale computationally driven dispersive mixing (Daus et al., 1985).
- Capturing concentration gradients driving diffusive storage and releases of contaminants to and from low-*k* zones can require mm–to–cm–scale spatial discretization of the domain of interest (Chapman et al., 2012) as discussed later in this section along with additional information on discretization.
- Groundwater flow models track the behavior of indifferentiable water molecules. As such, averaging by using scaling factors—for example, transmissivity (T) to scale up from hydraulic conductivity (K) for field-scale evaluations can be successful, as per our experience as well as the experience of Lewis and others (2016). Using solute transport models to track the movement of heterogeneously distributed solutes moving through heterogeneous domains of transmissive and low-*k* zones is a different matter. In our experience, the confidence gained through modeling groundwater flow does not carry over to solute transport modeling. Theis (1967) said the following.

*"The type of aquifer in which our homogeneous model of ground water flow is most grossly inadequate is that of dealing with transport phenomena… the simple and useful model for problems of wellfield development will mislead us if we apply it to problems of transport" (*p. 139).

Appealing aspects of numerical solute transport models include:

- the availability of well-tested codes with preprocessors, well-documented computational methods, and post processors, and
- the ability to model systems with complex geology, complex boundary conditions, and more less-idealized approaches for reactions.

Limitations to numerical solute transport modeling include:

- the need to computationally march through time and space to get to a position and time of interest;
- a need to parameterize many nodes or elements with multiple inputs;
- an increased potential for overparameterization, leading to nonunique forecasts;
- computational challenges to having sufficient spatial and temporal discretization's to capture storage and release of contaminants to and from low-*k* zones;
- a need for well-trained modelers with extensive familiarity with model codes, knowledge of the limitations of applied numerical methods, and abilities to manage large input and output data sets;
- a need for potentially expensive model licenses and/or computational resources; and

- potentially large levels of effort with related large costs.

Over the authors' careers, groundwater flow and solute transport codes (models) have seen tremendous advancement. Extrapolation of historical trends in numerical methods, computers, and modeling algorithms should leave all open to a future in which current constraints to numerical modeling may be addressed.

Numerical dispersion – Errors introduced using truncated series to approximate derivatives

Finite difference schemes do not necessarily provide accurate solutions. As shown in the following worksheet, numerical methods rely on approximations of first- and second-order derivatives using truncated Taylor series to approximate derivatives. As an example, the calculation vignette of Figure 84 shows the x direction is broken into increments of Δx. Similarly, other independent variables found in ODEs and PDEs derivatives including y, z, and t can be discretized. With increased numbers of spatial or temporal discretization, errors associated with truncated-series approximations increase. When using truncated-series approximations for derivatives, numerical spreading of contaminants, referred to as numerical dispersion, need to be appreciated.

Calculation Vignette
Errors Introduced Through Numerical Approximation of Derivatives

Head as a function of position x

$$h = f(x)$$

From the 1st principles of differential calculus

$$\frac{d}{dx}h = f`(x) = \lim_{\Delta x \to 0} \frac{(f(x+\Delta x) - f(x))}{\Delta x}$$

Applying Taylor's Theorem

$$f(x+\Delta x) = f(x) + \Delta x \frac{f`(x)}{1!} + \Delta x^2 \frac{f``(x)}{2!} + \sum_{n=1}^{\infty} \Delta x^{n+2} \frac{f^{n+2}(x)}{(n+2)!}$$

Solving for the 1st derivative using a forward difference scheme

$$\Delta x \frac{f`(x)}{1!} = f(x+\Delta x) - f(x) - \Delta x^2 \frac{f``(x)}{2!} + \sum_{n=1}^{\infty} \Delta x^{n+2} \frac{f^{n+2}(x)}{(n+2)!}$$

$$f`(x) = \frac{f(x+\Delta x) - f(x) - \Delta x^2 \frac{f``(x)}{2!} + \sum_{n=1}^{\infty} \Delta x^{n+2} \frac{f^{n+2}(x)}{(n+2)!}}{\Delta x}$$

$$f`(x) = \frac{f(x+h) - f(x)}{\Delta x} - \frac{\Delta x^2 \frac{f``(x)}{2!} + \sum_{n=1}^{\infty} \Delta x^{n+2} \frac{f^{n+2}(x)}{(n+2)!}}{\Delta x}$$

$$f`(x) = \frac{f(x+h) - f(x)}{\Delta x} - \Delta x \frac{f``(x)}{2!} + \sum_{n=1}^{\infty} \Delta x^{n+1} \frac{f^{n+2}(x)}{(n+2)!}$$

$$f`(x) = \frac{f(x+h) - f(x)}{\Delta x} - Error^{1st}_{Truncation} \qquad Error^{1st}_{Truncation}(\Delta x) = \Delta x \frac{f``(x)}{2!} + \sum_{n=1}^{\infty} \Delta x^{n+1} \frac{f^{n+2}(x)}{(n+2)!}$$

Solving for the 2nd derivative

$$f(x+\Delta x) = f(x) + \Delta x \frac{f`(x)}{1!} + \Delta x^2 \frac{f``(x)}{2!} + \sum_{n=1}^{\infty} \Delta x^{n+2} \frac{f^{n+2}(x)}{(n+2)!}$$

$$\Delta x^2 \frac{f``(x)}{2!} = f(x+\Delta x) - f(x) - \Delta x \frac{f`(x)}{1!} - + \sum_{n=1}^{\infty} \Delta x^{n+2} \frac{f^{n+2}(x)}{(n+1)!}$$

$$f``(x) = 2 \frac{f(x+\Delta x) - f(x) - \Delta x \frac{f`(x)}{1!} - \sum_{n=1}^{\infty} \Delta x^{n+2} \frac{f^{n+2}(x)}{(n+2)!}}{\Delta x^2}$$

$$f``(x) = 2 \frac{f(x+\Delta x) - f(x)}{\Delta x^2} - 2 \frac{\Delta x f`(x) - \sum_{n=1}^{\infty} \Delta x^{n+2} \frac{f^{n+2}(x)}{(n+2)!}}{\Delta x^2}$$

$$f``(x) = 2 \frac{f(x+\Delta x) - f(x)}{\Delta x^2} - 2\Delta x^{-1} f`(x) - \sum_{n=1}^{\infty} \Delta x^n \frac{f^{n+2}(x)}{(n+2)!}$$

$$f``(x) = 2 \frac{f(x+\Delta x) - f(x)}{\Delta x^2} - Error^{2nd}_{Truncation} \qquad Error^{2nd}_{Truncation}(\Delta x) = 2\Delta x^{-1} f`(x) - \sum_{n=1}^{\infty} \Delta x^n \frac{f^{n+2}(x)}{(n+2)!}$$

Figure 84 - Calculation vignette showing introduction of errors due to numerical approximation of derivatives.

Unfortunately, spatial and temporal discretization has often been limited by limited computer memory and speed. In the mid-1980s, numerical groundwater flow models with 100 or so elements executed on standard office computers might be run overnight to provide sufficient time to complete calculations. In the 2020s, improved office computational hardware have made one million or even 10 million node models computationally possible.

Discretization needs to be based on using sufficiently small sizes so that the employed truncated series approximations for derivatives are valid. Mathematically determining the necessary discretization is difficult (Thomas, 1995). As an alternative, we suggest that discretization be tested by (a) comparing results to exact analytical solutions when possible and (b) conducting numerical experiments to demonstrate convergence of results to constant values with decreasing discretization. The seminal text *Numerical Partial Differential Equations* (Thomas, 1995) states, "*. . . it is dangerous for a person who is using difference methods not to understand what it means for a solution to converge*" (pp. xi).

Finally, one approach to improving the fidelity of contaminant transport simulations is the use of Total Variation Diminishing (TVD) schemes within numerical groundwater models that must be assigned nonzero dispersivity vales (Langevin & Guo, 2006). TVD is not a standalone groundwater model but a numerical technique embedded in advection-dispersion solvers such as those in MT3DMS, SEAWAT, or similar transport codes. Unlike standard schemes, which are stable but overly diffusive, TVD schemes apply slope limiters that maintain stability and accuracy simultaneously. By ensuring that the "total variation" in concentration does not increase from one time step to the next, TVD formulations capture plume migration with reduced numerical artifacts, providing results that more closely represent physical transport processes in aquifers (Cox & Nishikawa, 1991).

5.5 Solute Transport Using Heterogeneous Advective Diffusive Reactive Models

Quoting Theis (1967) "*we need a new conceptual model, containing the known heterogeneities of the natural aquifer, to explain the phenomena of transport in groundwater*" (pp. 148). A central tenet of Modern Subsurface Contaminant Hydrology is to move beyond textbooks for students and practitioners that rely on hydrodynamic dispersion as a means of accounting for heterogeneities and, correspondingly, ignoring slow advective and diffusive-driven storage and release of contaminants in low-k zones. As advanced in this text and by others, critical flaws to the hydrodynamic dispersion approach to heterogeneities include potentially missing:

- rapid transport of solutes through fractional preferential transmissive zones with limited transverse mixing;
- early time assimilation of solutes in plumes into low-*k* zones via slow advection and diffusion;
- late time tailing concentrations of solutes in plumes due to hysteretic releases from low-*k* zones, leading to asymmetrical, non-Gaussian breakthrough curves; and
- nonuniform assimilation of contaminants via reactions in transmissive versus low-*k* zones.

Reflecting on the National Research Council's worry *"that the nation might be wasting large amounts of money on ineffective remediation efforts"* (1994, pp. 1), we find ourselves contemplating (a) the degree to which not accounting for contaminants stored in low-*k* zones may have hindered historical efforts by practitioners to conceptualize and manage risks posed by releases and (b) the opportunities posed by modern conceptualizations of transport. For example, we can ponder whether models predicated on using dispersion to account for heterogeneities, leading to Gaussian breakthrough curves, were a common basis for proceeding with pump and treat remedies that all too often failed to restore aquifers. Widely recognized limitations of pump and treat remedies for restoration of aquifers are documented in Doty and Travis (1991), EPA (1989), Mackay and Cherry (1989), and Mercer et al., (1990).

Section 5.5 explores solute transport modeling predicated on heterogeneous advective-diffusive and reactive (HADiffR) transport modeling. HADiffR modeling, versus advective-dispersive models (ADMs), has seen broad attention in publications but is largely absent in textbooks. Payne and others (2008) is a notable textbook exception. Herein, consideration is given to:

- models developed at the Universities of Waterloo and Guelph in Ontario, Canada;
- analytical solutions for a two-layer scenario developed at Colorado State University, USA;
- review of high-resolution numerical modeling efforts advanced by Steve Chapman and Beth Parker of Guelph University, Canada; and
- semi-analytical/numerical methods for modeling matrix diffusion developed by Ron Falta of Clemson University, USA, and his colleagues.

5.5.1 Models Developed at the University of Waterloo and the University of Guelph

Through the late 1970s and 1980s, publications by researchers at the University of Waterloo, Ontario, Canada, advanced conceptual and mathematical models for advective-diffusive transport in domains composed of transmissive and low-*k* zones, as described in this section.

Freeze and Cherry (1979) – Toward the end of this classic textbook the authors present a nascent conceptualization of solute transport through a transmissive fracture with diffusive assimilation of solutes in the fracture via transverse diffusion into adjacent porous low-*k* matrix blocks, enhanced by sorption in the matrix blocks. The cited reference for the conceptualization is Foster (1975). In hindsight, nearly half a century ago Freeze and Cherry (1979) were largely spot on as to the primary implications of diffusion in heterogeneous media.

Tang and others (1981) – Analytical and numerical solutions are advanced for solute transport through a fracture with diffusive assimilation of solutes into adjacent porous low-*k* matrix blocks. Solutions are derived using *"coupled, one-dimensional partial*

differential equations: one for the fracture and one for the porous matrix in a direction perpendicular to the fracture" (pp. 556). Analytical solutions are derived by equating fluxes between transmissive and low-*k* zones. Similar results are achieved using analytical and high-resolution numerical methods. Results show that given a constant source, assimilation of solutes in the transmissive zones via diffusion into low-*k* zones provides a safety mechanism that reduces solute fluxes in transmissive zones.

The complement to an assimilative safety mechanism proposed by Tang and others (1981) is storage of contaminants in low-*k* zones. Low-flow domains in which contaminants are stored in subsurface bodies are absent when using conventional homogeneous ADEs to capture the implication of heterogeneities. A critical flaw to models predicated on homogeneous aquifers is that they lack zones that hysteretically store and release contaminants.

Gillham, Robins, and others (1984) – Diffusive transport in materials used as *contaminant barriers* is considered. Results validate the use of Fick's first equation to resolve diffusive fluxes of solutes in low-*k* media. Effective diffusion coefficients for low-*k* zone media are shown to be a function of porosity, sorption, and tortuosity. Notably, effective diffusion coefficients are independent of permeability.

Sudicky and others (1985) – Laboratory tank studies and analytical solutions are advanced for a 3-cm layer of transmissive sand bounded by 10-cm layers of low-*k* silts in a 100-cm two-dimensional laboratory tank. A chloride tracer is flushed through the tank parallel to the layers. Effluent concentrations of chloride are measured through time (Figure 85).

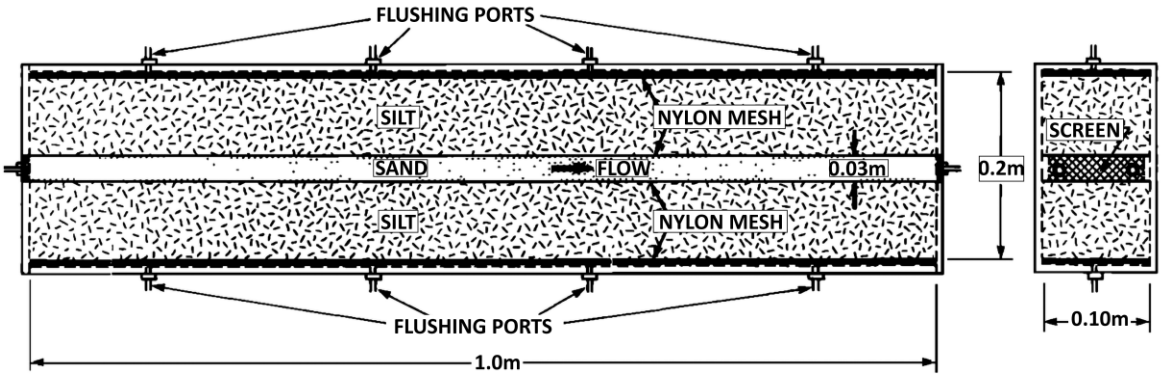

Figure 85 - Laboratory tank study with transmissive and low-*k* zones (modified from Sudicky et al., 1985**).**

Analytical solutions for nonreactive solutes are developed for solute concentrations in the transmissive zone. Following Tang and others (1981), heterogeneity is addressed using separate PDEs for transmissive and low-*k* zones. The PDEs are coupled using a boundary condition wherein fluxes between transmissive and low-*k* zones are equated. Complex analytical solutions for solute concentrations in the transmissive zone as a function of position and time are presented. Two solutions are advanced: a Thin-Layer Solution which assumes negligible transverse mixing within the sand layer (i.e., the

transverse concentration gradients across the thin sand are ignored), and a Thick-Layer Solution which assumes complete mixing within the sand layer. The following observations are drawn from the results (Figure 86).

- The arrival time of the tracer at the effluent end of the tank, 2 days, is accelerated relative to the bulk tank seepage velocity by preferential flow through the fractional (3-cm/20-cm) transmissive zone.
- Close agreement between laboratory and model results validates the principles of solute exchange between the transmissive and low-*k* zones via diffusion.
- After breakthrough at two days, effluent concentrations rise asymptotically toward a normalized concentration of 1. Over time, concentration gradients driving diffusion into the low-*k* silt layer decay and the rate at which the effluent concentration approaches the influent concentration slows. The area above the breakthrough curve reflects contaminant storage in the low-*k* zones. The area below the effluent curve, after the breakthrough of the source off signal at 9 days, reflects contaminants stored in low-*k* zones being released.
- Overall, the breakthrough curve is asymmetrical. The asymmetrical breakthrough response is contrary to Gaussian breakthrough curves associated with using ADE solutions, wherein hydrodynamic dispersion is used to address heterogeneities.

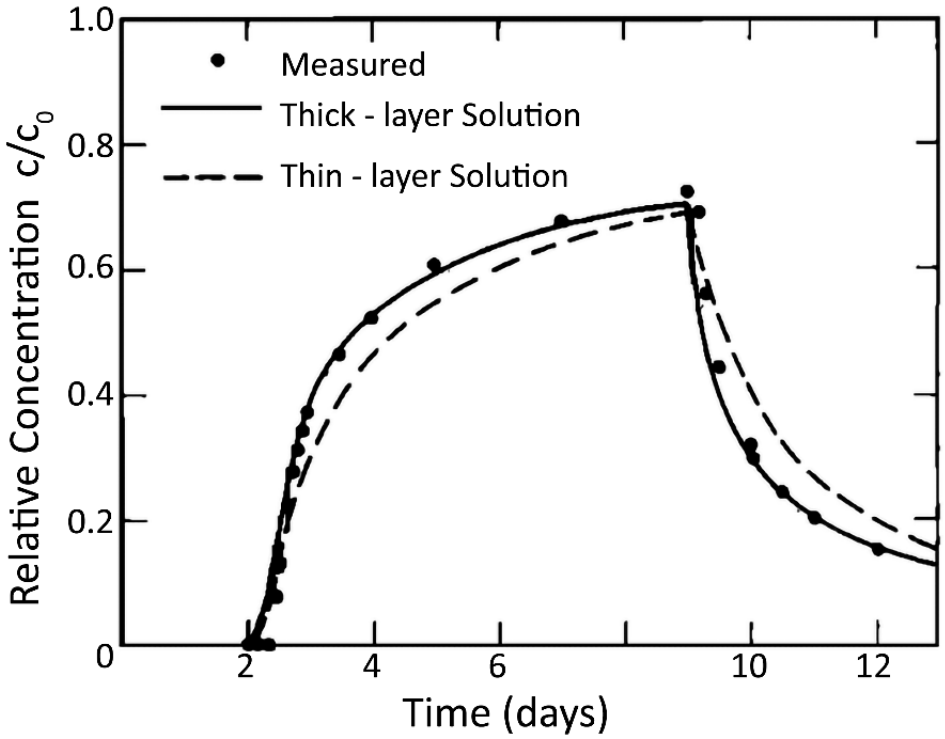

Figure 86 - Measured and modeled breakthrough curves from a laboratory tank study with transmissive and low-*k* zones, after Sudicky and others (1985). For the thick-layer solution, *Di* = 0 such that the sand layer is treated as completely mixed. For the thin-layer model *Di* ≠ 0 such that there is dispersion in the thin sand layer but *Dl* = 0 such that there is no dispersion in the surrounding silt (low-k zones)

We highlight the following key quotes from Sudicky and others (1985).

"Perhaps the most challenging problems facing groundwater hydrologists today concern the ability to make accurate prediction of arrival times and spatial patterns of toxic levels of a waste substance disposed of beneath the ground. Much of the difficulty can be attributed to the heterogeneous structure of the host medium which, for the most part, is comprised of an essentially unknown assemblage of strata having different hydraulic and chemical properties" (p. 1035).

"Because of the tailing of the breakthrough measurements, a departure from classical Fickian [dispersion based] transport is apparent" (p. 1035).

"Simulation of the measured breakthrough curves has demonstrated that molecular diffusion between strata is the main mechanism leading to strongly dispersed concentration patterns in layered porous media" (p. 1040).

"The observed tailing of the breakthrough curves, caused by the diffusive exchange of tracer between the strata in the layered system, is an indication of a significant departure from classical transport theory which assumes Fickian behavior when averaging is performed across the strata" (p. 1040).

"This [the paper] *suggests that conventional solute transport models based on an advection-dispersion equation that is integrated across the layering can lead to a significant error in the estimation of arrival times and spatial patterns of toxic concentrations during the development of the transport process in stratified aquifers"* (p. 1040).

Sudicky and McLaren (1992) – Development of a two-dimensional numerical model for steady state groundwater flow and transient contaminant transport in networks of randomly generated orthogonal fractures (FRACTRAN). Utilizes the Laplace Transform Galerkin (LTG) technique providing capability for larger-scale, long-term simulations. Recent papers utilizing this model include Parker and others (2010), Chapman and others (2013), Pierce and others (2018), Parker and others (2019), and Chapman and others (2021).

Therrien and Sudicky (1996) – Development of a three-dimensional discrete-fracture saturated-unsaturated numerical model for variably saturated flow and contaminant transport in porous or discretely fractured porous media (FRAC3DVS). This code has continued to evolve over the decades and is now referred to as HydroGeoSphere (HGS), which continues to be advanced and sold by Aquanty and has a strong user community. Papers utilizing this code for evaluation of diffusion/back-diffusion effects include Chapman and Parker (2005), Parker and others (2008) and Chapman and others (2012) described in more detail below.

Post-1980s publications addressing HADiffR transport by University of Guelph, Canada, and University of Waterloo, Canada, researchers are described in the following excerpts.

Chapman and Parker (2005) – High-resolution site characterization field data and modeling (using FRAC3DVS; Therrien & Sudicky, 1996) was advanced at an industrial field site with a chlorinated solvent DNAPL source zone. The site is a type 3 setting wherein a transmissive sand aquifer of *glaciofluvial origin* overlies a thick low-*k* silt-clay *glaciolacustrine aquitard*. Through the study period, the majority of the DNAPL source zone was isolated inside a sheet pile barrier. Field data and correlated high-resolution numerical modeling document the following observations:

- significant accumulation of contaminant mass in the underlying aquitard beneath the source zone and downgradient plume due to diffusion processes with mass storage enhanced by sorption;
- source isolation leading to diffusion-driven releases from the aquitard underlying the transmissive zone downgradient of the sheet-pile barrier;
- asymmetrical breakthrough curves consistent with laboratory scale studies advanced in Sudicky and others (1985);
- strong tailing of downgradient solute concentrations anticipated to exceed MCLs for periods of decades to centuries, with the highest concentrations at the aquifer-aquitard interface; and
- illumination of the principal problem at mature sites being contaminants stored in low-*k* zones.

Documenting a basis for modeling transport in heterogeneous media that works at both laboratory and field scales is a major advancement. Most notable is that models relying on dispersion to account for heterogeneities leads to the problem that dispersivity values used to estimate hydrodynamic dispersion are scale dependent (Gelhar, 1992). The corollary to scale-dependent dispersivity values is that results based on a single set of inputs are rigorously valid only at a single point in space and time. To quote Gelhar (1992):

> *"Both theoretical and experimental investigations have found that field-scale dispersivity are several orders of magnitude greater than lab-scale values for the same material; it is generally agreed that this difference is a reflection of the influence of natural heterogeneities which produce irregular flow patterns at the field scale"* (p. 1955).

Parker and others (2008) – Consideration is given to a type 3 setting wherein thin discontinuous low-*k* clay layers are embedded in a sandy transmissive zone. Field and modeling results using FRAC3DVS show that:

> *"back diffusion from one or a few thin clayey beds in a sand aquifer can cause contaminant persistence above MCLs in a sand aquifer long after the source zone initially causing the plume is isolated or removed."*(p. 86)

Furthermore, Parker and others (2008) states that:

> *"without careful inspection of continuous cores and high-resolution sampling, such thin clay beds, and their potential for causing long-term back-diffusion effects, can easily go unnoticed during site characterization"* (p. 86).

Parker and others (2008) underpins the principles that high-resolution site characterization and modeling can be essential to advancing sound SCMs.

Cherry (2023) – Cherry, adjunct professor in the School of Engineering at the University of Guelph (Guelph, Ontario, Canada), distinguished professor emeritus at the University of Waterloo (Waterloo, Ontario, Canada) and founder of the University Consortium for Field Focused Groundwater Research (since 1987), recognizes and expands upon the above issues associated with dispersion.

> *"I regret that it has taken me 43 years to get around to writing this warning about the established nonsense written about dispersion in the literature; unfortunately, this nonsense only became evident to me with the great advantage of hindsight"* (p. 145).
>
> *"The overall lesson I have taken away from this, and a few other experiences during my career, is that there are concepts published in books that, although they appear to be valid at face value, are nonetheless wrong. We must maintain inquiring minds and be vigilant to recognize when simulations deviate from the field evidence and be willing to adjust the written record and academic training accordingly. Concerning dispersion, more thinking is still needed"* (p. 147).
>
> *"The ADE (Advective Dispersive Equation) models can be useful and even necessary given lack of practical alternatives, if used with judgment and care"* (p. 146).

To the last point, the remaining sections of Section 5.5 present alternatives to ADE models. A relatively lengthy presentation of modeling results is predicated on the visions of advancing results from HAdiffR models for common scenarios for those who may not have the resources to conduct HAdiffR modeling. Notably, HAdiffR models are updated versions of classroom aquifers wherein stylized occurrences of low-*k* zones have been added. The main function of HAdiffR models is to redress historical omissions of storage and release of contaminants in and from low-*k* zones.

For us, embracing HADiffR models is analogous to recognizing that the sun, not the earth, is the center of the solar system. Given the correct conceptualization, all the pieces fall into an orderly assembly of logical principles that allow us to (a) understand and observe distributions of contaminants, (b) stylistically anticipate future conditions, and (c) advance better informed decisions regarding managing contaminant releases.

5.5.2 The Two-Layer Scenario and the Dandy-Sale Model

Inspired by Sudicky and others (1985), Chapman and Parker (2005), and the need for an alternative to ADMs, Sale and others (2008) advances an analytical solution for the two-layer scenario shown in Figure 87. This scenario provides an updated classroom

aquifer wherein storage and release of contaminants in low-*k* zones, with reactions, is accounted for. We encourage readers to work through the following two-layer scenario developments. Our rationale for advancing a detailed development includes the following goals:

- to illuminate processes governing transport in heterogeneous granular porous media with a DNAPL-like source wherein transport is governed by advection, diffusion, and reactions with unique transport parameters in transmissive and low-*k* zones;
- to provide a computational platform for students and practitioners for building intuition regarding transport in an idealized heterogeneous media by conducting calculations using the two-layer model (the model is made available via the Matrix Diffusion Tool Kit (Farhat et al., 2012), a Mathcad worksheet, and a MATLAB program, which can be obtained from the authors by email; and
- to build skills with mathematical methods that can be used to solve future problems.

In many ways, this text is as much about quantitative methods to address problems as it is about contaminant transport.

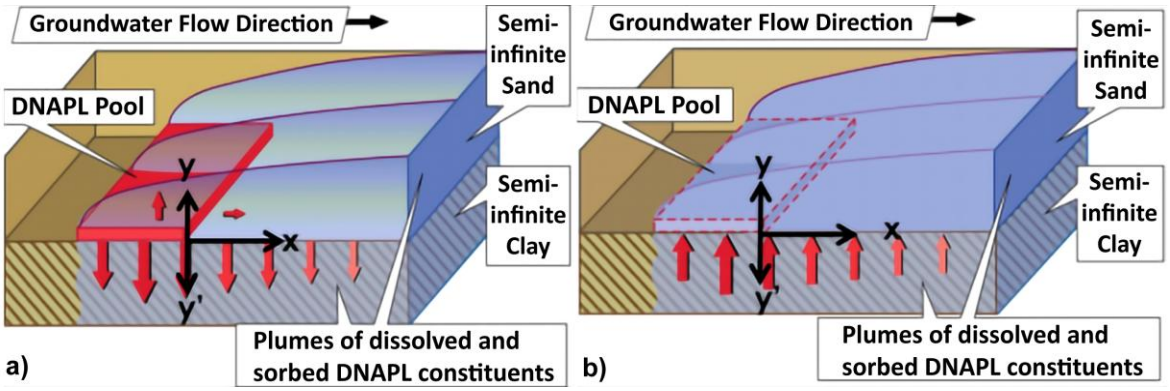

Figure 87 - The two-layer scenario (modified from Sale et al., 2008; and from Farhat et al., 2012). a) With a DNAPL pool as an upgradient source. b) After removal or natural depletion of the DNAPL pool (source).

Herein the two-layer scenario model is referred to as the Dandy–Sale model (DSM). Dandy and Sale are former full professors at Colorado State University, USA. Sale provided the conceptual foundations and Dandy developed the analytical solutions. Collaborating students at Colorado State University include master's candidate Doner (2008), doctoral candidate Bolhari (2011), bachelor's candidate Martin (2012), and master's candidate Wahlberg (2013).

The following advancement of solutions for the two-layer scenario draws on 1) an unpublished manuscript developed by Martin and Dandy; and 2) Wahlberg's master's thesis, Wahlberg (2013).

In hindsight, MathCAD-based worksheet applications in Sale and others (2008) suffer from inaccurate approximations of complex functions estimated over long times (more than 4 years). Computational limitations of the MathCAD platform were resolved by Martin in conjunction with Dandy. Martin and Dandy employ MATLAB as a

computational platform. Complex functions are resolved using series approximations in which the number of terms used in the series are iteratively tested for convergence for every combination of position and time of interest.

Mathematical foundations

This section presents the analytical solution for the two-layer scenario presented in Sale and others (2008) and updated in Wahlberg (2013). The solution shown in Equation (153) for the Dandy–Sale model (DSM) is based on separate PDEs for the transmissive zone.

$$\frac{\partial \rho_{aq}}{\partial t} = -\hat{v_w}\frac{\partial \rho_{aq}}{\partial x} + \widehat{D_t}\frac{\partial^2 \rho_{aq}}{\partial y^2} - \hat{\lambda}\rho_{aq} \qquad \text{for: y} \geq 0 \text{ and } 0 \leq x < \infty \tag{153}$$

For the low-*k* zone, Equation (154) applies.

$$\frac{\partial \rho_{aq}`}{\partial t} = \widehat{D_t`}\frac{\partial^2 \rho_{aq}`}{\partial y`^2} - \hat{\lambda}'\rho_{aq}` \quad \text{y`} < 0 \text{ and } 0 \leq x < \infty \tag{154}$$

Primes ' denote that the parameter describes the low-*k* layer. Hats ˆ indicate the parameter is divided by retardation factors as defined in Equation (155).

$$R = 1 + \frac{\rho_b}{\phi}K_D \quad \text{and} \quad R` = 1 + \frac{\rho_b`}{\phi`}K_D` \tag{155}$$

Assumptions include:

- transmissive and low-*k* zones are uniform;
- transport in the transmissive zone is driven by advection in the x direction and a combination of transverse diffusion and weak transverse hydrodynamic dispersion in the y direction based on $D_t = \alpha_x v_{aq} + D_e$;
- diffusive and dispersive transport in the direction of flow (longitudinal) in the transmissive zone is assumed to be negligible;
- the only significant transport process in the low-*k* layer is diffusion in the $y`$ (transverse) direction;
- advective and diffusive transport in the x direction, in the low-*k* zone, are negligible;
- sorption is based on linear isotherms defined by K_D and $K_D`$ for the transmissive and low-*k* zones, respectively;
- losses of aqueous phase contaminants through reactions are based on first-order reaction rate models defined by $\hat{\lambda}$ and $\hat{\lambda}'$ for the transmissive and low-*k* zones, respectively.

Initial conditions are defined by Equation (156).

$$\rho_{aq}(x, y, 0) = 0 \qquad \text{and} \qquad \rho_{aq}`(x, y`, 0) = 0 \tag{156}$$

Boundary conditions are provided in Equations (157) through (159).

The domains are semi-infinite transmissive and low-*k* zones where initial concentrations are zero.

$$\rho_{aq}(x, y^{\rightarrow\infty}, t) = 0 \qquad \text{and} \qquad \rho_{aq}^{`}(x, y^{`\rightarrow\infty}, t) = 0 \tag{157}$$

The PDEs are linked as follows. Absolute values of diffusive fluxes at the transmissive-low-k zone boundary are equal as shown in Equation (158).

$$\phi D_t \frac{\partial \rho_{aq}}{\partial y}(x, 0, t) = \phi D_t^{`} \frac{\delta \rho_{aq}^{`}}{\partial y}(x, 0, t) \tag{158}$$

Aqueous concentrations at the boundary between the transmissive and low-k zones are equal as shown in Equation (159).

$$\rho_{aq}(x, 0, t) = \rho_{aq}^{`}(x, 0, t) \tag{159}$$

In the DSM, following developments in Section 4.5.2, the source is analogous to a DNAPL pool in the transmissive zone immediately above the low-k zone located upgradient of $x = 0$ as defined in Equation (160).

$$\rho_{aq}(0, y, t) = \rho_0 e^{-by} \tag{160}$$

Aqueous concentrations at $(0, y)$ in the transmissive zone decay upward as governed by the source distribution constant b (1/L). Following Wahlberg (2013), equating the mass discharge from a pool into the transmissive zone to the mass discharge associated with Equation (124) leads to b being a function of the seepage velocity, the transverse diffusion coefficient, and the length of the DNAPL pool transverse to flow, as shown in Equation (161).

$$b = \frac{1}{2}\sqrt{\frac{v_{aq}}{L_{pool} D_t}} \tag{161}$$

Figure 88 is a calculation vignette documenting the imposed $\rho_{aq}(0, y, t)$ and the basis for estimating DSM source distribution constants.

Calculation Vignette
Estimation of DSM Model Source Distribution

Inputs (Consider PCE as the DNAPL source in sand)

$$\rho_{aqs} = 240\frac{mg}{L} \qquad \phi = 0.25 \qquad L_{pool} = 1\ m$$

$$v_{aq} = 0.27\frac{m}{day} \qquad S_w = 1 \qquad D_m = 7.5 \times 10^{-10}\frac{m^2}{sec}$$

$$y = 0\ cm,\ 0.1\ \ cm \ldots 100\ cm$$

Calculations

$$D_t = \phi^3\ \ S_w^3\ \ D_m = (4.7 \times 10^{-10})\frac{m^2}{s} \qquad b = \frac{1}{2}\ \sqrt{\frac{v_{aq}}{L_{pool}\ \ D_m}} = 32.3\frac{1}{m}$$

$$\rho_{aq}(y)\ = \rho_{aqs}\ \ e^{-(y\ b)}$$

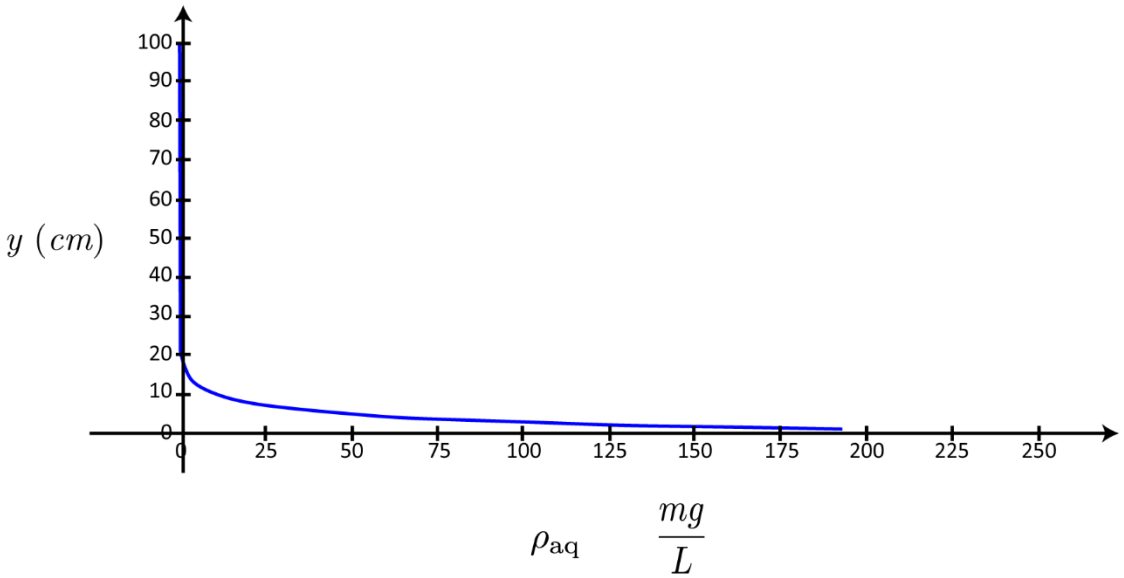

$$\text{Mass Discharge} = \phi\ \ \rho_{aqs}\ \ \sqrt{\frac{L_{pool}\ \ v_{aq}\ \ D_t}{\pi}} = 0.041\frac{kg}{yr\ \ m}$$

Figure 88 - Calculation vignette documenting the imposed $\rho_{aq}(0,y,t)$ and the basis for estimating the DSM source distribution constants b.

Aqueous concentrations for specific locations are used to calculate average aqueous concentrations in wells by integrating the concentrations over the vertical interval of interest (e.g., a screened interval such as $y_1 = 0$ m to $y_2 = 3$ m) in the transmissive layer and dividing by the length of the screened interval, as shown in Equation (162).

$$\overline{\rho_{aq}}(x,t) = \frac{\int_{y_1}^{y_2} \rho_{aq(x,y,t)dy}}{y_2 - y_1} \tag{162}$$

In Sale and others (2008), the source is on for $0 \leq t \leq t`$. Superimposing an equal and opposite source at time $t`$ turns the source off for $t > t`$. The on–off source is described mathematically by Equation (163).

$$\rho_{aq}(0,y,t) = \rho_{aq_s} e^{-by}[1 - H(t - t`)] \quad for \ y \geq 0 \tag{163}$$

Martin modified the source term such that the source strength can be reduced in increments as shown in Equation (164).

$$\rho_{aq}(0,y,t) = \begin{pmatrix} \rho_{aq_o} - [\rho_{aq_o} - \rho_{aq_1}]H(t - t`_1) \\ -[\rho_{aq_1} - \rho_{aq_2}]H(t - t`_2)\text{-...} \\ -[\rho_{aq_{n-1}} - \rho_{aq_n}]H(t - t`_n) \end{pmatrix} e^{-by} \tag{164}$$

In Equations (163) and (164), H is the Heaviside function. Using Martin's source term, one may choose any number of source strength reductions and corresponding durations. $t`_i$ denotes the time at which the source concentration is reduced.

Solutions

Complex solutions for aqueous concentrations in transmissive and low-*k* zones are presented in Sale and others (2008). Aqueous concentrations are a function of advection, diffusion, sorption, degradation, and source characteristics. Wahlberg (2013) presents updated solutions developed by Martin wherein complex functions are resolved using series approximations iteratively tested to verify that the necessary number of series terms are used to achieve convergence to constant results.

Wahlberg (2013)

Wahlberg's 2013 master of science thesis employs the DSM with Martin's series approximations to:

- illuminate the stylistic occurrences of contaminants in transmissive and low-*k* zones as a function of site conditions;
- document asymmetrical breakthrough curves; and
- track distributions of contaminants using the 14C model (Section 2.1.2) and losses due to degradation through time.

Primary model inputs for Wahlberg's thesis model are tabulated in Table 4.

Table 4 - Primary inputs used in the DSM in Wahlberg (2013).

Parameter	Values	Units
average linear groundwater seepage velocity, v_w	0.27	m/day
porosity of the transmissive layer, ϕ	0.25	dimensionless
porosity of the low-*k* layer, ϕ`	0.45	dimensionless
aqueous phase TCE solubility, ρ_{aq_o}	240	mg/L
bulk density of transmissive layer, ρ_b	1.99	gm/mL
bulk density of low-*k* layer, ρ_b`	1.46	gm/mL
retardation factor of the transmissive layer, R	1	dimensionless
retardation factor of the low-*k* layer, R`	1 - 15	dimensionless
exponential decay rate for the transmissive layer, λ	0 - 0.023	yr^{-1}
exponential decay rate for the low-*k* layer, λ'	0 - 0.231	yr^{-1}
effective transverse diffusion coefficient of the transmissive layer, D_{e_t}	4.54×10^{-9}	m^2/s
effective transverse diffusion coefficient of the low-permeability layer, D_{e_t}`	5.75×10^{-10}	m^2/s
source pool length, L	1	m
initial source persistence time, τ	10	yr

Aqueous concentrations in cross section

Figure 89 presents aqueous concentrations of PCE (ρ_{aq_o} = 240 mg/l) in cross section at 30 years given a steady source from 0 to 10 years. Aqueous concentrations are a function of advection and diffusion in the transmissive zone and diffusion and reactions (sorption and degradation) in the low-*k* zone. The domain is 7 m by 3 km. Assuming the use of a 1-cm^2 element, a finite difference numerical model would require 20 million nodes to resolve the modeled domain, and one would need to march through time calculating concentrations in 20 million nodes at each time step to get to a solution at 30 years. The required computational tasks would be daunting. Other than the DSM, the authors know of no other examples of HADiffR modeling being conducted at a scale of multiple kilometers. Aqueous concentrations are relevant due to resolving risks to human health based on consumption of groundwater (PCE MCL of 0.005 mg/L), and aqueous concentration gradients driving diffusion. The first column in Figure 89 considers a low-*k* zone with no sorption, R` value of 1. Sequentially, the second and third columns consider R` values of 5 and 15. Rows sequentially decrease contaminant half-lives (increasing reaction rates) in the low-*k* zone from 100 to 3 years. Increased retardation in the low-*k* zone reduces aqueous concentrations in the transmissive and low-*k* zones. Higher rates of degradation in low-*k* zones deplete aqueous concentrations in low-*k* zones and, correspondingly, increase aqueous concentration gradients drawing contaminants out of transmissive zones.

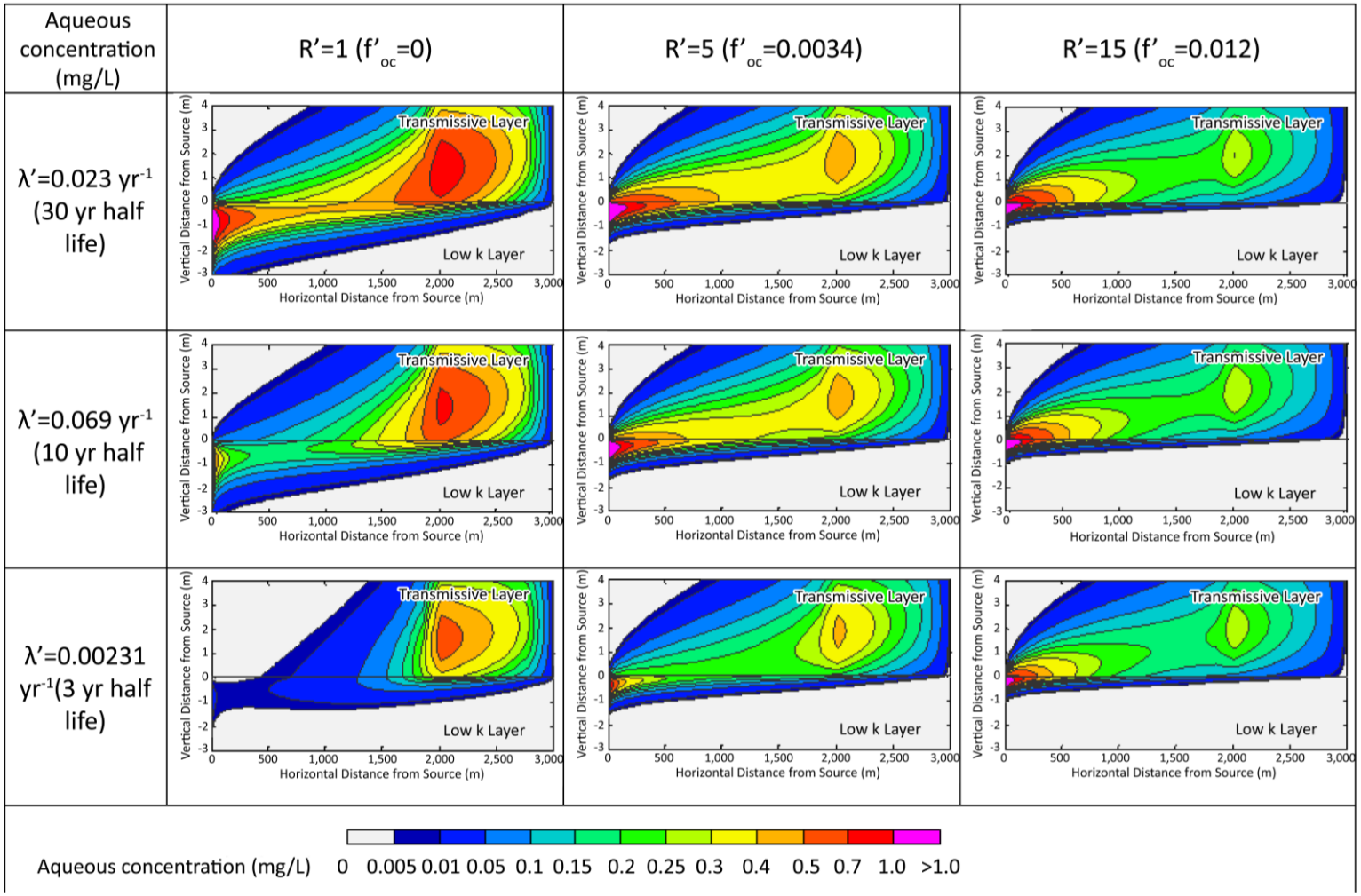

Figure 89 - Aqueous contaminant concentration (mg/L of water) as a function of retardation and degradation in the low-k zone after Wahlberg (2013). Input parameters: t=30 years, ϕ =0.25, ϕ'=0.45, τ=10 years, ρ_{aq_0} = 240 mg/L, D_t=4.54x10^{-9} m^2/s, D_e=5.75x10^{-10} m^2/s, L=1 m, R=1 (foc=0), k=0.023 yr^{-1} (30-year half-life), and v_w=0.27 m/day (modified from Wahlberg, 2013). Scanning the images from left to right with attention to the differences in the upper transmissive and lower low-k zones provides a visual sense of the impact of increasing sorption while scanning downward elucidates those of increasing rate of decay.

Total concentrations in cross section

Given the same conditions as described for Figure 89, Figure 90 presents total PCE concentrations (ω_T) in cross section using units of mg of PCE per kg of dry weight porous media. Total concentrations (aqueous and sorbed) speak to distributions and masses of contaminants that can sustain aqueous concentrations in transmissive zones (a primary risk driver) and might need to be addressed in a remediation effort. Notably, water-quality data alone misses sorbed phase CoCs.

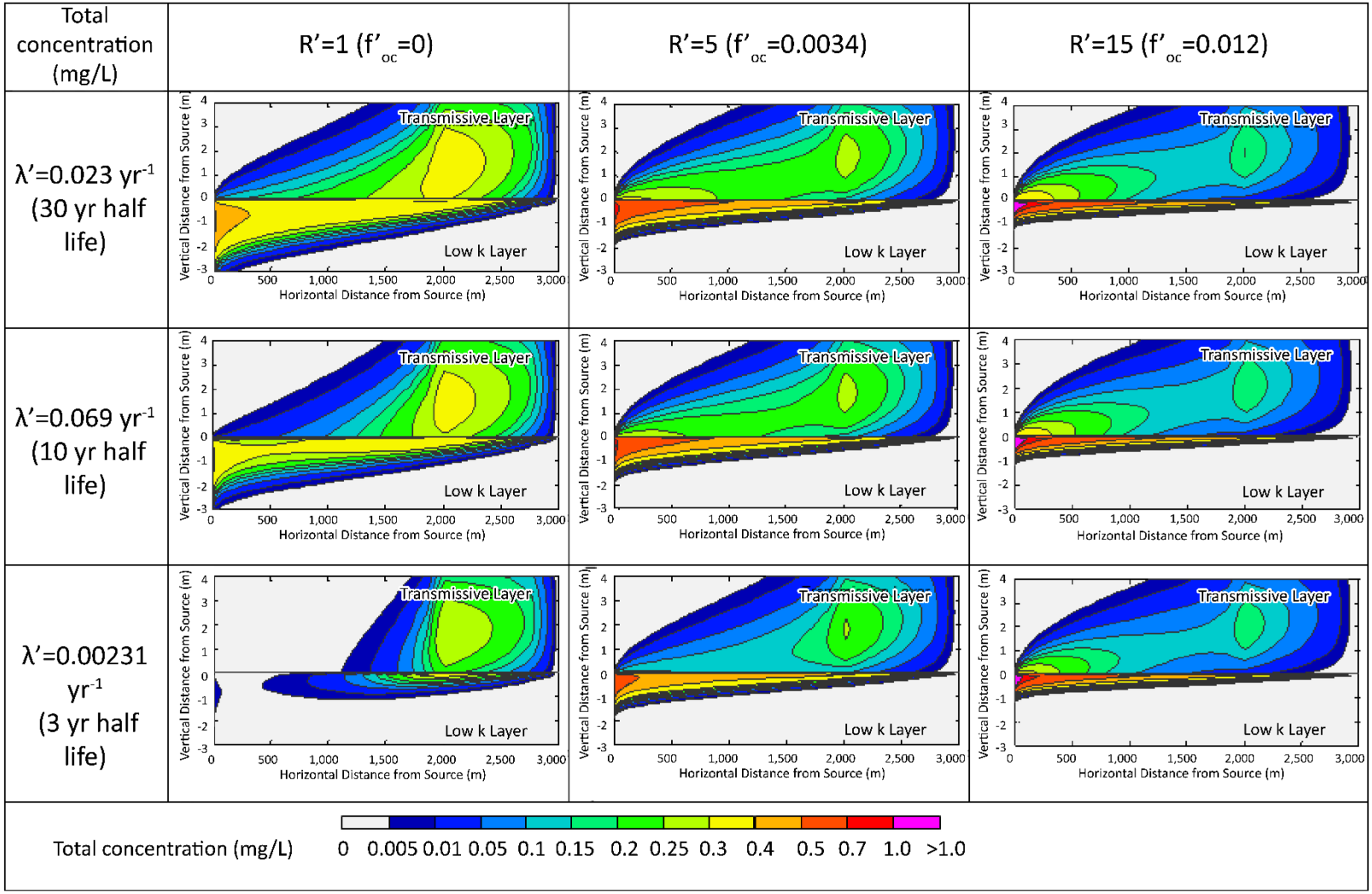

Figure 90 - Total contaminant concentration (mg/L of porous media) as a function of retardation and degradation in the low-k zone after Wahlberg (2013). Input parameters: t=30 years, ϕ =0.25, ϕ'=0.45, τ=10 years, ρ_{aq_0} = 240 mg/L, D_t=4.54x10^{-9} m^2/s, D_e=5.75x10^{-10} m^2/s, L=1 m, R=1 (foc=0), k=0.023 yr^{-1} (30-year half-life), and v_w=0.27 m/day (modified from Wahlberg, 2013). Scanning the images from left to right with attention to the differences in the upper transmissive and lower low-k zones provides a visual sense of the impact of increasing sorption while scanning downward elucidates those of increasing rate of decay.

Increasing retardation in the low-*k* zones leads to 1) higher total contaminant concentration in low-*k* zones at the transmissive-low-*k* zone contact and 2) higher total contaminant concentration in low-*k* zones. With respect to the latter, the DSM assumes losses due to degradation are proportional to aqueous concentrations, as in Equation (165).

$$M'_{Deg} = \lambda'_{aq}\rho'_{aq} \tag{165}$$

wherein:

$$\rho'_{aq} = \frac{\rho'_T}{R'} \tag{166}$$

Per the assumptions employed, sorbed masses are not available for degradation and sorption reduces losses through transformation reactions. An argument can be made that microorganisms mediating degradation can attach to sorption sites and that sorbed contaminants are available for degradation. The specifics as to whether rates of transformation are proportional to aqueous or total concentrations needs further attention.

Aqueous concentrations in monitoring wells

The most common metric used to evaluate subsurface contamination is vertically averaged aqueous concentrations of contaminants from transmissive zones based on water samples from monitoring wells $(\overline{\rho_{aq}})$ with modest screened intervals (e.g., 3 m). Using Equation (162), Figure 91 plots vertically averaged aqueous concentrations in wells $(\overline{\rho_{aq}})$ screened from 0 to 3 m above the low-*k* zone contact. Modeled monitoring wells are located 1, 10, 100 and 500 m downgradient of the source for 0 to 30 years. At times, less than the 10-year source duration, monitoring-well based aqueous concentrations increase at an ever-declining rate through time. At times greater than 10 years, aqueous concentrations initially decrease sharply, but continue to exceed MCLs for decades. As advanced by Sudicky and others (1985) and Chapman and Parker (2005), breakthrough curves are asymmetrical with problematic long-term exceedances of MCLs, not Gaussian as anticipated by applications of ADMs predicated on using dispersion to account for heterogeneities.

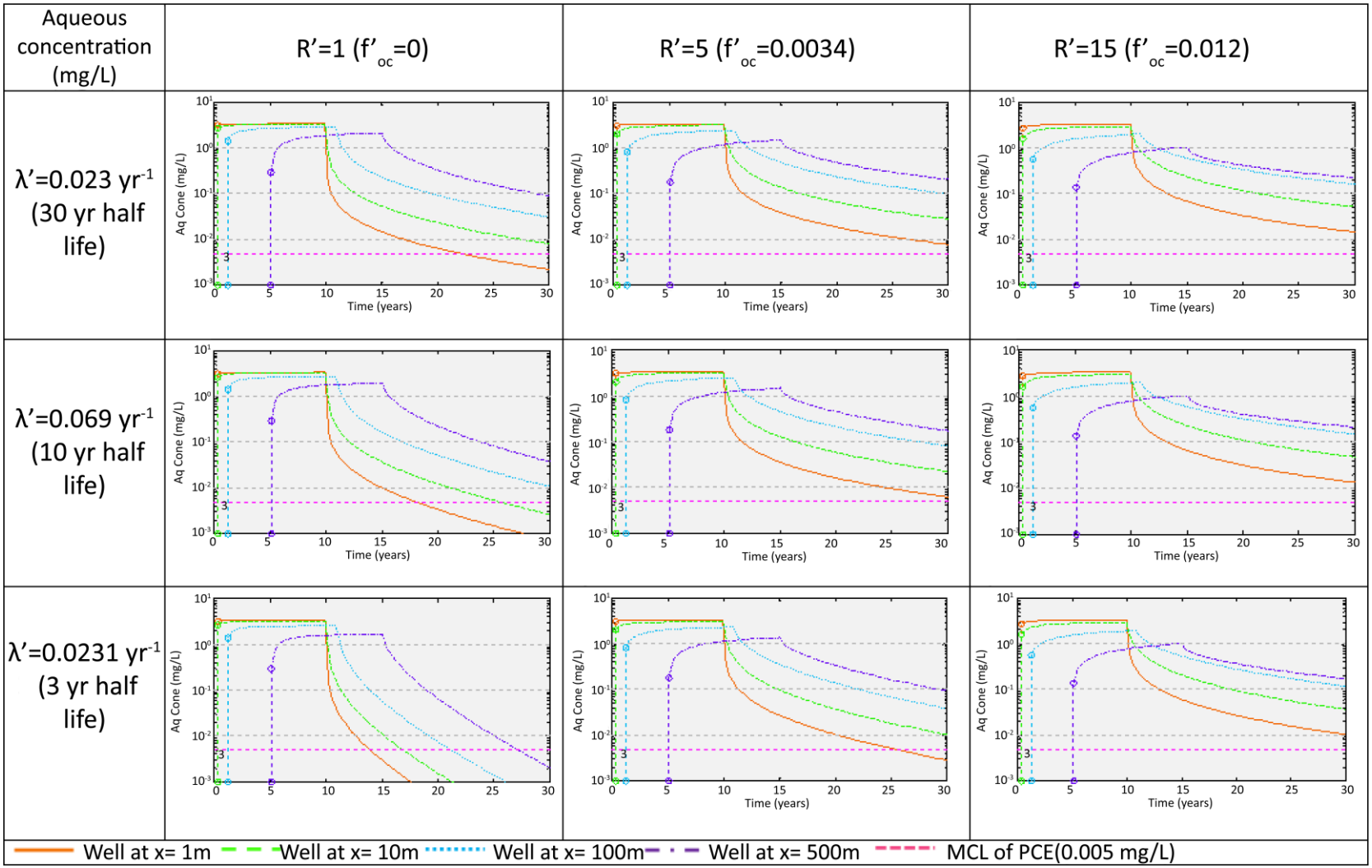

Figure 91 - Well concentrations versus time for wells located 1, 10, 100, and 500 m downgradient of the source as a function of low-*k* zone retardation and contaminant half-lives (modified from Wahlberg, 2013). Scanning the images from left to right with attention to the differences in the upper transmissive and lower low-*k* zones provides a visual sense of the impact of increasing sorption while scanning downward elucidates those of increasing rate of decay.

The best-case scenario for downgradient wells reaching MCLs occurs with low sorption and short half-lives in low-*k* zones (lower-left cell of Figure 89, Figure 90, and Figure 91). The worst-case scenario for downgradient wells reaching MCLs occurs with high sorption and large half-lives in low-*k* zones (upper-right cell of Figure 89, Figure 90, and Figure 91). Most importantly, the asymmetrical aqueous concentration versus time plots (i.e., the breakthrough curves of Figure 91) are inconsistent with Gaussian breakthrough curves associated with ADE modeling. First, the timing of downgradient water quality is governed by seepage velocities in transmissive zones as opposed to the average velocity in the averaged, combined transmissive and low-*k* zones. Secondly, eliminating upgradient sources via source removal or containment does not lead to near-term attainment of concentrations below MCLs.

Transient occurrences of contaminant phases in source zone and plumes within transmissive and low-k zones

Per the 14C model, all potential contaminant phases in both source zones and plumes within both the transmissive and low-*k* zones need to be recognized along with the associated occurrence and evolution of contaminants through time. Using the DSM and MATLAB code of Martin, Wahlberg (2013) resolved distributions of contaminants in all 14 compartments as well as contaminant losses due to degradation through time as shown in Figure 92 through Figure 96. Full details of the analysis are provided by Wahlberg (2013).

An initial release of PCE DNAPL is introduced and persists for ten years with a constant loss rate per Equation (160). Model inputs are listed in Table 4 with specific retardation coefficients and reaction rates included in the figure captions. Selected retardation and degradation rate coefficients reflect commonly occurring greater sorption and higher rates of reductive dechlorination in low-*k* zones. Elevated sorption and higher rates of reductive dechlorination (i.e., lower redox) is predicated on more quiescent depositional conditions for low-*k* zones in which NOM (natural organic material) is likely to be elevated.

Figure 92 documents the initial condition ($t = 0$ years) for the conceptual model shown in Figure 87 and parameterized as indicated in Table 4, when all of the PCE is present as DNAPL in the transmissive portion of the source zone. Unfortunately, resolution of occurences of vapor in source zones and plumes, and low-*k* zones and aqueous and sorbed phases in source zones, is beyond the scope of the DSM.

Time = 0 years

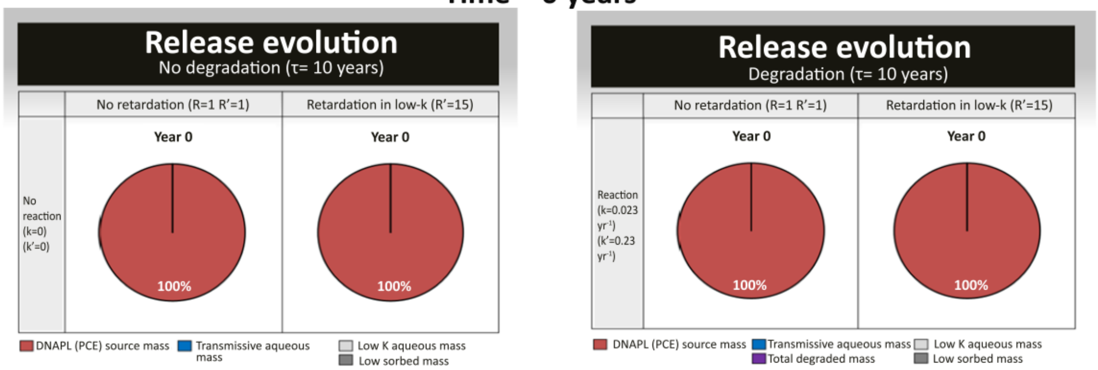

No retardation

	Source Zone		Plume	
Phase/Zone	Low Permeability	Transmissive	Transmissive	Low Permeability
Vapor				
DNAPL		100%	NA	NA
Aqueous				
Sorbed				

Reactions w no retardation

	Source Zone		Plume	
Phase/Zone	Low Permeability	Transmissive	Transmissive	Low Permeability
Vapor				
DNAPL		100%	NA	NA
Aqueous				
Sorbed				

0%

With retardation in low-k

	Source Zone		Plume	
Phase/Zone	Low Permeability	Transmissive	Transmissive	Low Permeability
Vapor				
DNAPL		100%	NA	NA
Aqueous				
Sorbed				

Reactions w retardation in low-k

	Source Zone		Plume	
Phase/Zone	Low Permeability	Transmissive	Transmissive	Low Permeability
Vapor				
DNAPL		100%	NA	NA
Aqueous				
Sorbed				

0%

Figure 92 - Distribution of contaminants in the 14C model and losses due to reactions at t = 0 years for the conceptual model shown in Figure 87 and parameterized as indicated in Table 4, when all of the PCE is present as DNAPL in the transmissive portion of the source zone (adapted from Wahlberg, 2013).

Figure 93 documents distributions of PCE after 4 years, including losses due to degradation of PCE (presumptively mineralized to chloride and carbonates). Scenarios considered include:

- no retardation or degradation,
- low-*k* zone retardation,
- no retardation with degradation in transmissive and low-*k* zones, and
- low-*k* zone retardation with degradation in transmissive and low-*k* zones.

After 4 years, 40 percent of the PCE DNAPL has been transformed to other phases, 12 to 25 percent of the PCE is present in the aqueous phase in transmissive portions of the plume, 11 to 28 percent of the PCE is in low-*k* zones as aqueous and sorbed phases, and 0 to 7 percent of the PCE has been mineralized.

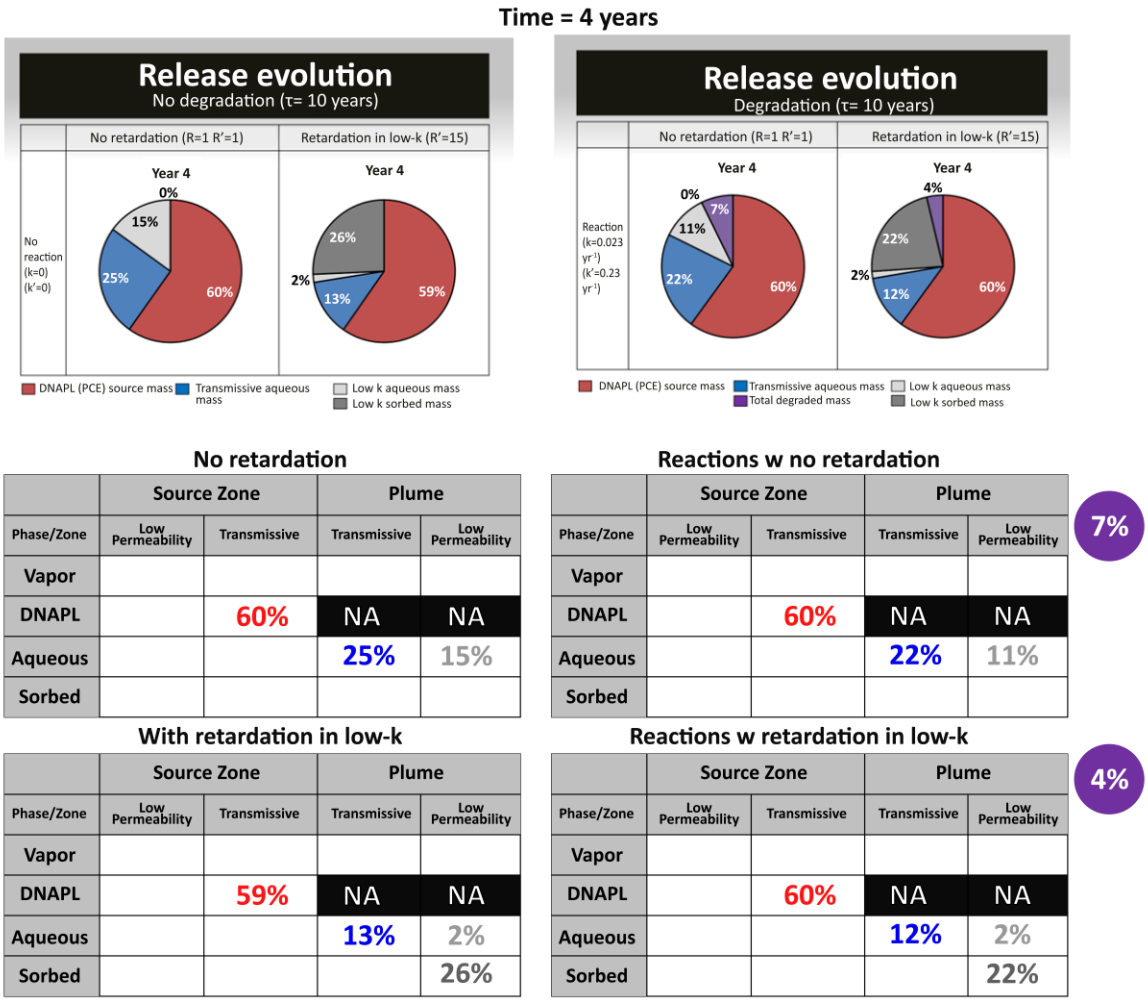

Figure 93 - Distribution of contaminants in the 14C model and losses due to reactions at t = 4 years for the conceptual model shown in Figure 87 and parameterized as indicated in Table 4 (adapted from Wahlberg, 2013).

Figure 94 addresses PCE occurrences at 10 years. At 10 years, all the PCE DNAPL has been transformed to other phases, 28 percent to 62 percent of the PCE is present in the aqueous phase in transmissive portions of the plume, 19 percent to 70 percent of the PCE

is in low-*k* zones as aqueous and sorbed phases, and 0 percent to 34 percent of the PCE has been mineralized.

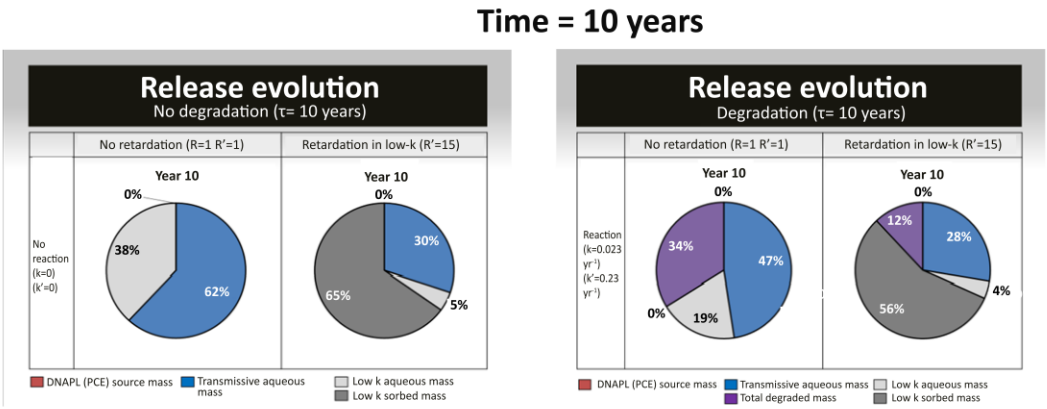

No retardation

	Source Zone		Plume	
Phase/Zone	Low Permeability	Transmissive	Transmissive	Low Permeability
Vapor				
DNAPL		0%	NA	NA
Aqueous			62%	38%
Sorbed				

Reactions w no retardation

	Source Zone		Plume	
Phase/Zone	Low Permeability	Transmissive	Transmissive	Low Permeability
Vapor				
DNAPL		0%	NA	NA
Aqueous			47%	19%
Sorbed				

34%

With retardation in low-k

	Source Zone		Plume	
Phase/Zone	Low Permeability	Transmissive	Transmissive	Low Permeability
Vapor				
DNAPL		0%	NA	NA
Aqueous			30%	5%
Sorbed				65%

Reactions w retardation in low-k

	Source Zone		Plume	
Phase/Zone	Low Permeability	Transmissive	Transmissive	Low Permeability
Vapor				
DNAPL		0%	NA	NA
Aqueous			28%	4%
Sorbed				56%

12%

Figure 94 - Distribution of contaminants in the 14C model and losses due to reactions at t = 10 years for the conceptual model shown in Figure 87 and parameterized as indicated in Table 4 (adapted from Wahlberg, 2013).

Figure 95 addresses PCE occurrences at 20 years, 10 years after the DNAPL source has been fully depleted. At 20 years, 21 percent to 62 percent of the PCE is present in the aqueous phase in transmissive portions of the plume, 5 percent to 71 percent of the PCE is in low-*k* zones as aqueous and sorbed phases, and 0 to 66 percent of the PCE has been mineralized.

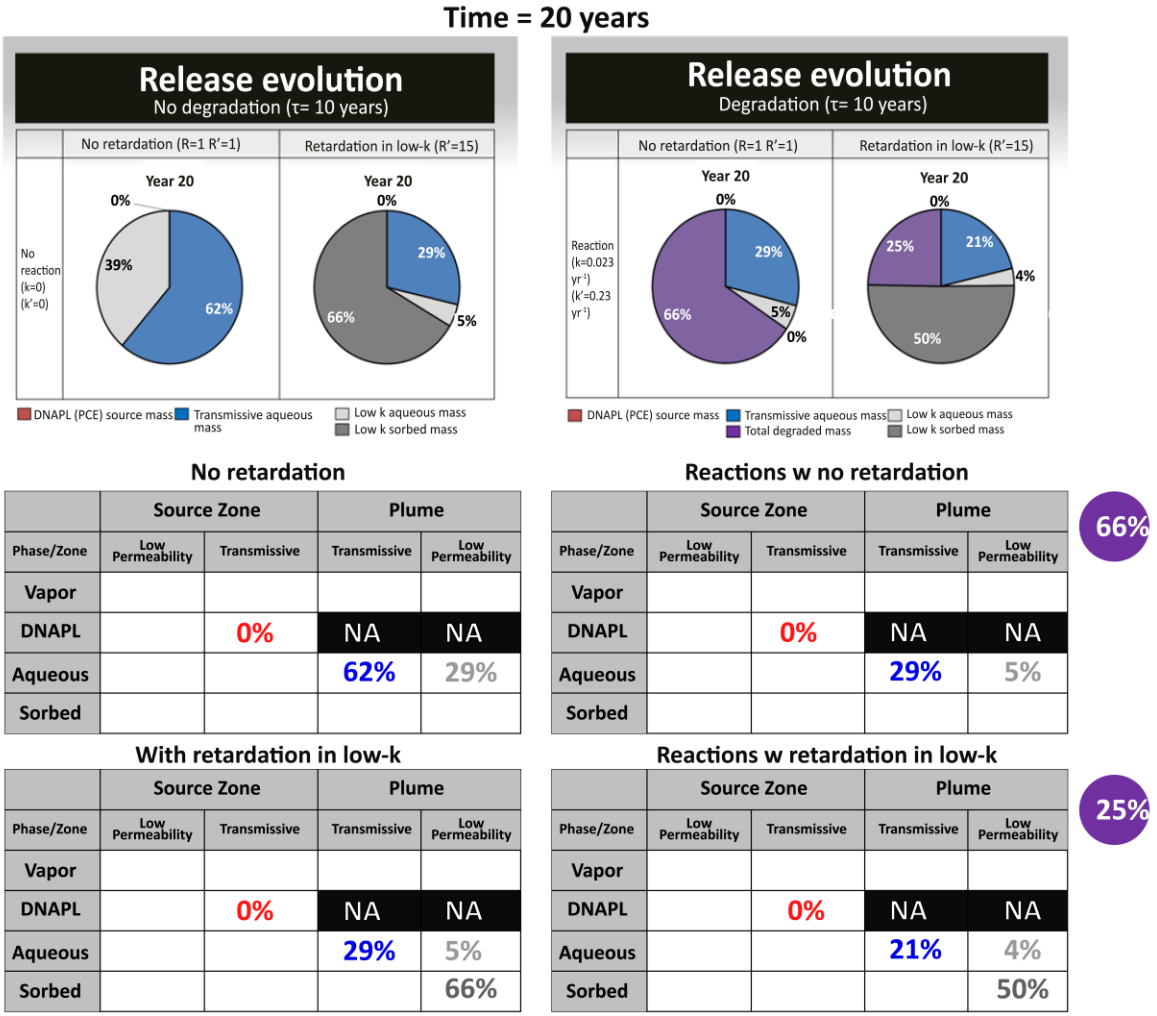

Figure 95 - Distribution of contaminants in the 14C model and losses due to reactions at t = 20 years for the conceptual model shown in Figure 87 and parameterized as indicated in Table 4 (adapted from Wahlberg, 2013).

Lastly, Figure 96 addresses PCE occurrences at 30 years, 20 years after the DNAPL source has been fully depleted. At 30 years, 17 percent to 61 percent of the PCE is present in the aqueous phase in transmissive portions of the plume, 2 percent to 72 percent of the PCE is in low-*k* zones as aqueous and sorbed phases, and 0 percent to 79 percent of the PCE has been mineralized.

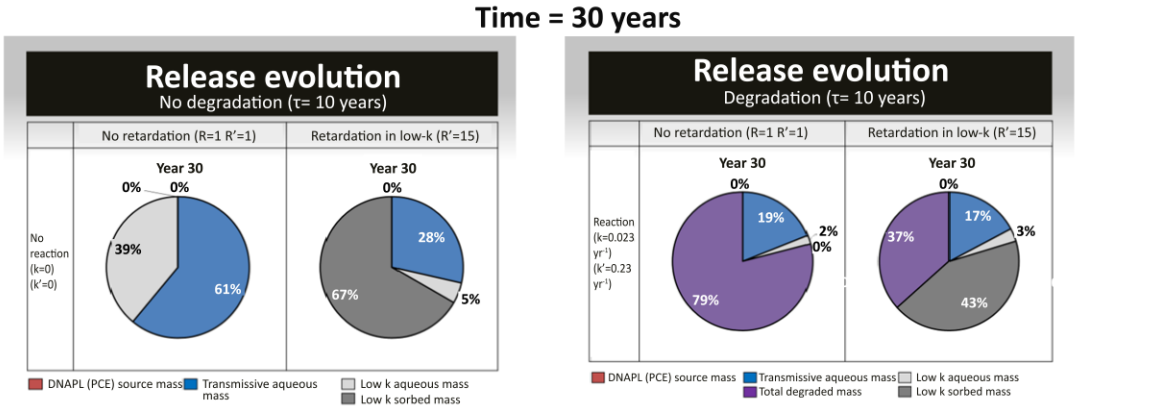

No retardation

	Source Zone		Plume	
Phase/Zone	Low Permeability	Transmissive	Transmissive	Low Permeability
Vapor				
DNAPL		0%	NA	NA
Aqueous			61%	39%
Sorbed				

Reactions w no retardation

	Source Zone		Plume	
Phase/Zone	Low Permeability	Transmissive	Transmissive	Low Permeability
Vapor				
DNAPL		0%	NA	NA
Aqueous			19%	2%
Sorbed				

79%

With retardation in low-k

	Source Zone		Plume	
Phase/Zone	Low Permeability	Transmissive	Transmissive	Low Permeability
Vapor				
DNAPL		0%	NA	NA
Aqueous			28%	5%
Sorbed				67%

Reactions w retardation in low-k

	Source Zone		Plume	
Phase/Zone	Low Permeability	Transmissive	Transmissive	Low Permeability
Vapor				
DNAPL		0%	NA	NA
Aqueous			37%	3%
Sorbed				43%

37%

Figure 96 - Distribution of contaminants in the 14C model and losses due to reactions at t = 30 years for the conceptual model shown in Figure 87 and parameterized as indicated in Table 4 (adapted from Wahlberg, 2013).

The primary take-away from Figure 92 to Figure 96 is that chlorinated solvent DNAPL releases are dynamic problems. In time, DNAPL sites are transformed into low-*k* zone sites and, under select conditions, natural assimilation processes can play a primary role in depleting remaining CoCs.

Work by Martin

Per an EPA-funded expert panel (Kavanaugh et al., 2003), "*The potential benefits of DNAPL source depletion have been the subject of significant on-going technical and policy debates*" (p. xi). In the mid-2000s, the issues were twofold. First, source zone remediation technologies typically achieve fractional depletion of DNAPL in source zones and correspondingly fractional reductions in mass discharge from source zones (McWhorter & Sale, 2003; Rao & Jawitz, 2003; Sale & McWhorter, 2001). As an analogy, one might wonder whether, if you had two feet of creosote-based wood-treating oil in your kitchen, you would be better off in the near term if you reduced the creosote in your kitchen to 1 foot. Correspondingly, how would the benefits of fractional depletion of DNAPLs play out in the long term?

Secondly, even when mass discharges from source zones are reduced to near zero (e.g., via source excavation, source containment, or emplacement of permeable reactive barriers), aqueous concentrations in downgradient wells often remain well above MCLs for extended periods (e.g., Chapman & Parker, 2005; Sale et al., 2008). As an alternative to often-difficult-to-achieve concentrations below MCLs in water, one can consider the benefits of reducing downgradient mass discharge at sources and in plumes (e.g., Kavanaugh et al., 2003).

Martin, in collaboration with Dandy and Sale, employed his DSM MATLAB code (relying on series approximations for complex functions) in 2013 to evaluate the potential benefits of DNAPL source depletion. Results from the Martin-Dandy-Sale 2013 study are provided.

Modeled domain and aqueous concentrations

Martin's model domain extends 10 m vertically and 4 km horizontally. Contaminant concentrations as a fraction of aqueous solubility are shown at 50 years in Figure 97. The source is active from 0 to 20 years and off from 20 to 50 years. Basic input values are presented in Table 5 with variations presented later in this section. Figure 97 shows aqueous concentrations normalized to the solubility of PCE in water (240 mg/L). A normalized aqueous concentration of $2x10^{-5}$ equates to the PCE MCL of 0.005 mg/L. Based on Figure 97, the MCL for PCE is exceeded in almost all of the model domain at 50 years.

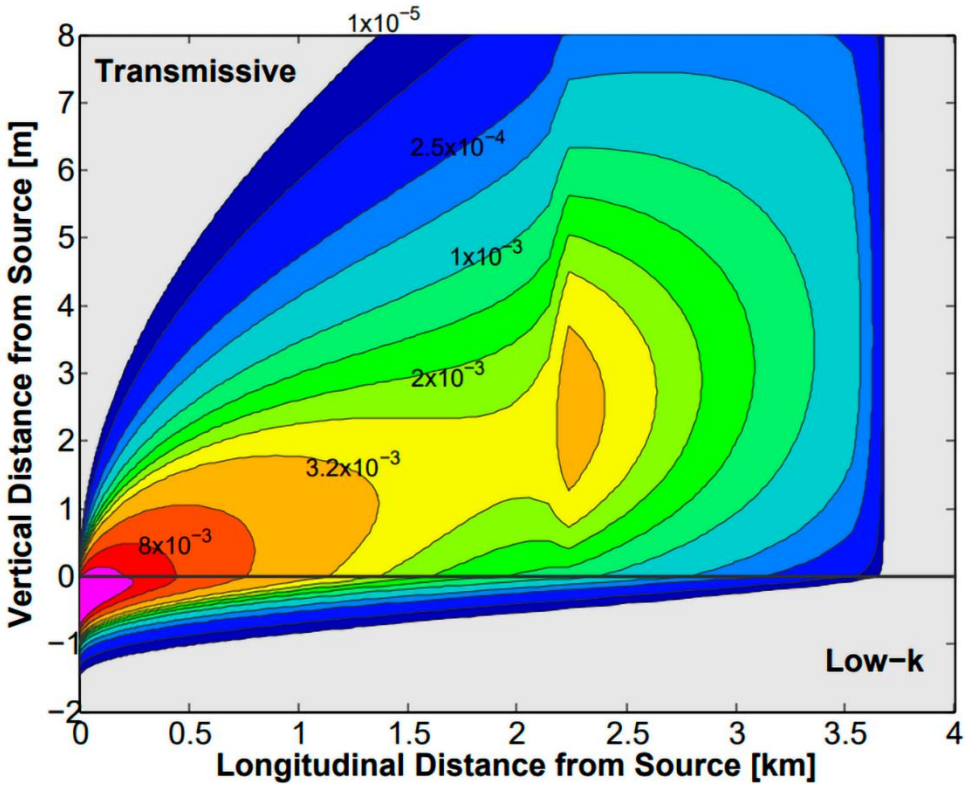

Figure 97 - Contour plot of normalized (as a fraction of aqueous solubility) contaminant concentrations in plume with a vertical exaggeration of approximately 300 for Martin's two-layer scenario (Figure 97 and Table 5) in the DSM (Figure 87). R'=15; k'=6.3×10^{-5} day^{-1} (30-year half-life); t=50 years; $t`$=20 years.

Table 5 - Primary inputs used by Martin for the two-layer scenario in the DSM.

Parameter	Values	Units
average linear groundwater seepage velocity, v_{aq}	0.2	m/day
porosity of the transmissive layer, ϕ	0.25	dimensionless
porosity of the low-permeability layer, ϕ`	0.45	dimensionless
aqueous phase TCE solubility, ρ_{aq_s}	240	mg/L
bulk density of transmissive layer, ρ_b	1.99	g/mL
bulk density of low-permeability layer, ρ_b`	1.46	g/mL
retardation factor of the transmissive layer, R	1	dimensionless
retardation factor of the low-permeability layer, R`	15	dimensionless
exponential decay rate for the transmissive layer, k	0	yr^{-1}
exponential decay rate for the low-permeability layer, k'	6.3×10^{-5}	day^{-1}
effective transverse diffusion coefficient of the transmissive layer, D_{e_t}	9.4×10^{-10}	m^2/s
effective transverse diffusion coefficient of the low-permeability layer, D_{e_t}`	3.1×10^{-10}	m^2/s
source pool length, L	1	m
initial source persistence time, τ	20	yr

Fractional source versus plume flux reductions

Figure 98 shows flux reductions at downgradient wells, screened 3 m above the low-*k*-zone versus flux reductions at the source. When downgradient flux reduction is compared to flux reduction at the source, a linear relationship is observed. Mathematically, this is expected because the DSM assumes a linear relationship between source concentration reduction and source flux reduction. As downgradient distances increase, less benefit is seen from fractional reductions in the contaminant flux from the source zone. Diminished downgradient benefits reflect more space and time for back diffusion to constrain the benefits of source reduction. The ratio of well flux reduction to source flux reduction is 1:1 at the upgradient end of the source zone and decreases with increasing distance.

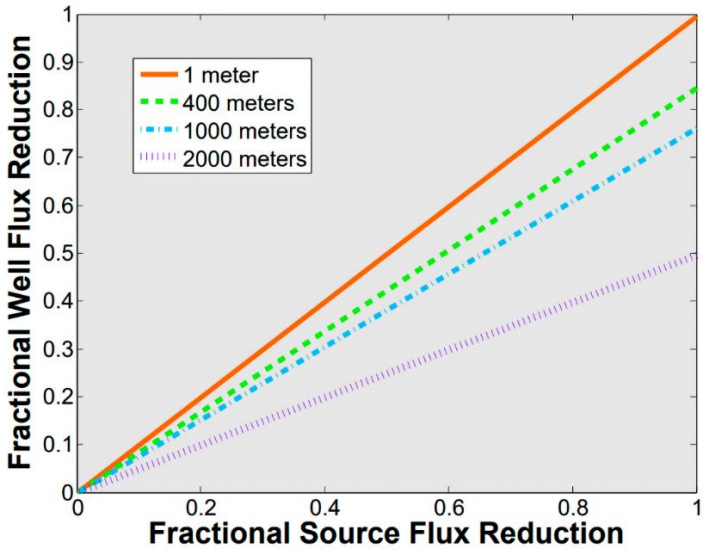

Figure 98 - Fractional flux reduction at a well versus fractional flux reduction at the source for Martin's two-layer scenario (Figure 97 and Table 5) in the DSM (Figure 87). *R'*=15; *k'*=6.3×10^{-5} day^{-1} (30-year half-life); *t*=50 years; *t*`=20 years.

Source reduction efficiencies

Due to the linear relationship between well flux and source flux, it is possible to study only the resulting slopes, which correspond to SRE (source reduction efficiency). SRE is defined as the quotient of [downgradient contaminant flux with source reduction] and [downgradient contaminant flux without source reduction]. Using this metric, the effectiveness of source zone remediation can be quantified more concisely.

Figure 99 shows SREs as a function of varying retardation and reaction rates in the low-*k* layer and of longitudinal distances from the source. At the source, SRE is unity, indicating a 1:1 relationship between source strength reduction and well flux reduction. This is the case because, essentially, there has been no time for diffusion into the transmissive layer to occur. Conversely, SRE approaches zero as the downgradient distance nears the distance at which we see the downstream peak concentrations 50 years after the source was emplaced. At this time and distance, the effects of source reduction have not yet been encountered. It is apparent that source flux reduction can have a larger positive effect on SRE in the case of low retardation and high rate of reaction. However, in the case of high retardation in the low-*k* layer, a high degradation rate source flux reduction does little to reduce downgradient contaminant fluxes. Per Sale and others (2008) and Wahlberg (2013), it is assumed that only aqueous phase contaminants are available for degradation. Furthermore, Figure 99 highlights the extent to which plume concentrations are governed by storage and release from low-*k* layers. Proceeding downgradient from the source, the cumulative effects of releases from low-*k* zones (back diffusion) lead to lower SRE.

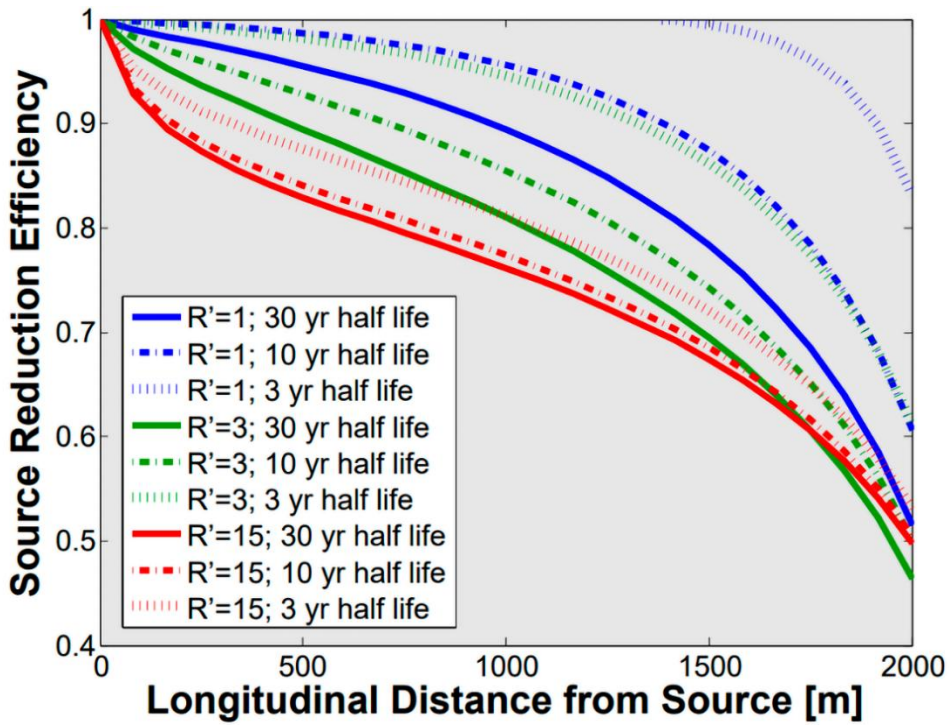

Figure 99 - Source reduction efficiency versus downgradient well distance with varying retardation and reaction rates in the low-*k* layer for Martin's two-layer scenario (Figure 97 and Table 5) in the DSM (Figure 87). *t*=50 years; *t*`=20 years.

Benefits of early reductions in mass discharge from sources

The DSM can also be used to gain insights into the benefits of early reduction in releases from source zones. Figure 100 illustrates the detriment of delay in addressing mass discharge from source zones. Given source reduction at year 5, SRE is greater than 90 percent 2 km downgradient at year 50. However, if remediation occurs 20 years after source introduction, efficiency is less than 50 percent at the same time and distance, meaning that even with a 100-percent reduction in source strength, only a two-fold decrease occurs in downgradient flux. These trends are intuitive given the conceptual model of transmissive and low-*k* zones with diffusion-driven exchanges.

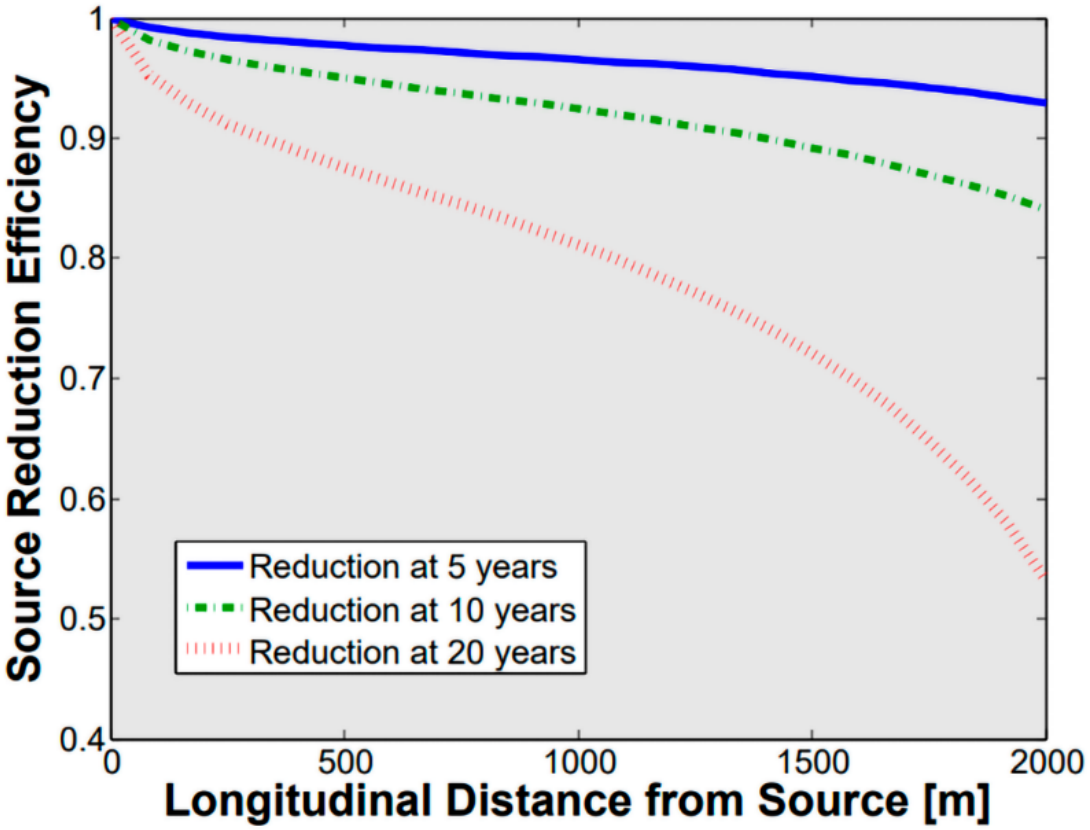

Figure 100 - Source reduction efficiency versus downgradient well distance with varying source duration for Martin's two-layer scenario (Figure 97 and Table 5) in the DSM (Figure 87). R'=15; k'=6.3×10^{-5} day^{-1} (30-year half-life). The dotted red line corresponds to the dotted red line in Figure 99.

Summary of the findings of Martin's work

Returning to the question of when source zone remediation is beneficial, the answer depends on processes and parameters governing transport in heterogeneous domains. While Martin's results, and the DSM in general, are founded on gross simplifications of subsurface media, they provide valuable insights. Specifically, they advance our intuition regarding what to expect from remedial measures and, therein, provide a foundation for sound site-management decisions.

A Review of High-Resolution Numerical Modeling by Chapman and Parker

In this Section 5.5.3, we explore the validity of numerical modeling using high-resolution numerical methods with sufficiently small spatial and temporal discretizations in more complex Type 3 and Type 5 settings. We summarize Chapman's and Parker's contribution to *Management of Contaminants Stored in Low Permeability Zones* by Sale and others (2013). We reference their work here as Chapman and Parker (2013). This and supporting publications are primary references for those wanting to know more about high-resolution numerical modeling of contaminant transport. The project team for Sale and others (2013) received the prestigious 2014 SERDP Environmental Restoration Project of the Year Award.

Validating High-resolution numerical models

Chapman and Parker (2013) compare MathCad-based analytical solutions for the DSM to numerical modeling results using multiple numerical models. The model domain is 1.2 m in the vertical direction and 100 m long. Figure 101 compares results from a MathCad worksheet for the analytical solutions in Sale and others (2008) to HydroGeoSphere results. As a first step in applying HydroGeoSphere, Chapman and Parker (2013) iteratively reduced scales of discretization until the results converged to near-constant values. The final spatial discretization of the two-dimensional domain is approximately 1,000 node/m^2 (regularly spaced) for the modeled domain. Additional information regarding the modeling in Figure 101 is presented in Chapman and Parker (2013).

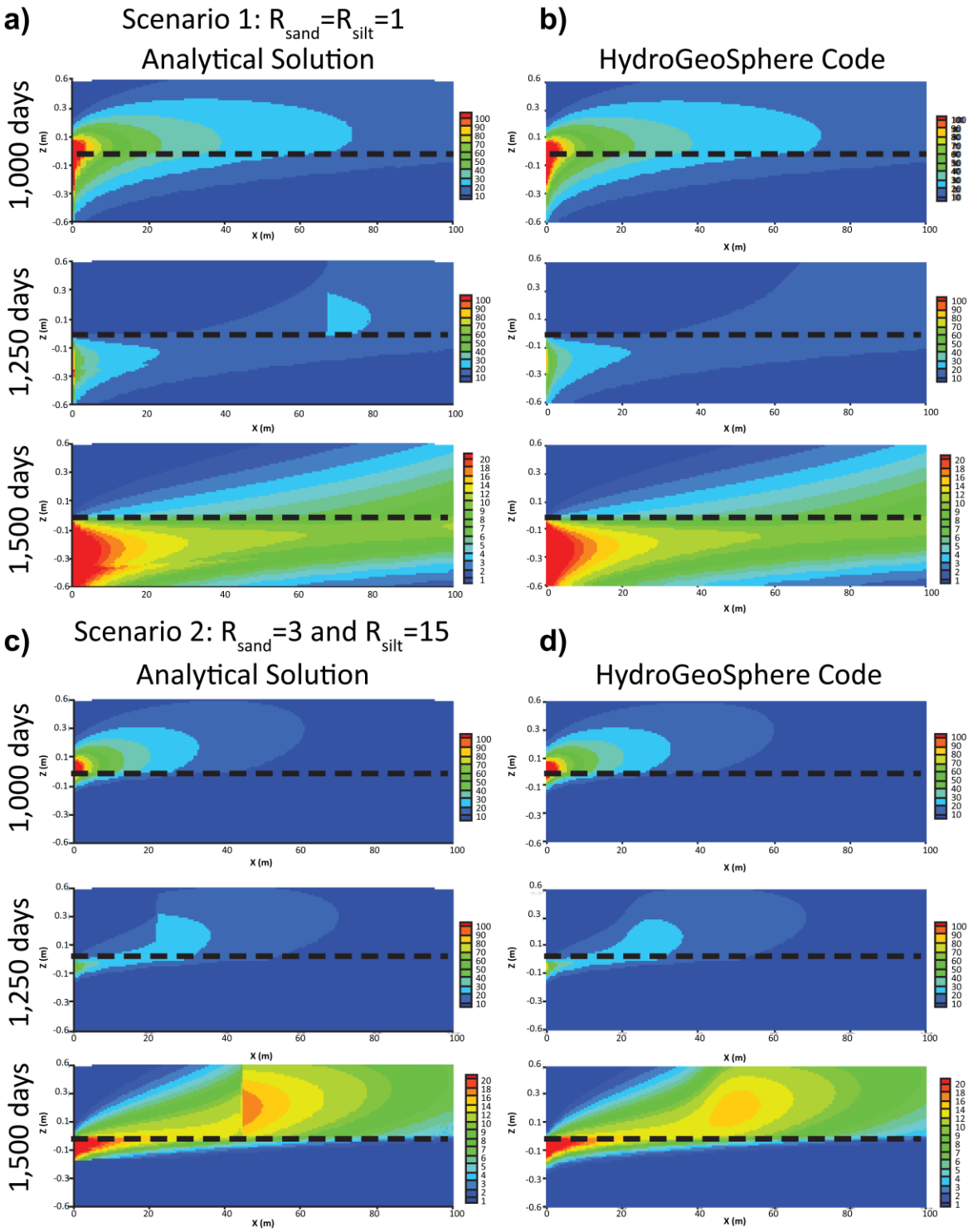

Figure 101 - Comparison of results from the DSM analytical solution using a Mathcad worksheet to numerical modeling results from HydroGeoSphere. a) Results of the analytical and b) numerical modeling for no sorption in the transmissive and low-*k* zones. c) Results of the analytical and d) numerical modeling for retardation of 3 and 15 in the transmissive and low-*k* zones, respectively. (modified from Chapman & Parker, 2013).

In the big picture, results from the analytical and high-resolution numerical models agree. Upon more careful inspection, two differences can be seen. First, an irregularity occurs in the analytical solution in the low-*k* zone that is initially apparent at 1,250 days and readily apparent at 1,500 days for scenario 1. The anomaly is attributed to flawed MathCad

estimates of complex functions given small error function arguments at large times. Problems with MathCad estimates of complex functions were subsequently resolved by Martin using Taylor series approximations with iterative testing for the number of series terms needed for the series approximations to converge at every time-point of interest.

Secondly, the analytical solution shows sharper plume edges in the transmissive zone, reflecting the DSM assumption of no longitudinal hydrodynamic dispersion. In contrast, the HydroGeoSphere models show mixing at the edges of the plumes in the transmissive zone. The HydroGeoSphere modeling uses nonzero dispersion coefficients. The values used are presented in the calculation vignette of Figure 102.

Calculation Vignette
Longitudinal and Transverse Dispersion Coefficients
Used in the HydroGeoSphere Two-Layer Model

Molecular Diffusion Coefficient in Water

$$D_m = 9.2 \times 10^{-10} \frac{m^2}{sec}$$

Tortuosity for Transmissive and Low-k zones

$$\tau_{\text{Trans}} = \frac{1}{0.4} = 2.5 \qquad \tau_{\text{Low-k}}^{`} = \frac{1}{0\ 585} = 1.7$$

Porosity

$$\phi_{\text{Trans}} = 0.25 \qquad \phi_{\text{Low-k}}^{`} = 0.45$$

Effective Diffusion Coefficien

$$D_{E_{\text{Trans}}} = \frac{D_m \quad \phi_{\text{Trans}}}{\tau_{\text{Trans}}} = (9.2 \times 10^{-11}) \frac{m^2}{s}$$

$$D_{E_{\text{Low-k}}} = \frac{D_m \cdot \phi_{\text{Low-k}}^{`}}{\tau_{\text{Low-k}}^{`}} = (2.4 \times 10^{-10}) \frac{m^2}{s}$$

Transmissive Zone Dispersivity Values

$$\alpha_{T_{\text{Long}}} = 0.2 \quad m \qquad \alpha_{T_{\text{Trans}}} = 0.0014 \quad m$$

Aqueous Seepage Velocity

$$v_{\text{aqTrans}} = 0.27 \frac{m}{day} \qquad v_{\text{aqLow-k}} = \frac{0.27}{1000} \frac{m}{day}$$

Transmissive Zone Mixing Coefficients

$$D_{L_{\text{Trans}}} = D_{E_{\text{Trans}}} + \alpha_{T_{\text{Long}}} \quad v_{\text{aqTrans}} = (6.251 \times 10^{-7}) \frac{m^2}{s}$$

$$D_{T_{\text{Trans}}} = D_{E_{\text{Trans}}} + \alpha_{T_{\text{Trans}}} \quad v_{\text{aqTrans}} = (4.467 \times 10^{-9}) \frac{m^2}{s}$$

Low-k Zone Effective Diffusion Coefficients

$$D_{T_{\text{Low-k}}} = D_{E_{\text{Low-k}}} + \alpha_{T_{\text{Trans}}} \quad v_{\text{aqLow-k}} = (2.466 \times 10^{-10}) \frac{m^2}{s}$$

Figure 102 - Calculation vignette showing the basis for the longitudinal and transverse dispersion coefficients used in the two-layer HydroGeoSphere model.

The bottom line in comparing analytical and numerical approaches is that equivalent results can be obtained all while both approaches have computational limitations. In truth, all complex models have computational limitations. Putting foundational assumptions and computational limitations in perspective, Theis (1967) notes that errors introduced by uncertainties in input parameter values can be even larger than errors associated with mathematical methods. That said, the results of both approaches are sufficient to provide guidance on useful approaches to management of contaminated sites.

Complex type 3 settings

Type 3 settings are common. The two-layer scenario is a simple type 3 setting. Chapman and Parker (2013) provide further consideration of more complex stylistic Type 3 settings, including periodic layers of transmissive and low-*k* zones, and two-layer scenarios wherein thin low-*k* zone inclusions are present in the transmissive zone.

Periodic layer scenario

A periodic-layer scenario is shown in Figure 103a. The model domain is 7 m by 500 m. The periodic-layer scenario is analogous to a heat exchanger such as an automobile radiator. Red bars indicate constant concentration boundaries analogous to DNAPL sources in the transmissive zones. Sources are active for specified periods ($0 > t \leq t'$) and subsequently turn off ($t > t'$). Figure 103b illustrates the spatial discretization used in the HydroGeoSphere model of this scenario as presented in Chapman and Parker (2013). To date, the authors of this text have not succeeded in developing an analytical solution for the periodic-layer scenario.

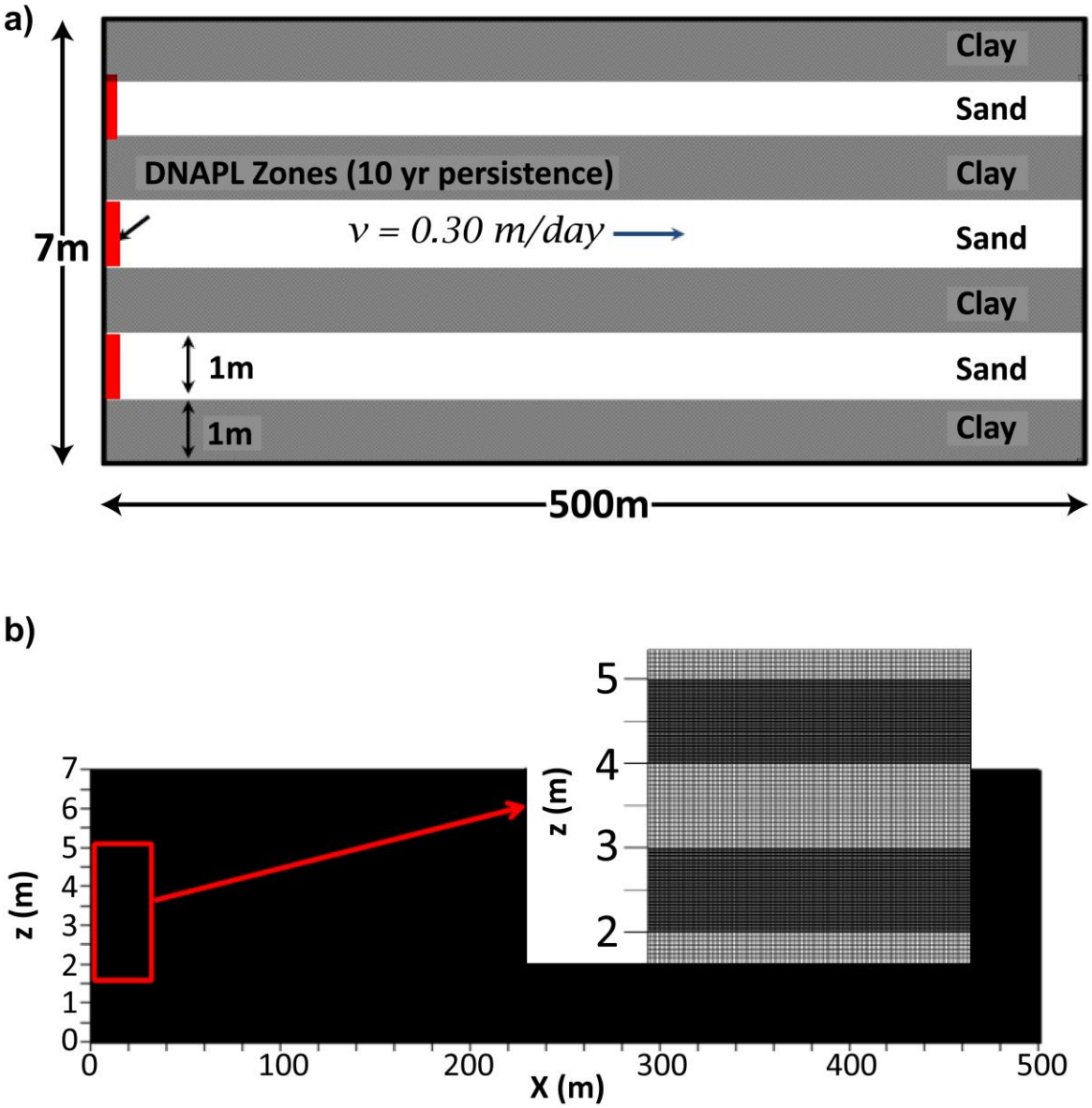

Figure 103 - Periodic-layer scenario simulated by Chapman and Parker (2013): a) periodic transmissive and low-*k* zone layers and b) domain discretization.

Figure 104 presents aqueous concentrations normalized to aqueous influent concentrations for active source periods ranging from 1 to 10 years followed by a source off period ranging from 19 to 90 years. In all cases, storage of contaminants in low-*k* zones leads to assimilation of contaminants in transmissive zones. After the source is turned off, persistent releases from low-*k* zones leads to sustained contaminant concentrations in transmissive zones.

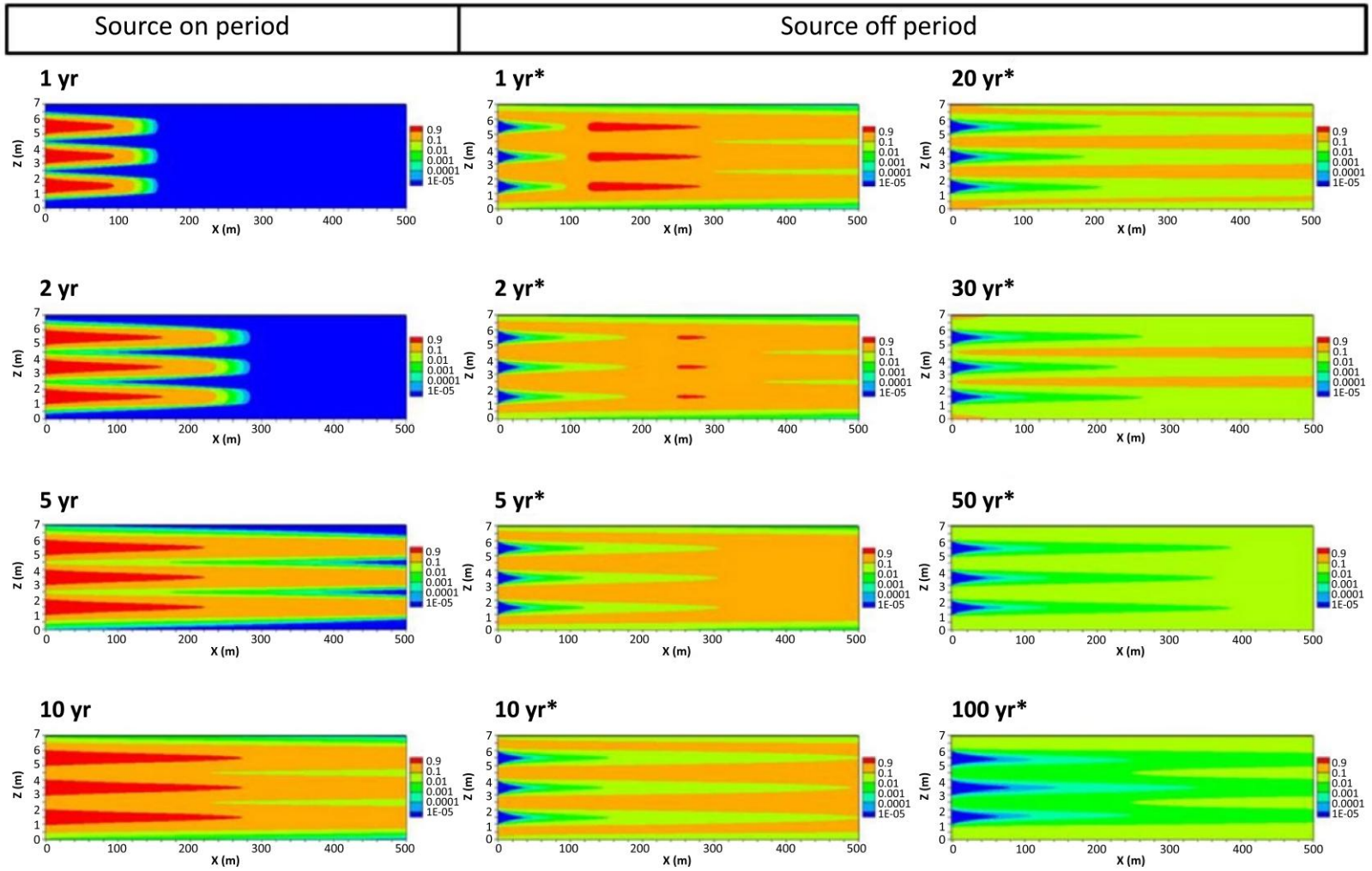

Figure 104 - Aqueous concentrations normalized to initial influent aqueous concentrations in a periodically layered system of transmissive and low-*k* zones for a range of source on and source-off periods given $R` = 2$ and no degradation. An * indicates time is measured from when the source was turned off. Given that there is no sorption or decay, the differences reflect the impact of source duration.

Figure 105 introduces analog monitoring wells located at 10, 50, 100, 200, and 500 m downgradient of the source in the transmissive layer as well as at points of interest collocated with wells at the transmissive low-k zone contact and the midpoint of the transmissive zone for the simulated by Chapman and Parker (2013). The graphs of Figure 105 presents aqueous concentrations normalized to initial influent aqueous concentrations for monitoring wells ($\overline{\rho_{aq}}$) and points of interest (ρ_{aq}). As with the two-layer scenario, breakthrough curves are asymmetrical, not Gaussian as per ADMs. Post-source-removal releases of contaminants from low-k zones sustain normalized concentrations greater than 10^{-5} (equivalent to the MCL for chlorinated solvents) for extended periods of time. A notable difference from the two-layer scenario is the log of normalized concentration versus time decays linearly at large times due to back diffusion yielding potentially slow return low concentrations. Post-source asymptotic log values of concentration tails in two-layer systems, versus log linear tails in periodically layered systems, speak to the importance of the architecture of transmissive and low-k zones.

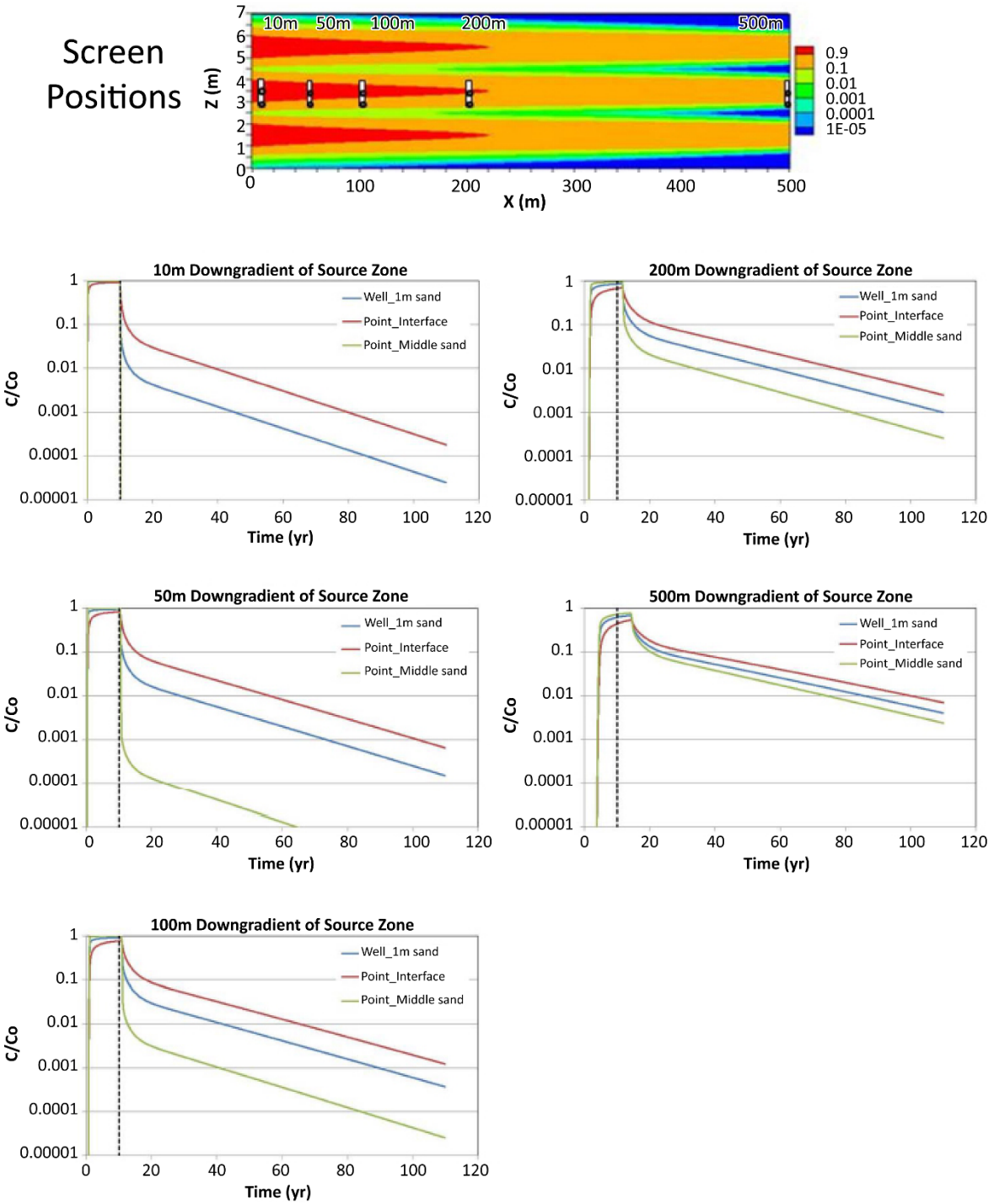

Figure 105 - Aqueous concentrations in monitoring wells and at points of interest in transmissive zones (normalized to initial influent aqueous concentrations) in a periodically layered system of transmissive and low-k zones for a range of source-on and source-off periods given $R' = 2$ and no degradation, as simulated by Chapman and Parker (2013) and presented in Figure 103 and Figure 104.

Two-layer scenario with low-k zone inclusions in the transmissive zone

The two-layer scenario with low-k zone inclusions in the transmissive zone and DNAPL sources is illustrated in Figure 106a. The domain is 10 m by 500 m. Figure 106b illustrates spatial discretizations used in a HydroGeoSphere model simulated by Chapman and Parker (2013). Figure 107 presents aqueous concentrations normalized to initial

influent aqueous concentrations, versus time and position, for a range of source durations. Notably, greater source durations lead to greater plume durations, and the thicker, lower low-*k* zone is a more persistent source of PCE after the source is turned off than the smaller low-*k* zone inclusions in the transmissive zone. Thicker low-*k* zones sustaining plumes for greater periods of time is also addressed by Falta and Wang (2017), Falta and others (2019), and Borden and Cha (2021).

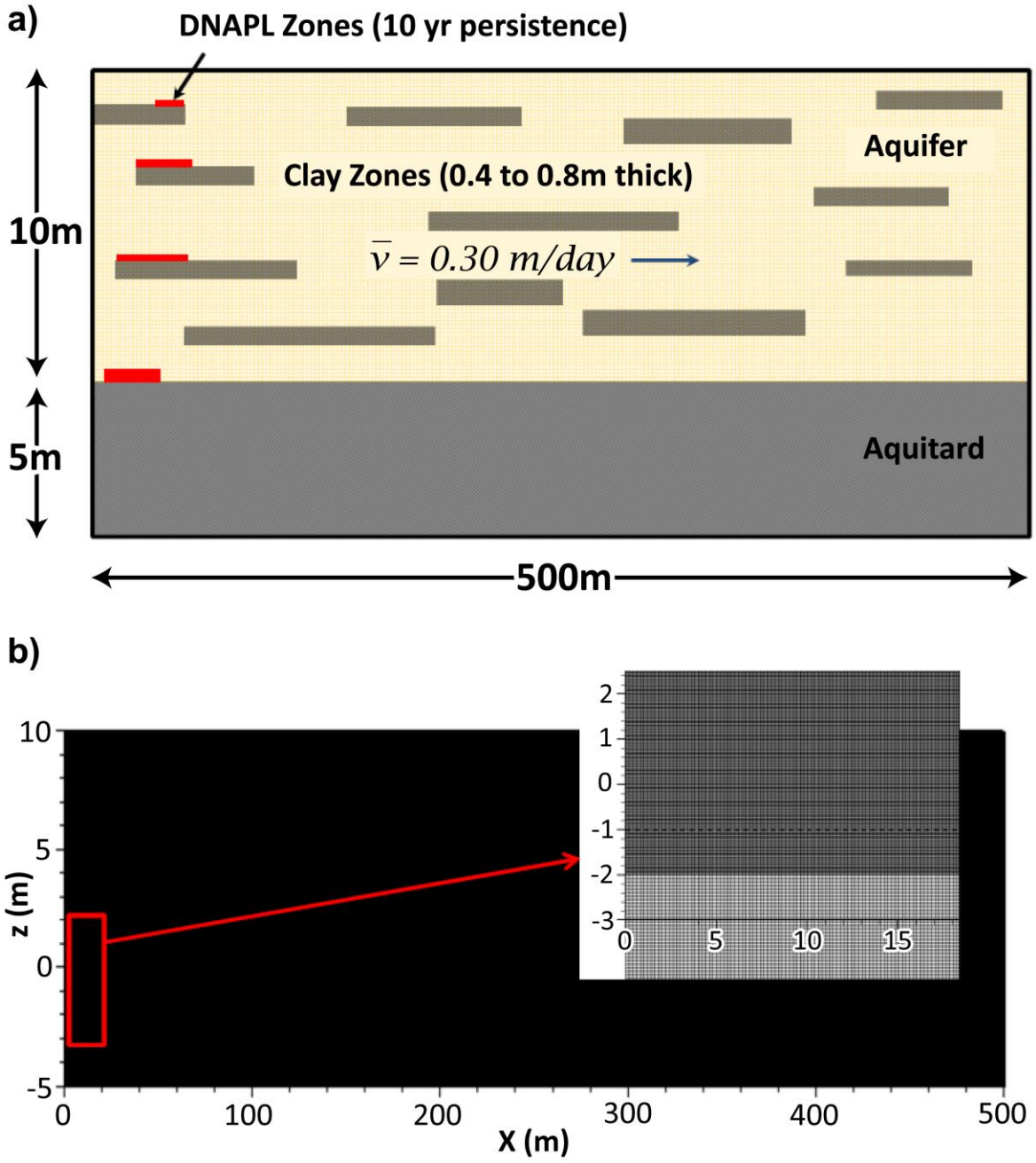

Figure 106 - Two-layer scenario with a) low-*k* zone inclusions in the transmissive layer and DNAPL sources and b) the model discretization for simulation by Chapman and Parker (2013).

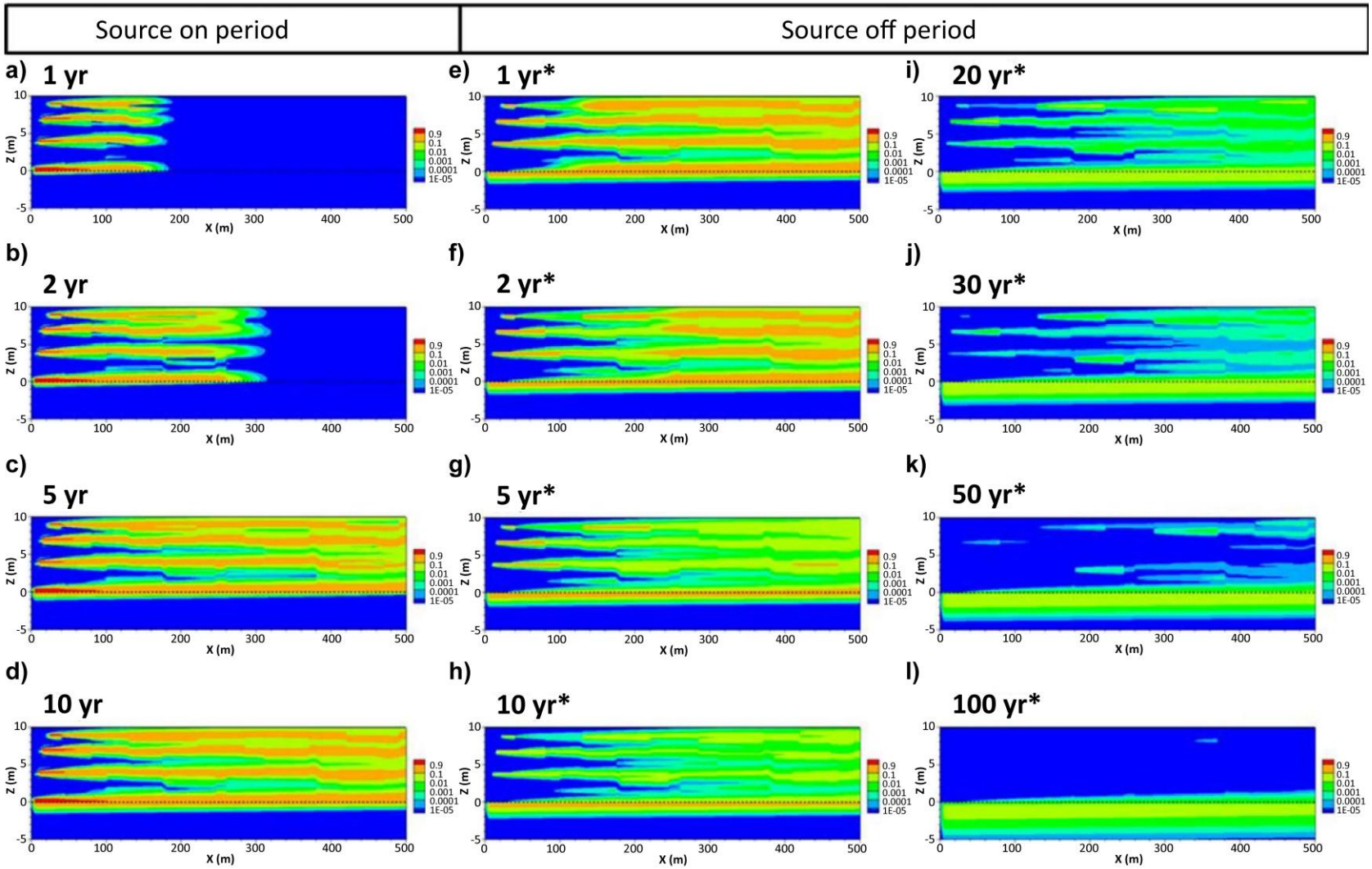

Figure 107 - Normalized aqueous concentration in a two-layer system with low-*k* inclusions in the transmissive zone. An * indicates time is measured from when the source was turned off. Greater source durations lead to greater plume durations, and the thicker, lower, low-*k* zone is a more persistent source of PCE after the source is turned off than the smaller low-*k* zone inclusions in the transmissive zone. (modified from Chapman & Parker, 2013).

Figure 108 introduces analog multiple-level sampling devices with 1-m vertical screens in the transmissive zone located at 500 m in the modeled domain. Aqueous concentrations normalized to initial influent aqueous concentrations are plotted for multiple level sampling devices as a function of time. As with the two-layer scenario, breakthrough curves are asymmetrical, not Gaussian, and releases of contaminants from low-*k* zones sustain normalized concentrations greater than 10^{-5} for extended periods of time. Aqueous concentration breakthrough curves from points near the basal low-*k* zone (W5a and W5c) are stylistically similar to two-layer scenario breakthrough curves. Aqueous concentration breakthrough curves for points above the basal low-*k* zone (W5e, W5g and W5i) are stylistically similar to breakthrough curves from the periodically layered scenario.

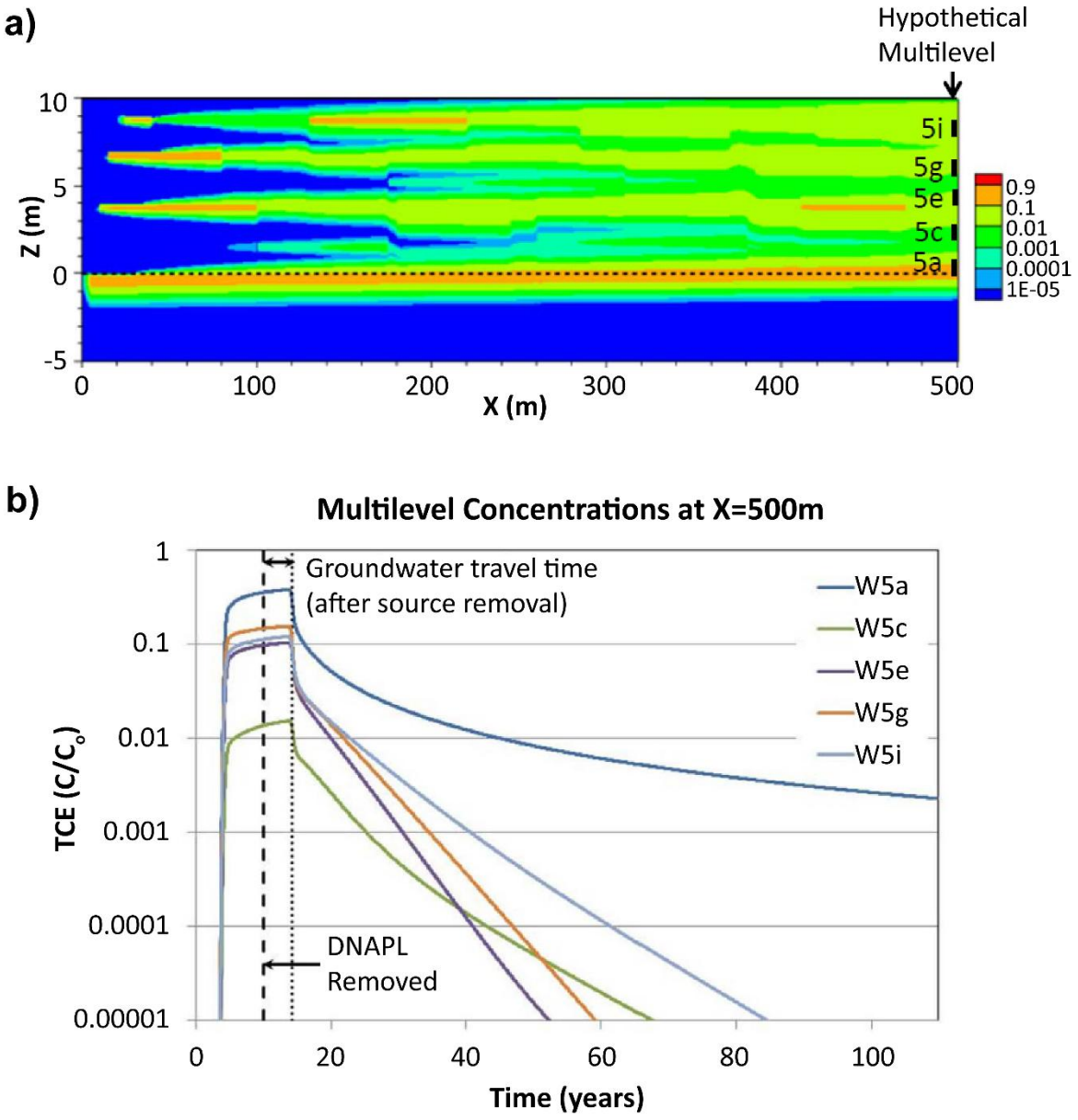

Figure 108 - Multiple level sampling system breakthrough curves for a two-layer system with low-*k* zone inclusions in the transmissive zone (modified from Chapman & Parker, 2013); a) locations of multiple level sampling systems and b) normalized aqueous concentrations versus time.

Type 5 setting – Fractured rock with porous matrix blocks

As presented by Chapman and Parker (2013), Figure 109 presents a Type 5 setting composed of a network of interconnected transmissive fractures within a body of porous low-*k* matrix blocks. Examples of Type 5 settings include fractured carbonates (limestone and dolomite), fractured shales, and fractured sandstones. Constant concentration nodes in the upper left-hand portion of the domain provide an analogous DNAPL source that is active from 0 to 20 years.

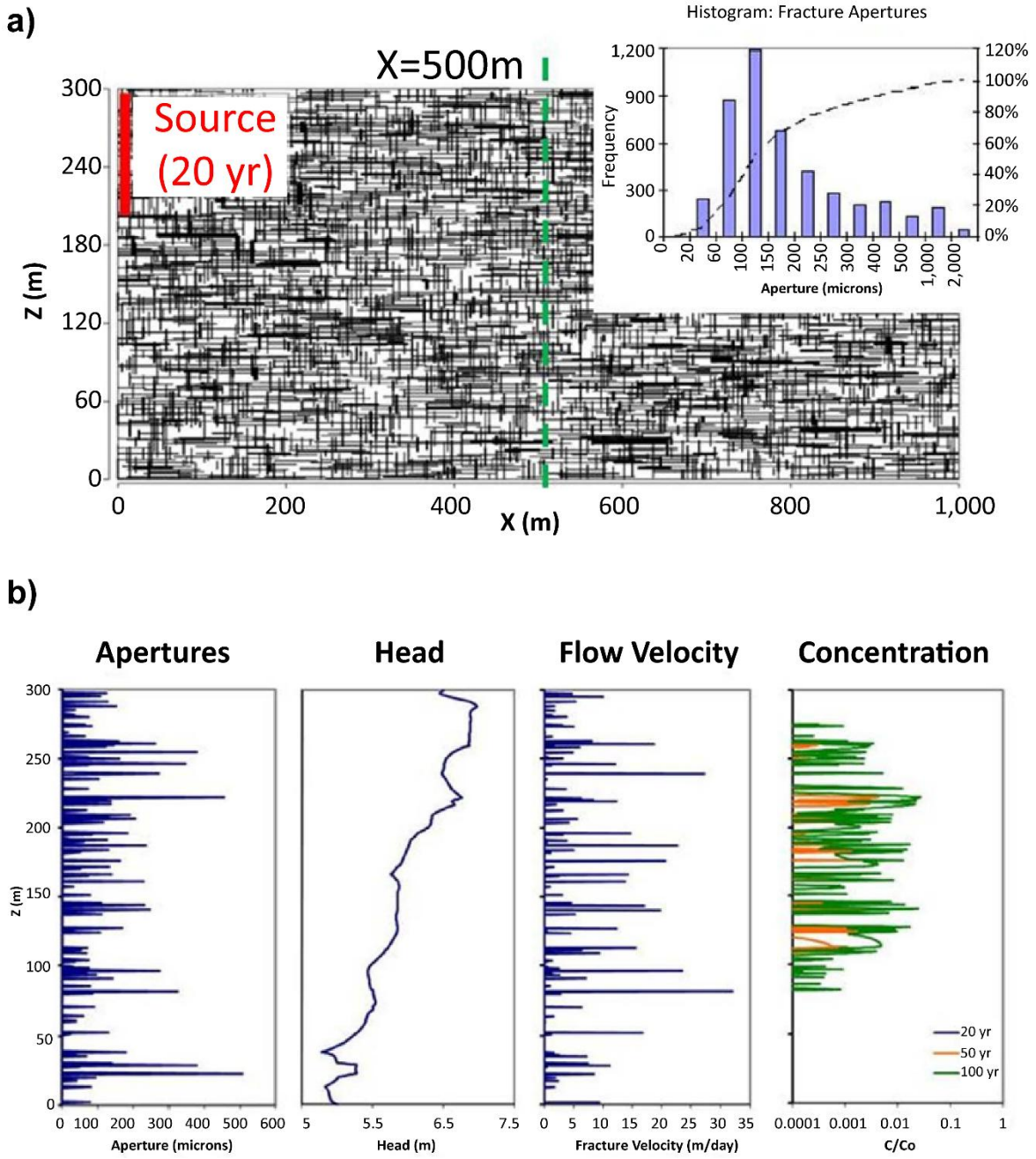

Figure 109 - FRACTRAN modeling of a fracture network in a sandstone. a) Model domain. b) Apertures, heads, flow velocities, and concentrations at 500 m (modified from Chapman & Parker, 2013).

The domain shown in Figure 109 is 300 m by 1 km with a contaminant half-life of ten years in both transmissive and low-k zones. Modeling was conducted using FRACTRAN (Sudicky & McLaren, 1992), a numerical model developed to simulate groundwater flow and contaminant transport in networks of statistically generated discrete fractures. The model incorporates key processes governing transport in fractured porous media, including matrix diffusion, sorption, and first-order degradation.

The low-k zone fraction f_{lk} is large and, correspondingly, the transmissive zone fraction f_T is small. Given a high f_{lk}, the domain is dominated by low-k space where contaminants can be stored and released. Given a low f_T transmissive zone, seepage velocities (up to 20 m/day) are larger than seepage velocities in Type 1 and Type 3 settings with equivalent volumetric discharges of groundwater.

Figure 110 presents aqueous concentrations normalized to initial influent aqueous concentrations in transmissive and low-k zones at 20, 50, and 100 years. Amazingly, given transmissive zone seepage velocities ranging up to tens of meters a day (thousands of meters a year), the plumes have only advanced to approximately 600, 700, and 1,000 m after 20, 50, and 100 years, respectively. Apparent transport velocities slow with time—0.08, 0.04, and 0.03 m/day after 20, 50, and 100 years, respectively. Slowing apparent transport velocities are attributed to ever larger volumes of subsurface media assimilating contaminants and ever larger periods of time for contaminants to degrade. Above all the examples advanced in this section, Figure 110 provides the most vivid illustration of contaminant assimilation via storage in low-k zones with modest rates of contaminant degradation.

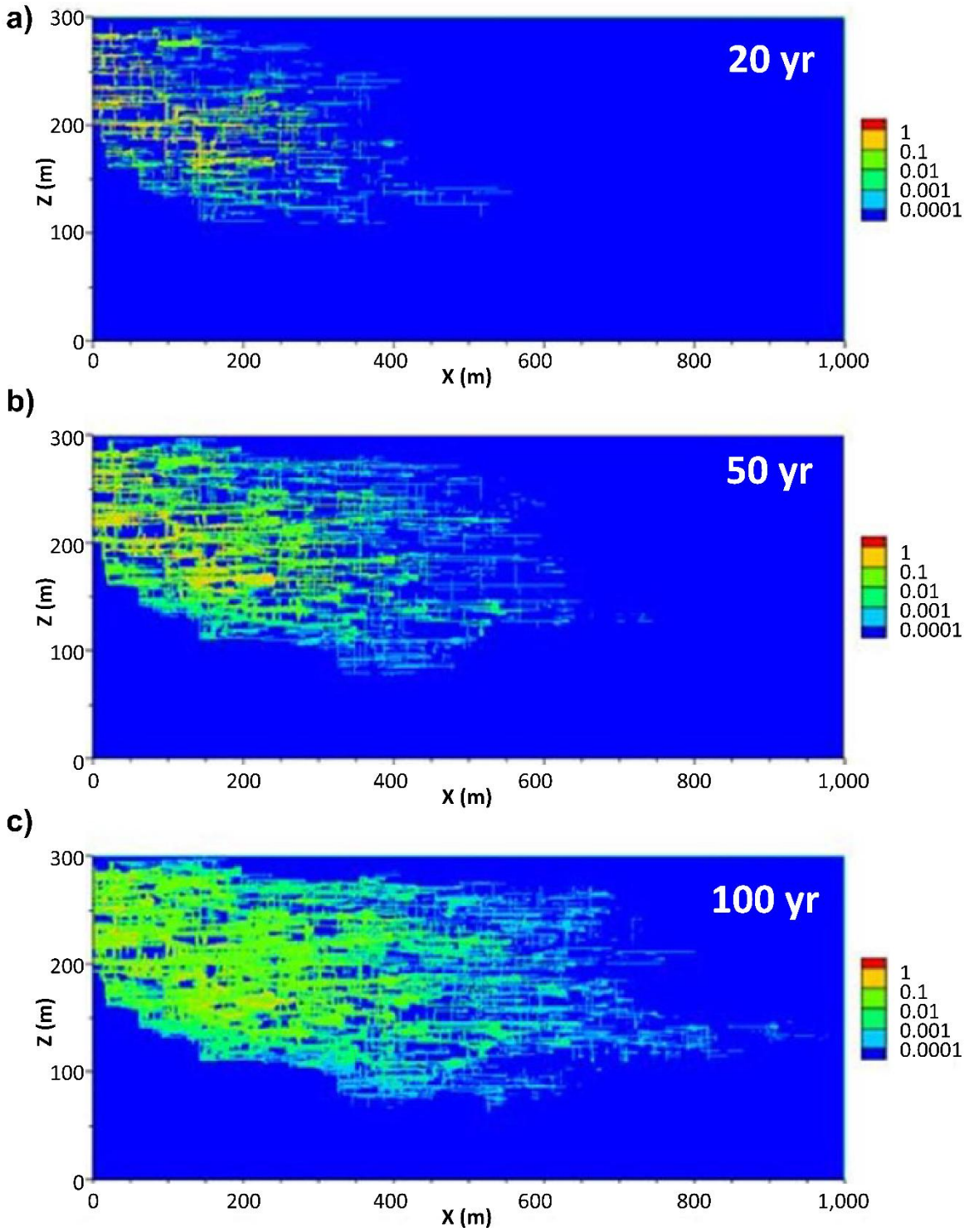

Figure 110 - Normalized aqueous concentrations in a fracture network in a sandstone at 20, 50, and 100 years given a contaminant half-life in transmissive and low-*k* zones of 10 years (modified from Chapman & Parker, 2013; Parker et al., 2012).

In closing, readers can contemplate the question of whether it is better to release contaminants into a Type 3 or a Type 5 setting. Given the complexities of managing risks associated with releases, one might consider answering by saying "*It all depends on. . .*" As we have touched on a subset of the scenarios in Chapman and Parker (2013), we encourage those wanting to know more to read Chapman and Parker (2013) and supporting

publications. Furthermore, we encourage interested readers to look for more recent modeling tools (as of 2025). These include FRACTRAN (Sudicky & McLaren, 1992) and FRAC3DVS (Therrien & Sudicky 1996) which evolved into HydroGeoSphere) and other less familiar codes including FracDNT (Parker et al. 2018) and Compflow (Slough et al., 1999; Sudicky 2014).

5.5.3 Semi-Analytical/Numerical Methods for Modeling Matrix Diffusion

Building on described analytical and high-resolution numerical modeling methods addressing contaminants in low-*k* zones, Dr. Ron Falta at Clemson University, USA, and colleagues have taken a new approach to modeling storage and release of contaminants in low-*k* zones, in plumes at field scales. Numerical methods are employed in transmissive zones and analytical methods are employed in low-*k* zones. First order reaction models capture transformations of CoC to new compounds (degradation products) and their subsequent transport. A primary advantage to the methods of Falta and collaborators is that only transmissive zones need to be spatially discretized improving computation efficiencies as compared to models employing high resolution numerical methods in both transmissive and low-*k* zones. Furthermore, tracking transport of CoCs and related degradation products is a large step forward.

Quoting Falta and Wang (2017) *"This method is an adaptation and extension of the* heat conduction *method of Vinsome and Westerveld (1980) used to simulate heat losses during thermally enhanced oil recovery"* (p. 39). Per Section 2.10 - Foundations - A demonstrative thought experiment, we embrace analogies between heat transfer in heterogeneous media and contaminant transport in heterogeneous media. Following mathematical principles and Carslaw and Jaeger (1959) it comes as no surprise that methods for modeling heat transfer in heterogeneous media can be employed to model contaminant transport in heterogeneous subsurface settings. A notable difference is that heat transfer models generally do not address reactions. The following provides a summary of publications advancing semi-analytical methods for addressing storage and release of contaminants in low-*k* zones in heterogeneous systems. Together, these studies establish and operationalize semi-analytical modeling as an efficient and accurate modeling approach for simulating transport in heterogeneous environments.

- **Falta and Wang (2017)** – Consideration is given to 1) a two-layer system of a transmissive zone overlying an infinite aquitard following Figure 87 and Figure 2; and 2) a single thin transmissive zone, analogous to a fracture, surrounded by low-*k* zones on both sides following Figure 85. Source strengths vary with time. Semi-analytical solutions for diffusion into and out of low-*k* zones yield close agreement with exact analytical solutions. Comparisons between high resolution MT3DMS numerical modeling and semi-analytical/numerical methods also show close agreement. Overall Falta and Wang (2017) advance the validity of semi-analytical methods for addressing

storage and release from low-*k* zones with the advantage of improved computational efficiency.

- **Muskus and Falta (2018)** – Expands on Falta and Wang (2017) by employing semi-analytical methods to address more complex settings and first-order transformation of CoCs to degradation products. Considered settings include systems of parallel fractures, matrix diffusion in a thin layer, matrix diffusion with embedded low permeability zones. Agreement between experimental laboratory results and high-resolution numerical models supports the proposed semi-analytical methods. Furthermore, contrary to models relying on dispersion to address low-*k* zones, results illustrate non-Gaussian, asymmetrical breakthrough curves as described by Sudicky and others (1985), Chapman and Parker (2005), and Sale and others (2007).
- **Farhat and others (2022)** – Applies the semi-analytical methods for matrix diffusion advanced in Falta and Wang (2017) and Muskus and Falta (2018) to perfluoroalkyl acids. Perfluoroalkyl acids are widely viewed as non-degrading CoCs. Results illustrate that given proper modeling methods, "*matrix diffusion can serve as an attenuation mechanism for the leading edge of a plume of non-degrading compounds like perfluoroalkyl acids (PFAAs), including perfluoro octane sulfonate (PFOS).*" (p. 1)
- **Falta and others (2023)** – Documents a flow and transport model in MODFLOW based on semi-analytical methods for matrix diffusion in heterogeneous media advanced in Falta and Wang (2017) and Muskus and Falta (2018). Falta and others (2023) provides access to a model that captures contaminant storage and release in low-*k* zones that can be used by wide audiences. We encourage parties interested in modeling transport in heterogeneous media to read Falta and others (2023).

A planning-level approach to semi-analytical/numerical modeling of matrix diffusion at impacted groundwater sites for approximations of contaminant extent and duration is REMChlor-MD. This modeling approach overcomes the need for centimeter-order grid resolutions to simulate matrix diffusion in many existing models (e.g., MODFLOW/MT3D; Chapman et al., 2012; Rasa et al., 2011). The development of REMChlor-MD is described by Newell and others (2024) and Newell and others (2025). REMChlor-MD was developed from a heat diffusivity strategy to simulate diffusion between high- and low-*k* zones and first order decay kinetics. Further information about REMChlor-MD, including links to access the REMChlor-MD Toolkit package are available at EnvrioWiki (https://www.enviro.wiki/index.php?title=REMChlor_-_MD↗).

5.6 Key Takeaways from Modeling Systems of Transmissive and Low-*k* Zones

Key takeaways from modeling systems of transmissive and low-*k* zones include the following.

- With time, releases of soluble DNAPLs progress from problems of DNAPLs in the transmissive zone within source zones to problems of aqueous and sorbed phases in low-*k* zones. Given the prevalence of sites where releases occurred in the 1970s and 1980s, in the 2020s the primary problem at many sites is contaminants in low-*k* zones. Given that conventional ADMs, as applied in analytical solutions or numerical models with coarse discretization, don't have low-*k* zones, ADMs typically fail to recognize the often-primary problem of contaminants in low-*k* zones.
- Homogeneous ADM Gaussian breakthrough curves versus asymmetrical HADiffR breakthrough curves miss early assimilation of contaminants in low-*k* zones, early arrival of plumes due to preferential flow through fractional transmissive zones, and persistent post-source removal exceedances of MCLs in transmissive zones.
- Over decades, modest rates of CoC degradation in low k zones can lead to depleting a majority of the released PCE. The potential importance of even slow degradation rates is a point Dr. Beth Parker has been advocating since the late 1990s.
- Absent significant degradation, allowing sources to persist for extended periods leads to potentially problematic accumulations of contaminants in low-*k* zones. Early reductions of mass discharge from sources can be far more effective than late reductions in mass discharge from sources.
- The distributions of PCE in considered compartments and losses due to degradation is dependent on heterogeneous occurrence of sorption and redox conditions (governing PCE half-lives) in transmissive and low-*k* zones. The bottom line is that heterogeneous occurrences of permeability, sorption, and reactions are a key part of modeling transport.
- Having seen HADiffR models, accepting conventional homogeneous ADMs is difficult. It seems likely that flawed ADMs have led to ineffective use of social resources, including failed deployments of pump and treat systems and source control remedies.
- Solely seeing subsurface contamination through the lens of monitoring wells (vertically averaged aqueous phase contaminants in transmissive zones), only two of fourteen compartments, can be grossly misleading. We need to look beyond water quality from monitoring wells as a primary basis for characterizing sites. The 14C model provides a useful point of embarkation for characterizing and managing releases.
- Stylistic modeling advanced herein for two-layer, periodic layer, two-layer with inclusions of low-*k* zones, and fractured rock with porous matrix blocks yield stylistic results that are missed using ADMs. Per the observational approach (Peck, 1969), valid stylistic results provide an essential basis for anticipating future conditions, identifying plausible alternative outcomes, resolving monitoring to resolve actual outcomes, and developing contingency plans for variations for alternative outcomes.

- While all models are wrong at some level, many models can be essential to building sound foundations for understanding contaminant transport and, correspondingly, efficiently managing sites.

5.7 Exercises Related to Section 5

After studying Section 5, the reader should be able to complete the following exercises: Exercise 30, Exercise 31, Exercise 32, Exercise 33, Exercise 34, Exercise 35, Exercise 36, Exercise 37, Exercise 38, and Exercise 39.

6 Finale

In retrospect, Theis was right in stating "The type of aquifer in which our homogeneous model of groundwater flow is most grossly inadequate is that of dealing with transport phenomena... the simple and useful model for problems of wellfield development will mislead us if we apply it to problems of transport" Theis (1967, pp. 139 and 146).

Despite Theis's words of caution, and perhaps driven by computational pragmatism, our principal approach to understanding contaminant transport in textbooks has been to employ a homogeneous-isotropic model of groundwater flow, classroom aquifers. The authors note that, with more than a half century of cumulative experience at field sites, the only place we have encountered classroom aquifers is in classrooms.

Following first principles, the standard approach found in textbooks has been to employ a single PDE, the heat equation, with boundary conditions, to a homogeneous domain with uniform groundwater flow. Advection of fluids carries contaminants, dispersion drives transverse and longitudinal mixing, and reactions modify transport. Primary arguments for invoking dispersion are that it provides a means of accounting for spreading associated with inevitable spatial variations in permeability and that it produces dilute concentrations observed in conventional monitoring wells. Notably, dilute concentrations observed in conventional monitoring wells are likely to be more about in-well mixing as compared to dispersion in aquifers.

The shortcomings of invoking dispersion include these three: (1) There is no clear basis for treating dispersion as a Fickian process, (2) there are limited means by which to resolve scale dependent dispersivity values, and (3) it fails to recognize storage and release of contaminants in low-k zones. The third is, in our opinion, the most consequential.

A common argument for using homogeneous models of groundwater flow for contaminant transport is the lack of practical alternatives. We disagree with this position. Per this text and supporting references, alternatives include:

- analytical solutions wherein separate PDEs are employed for transmissive and low-*k* zones, and fluxes and/or concentrations are equated at boundaries between transmissive and low-*k* zones;
- high-resolution numerical models wherein sufficient discretization of space and time is verified via testing for convergence of results to constant values with sequential reductions of discretizations; and
- semi-analytical/numerical methods predicated on heat transfer models wherein numerical methods are used in transmissive zones and analytical methods are used in low-*k* zones (e.g., REMChlor-MD; MODFLOW-USG-T; USGT-PFAS; and the upcoming REMFluor-MD model).

Another defense for using a homogeneous model of groundwater flow for contaminant transport has been that in classroom settings one needs to start with simple systems. We do not object to starting with simple systems. We do have a problem with not moving beyond simple systems if they provide misleading results.

The value of models recognizing storage and release of contaminants in low-*k* zones, with reactions, is that they provide stylistic insights as to governing processes that are consistent with what we see at field sites employing high-resolution site characterization methods. Given advanced stylistic understandings of governing processes and proper management of ever-present uncertainties (i.e., Peck's observational approach), we are in a far better position to provide better returns on resources invested in managing subsurface releases.

Lastly, can we expect our "practical" alternative models to rigorously forecast contaminant concentrations and fluxes at large times? As of 2025, the answer seems to be, probably not. Per Bredehoeft (2003, 2005), it seems naive to think we are past being surprised by things we have missed. Nevertheless, we feel satisfaction in realizing our progress in solving the riddles of contaminant transport and best management practices for releases. As the Rolling Stones sang in 1969, "You can't always get what you want, but if you try sometimes, you just might find you get what you need."

We hope others will sustain our vision of advancing *Modern Subsurface Contaminant Hydrology*. Surely this is not the end of the journey. Regrettably, efficient management of subsurface releases remains a leading global challenge. Managing contaminants in low-*k* zones needs more attention—specifically, managing them in ways that mitigate plausible exposure pathways, including human consumption of groundwater produced from transmissive zones. To get started, we point readers to these works:

- Sale and others (2013): *Management of contaminants stored in low permeability zones – A state of the science review*
- Wilson and others (2018): Treatment of aquifer matrix back diffusion
- Brooks and others (2020): *Strategies for managing risk due to back diffusion*
- Bolhari and Sale (2023): *Processes governing treatment of contaminants in low permeability zones*

Finally, we need to advance better understandings of how natural assimilation processes can responsibly be relied upon to address risks posed to human health and the environment by subsurface contaminants. Standardization is needed in how assimilative capacity is quantified, and regulatory frameworks need updating as we move to thoughtful site-closure decision-making (Devlin et al., 2024).

In closing, we hope many will embrace this work through study, practice, and future editions of this book.

7 Exercises

Exercise 1

How many of the compartments in the 14C model are informed by groundwater data from monitoring wells in

- source zones?
- plumes?

Solution to Exercise 1

Return to where text linked to Exercise 1

Exercise 2

Do the answers to Exercise 1 illustrate a problem? If yes, state why.

Solution to Exercise 2

Return to where text linked to Exercise 2

Exercise 3

What are three primary processes governing transport in heterogeneous aquifers?

Solution to Exercise 3

Return to where text linked to Exercise 3

Exercise 4

Given transmissive and low-*k* zones, why is advection limited in low-*k* zones?

Solution to Exercise 4

Return to where text linked to Exercise 4

Exercise 5

What can be learned from a site's depositional environment?

Solution to Exercise 5

Return to where text linked to Exercise 5

Exercise 6

In addition to permeability, what other important physical properties are nonuniformly (heterogeneously) distributed in subsurface media?

Solution to Exercise 6

Return to where text linked to Exercise 6

Exercise 7

Name two reasons to embrace mathematics as an essential foundation for studying the transport of contaminants in subsurface media.

Solution to Exercise 7

Return to where text linked to Exercise 7

Exercise 8

How might an assumed uniform aquifer bias anticipated arrival times?

Solution to Exercise 8

Return to where text linked to Exercise 8

Exercise 9

What is the value of a transmissive–low-*k* conceptualization of subsurface settings if it is only a stylistic approximation of actual conditions?

Solution to Exercise 9

Return to where text linked to Exercise 9

Exercise 10

Add lines delineating transmissive and low-*k* zones to Fred Payne's photo.

Solution to Exercise 10

Return to where text linked to Exercise 10

Exercise 11

1. Given the flow net in Figure 23, how would f_T values of 0.1 and 0.5 effect travel times from X to pumping well 1?
2. If X marks the spot in Figure 23 of a uniform constant source of TCE with a concentration of 100 ug/L and plug flow occurs in that flow tube, what will the concentration be at well 1?
3. How would storage of TCE in low-k zones via diffusion affect concentrations at well 1 while the source is active and after the source is removed?
4. What would happen if the source at X was instantaneously removed?

Solution to Exercise 11
Return to where text linked to Exercise 11

Exercise 12

Absent secondary permeability features, would you expect to find NAPLs in water-saturated low-permeability zones in source zones?

Solution to Exercise 12
Return to where text linked to Exercise 12

Exercise 13

Why might secondary low-*k* zone permeability features allow NAPLs to be present in low-*k* zones?

Solution to Exercise 13
Return to where text linked to Exercise 13

Exercise 14

Is it possible for low-permeability zones above the water table to be saturated with water?

Solution to Exercise 14
Return to where text linked to Exercise 14

Exercise 15

What is the necessary condition for a nonwetting phase to displace a wetting phase in a saturated media?

Solution to Exercise 15
Return to where text linked to Exercise 15

Exercise 16

How does having multiple fluids in a porous media affect the capacity of the media to conduct fluids?

Solution to Exercise 16
Return to where text linked to Exercise 16

Exercise 17

Given the challenges of parameterizing multiple-immiscible-fluid models, what is the value of multiple-phase models?

Solution to Exercise 17
Return to where text linked to Exercise 17

Exercise 18

Name three important points from the introduction to multiple immiscible phases in porous media provided in Section 3.2.

Solution to Exercise 18
Return to where text linked to Exercise 18

Exercise 19

Explain the processes governing diffusion.

Solution to Exercise 19
Return to where text linked to Exercise 19

Exercise 20

Given 25- and 40-percent porosities, respectively, in transmissive and low-*k* zones, which unit will have the larger effective diffusion coefficient?

Solution to Exercise 20
Return to where text linked to Exercise 20

Exercise 21

What makes storage and release from low-*k* zones a hysteretic process?

Solution to Exercise 21
Return to where text linked to Exercise 21

Exercise 22

What are the implications of hysteretic processes associated with storage and release from low-*k* zones?

Solution to Exercise 22

Return to where text linked to Exercise 22

Exercise 23

How does sorption in low-*k* zones affect storage and releases of stable contaminants from low-*k* zones?

Solution to Exercise 23

Return to where text linked to Exercise 23

Exercise 24

Based on typical depositional environments, why might low-*k* zones have greater sorptive capacities?

Solution to Exercise 24

Return to where text linked to Exercise 24

Exercise 25

Is there storage and release of contaminants in plumes in classroom aquifers?

Solution to Exercise 25

Return to where text linked to Exercise 25

Exercise 26

List three field phenomena that are not observed in classroom aquifers.

Solution to Exercise 26

Return to where text linked to Exercise 26

Exercise 27

How can a plume have stable extent when loading from sources are constant and contaminants are moving in the plume?

Solution to Exercise 27

Return to where text linked to Exercise 27

Exercise 28

Provide a list of field evidence for the following processes.

- dissolution of NAPL
- sorption
- transformation

Solution to Exercise 28
Return to where text linked to Exercise 28

Exercise 29

What might you miss if you looked only at CoCs in groundwater?

Solution to Exercise 29
Return to where text linked to Exercise 29

Exercise 30

How close do our models come to capturing processes in heterogeneous media that govern:

- dissolution of NAPL?
- sorption?
- transformation?

Solution to Exercise 30
Return to where text linked to Exercise 30

Exercise 31

Are there significant uncertainties associated with the input parameters used for our reaction models?

Solution to Exercise 31
Return to where text linked to Exercise 31

Exercise 32

Name three general approaches to modeling.

Solution to Exercise 32
Return to where text linked to Exercise 32

Exercise 33

Would you have more or less confidence in short- or long-term forecasts of contaminant concentrations in plumes?

Solution to Exercise 33

Return to where text linked to Exercise 33

Exercise 34

When can numerical methods create numerical dispersion that has nothing to do with contaminant transport?

Solution to Exercise 34

Return to where text linked to Exercise 34

Exercise 35

Name two mathematical approaches that can capture preferential transport in transmissive zones, diffusive exchanges of contaminants between transmissive and low-*k* zones, and spatially varying reactions in transmissive and low-*k* zones.

Solution to Exercise 35

Return to where text linked to Exercise 35

Exercise 36

What are models good for?

Solution to Exercise 36

Return to where text linked to Exercise 36

Exercise 37

What are models not good for?

Solution to Exercise 37

Return to where text linked to Exercise 37

Exercise 38

Was Theis correct when he stated in 1967 that "*[t]he type of aquifer in which our homogeneous model of groundwater flow* is most grossly inadequate is that of dealing with transport phenomena. . . *the simple and useful model for problems of wellfield development will mislead us if we apply it to problems of transport*"?

Solution to Exercise 38

Return to where text linked to Exercise 38

Exercise 39

Given uncertainty in results from models, how can we move forward?

Solution to Exercise 39

Return to where text linked to Exercise 39

8 References

Abbott, M. B., Bathurst, J. C., Cunge, J. A., O'Connell, P. E., & Rasmussen, J. (1986). An introduction to the European Hydrological System—Systeme Hydrologique Europeen, "SHE", 1: history and philosophy of a physically-based, distributed modelling system. *Journal of Hydrology, 87*(1–2), 45–59. https://doi.org/10.1016/0022-1694(86)90114-9↗.

Allen-King, R. M., Grathwohl, P., Ball, W. P. (2002). New modeling paradigms for the sorption of hydrophobic organic chemicals to heterogeneous carbonaceous matter in soils, sediments, and rocks. *Advances in Water Resources, 25*(8–12), 985–1016. https://doi.org/10.1016/S0309-1708(02)00045-3↗.

Allen-King, R. M., Loarah, M., Goode, D., Imbrigiotta, T., Tiedeman, C. I., & Shapiro, A. (2021). *A field method to quantify chlorinated solvent diffusion, sorption, abiotic and biotic degradation in low-permeability zones* (Final report, project ER-2533). SERDP-ESTCP.

Amos, R. T., Mayer, K. U., Bekins, B. A., Delin, G. N., &Williams, R. L. (2005). Use of dissolved and vapor-phase gases to investigate methanogenic degradation of petroleum hydrocarbon contamination in the subsurface. *Water Resources Research 41*(2). https://doi.org/10.1029/2004WR003433↗.

Anderson M. P., & Woessner, W. W. (2002). *Applied groundwater modeling simulation of flow advective transport*. Academic Press, Elsevier.

Anderson, M. R., Johnson, R. L., & Pankow, J. F. (1992). Dissolution of Dense Chlorinated Solvents into Groundwater. 3. Modeling of contaminant plumes from fingers and pools of solvent. *Environmental Science and Technology, 26*(5), 901–8. https://doi.org/10.1021/es00029a005↗.

Arnold, A. A., & Roberts, A. L. (2000). Pathways and kinetics of chlorinated ethylene and chlorinated acetylene reaction with Fe(0) particles. Environmental Science & Technology, *34*(9), 1794–1805. https://doi.org/10.1021/es990884q↗.

ASTM. (2016). *Standard guide for describing the functionality of a groundwater modeling code, american standard testing methods* (ASTM D6033-16, updated December 17, 2016).

Back, W., Rosenshein, J. S., & Seaber, P. R. (Eds.). (1988). *Hydrogeology: the geology of North America* (Vol. O–2). The Geologic Society of America. https://doi.org/10.1130/DNAG-GNA-O2↗.

Bear, J. (1972). *Dynamics of Fluids in Porous Media.* Dover Publications, Inc.

Betts, H. C., Puttick, M. N., Clark, J. W., Williams, T. A., Donoghue, P. C., & Pisani, D. (2018). Integrated genomic and fossil evidence illuminates life's early evolution and eukaryote origin. *Nature Ecology & Evolution, 2*(10), 1556–62. https://doi.org/10.1038/s41559-018-0644-x↗.

Bird, R. B., Stewart, W. E. & Lightfoot, E. N. (2002). *Transport phenomena* (2nd ed.). John Wiley & Sons, Inc.

Boggs, M. J., Young, S. C., Beard, L. M., Gelhar, L. W., Rehfeldt, K. R., & Adams, E. E. (1992). Field study of dispersion in a heterogeneous aquifer: 1. Overview and site description. *Water Research, 28*(12), 3281–91. https://doi.org/10.1029/92WR01756↗.

Bolhari, A. (2011). *Resolving the feasibility of treating chlorinated solvents stored in low permeability zones in sandy aquifers* [Doctoral dissertation, Department of Civil and Environmental Engineering, Colorado State University, Fort Collins, Colorado, US]. Proquest. https://www.proquest.com/openview/58d7bcd52ceaa78b708fb02b926cfbc0/1?cbl=18750&pq-origsite=gscholar↗.

Bolhari, A., & Sale, T. C. (2023). Processes governing treatment of contaminants in low permeability zones. *Science of The Total Environment*, *879*, 163010. https://doi.org/10.1016/j.scitotenv.2023.163010↗.

Borden, R. C., & Cha, K. Y. (2021). Evaluating the impact of back diffusion on groundwater cleanup time. *Journal of Contaminant Hydrology*, *243*. https://doi.org/10.1016/j.jconhyd.2021.103889↗.

Box, G. E. P. (1976). Science and Statistics, Journal of the American Statistical Association, 71 (356): 791–799, doi:10.1080/01621459.1976.10480949↗.

Bredehoeft, J. (2003). From models to performance assessment: the conceptualization problem: *Groundwater, 41*, 571–7. https://doi.org/10.1111/j.1745-6584.2003.tb02395.x↗.

Bredehoeft, J. (2005). The conceptual model problem—surprise. *Hydrogeology Journal, 13*, 37–46. https://doi.org/10.1007/s10040-004-0430-5↗.

Brooks, M. C., Yarney, E., & Huang, J. (2020). Strategies for managing risk due to back diffusion. *Groundwater Monitoring and Remediation, 41*(1), 76–98. https://doi.org/10.1111/gwmr.12423↗.

Brooks, R. H., & Corey, A. T. (1964). Hydraulic properties of porous media. *Hydrology Paper, 3*, 1–27.

Brown, R. (1828). *A brief account of microscopical observations on the particles contained in the pollen of plants and the general existence of active molecules in organic and inorganic bodies*. Richard Taylor.

Burdine, N. T. (1953). Relative permeability calculations from pore size distribution data, *Journal of Petroleum Technology, 5*(3), 71–7. https://doi.org/10.2118/225-G↗.

Campbell, C. E. (2017). *Effects of capping material on longevity of degradable contaminants in sediments* [Master's thesis, Colorado State University]. ProQuest. https://www.proquest.com/openview/e0d110f0f1212c0aa2788ed13bd39f0b/1?cbl=18750&pq-origsite=gscholar↗.

Carslaw, H. S., & Jaeger, J. C. (1959). *Conduction of heat in solids* (2nd ed.). Oxford University Press.

Carson, R. (1962). *Silent spring*. Houghton Mifflin Harcourt.

Chapman, S. W., & Parker, B. L. (2005). Plume persistence due to aquitard back diffusion following dense nonaqueous phase liquid source removal or isolation. *Water Resources Research, 41*(12). https://doi.org/10.1029/2005WR004224↗.

Chapman, S. W., & Parker, B. L. (2013) *State-of-the-science review management of contaminants stored in low permeability zones* (Chapter 5.0). TYPE SITE SIMULATIONS, SERDP Project ER-1740. https://apps.dtic.mil/sti/pdfs/ADA619819.pdf↗.

Chapman, S. W., Parker, B. L., Al, T., Wilkin, R., Cutt, D., Mishkin, K., & Nelson, S. (2021). Laboratory and modeling evidence for strong attenuation of a Cr (VI) plume in a mudstone aquifer due to matrix diffusion and reaction processes. *Soil Systems*, *5*(1), 18. https://doi.org/10.3390/soilsystems5010018↗.

Chapman, S. W., Parker, B. L., Cherry, J. A., McDonald, S. D., Goldstein, K. J., Frederick, J. J., St. Germain, D. J., Cutt, D. M., & Willams, C. E. (2013). Combined MODFLOW-FRACTRAN application to assess chlorinated solvent transport and remediation in fractured sedimentary rock. *Remediation, 23*(3), 7–35. https://doi.org/10.1002/rem.21355↗.

Chapman, S. W., Parker, B. L., Sale, T. C., & Doner, L. A. (2012). Testing high resolution numerical models for analysis of contaminant storage and release from low permeability zones. *Journal of Contaminant Hydrology, 136–137*, 106–16. https://doi.org/10.1016/j.jconhyd.2012.04.006↗.

Chen, W., Kan, A. T., Newell, C. J., Moore, E., & Tomson, M. B. (2002). More realistic soil cleanup standards with dual-equilibrium desorption. *Groundwater*, *40*(2), 153–64. https://doi.org/10.1111/j.1745-6584.2002.tb02500.x↗.

Chen, Y., Hou, D., Lu, C., & Spain, J. C. (2016). Effects of rate-limited mass transfer on modeling vapor intrusion with aerobic biodegradation. *Environmental Science & Technology, 50*(17), 9400–6. https://doi.org/10.1021/acs.est.6b01840↗.

Cherry, J. A. (2023). In my experience: the lessons from dispersion—don't believe everything you read. *Groundwater Monitoring and Remediation, 43*(3), 145–7. https://doi.org/ 10.1111/gwmr.12603↗.

Clark, C. W. (1971). *Einstein: the life and times*. The World Publishing Company.

Cohen, R. M., & Mercer, J. W. (1993). *DNAPL Site Evaluation*. C.K. Smoley, CRC Press.

Corey, A. T. (1994). *Mechanics of immiscible fluids in porous media*. The Groundwater Project. https://gw-project.org/books/mechanics-of-immiscible-fluids-in-porous-media↗.

Corson-Dosch, H. R., Nell, C. S., Volentine, R. E., Archer, A. A., Bechtel, E., Bruce, J. L., Felts, N., Gross, T. A., Lopez-Trujillo, D., Riggs, C. E., & Read, E. K. (2023). The water cycle (General Information Product 221). US Geological Survey. https://doi.org/10.3133/gip221↗.

Cox, R., A., and Nishikawa, T. (1991). A new total variation diminishing scheme for the solution of advective-dominant solute transport. Water Resources Research, 27(10): 2645-2654. https://doi.org/10.1029/91WR01746↗.

Daus, A. D., Frind, E. O., & Sudicky, E. A. (1985). Comparative error analysis in finite element formulations of the advection–dispersion equation. *Advances in Water Resources, 8*(2), 86–95. https://doi.org/10.1016/0309-1708(85)90005-3↗.

Davis, S. N., & DeWeist, R. J. M. (1966). *Hydrogeology*. Wiley.

Devlin J. F., Parker, B. L., Rhoades, A. J. H., Stuetzle, R. J., Mahendra, S., Scalia, J., & Blotevogel, J. (2024). Assimilative capacity is an under-utilized concept for regulating soil and groundwater contamination with important implications for site closure. *Groundwater Monitoring and Remediation, 44*(2), 3–4. https://doi.org/10.1111/gwmr.12650↗.

Doner, L. A. (2008). Tools to Resolve Water Quality Benefits of Upgradient Flux Reduction [Unpublished master's thesis]. Colorado State University.

Doty, C. B., & Travis, C. C. (1991). *The effectiveness of groundwater pumping as a restoration technology* (Technical report). USDOE. https://doi.org/10.2172/5737063↗.

Einarson, M., & Mackay, D. (2001). Peer reviewed: predicting impacts of groundwater contamination. *Environmental Science & Technology, 35*(3), 66A–73A. https://doi.org/10.1021/es0122647↗.

Einstein, A. (1905). Über die von der molekularkinetischen Theorie der Wärme geforderte Bewegung von in ruhenden Flüssigkeiten suspendierten Teilchen [On the movement of small particles suspended in stationary liquids required by the molecular-kinetic theory of heat]. *Annalen der Physik, 322*(8), 154–60. http://dx.doi.org/10.1002/andp.19053220806↗.

EPA. (1989). *Evaluation of groundwater extraction remedies* (EPA/540 2-89/054). US Environmental Protection Agency.

EPA. (2016). *A citizen's guide to radon* (EPA 4 02/K-12/002). US Environmental Protection Agency. www.epa.gov/radon↗.

Eykholt, G. R. (1999). Analytical solution for networks of irreversible first-order reactions. *Water Research, 33*(3), 814–26. https://doi.org/10.1016/S0043-1354(98)00273-5↗.

Falta, R. (2019). *A practical approach for modeling matrix diffusion effects in REMChlor-MD* (Certification Program Project ER-201426). SERDP-ESTCP https://serdp-estcp.mil/resources/details/c9b9f7a2-29ce-40ee-b181-cb9a37b65ba9↗.

Falta, R., Farhat, S., & Lemon, A. (2023). *Incorporating Matrix Diffusion in the New MODFLOW Flow and Transport Models for Unstructured Grids* (Project ER19-5028). SERDP-ESTCP.

Falta, R., Newell, C., & Farhat, S. (2019). *The REMChlor-MD groundwater transport and remediation model for sites with matrix diffusion* (Project ER-201426). SERDP-ESTCP. https://serdp-estcp.mil/resources/details/7f54ceb6-df12-4cae-8a6c-525f54a5b228↗.

Falta, R. W., & Wang, W. (2017). A Semi-Analytical Method for Simulating Matrix Diffusion in Numerical Transport Models. *Journal of Contaminant Hydrology, 197*, 39–49. https://doi.org/10.1016/j.jconhyd.2016.12.007↗.

Farhat, S. K., Adamson, D. T., Gavaskar, A. R., Lee, S. A., Falta, R. W., & Newell, C. J. (2020). Vertical Discretization Impact in Numerical Modeling of Matrix Diffusion in Contaminated Groundwater. *Groundwater Monitoring and Remediation*, *40*(2), 52–64. https://doi.org/10.1111/gwmr.12373↗.

Farhat, S. K., Newell, C. J., Lee, S. A., Looney, B. B., & Falta, R. W. (2022). Impact of matrix diffusion on the migration of groundwater plumes for Perfluoroalkyl acids (PFAAs) and other non-degradable compounds. *Journal of Contaminant Hydrology*, *247*, 103987. https://doi.org/10.1016/j.jconhyd.2022.103987↗.

Farhat, S. K., Newell, C. J., Sale, T. C., Dandy, D. S., Wahlberg, J. J., Seyedabbasi, M. A., McDade, J. M., & Mahler, N. T. (2012). *Matrix diffusion toolkit* [Developed for the Environmental Security Technology Certification Program (ESTCP)]. GSI Environmental Inc.

Farr, A. M., Houghtalen, J. R., & McWhorter, D. B. (1990). Volume estimation of light nonaqueous phase liquids in porous media. *Groundwater*, *28*(1), 48–56. https://doi.org/10.1111/j.1745-6584.1990.tb02228.x↗.

Feenstra, S., Cherry, J. A., & Parker, B. L. (1996). Conceptual Models for the Behavior of Dense Non-Aqueous Phase Liquids (DNAPLs) in the Subsurface. In J. F. Pankow, & J. A. Cherry, *Dense chlorinated solvents and other DNAPLs in groundwater* (ch 3). The Groundwater Project. https://gw-project.org/books/dense-chlorinated-solvents-and-other-dnapls-in-groundwater/↗.

Fetkovich, M. J., Fetkovich, E. J., & Fetkovich, M. D. (1996). Useful Concepts for Decline Curve Forecasting, Reserve Estimation, and Analysis. *Society of Petroleum Engineers*, *11*(1), 13–22. http://dx.doi.org/10.2118/28628-PA↗.

Fetter, C. W. (1999). *Contaminant Hydrogeology* (2nd ed.). Prentice Hall. https://doi.org/10.1029/99EO00097↗.

Fick, A. (1855). On liquid diffusion. *The London, Edinburgh, and Dublin Philosophical Magazine and Journal of Science*, *10*(63), 30–39. https://doi.org/10.1080/14786445508641925↗.

Fitts, C. R. (2002). *Groundwater science*. Academic Press.

Foster, S. S. D. (1975). The chalk triduum anomaly: a possible explanation. *Journal of Hydrology 25*, 159–65.

Freeze, R. A., & Cherry, J. A. (1979). *Groundwater*. The Groundwater Project. https://gw-project.org/books/groundwater/↗.

Gamlin, J., Newell, C. J., Holton, C., Kulkarni, P. R., Skaggs, J., Adamson, D. T., Blotevogel, J., & Higgins, C. P. (2024). Data Evaluation Framework for Refining PFAS Conceptual Site Models. *Groundwater Monitoring & Remediation*, *44*(4) 53–66. https://doi.org/10.1111/gwmr.12666↗.

Garg, S., Newell, C. J., Kulkarni, P. R., King, D. C., Adamson, D. T., Irianni Renno, M. M., & Sale, T. C. (2017). Overview of natural source zone depletion: processes, controlling factors, and composition change. *Groundwater Monitoring & Remediation*, *37*(3), 62–81. https://doi.org/10.1111/gwmr.12219↗.

Gelhar, L. W., C. Welty, C., & Rehfeldt, K. R. (1992). A critical review of data on field-scale dispersion in aquifers. *Water Resources Research, 28*(7), 1955–74. https://doi.org/10.1029/92WR00607↗.

Gilbert, D, & Sale, T. C. (2002). *Prototype field demonstration of an electrolytic permeable reactive barrier (PRB)* [Unpublished raw data]. Canadian Forces Base, Borden, Ontario, CA.

Gillham, R. W., & O'Hannesin, S. F. (1994). Enhanced degradation of halogenated aliphatics by zero-valent iron. *Groundwater, 32*(6), 958–67. https://doi.org/10.1111/j.1745-6584.1994.tb00935.x↗.

Gillham, R. W., Robin, M. J. L., Dytynyshyn, K. J., & Johnston, H. M. (1984). Diffusion of nonreactive and reactive solutes through fine-grained barrier materials. *Canadian Geotechnical Journal, 21*, 117–23. https://doi.org/10.1139/t84-056↗.

Gillham, R. W., Sudicky, E. A., Cherry, J. A., & Frind, E. O. (1984). An advection-diffusion concept for solute transport in heterogeneous unconsolidated geological deposits. *Water Resources Research, 20*(3), 369–78. https://doi.org/10.1029/WR020i003p00369↗.

Guilbeault M. A., Parker, B. l., & Cherry, J. A. (2005). Mass and flux distributions from DNAPL zones in sandy aquifers. *Groundwater, 43*(1), 70–86. https://doi.org/10.1111/j.1745-6584.2005.tb02287.x↗.

Hadley, P. W., & Armstrong, R. (1991). "Where's the Benzene?"—Examining California Ground-Water Quality Surveys. *Groundwater, 29*(1), 35–40. https://doi.org/10.1111/j.1745-6584.1991.tb00494.x↗.

Hadley, P. W., & Newell, C. (2014). The New Potential for Understanding Groundwater Contaminant Transport. *Groundwater, 52*(2), 174–86. https://doi.org/10.1111/gwat.12135↗.

Harvey, C. F., & Gorelick, S. M. (2000). Rate-limited mass transfer on macrodispersion: which dominates plume evolution at the macrodispersion experiment (MADE) site? *Water Resources Research*, *36*(3), 637–50. https://doi.org/10.1029/1999WR900247↗.

Hem, J. D. (1992). Study and interpretation of the chemical characteristics of natural water (3rd ed.) (Water-Supply Paper 2254). US Geological Survey.

Hendrickson, J. B., Cram, D. J., & Hammond, G. (1970). *Organic Chemistry*. McGraw Hill.

Hughes, J. D., Langevin, C. D., & Banta, E. R. (2017). *Documentation for the MODFLOW 6 framework* (Series no. 6-A57, Index ID tm6A57). US Geological Survey.

Hunkeler, D., Aravena, R., & Butler, B. J. (1999). Monitoring microbial dechlorination of tetrachloroethene (PCE) in groundwater using compound-specific stable carbon isotope ratios: microcosm and field studies. *Environmental Science & Technology, 33*(16), 2733–8. https://doi.org/10.1021/es981282u↗.

International Network for Acid Prevention (INAP). (2024). *Global Acid Rock Drainage Guide* (GARD). The International Network for Acid Prevention. www.gardguide.com↗.

Interstate Technology and Regulatory Council. (2009). *Evaluating Natural Source Zone Depletion at Sites with LNAPL*.

Irianni-Renno, M., Akhbari, D., Olson, M. R., Byrne, A. P., Lefevre, E., Zimbron, J., Lyverse, M., Sale, T. C., & De Long, S. K. (2015). Comparison of bacterial and archaeal communities in depth-resolved zones in an LNAPL body. *Applied Microbiology and Biotechnology*, *100*(7), 3347–60. https://doi.org/10.1007/s00253-015-7106-z↗.

Kan, A. T., Fu, G., Hunter, M., Chen, W., Ward, C. H., & Tomson, M. B. (1998). Irreversible sorption of neutral hydrocarbons to sediments: experimental observations and model predictions. *Environmental Science & Technology*, *32*(7), 892–902. https://doi.org/10.1021/es9705809↗.

Karimi Askarani, K., Stockwell, E. B., Piontek, K., & Sale, T. C. (2018). Thermal monitoring of natural source zone depletion. *Groundwater Monitoring & Remediation*, *38*(3), 43–52. https://doi.org/10.1111/gwmr.12286v↗.

Kavanaugh, M. C., Rao, P. S., & Wood, A. L. (2003) The DNAPL remediation challenge: is there a case for source depletion? (Expert Panel Report, EPA/600/R-03/143). US Environmental Protection Agency. https://cfpub.epa.gov/si/si_public_record_report.cfm?Lab=NRMRL&dirEntryId=84765↗.

Kiaalhosseini, S., Sale, T. C., Rogers, R., Irrianni-Renno, M., & Johnson, R. (2025). Cryogenic Core Collection and High-Resolution Sample Analysis to Support Subsurface Remediation. In R. Naidu, J. Sadeque, & A. Lal (Eds.), *Sampling and Assessment of Contaminated Sites* (in print). World Scientific Publishing Company.

Kulkarni, P. R., Walker, K. L., Newell, C. J., Askarani, K. K., Li, Y., & McHugh, T. E. (2022). Natural source zone depletion (NSZD) insights from over 15 years of research and measurements: a multi-site study. Water Research, *225*, 119170. https://doi.org/10.1016/j.watres.2022.119170↗.

Langevin, C D.., & Guo, W. (2006) MODFLOW/MT3DMS-Based Simulation of Variable-Density Ground Water Flow and Transport. *Groundwater*, *44(3)*, 339-351. http://doi.org/10.1111/j.1745-6584.2005.00156.x↗.

Leopold, A. (1949). *A Sand County almanac*. Oxford University Press.

Lewis A. R., Ronayne, M. J., & Sale, T. C. (2016). Estimating aquifer properties using derivative analysis of water level time series from active well fields. *Groundwater*, *54*(3), 414–24. https://doi.org/10.1111/gwat.12368↗.

Lindsay, W. L. (1979). *Chemical Equilibria in Soils*. John Wiley and Sons.

Mackay, D., & Cherry, J. A. (1989). Groundwater contamination: pump and treat remediation. *Environmental Science Technology*, *23*(6), 630–6. https://doi.org/10.1021/es00064a001↗.

Mackay, D. M., Allen King, R. M, & Rixey, W. G. (2024). *Properties of Organic Contaminants*, The Groundwater Project. https://doi.org/10.62592/XFAF9509↗.

Mahler, N., Sale, T., & Lyverse, M. (2012). A mass balance approach to resolving LNAPL stability. *Groundwater*, *50*(6), 861–71. https://doi.org/10.1111/j.1745-6584.2012.00949.x↗.

Marinelli, F. (2024). *Darcy's law in variable density groundwater systems*. The Groundwater Project. https://gw-project.org/books/darcys-law-in-variable-density-groundwater-systems/↗.

McCoy, K., Zimbron, J., Sale, T. C., & Lyverse, M. (2015). Measurement of natural losses of LNAPL using CO_2 traps. *Groundwater*, *53*(4), 658–67. https://doi.org/10.1111/gwat.12240↗.

McWhorter, D. and J. Nelson, (1980). Seepage in the Partially Saturated Zone Beneath Tailings Impoundments. Mining Engr., April. pp. 432-439.

McWhorter, D. B. (2021). *Flux equations for gas diffusion in porous media*. The Groundwater Project. https://gw-project.org/books/flux-equations-for-gas-diffusion-in-porous-media/↗.

McWhorter, D. B., & Sale, T. C. (2003). [Reply to comment by P. S. C. Rao, & J. W. Jawitz on the article "Steady state mass transfer from single-component dense nonaqueous phase liquids in uniform flow fields" found at https://doi.org/10.1029/2000WR900236↗. https://agupubs.onlinelibrary.wiley.com/doi/full/10.1029/2002WR001423↗.

McWhorter, D. B., & Sunada, D. K. (1977). *Groundwater hydrology and hydraulics*. The Groundwater Project. https://gw-project.org/books/groundwater-hydrology-and-hydraulics/↗.

Mercer, J. W., & Cohen, R. M. (1990). A review of immiscible fluids in the subsurface: properties, models, characterization, and remediation. *Journal of Contaminant Hydrology*, *6*(2), 107–63. https://doi.org/10.1016/0169-7722(90)90043-G↗.

Mercer, J. W, Skipp, D. C., & D. Giffin, D. (1990). *Basics of pump-and-treat ground-water remediation technology* (Special report). US Environmental Protection Agency.

Merck. (2006). The Merck index: an encyclopedia of chemicals, drugs, and biologicals (14th ed.). Merck & Co. Inc.

Merriam-Webster. (n.d.). Empirical. In Merriam-Webster's unabridged dictionary. Retrieved June 1, 2025, from https://unabridged.merriam-webster.com/unabridged/empirical↗.

Millington, R. J., & Quirk, J. M. (1961). Permeability of Porous Solids. *Transactions of the Faraday Society*, *57*, 1200–7. https://doi.org/10.1039/TF9615701200↗.

Milton, J., 1608–1674. (2000). *Paradise lost*. Penguin Books.

Mumford, G. M., Kueper, B. H., & Lenhard, R. J. (2024). *Flow and distribution of non-aqueous phase liquids*. The Groundwater Project. https://gw-project.org/books/flow-and-distribution-of-non-aqueous-phase-liquids/↗.

Muskus, N., & Falta, R. W. (2018). Semi-analytical method for matrix diffusion in heterogeneous and fractured systems with parent-daughter reactions. *Journal of Contaminant Hydrology*, *218*, 94–109. https://doi.org/10.1016/j.jconhyd.2018.10.002↗.

National Research Council (NRC). (1994). *Alternatives for ground water cleanup*. National Academies Press.

National Research Council (NRC). (2003). *Environmental cleanup at Navy facilities*. National Academies Press.

National Research Council (NRC). (2005). *Contaminants in the subsurface*. National Academies Press.

National Research Council (NRC). (2013). *Alternatives for managing the nation's complex contaminated groundwater sites*. National Academies Press. https://doi.org/10.17226/14668↗.

Newell, C. J., Kulkarni, P. R., Stockwell, E. B., Cook, J. S., & Mathioudakis, M. R. (2025). REMChlor-MD technical guidance and adaptation for Per- and Polyfluoroalkyl substances (PFAS). Air Force Civil Engineer Center.

Newell, C. J., Kulkarni, P. R., Stockwell, E., Mathioudakis, M. R., & Cook, J. S. (2024). Final technical report: can the REMChlor-MD model be used to evaluate passive and active PFAS remediation alternatives? Prepared for Air Force Civil Engineer Center (AFCEC).

Pankow, J. F. (1991). *Aquatic chemistry concepts*. Lewis Publishers. https://doi.org/10.1201/9781315137742↗.

Pankow, J. F., & Cherry, J. A. (1996). *Dense chlorinated solvents and other DNAPLs in groundwater*. The Groundwater Project. https://gw-project.org/books/dense-chlorinated-solvents-and-other-dnapls-in-groundwater/↗.

Parker, B. L., Chapman, S. W., & Cherry, J. A. (2010). Plume persistence in fractured sedimentary rock after source zone removal. *Groundwater*, *48*(6), 799–808. https://doi.org/10.1111/j.1745-6584.2010.00755.x↗.

Parker, B. L., Chapman, S. W., Goldstein, K. J., & Cherry, J. A. (2019). Multiple lines of field evidence to inform fracture network connectivity at a shale site contaminated with dense non-aqueous phase liquids. In U. Ofterdinger, A. M. MacDonald, J.-C. Comte, & M. E. Young (Eds.), *Groundwater in Fractured Bedrock Environments: Managing Catchment and Subsurface Resources* (pp. 101–127). The Geological Society of London. https://doi.org/10.1144/SP479.8↗.

Parker, B. L., Chapman, S. W., & Guilbeault, M. A. (2008). Plume persistence caused by back diffusion from thin clay layers in a sand aquifer following TCE source-zone hydraulic isolation. *Journal of Contaminant Hydrology, 102*(1–2), 86–104. https://doi.org/10.1016/j.jconhyd.2008.07.003↗.

Parker, B. L., Cherry, J. A., & Chapman, S. W. (2012). Discrete fracture network approach for studying contamination in fractured rock. *AQUA mundi, 3*(2), 101–16. https://citeseerx.ist.psu.edu/document?repid=rep1&type=pdf&doi=10baa8f32d0032dbcbdb4a366e8f7eee52347e89↗.

Payne, F. C., Quinnan, J. A., & Potter, S. T. (2008). *Remediation Hydraulics*. CRC Press. https://doi.org/10.1201/9781420006841↗.

Peck, R. B. (1969) advantages and limitations of the observational method in applied soil mechanics. *Géotechniques, 19*(2) 171–87. https://doi.org/10.1680/geot.1969.19.2.171↗.

Pierce, A. A., Chapman, S. W., Zimmerman, L. K., Hurley, J. C., Aravena, R., Cherry, J. A., & Parker, B. L. (2018). DFN-M field characterization of sandstone for a process-based site conceptual model and numerical simulations of TCE transport with degradation. *Journal of Contaminant Hydrology, 212*, 96–114. https://doi.org/10.1016/j.jconhyd.2018.03.001↗.

Poeter, E., & Hsieh, P. (2020). *Graphical construction of groundwater flow nets*. The Groundwater Project. https://gw-project.org/books/graphical-construction-of-groundwater-flow-nets/↗.

Poeter, E., Fan, Y., Cherry, J. A., Woods, W., & Mackay, D. (2020). *Groundwater in our water cycle*. The Groundwater Project. https://gw-project.org/books/groundwater-in-our-water-cycle/↗.

Post, V. E. A., & Simmons, C. T. (2022). *Variable-density groundwater flow*. The Groundwater Project. https://gw-project.org/books/variable-density-groundwater-flow/↗.

Rao, P. S. C., & Jawitz, J. W. (2003). [Comment on "Steady state mass transfer from single-component dense nonaqueous phase liquids in uniform flow fields" by T. C. Sale and D. B. McWhorter found at https://doi.org/10.1029/2000WR900236↗]. https://doi.org/10.1029/2001WR000599↗.

Rasa, E., Chapman, S. W., Bekins, B. A., Fogg, G. E., Scow, K. M., & Mackay, D. M. (2011). Role of back diffusion and biodegradation reactions in sustaining an MTBE/TBA plume in alluvial media, J*ournal of Contaminant Hydrology, 126*(3–4), 235–47. https://doi.org/10.1016/j.jconhyd.2011.08.006↗.

Ritter, D. F., Kochel, R. C., & Miller, J. R. (1995). *Process geomorphology* (3rd ed.). Wm. C. Brown Publishers.

Rittmann, B. E. (2023). *Biotic transformations of organic contaminants*. The Groundwater Project. https://gw-project.org/books/biotic-transformations-of-organic-contaminants/↗.

Roads, E. (2020). *Analysis of contaminant mass in place in transmissive and low-k zones* [Master's thesis, Colorado State University]. ProQuest. https://www.proquest.com/openview/8a57598034149098795a54335ad8ff9a/1?cbl=18750&diss=y&pq-origsite=gscholar↗.

Roberts, P. V., Goltz., M. N., & Mackay, D. M. (1986). A natural gradient experiment on solute transport in a sand aquifer 3. retardation estimates and mass balances for organic solutes. *Water Resources Research, 22*(13), 2047–58. https://doi.org/10.1029/WR022i013p02047↗.

Robertson, W. (2021). *Septic system impacts on groundwater quality*. The Groundwater Project. https://gw-project.org/books/septic-system-impacts-on-groundwater-quality/↗.

Sale, T. C. (1998). *Interphase mass transfer from single component DNAPLs* [Doctoral dissertation, Colorado State University]. ProQuest. https://www.proquest.com/openview/36af92f2a70840a78c8257cc7ae0fda2/1?cbl=18750&diss=y&pq-origsite=gscholar↗.

Sale, T. C. (2001). *Methods for determining inputs to environmental petroleum hydrocarbon mobility and recovery models* (Technical Report API 4711). American Petroleum Institute.

Sale, T. C., & Applegate, D. (1997). Mobile NAPL recovery: conceptual, field, and mathematical considerations. *Groundwater, 35*(3), 418–26. https://doi.org/10.1111/j.1745-6584.1997.tb00101.x↗.

Sale, T. C., Gallo, S., Askarani, K. K., Iranni-Renno, M., Lyverse, M., Hopkins, H., Blotevogel, J., & Burge, S. (2021). Real-time soil and groundwater monitoring via spatial and temporal resolution of biogeochemical potentials. *Journal of Hazardous Materials*, *408*, 124403. https://doi.org/10.1016/j.jhazmat.2020.124403↗.

Sale, T. C., Hopkins, H., & Kirkman, A. (2018). *Managing Risks at LNAPL Sites* (2nd ed.). American Petroleum Institute, Soils and Groundwater Research Program, Bulletin 18.

Sale, T. C., Illangasekare, T., Zimbron, J., Rodriguez, D., Wilking, B., & Marinelli, F. (2007). *AFCEE Source Zone Initiative* (Project report). Air Force Center for Environmental Excellence.

Sale, T. C., & McWhorter, D. B. (2001). Steady state mass transfer from single-component dense nonaqueous phase liquids in uniform flow fields. *Water Resources Research, 37*(2), 393–404. https://doi.org/10.1029/2000WR900236↗.

Sale, T. C., & Newell, C. (2010). Implications of Source Management on Chlorinated Solvent Plumes. In H. F. Stoo, & C. H. Ward (Eds.), In situ *remediation of chlorinated solvent plumes* (pp. 185–216). Springer. https://link.springer.com/chapter/10.1007/978-1-4419-1401-9_7↗.

Sale, T. C., & Newell, C. (2011). *A guide for selecting remedies for subsurface releases of chlorinated solvents* (ESTCP Project ER-200530). GSI Environmental, Inc. https://agris.fao.org/search/en/providers/122415/records/647368c853aa8c89630d64bf↗.

Sale, T. C., Olson, M., Gilbert, D., & Petersen, M. (2010). *Field demonstration/validation of electrolytic barriers for energetic compounds at Pueblo chemical depot* (ESTCP Project ER-0519). Environmental Security Technology Certification Program. https://clu-in.org/download/techfocus/prb/prbs-er-0519-fr.pdf↗.

Sale, T. C., Parker, B. L., Newell, C. J., & Devlin, J. F. (2013). *Management of contaminants stored in low permeability zones a state-of-the-science review* (SERDP Project ER-1340). https://apps.dtic.mil/sti/pdfs/ADA619819.pdf↗.

Sale, T. C., Zimbron, J. A., & Dandy, D. S. (2008). Effects of reduced contaminant loading on downgradient water quality in an idealized two-layer granular porous media. *Journal of Contaminant Hydrology, 102*(1–2), 72–85. https://doi.org/10.1016/j.jconhyd.2008.08.002↗.

Schwarzenbach, R., Gschwend, P. M., & Imboden, D. M. (1993). *Environmental organic chemistry*. Wiley.

Schwarzenbach, R., Gschwend, P. M., & Imboden, D. M. (2017). *Environmental organic chemistry* (3rd ed.). Wiley.

Schwille, F. (1984). Leichtfluchtige Chlorkohlenwasserstoffe in porosen und kliiftigen Medien, Besondere Mitteilungen zum Deutschen Gewasserkundlichen Jahrbuch, Nr. 46 [Volatile chlorinated hydrocarbons in porous and fibrous media, Special Reports on the German Hydrological Yearbook, No 46], Bundesanstalt fur Gewasserkunde [Federal Institute of Hydrology].

Schwille, F., & Pankow, J. F. (1988) *dense chlorinated solvents in porous and fractured media: model experiments*. Lewis Publishers. https://www.osti.gov/biblio/6419077↗.

Slough, K., J., Sudicky, E., A., & Forsyth, P. A. (1999). Numerical simulation of multiphase flow and phase partitioning in discretely fractured geologic media. *Journal of Contaminant Hydrology*, 40(2), 107-136. https://www.doi.org/10.1016/S0169-7722(99)00051-0↗.

Shackelford, C. D. (1991). Laboratory diffusion testing for waste disposal—a review. *Journal of Contaminant Hydrology*, *7*(3), 177–217. https://doi.org/10.1016/0169-7722(91)90028-Y↗.

Shapiro, A. M. (2019). *The retention and release of groundwater contaminants in fractured rock and other dual-porosity media by matrix diffusion and "effective" matrix diffusion*. US Geological Survey.

Skinner, A. M. (2013). *LNAPL longevity as a function of remedial actions: tools for evaluating LNAPL remedies* [Master's thesis, Colorado State University]. ProQuest. https://www.proquest.com/openview/df12b3d5e6083343035b7ed6723659e6/1?cbl=18750&pq-origsite=gscholar↗.

Skogen, M. D., Ji, R., Akimova, A., Daewel, U., Hansen, C., Hjøllo, S. S., van Leeuwen, S. M., Maar, M., Macias, D., Mousing, E. A., Almoroth-Rosell, E., Ssailley, S. F., Spence, M. A., Troost, T. A., & van de Wolfshaar, K. (2021). Disclosing the truth: Are models better than observations? Marine Ecology Progress Series, *680*, 7–13. https://doi.org/10.3354/meps13574↗.

Strack, O. D. L. (2017). *Analytical groundwater mechanics*. Cambridge University Press.

Stumm, W., & Morgan, J. J. (1995). *Aquatic chemistry: chemical equilibria and rates in natural waters* (3rd ed.). Wiley.

Sudicky, E. A. (2014). Computational and experimental investigation of contaminant plume response to DNAPL source zone architecture and depletion in porous and fractured media. (SERDP Project ER-1610). https://serdp-estcp.mil/projects/details/c6302f46-5618-4f6d-80c1-cd6b4a38c12a↗.

Sudicky, E. A., Gillham, R. W., & Frind, E. O. (1985). Experimental investigation of solute transport in stratified porous media: 1. the nonreactive case. *Water Resources Research 21*(7), 1035–1041. https://doi.org/10.1029/WR021i007p01035↗.

Sudicky, E. A., & McLaren, R. G. (1992). The Laplace Transform Galerkin Technique for long-scale simulation of mass transport in discretely fractured porous formations. *Water Resources Research, 28*(2), 499–512. https://doi.org/10.1029/91WR02560↗.

Taggart, D. M., & Key, T. A. (2024). Molecular Biological Tools Used in Assessment and Remediation of Petroleum Hydrocarbons in Soil and Groundwater. In *Advances in the Characterization and Remediation of Sites Contaminated with Petroleum Hydrocarbons* (pp. 329–59). Springer.

Tang, D. H., Frind, E. O., & Sudicky, E. A. (1981). Contaminant transport in fractured porous media: analytical solution for a single fracture. *Water Resources Research, 17*(3), 555–64. https://doi.org/10.1029/WR017i003p00555↗.

Theis, C. V. (1935). The relationship between the lowering of the piezometric surface and the rate and duration of discharge of a well using groundwater storage. *Eos American Geophysical Union Transactions, 16*(2), 519–24. https://doi.org/10.1029/TR016i002p00519↗.

Theis, C. V. (1967). *Aquifers and models, symposium on ground-water hydrology, San Francisco, California, US*. American Water Resources Association.

Therrien, R., & Sudicky, E. A. (1996). Three-dimensional analysis of variably-saturated flow and solute transport in discretely-fractured porous media. Journal of Contaminant Hydrology, 23(1-2), 1-44. https://doi.org/10.1016/0169-7722(95)00088-7↗.

Thomas, J. W. (1995). *Numerical partial differential equations: finite difference methods.* Springer.

Thornton, S. F., Nicholls, H. C. G., Rolfe, S. A., Mallinson, H. E. H., & Spence, M. J. (2020). Biodegradation and fate of ethyl *tert*-butyl ether (ETBE) in soil and groundwater: a review. *Journal of Hazardous Materials, 391*, 122046. https://doi.org/10.1016/j.jhazmat.2020.122046↗.

Thiem, G. (1906). Hydrologische methoden (Hydrologic methods) : Leipzig, J. M. Gebhardt, 56 p.

Todd, D. K. (1980). *Groundwater hydrology* (2nd ed.). Wiley.

Tratnyek, P. G., Johnson, R. L., Lowry, G. V., & Brown, R. A. (2014). *In situ* chemical reduction for source remediation. In B. H. Kueper, H. F. Stroo, C. M. Vogel, & C. H. Ward (Eds.), *Chlorinated Solvent Source Zone Remediation* (pp. 307–51). Springer. https://doi.org/10.1007/978-1-4614-6922-3_10↗.

US Nuclear Regulatory Commission. (2000). *A performance assessment methodology for low-level radioactive waste disposal facilities*. Office of Nuclear Materials Safety and Safeguards.

van der Kamp, G., Luba, L. D., Cherry, J. A., & Maathuis, H. (1994). Field study of a long and very narrow contaminant plume. *Groundwater, 32*(6), 1008–16. https://doi.org/10.1111/j.1745-6584.1994.tb00940.x↗.

van Genuchten, M. T. (1980). A closed-form equation for predicting the hydraulic conductivity of unsaturated soils. *Soil Science Society of America Journal, 44*(5), 892–8. https://doi.org/10.2136/sssaj1980.03615995004400050002x↗.

Vinsome, P. K. W., & Westerveld, J. (1980). A simple method for predicting cap and base rock heat losses in thermal reservoir simulators. *The Journal of Canadian Petroleum Technology, 19*(3), 87–90. https://doi.org/10.2118/80-03-04↗.

Wahlberg, J. J. (2013). *Retardation and reaction in low permeability layers in groundwater plumes* [Unpublished master's Thesis]. Colorado State University.

Wang, L., Li, L., Chen, X., Tian, X., Wang, X., & Luo, G. (2014). Biomass Allocation Patterns across China's Terrestrial Biomes. *PLoS ONE 9*(4), e93566. https://doi.org/10.1371/journal.pone.0093566↗.

Merriam-Webster's Unabridged Dictionary (2025), Merriam-Webster, https://unabridged.merriam-webster.com/unabridged/empirical.

Wiedemeier, T. H., Rifai, H. S., Newell, C. J., & Wilson, J. T. (1999). *Natural attenuation of fuels and chlorinated solvents in the subsurface*. Wiley.

Wiedemeier, T. H., Swanson, M. A., Moutoux, D. E., Gordon, E. K., Wilson, J. T., Wilson, B. H., Hansen, J. E., Haas, P., & Chapelle, F. H. (1996). *Technical protocol for evaluating natural attenuation of chlorinated solvents in groundwater*. US Air Force Center for Environmental Excellence.

Wilson, J. L., Conrad, S. H., Mason, W. R., Peplinski, W., & Hagan, E. (1990). *Laboratory investigation of residual liquid organics from spills, leaks, and the disposal of hazardous wastes in groundwater* (EPA/600/6-90/004, NTIS 90-235797). US Environmental Protection Agency.

Wilson, S. B., Mork, B. V., Birnstingl, J., & Thoreson, K. A. (2018). *Treatment of aquifer matrix back diffusion* (US Patent No. US9776898B2). US Patent and Trademark Office. https://patents.google.com/patent/US9776898B2/en↗.

Woessner, W. W. (2020). *Groundwater-surface water exchange*. The Groundwater Project. https://gw-project.org/books/groundwater-surface-water-exchange/↗.

Woessner, W. W., & Poeter, E. P. (2020). *Hydrogeologic properties of earth materials and principles of groundwater flow*. The Groundwater Project. https://gw-project.org/books/hydrogeologic-properties-of-earth-materials-and-principles-of-groundwater-flow/↗.

You, X., Liu, S., Dai, C., Zhong, G., Duan, Y., & Tu, Y. (2020). Acceleration and centralization of a back-diffusion process: effects of EDTA-2Na on cadmium migration in high- and low-permeability systems. *Science of The Total Environment, 706*, 135708. https://doi.org/10.1016/j.scitotenv.2019.135708↗.

Zech, A., Attinger, S., Bellin, A., Cvetkovic, V., Dagan, G., Dietrich, P., Fiori, A., & Teutsch, G. (2023). Evidence based estimation of macrodispersivity for groundwater transport. *Groundwater, 61*(3), 346–62. https://doi.org/10.1111/gwat.13252↗.

Zech, A., Attinger, S., Bellin, A., Cvetkovic, V., Dietrich, P., Fiori, A., Teutsch, G., & Dagan, G. (2019). A critical analysis of transverse dispersivity field data. *Groundwater, 57*(4), 632–39. https://doi.org/10.1111/gwat.12838↗.

Zech, A., Attinger, S., Cvetkovic, V., Dagan, G., Dietrich, P., Fiori, A., Rubin, Y., & Teutsch, G. (2015). Is unique scaling of aquifer macrodispersivity supported by field data? *Water Resources Research*, *51*(9), 7662–79. https://doi.org/10.1002/2015WR017220↗.

9 Boxes

Box 1 - Acronyms

1D	one dimensional
2D	two dimensional
3D	three dimensional
ADE	advective dispersive equation
cis DCE	cis-dichloroethylene
csia	compound specific isotope analysis
CMs	conceptual models
CoCs	contaminants of concern
CT	carbon tetrachloride
CCR	coal combustion residual
CF	chloroform
CM	chloromethane or conceptual model
CT	carbon tetrachloride
CST	conceptual site model
CWA	Clean Water Act
DCA	dichloroethane
DDT	dichlorodiphenyltrichloroethane
DNAPL	dense nonaqueous phase liquids
DNT	Dinitrotoluene
DSM	Dandy–Sale model
ESTCP	Environmental Security Technology Certification Program
erfc	error function complementary
HADiffR	heterogeneous advective-diffusive and reactive
HMX	high-melting explosive
LNAPL	light nonaqueous phase liquids
low-*k*	low permeability
M	methane
MC	methylene chloride
MCL	maximum contaminant level
MTBE	methyl-tert-butyl-ether
NA	natural attenuation
NAPL	nonaqueous phase liquid
NOM	natural organic material
NSZD	natural source zone depletion
14C model	fourteen compartment model
NRC	National Research Council

ODE	ordinary differential equation
OoM	order of magnitude
PAHs	polynuclear aromatic hydrocarbons
PCA	perchloroethane
PCB	polychlorinated biphenyl
PCE	perchloroethene
PDE	partial differential equation
PFAS	per- and polyfluoroalkyl substances
PRB	permeable reactive barrier
REV	representative elements of volume
RDX	Research Department Explosive
RCRA	Resource Conservation and Recovery Act
SCMs	site conceptual models
SERDP	Strategic Environmental Research Development Program
SRE	source reduction efficiency
SWDA	Solid Waste Disposal Act
TCA	trichloroethane
TCE	trichloroethene
TDS	total dissolved solids
TNT	trinitrotoluene
TVD	total variation diminishing
VC	vinyl chloride

Back to where text linked to Box 1

Box 2 - Derivation of an Analytical Solution for Waterflood DNAPL Recovery

1.8 M gallons (≈ 6800 cubic meters) recovered

Background

Mobile NAPL Recovery: Conceptual, Field, and Mathematical Considerations

by Tom Sale[a] and David Applegate[b]

Abstract

Recovery of mobile Nonaqueous Phase Liquids (NAPLs), referred to as "oil recovery," is one of the most common remedial technologies currently being implemented at sites where NAPLs have been released. The rationale for oil recovery typically includes resource recovery, mitigation of further NAPL migration, and compliance with regulatory mandates for source reduction. Efficient oil recovery can be achieved by optimizing conditions within the oil flow path. This concept is referred to as flow path management. Building on this concept, a waterflood oil recovery technique utilizing dual recovery and parallel delivery drainlines has been developed for recovery of creosote-based wood-treating oil, a Dense Nonaqueous Phase Liquid (DNAPL). Full-scale application of this technique at a contaminated site has yielded 1.5 million gallons of DNAPL. Furthermore, an operational endpoint of 95 percent recovery of the mobile oil is being achieved. Building on the concept of flow path management and the observed performance of the waterflood oil recovery system, a first-order analytical solution for DNAPL flow to a drainline has been derived and validated using field data. This solution leads to a set of useful design equations and further insight into the factors that control oil recovery.

Figure Box 2-1 - Sale & Applegate (1997). Mobile NAPL recovery: Conceptual, field, and mathematical considerations. *Groundwater, 35*(3), 418–426. Peer Reviewed/Refereed

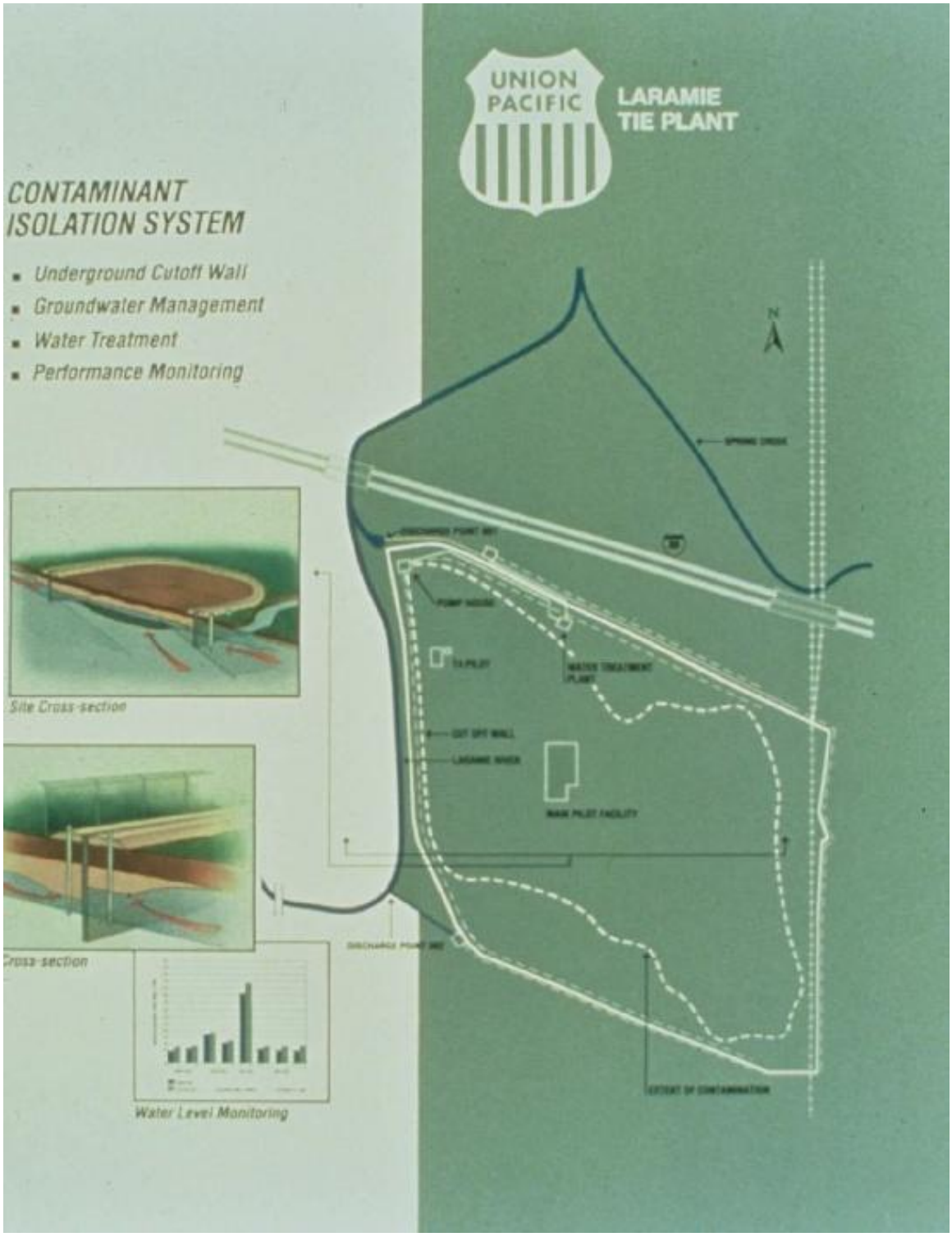

Figure Box 2-2 - Laramie Tie Plant Contaminant Isolation System. dashed interior line delineates the extent of the DNAPL pool.

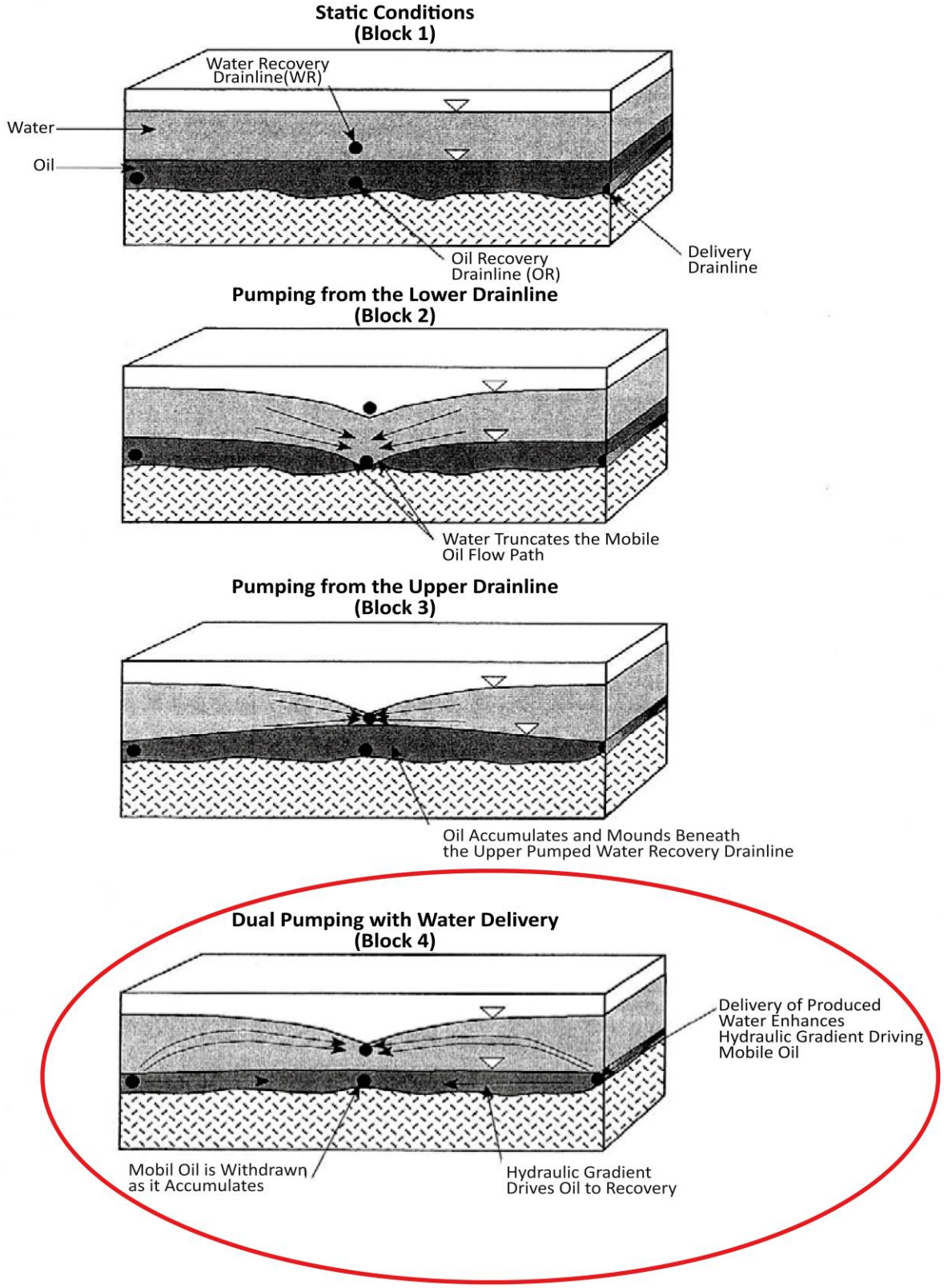

Figure Box 2-3 - Principles behind waterflood DNAPL recovery. The red oval shows the applied operation of the system.

Figure Box 2-4 – DNAPL recovery Modules 1 (right) and 2 (left) at a former wood treating facility.

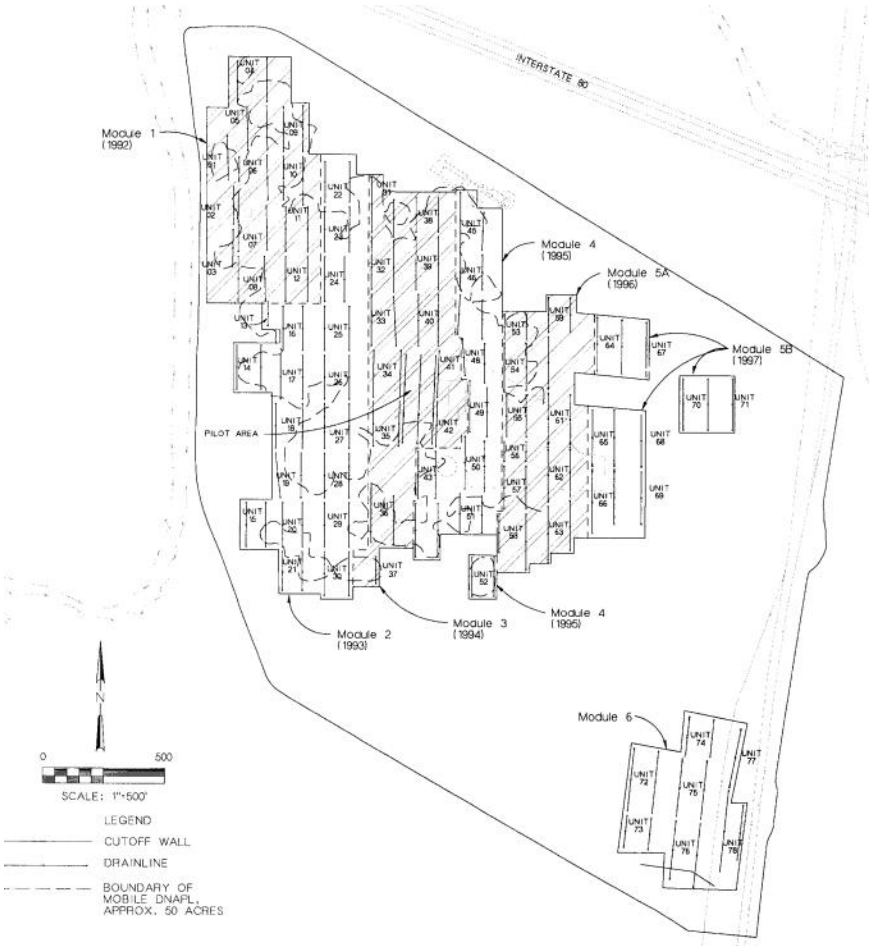

Figure Box 2-5 - DNAPL: recovery modules 1 – 6 at a former wood treating facility.

Derivation

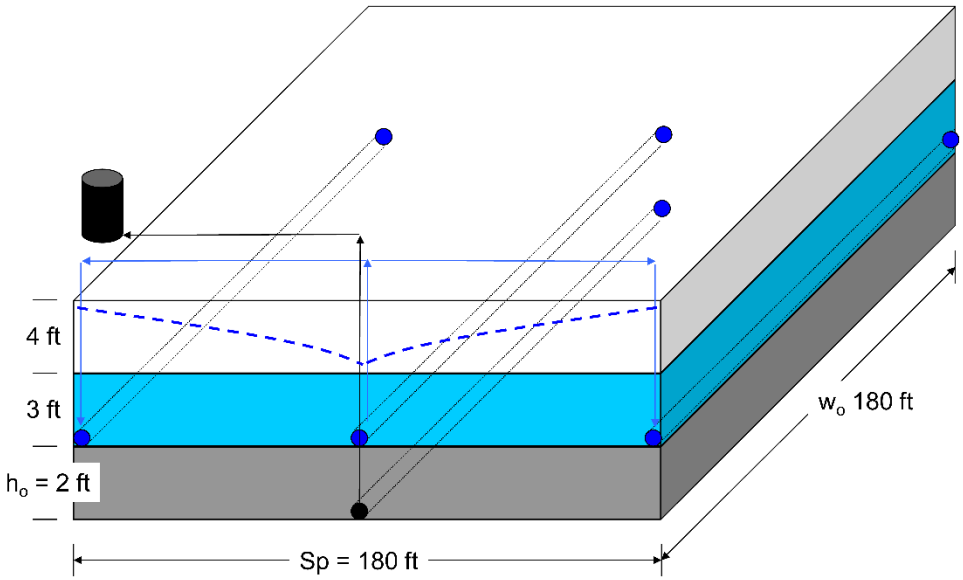

Figure Box 2-6 - Conceptual model for a volume of porous media between two drains with spacing (*Sp*) and width of oil (w_o) and depth of oil (h_o).

Consider the volume of porous media between two drains as the model domain. This is one half of the image shown in Figure Box 2-6.

Subscripts "o" (oil) and "w" (water) refer to nonwetting and water wetting fluids, respectively.

$V_o(t)$ is the amount of oil remaining. V_{max} is the maximum amount of oil that could be recovered.

Outflow rate − Inflow rate = Rate of volume collected

Assuming one-dimensional horizontal flow, incompressible fluids, and inflow=0

$$-\frac{kk_{ro}\rho_o g}{\mu_o}h_o w_o \frac{dP^*}{dx} - 0 = -\frac{dV_o}{dt}$$

$$\frac{dV_o}{dt} = \frac{kk_{ro}\rho_o g}{\mu_o}h_o w_o \frac{dP^*}{dx}$$

$$P^* = \frac{P_o}{\rho_o g} + z$$

By substitution

$$\frac{dV_o}{dt} = \frac{kk_{ro}\rho_o g}{\mu_o}h_o w_o \frac{d}{dx}\left(\frac{P_o}{\rho_o g} + z\right)$$

Employing the definition of capillary pressure

$$P_c = P_o - P_w \text{ and therefore } P_o = P_c + P_w$$

$$\frac{dV_o}{dt} = \frac{kk_{ro}\rho_o g}{\mu_o}h_o w_o \frac{d}{dx}\left(\frac{P_c}{\rho_o g} + \frac{P_w}{\rho_o g} + z\frac{\rho_o g}{\rho_o g}\right)$$

Pull $\rho_o g$ out of the derivative

$$\frac{dV_o}{dt} = \frac{kk_{ro}}{\mu_o} h_o w_o \frac{d}{dx}(P_c + P_w + z\rho_o g)$$

Employ

$$P_c = (\rho_o - \rho_w) g h_o \text{ and}$$

$$h_w = \frac{P_w}{\rho_w g} + z \quad \rightarrow \quad P_w = \rho_w g (h_w - z)$$

By substitution

$$\frac{dV_o}{dt} = \frac{kk_{ro} h_o w_o}{\mu_o} \frac{d}{dx}\left((\rho_o - \rho_w) g h_o + \rho_w g (h_w - z) + z\rho_o g\right)$$

Rearranging the term in the derivative

$$(\rho_o - \rho_w) g h_o + \rho_w g (h_w - z) + z\rho_o g \rightarrow \Delta\rho g (z + h_o) + \rho_w g h_w$$

Assume the top of the oil is initially horizontal and that the height of the top of the oil decays uniformly with time.

$$\frac{d}{dx}(\Delta\rho g (z + h_o)) = 0$$

Therefore,

$$\frac{dV_o}{dt} = \frac{kk_{ro} h_o w_o}{\mu_o} \frac{d}{dx}(\rho_w g h_w)$$

$$\frac{dV_o}{dt} = \frac{kk_{ro} h_o w_o \rho_w g}{\mu_o} \frac{dh_w}{dx}$$

Employing Darcy's Equation

$$Q_w = \frac{-kk_{rw}\rho_w g}{\mu_w} h_w w_w \frac{dh_w}{dx} \quad \rightarrow \quad \frac{dh_w}{dx} = \frac{Q_w \mu_w}{-kk_{rw}\rho_w g h_w w_w}$$

$$\frac{dV_o}{dt} = \frac{kk_{ro}\rho_w g}{\mu_o} h_o w_o \frac{Q_w \mu_w}{-kk_{rw}\rho_w g h_w w_w}$$

k and g, $\rho_w$and w_w cancel out

$$-\frac{dV_o}{dt} = Q_w \frac{k_{ro}\mu_w}{k_{rw}\mu_o} \frac{h_o}{h_w}$$

Finally, assuming a constant $S_o$with h_o, then by mass balance

$$h_o = h_{o_{initial}}\left[1 - \frac{V_o}{V_{max}}\right]$$

Substituting

$$-\frac{dV_o}{dt} = Q_w \frac{k_{ro}\mu_w}{k_{rw}\mu_o} \frac{h_{o_{initial}}}{h_w}\left[1 - \frac{V_o}{V_{o\,max}}\right]$$

Assuming all variables except V_o are constant

$$\int \frac{1}{1-\frac{V_o}{V_{max}}} dV_o = Q_w \frac{k_{ro}\mu_w}{k_{rw}\mu_o} \frac{h_{o_{initial}}}{h_w} \int dt$$

$$V_o(t) = V_{max}\, exp(-\frac{k_{ro}\mu_w}{k_{rw}\mu_o} \frac{h_w}{h_{o_{initial}}} \frac{Q_w}{V_{max}} t) + C$$

Applying the initial condition for volume of oil in the reference volume, $V_o=V_{max}$ where V_{max} is the volume of oil at t=0 which is represented by t_o

$$V_o(t) = V_{max}\, exp(-\frac{k_{ro}\mu_w}{k_{rw}\mu_o} \frac{h_w}{h_{o_{initial}}} \frac{Q_w}{V_{max}} t)$$

Define the Volume of Oil Produced as $V_{op}(t)=V_{Max} - V_o(t)$

$$V_{op}(t) = V_{max} - V_{max}\, exp(-\frac{k_{ro}\mu_w}{k_{rw}\mu_o} \frac{h_w}{h_{o_{initial}}} \frac{Q_w}{V_{max}} t)$$

Taking the derivative of with respect to time

$$\frac{d}{dt} V_{op}(t) = Q_o$$

$$Q_o = \frac{k_{ro}\mu_w}{k_{rw}\mu_o} \frac{h_w}{h_{o_{initial}}} Q_w\, exp(-\frac{k_{ro}\mu_w}{k_{rw}\mu_o} \frac{h_w}{h_{o_{initial}}} \frac{Q_w}{V_{max}} t)$$

Or, dividing through by $V_{o_{max}}$, then V_{op}^* is the fraction of the maximum oil produced at time t.

$$V_{op}^*(t) = 1 - exp(-\frac{k_{ro}\mu_w}{k_{rw}\mu_o} \frac{h_w}{h_{o_{initial}}} \frac{Q_w}{V_{max}} t)$$

$$V_{op}(t) = V_{max} - V_{max}\, exp(\frac{k_{ro}\mu_w}{k_{rw}\mu_o} \frac{h_w}{h_{o_{initial}}} \frac{Q_w}{V_{o_{max}}} t)$$

$$\lambda = \frac{k_{ro}\mu_w}{k_{rw}\mu_o} \frac{h_w}{h_{o_{initial}}} \frac{Q_w}{V_{o_{max}}}$$

$$t_{1/2} = \frac{ln(2)}{\lambda}$$

Total production after n half lives$=1-.5^n$

n=4 would yield 0.94 of recoverable DNAPL

Graphs of the volume of oil produced as a function of time from some of the units on the site are shown in Figure Box 2-7. A calculation vignette is setup and resulting oil volumes produced for a few different water injection rates are shown in Figure Box 2-8. Figure Box 2-9 shows oil production rates as a function of time for few different water injection rates, as well as oil production rates as a function of the volume of oil that has been produced.

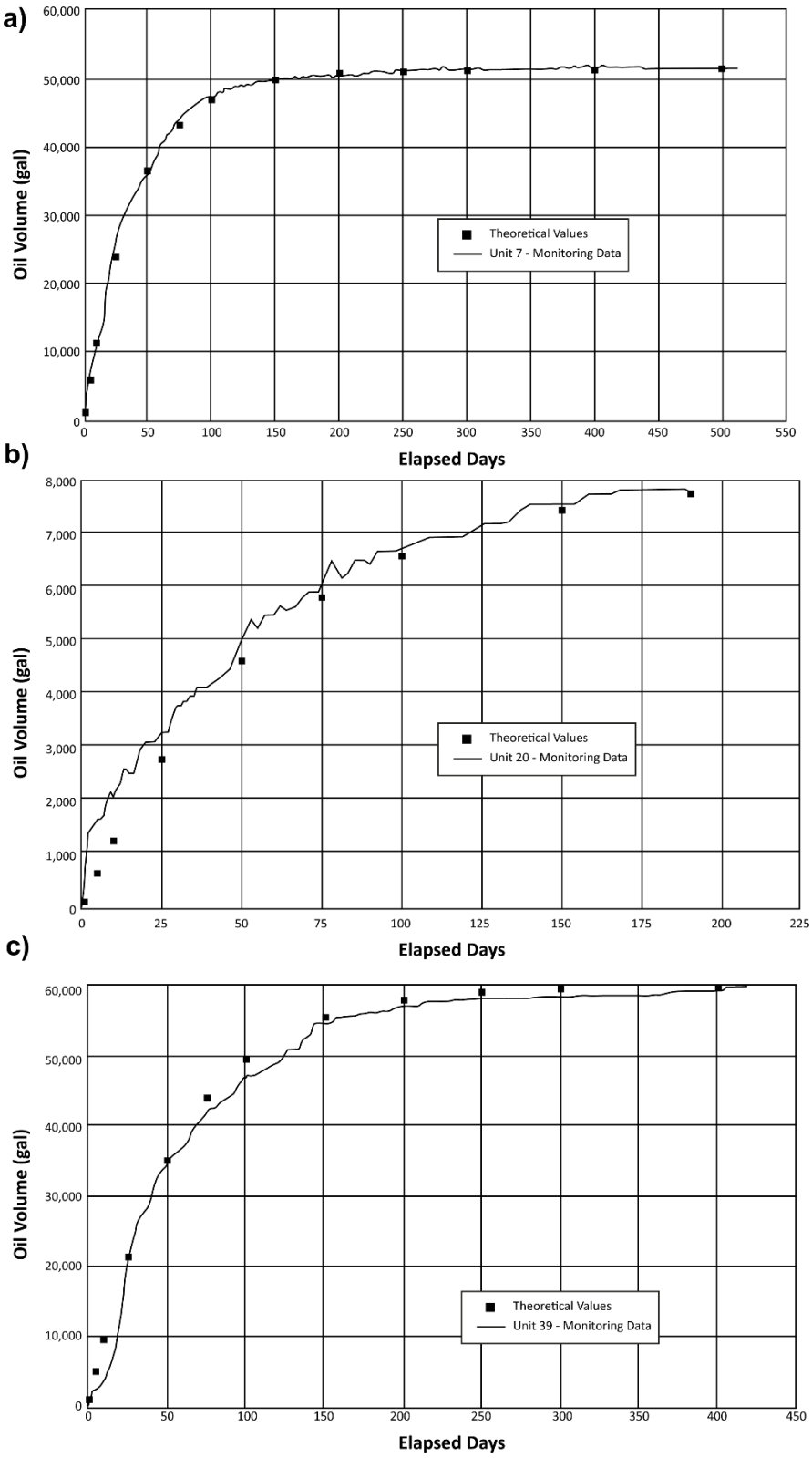

Figure Box 2-7 - Modeled versus observed oil production for remediation Units 7, 20, and 39.

Inputs

$k_{ro} = 0.5$ $k_{rw} = 1$ $h_w := 6 \cdot ft$ $\mu_w = 0.01\,poise$

$\mu_o = 0.54\,poise$ $h_o = 2\ ft$ $w = 180\ ft$ $spacing = 180\ ft$

$t = 1\ day, 2\ day \ldots 500\ day$

Setup Calculations

$$V_{omax} = w \cdot spacing \cdot h_o \cdot (0.8 - 0.1)$$

$$Q_o(t, Q_w) = \frac{k_{ro}\,\mu_w}{k_{rw}\,\mu_o} \frac{h_w}{h_o} \frac{Q_w}{2} \exp\left[-\left(\frac{k_{ro}\,\mu_w}{k_{rw}\,\mu_o} \frac{h_w}{h_o} \frac{Q_w}{V_{omax}}\right) t\right]$$

$$V_o(t, Q_w) = V_{omax} - V_{omax} \exp\left[-\left(\frac{k_{ro}\,\mu_w}{k_{rw}\,\mu_o} \frac{h_w}{h_o} \frac{Q_w}{V_{omax}}\right) t\right]$$

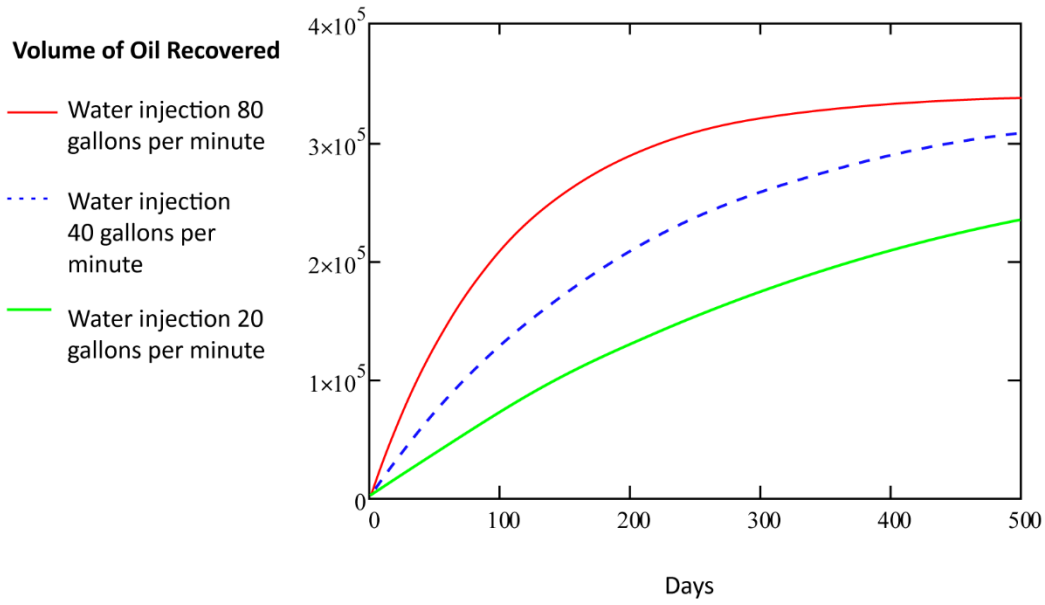

Figure Box 2-8 - Mathcad calculation setup for oil recovery as a function of time for water injection rates of 20, 40, and 80 gallons per minute, with a graph showing volume of oil recovered as a function of time.

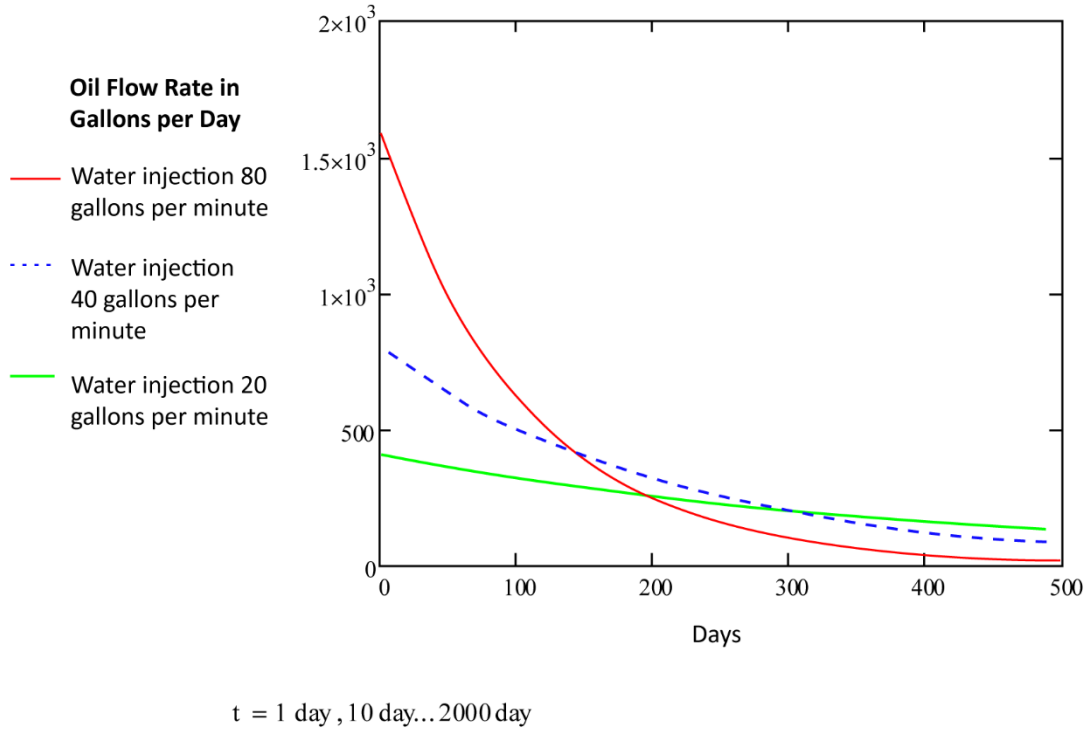

$t = 1\,\text{day}, 10\,\text{day} \ldots 2000\,\text{day}$

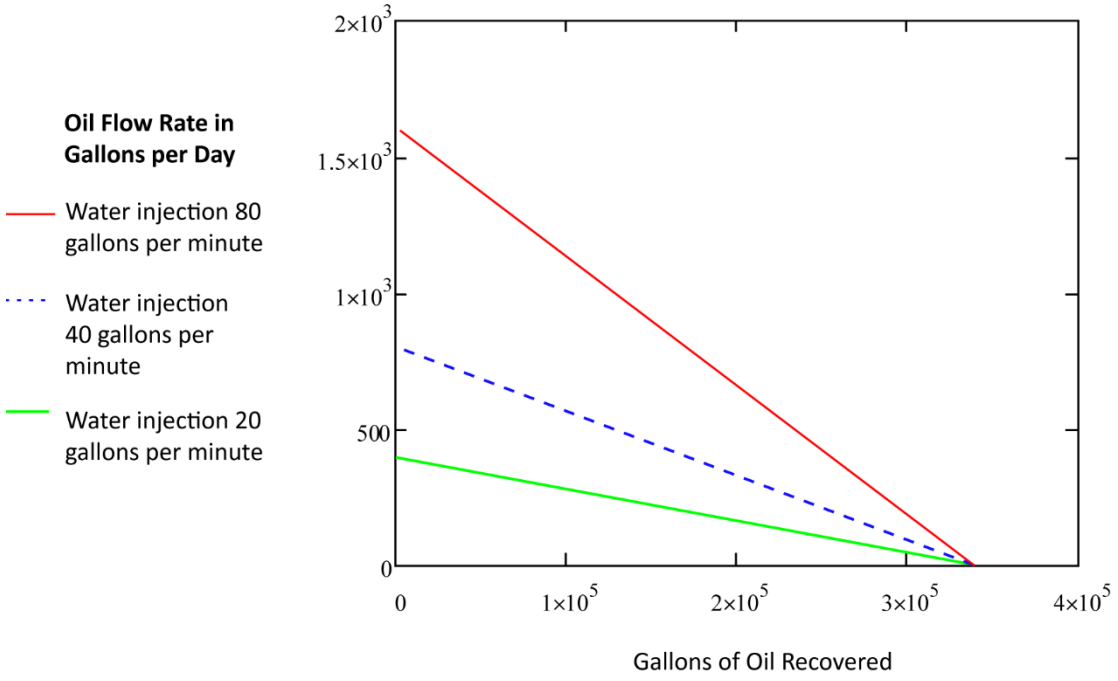

Figure Box 2-9 - Oil production rates as a function of time for water injection rates of 20, 40, and 80 gallons per minute, and oil production rates as a function of the volume of oil that has been produced for the same water injection rates.

Back to where text linked to Box 2

Box 3 - Derivation of a solution for 1D diffusion into a low-*k* zone

Based on Bird and others (1960) and Sale (1997)

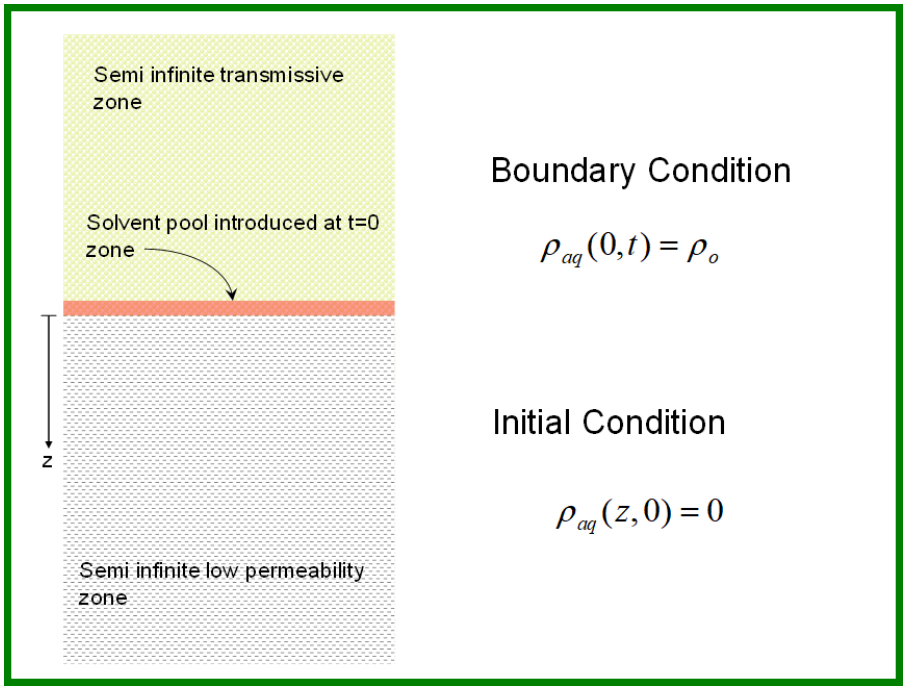

Figure Box 3-1 - Conceptual model for one-dimensional diffusion into a low-*k* zone.

To derive a solution for one-dimensional diffusion into a low-*k* zone, we start with a fundamental PDE for transport.

$$q_{aq}\frac{\delta\rho_{aq}}{\delta x} + D_x^*\frac{\delta^2\rho_{aq}}{\delta x^2} + D_y^*\frac{\delta^2\rho_{aq}}{\delta y^2} + D_z^*\frac{\delta^2\rho_{aq}}{\delta z^2} + \frac{R_m}{\phi} + \frac{G_m}{\phi} = \phi R\frac{\delta\rho_{aq}}{\delta t}$$

R_m and G_m are sink and source terms, respectively.

List of assumptions

1. No advection, therefore $q_{aq}\frac{\partial\rho}{\partial x} = 0$
2. Infinite horizontal pool therefore $\frac{\partial^2\rho_i}{\delta x^2} = 0$ and $\frac{\delta^2\rho_i}{\partial y^2}$=0
3. No reactions (i.e., sinks), therefore $\frac{G_m}{\phi} = 0$
4. No mass production (i.e., sources), therefore $\frac{R_m}{\phi} = 0$

Apply assumptions.

$$D_z^*\frac{\delta^2\rho_{aq}}{\delta z^2} = \phi R\frac{\delta\rho_{aq}}{\delta t}$$

If $\alpha = \frac{D_z}{\phi R}$, substituting gives $\alpha\frac{\delta^2\rho_{aq}}{\delta z^2} = \frac{\delta\rho_{aq}}{\delta t}$

This is the heat equation.

Define boundary and initial conditions.

$$\rho_i(0,t) = \rho_o$$
$$\rho_{aq}(z,0) = 0$$

Reduce the PDE (two independent variables) to an ODE (one independent variable) using the Boltzmann transform variable.

$\eta = \frac{z}{\sqrt{4\alpha t}}$ Boltzmann transform variable

Substitutions.

For the RHS

$$\frac{\delta\rho_{aq}}{\delta t} = \frac{\delta\rho_{aq}}{\delta\eta}\frac{\delta\eta}{\delta t} = \frac{\delta\rho_{aq}}{\delta\eta}\frac{\delta}{\delta t}\frac{z}{\sqrt{4\alpha t}}$$
$$\frac{\delta}{\delta t}\frac{z}{\sqrt{4\alpha t}} = -\frac{z}{2\sqrt{4\alpha}t^{\frac{3}{2}}}$$
$$\frac{\delta\rho_{aq}}{\delta t} = \frac{\delta\rho_{aq}}{\delta}\left(-\frac{z}{2\sqrt{4\alpha}t^{\frac{3}{2}}}\right) = \frac{\delta\rho_{aq}}{\delta\eta}\left(-\frac{z}{2x\sqrt{4\alpha t}}\right) = \frac{\delta\rho_{aq}}{\delta\eta}\left(\frac{\eta}{-2t}\right)$$
$$= \frac{\eta}{-2t}\frac{\delta\,\rho_{aq}}{\delta\eta}$$

For the LHS

$$\alpha\frac{\delta^2\rho_{aq}}{\delta z^2} = \alpha\frac{\delta}{\delta z}\left(\frac{\delta\rho_{aq}}{\delta\eta}\frac{\delta\eta}{\delta z}\right) = \alpha\frac{\delta}{\delta z}\left(\frac{\delta\rho_{aq}}{\delta\eta}\frac{\delta}{\delta z}\frac{z}{\sqrt{4\alpha t}}\right) = \alpha\frac{\delta}{\delta\eta}\left(\frac{\delta\rho_{aq}}{\delta\eta}\frac{\delta}{\delta z}\frac{z}{\sqrt{4\alpha t}}\right)\frac{\delta\eta}{\delta z}$$
$$= \alpha\frac{\delta}{\delta\eta}\left(\frac{\delta\rho_{aq}}{\delta\eta}\frac{\delta}{\delta z}\frac{z}{\sqrt{4\alpha t}}\right)\frac{\delta}{\delta z}\frac{z}{\sqrt{4\alpha t}}$$
$$\frac{\delta}{\delta z}\frac{z}{\sqrt{4\alpha t}} = \frac{1}{\sqrt{4\alpha t}}$$
$$\alpha\frac{\delta^2\rho_{aq}}{\delta z^2} = \alpha\frac{\delta}{\delta\eta}\left(\frac{\delta\rho_{aq}}{\delta\eta}\frac{1}{4\alpha t}\right) = \frac{1}{4t}\frac{\delta^2\rho_{aq}}{\delta\eta^2}$$

LHS=RHS

$$\frac{1}{4t}\frac{\delta^2\rho_{aq}}{\delta\eta^2} = \frac{\eta}{-2t}\frac{\delta\rho_{aq}}{\delta\eta}$$
$$\frac{\delta^2\rho_{aq}}{\delta\eta^2} = -2\eta\frac{\delta\rho_{aq}}{\delta\eta} \text{ or}$$
$$\frac{\delta^2\rho_{aq}}{\delta\eta^2} + 2\eta\frac{\delta\rho_{aq}}{\delta\eta} = 0$$

This is an ODE with η the only independent variable and ρ_{aq} as the dependent variable.

Define boundary conditions in terms of η using the definition $\eta = \frac{z}{\sqrt{4\alpha t}}$.

$$\rho_{aq}(0,t) = \rho_o \text{ and } \eta = 0, \rho_{aq} = \rho_o$$
$$\rho_{aq}(z,0) = 0 \text{ and } \eta = \infty, \ \rho_{aq} = 0$$

This gives an ODE, which can be solved through two integration steps.

First integration:

$$\text{If } \psi = \frac{d\rho_{aq}}{d\eta}, \text{ substituting gives } \frac{d\psi}{d\eta} + 2\eta\psi \text{ or } \frac{d\psi}{d\eta} = -2\eta\psi$$

$$\int \frac{1}{\psi} d\psi = \int -2\eta d\eta$$

$$ln\psi = -\frac{2}{2}\eta^2 + C_1$$

$$\psi = C_1 e^{-\eta^2}$$

Second integration:

$$\frac{d\rho_{aq}}{d\eta} = C_1 e^{-\eta^2}$$

$$\rho_{aq}(\eta) - \rho_{aq}(0) = C_1 \int_0^{\eta} e^{-\eta^2} d\eta + C_2$$

$$\rho_{aq}(\eta) = \left(C_1 \int_0^{\eta} e^{-\eta^2} d\eta + C_2 \right) + \rho_o$$

$$\rho_{aq}(0) = \rho_0 = \left(C_1 \int_0^{0} e^{-\eta^2} d\eta + C_2 \right) + \rho_o, \text{ therefore } C_2 = 0$$

$$\rho_{aq}(\eta) = C_1 \int_0^{\eta} e^{-\eta^2} d\eta + \rho_o$$

$$\rho_{aq}(\infty) = 0 = C_1 \int_0^{\infty} e^{-\eta^2} d\eta + \rho_o \text{, therefore } C_1 = \frac{\rho_o}{\int_0^{\infty} e^{-\eta} d\eta}$$

$$\rho_{aq}(\eta) = -\rho_0 \frac{\int_0^{\eta} e^{-\eta^2} d\eta}{\int_0^{\infty} e^{-\eta} d\eta} + \rho_o$$

$$\frac{\rho_{aq}(\eta)}{\rho_o} = -\frac{\int_0^{\eta} e^{-\eta^2} d\eta}{\int_0^{\infty} e^{-\eta} d\eta} + 1 = 1 - \frac{2}{\sqrt{\pi}} \int_0^{\eta} e^{-\eta^2} d\eta = erfc(\eta)$$

Substituting the definition of η.

$$\rho_i(z,t) = \rho_o erfc\left(\frac{z}{\sqrt{4\alpha t}} \right)$$

Substituting the definition of α.

$$\rho_i(z,t) = \rho_o erfc\left(\frac{z}{\sqrt{4\frac{D_z}{\phi R} t}} \right)$$

Simplifying.

$$\rho_i(z,t) = \rho_e erfc\left(\frac{1}{2} \frac{z}{\sqrt{\frac{D_z}{\phi R} t}} \right)$$

Back to where text linked to Box 3

Box 4 - pe–pH stability fields

Master variables, pe and pH, govern the stability of water, minerals, and CoCs. Box 4 presents four problem sets with answers. We assume the activity coefficients (γ) for all species are 1. Other assumptions described herein are very general. Soil–water systems have additional components that make things more complicated. The intent of these example problems is to give you a general sense of the hierarchy of redox reactions commonly associated with remediation efforts. The equilibrium coefficients except for zero-valent-iron ⟷ ferrous-iron come from Lindsay (1979). The valent-iron⟷ferrous-iron equilibrium comes from a power point presentation developed by Jens Blotevogel.

Problem 1) – Develop a plot of the stability field for water

Given

$$H_2O \longleftrightarrow H^+ + e^- + \frac{1}{4}O_{2\,(g)} \qquad K_o = 10^{-20.78}$$

1) Equate the equilibrium constant to the molar concentration of the products divided by the molar concentrations of the reactants.

$$\frac{[H^+][e^-][O_2]^{\frac{1}{4}}}{[H_2O]} = 10^{-20.78}$$

2) Take the log of both sides to develop the following expression (recalling pe=-log[H^+] and pH=-log[e^-]

$$pe + pH = -20.78 + \tfrac{1}{4} \log O_{2\,(g)}$$

3) Assume O_2 is present at 1 atmosphere (log[O_2]=log[1]=0) and solve for pe as a function of pH

$$pe = 20.78 + \tfrac{1}{4} \log (1) - pH$$

$$pe(pH) = 20.78 - pH$$

4) Describe what will happen in an open aqueous system at standard conditions if pe+pH>20.78 – *Water is unstable and it disassociates to oxygen and protons.*

5) Given

$$H_2O + e^- \longleftrightarrow \tfrac{1}{2}\, H_2 + OH^-$$

$$H^+ + OH^- \longleftrightarrow H_2O$$

$$H^+ + e^- \longleftrightarrow \tfrac{1}{2}\, H_{2gas}$$

The equilibrium constant or this reaction is 1 and Log (1)=0

$$pe + pH = 0$$

or

$$pH(pe)=-pe$$

6) Describe what will happen in an open aqueous system at standard conditions if pe+pH>0

Assume an activity coefficient of 1 and given

$$H_2O \leftrightarrows H^+ + e^- + \frac{1}{4}O_{2\,(g)} \qquad K_o=10^{-20.78}$$

Plot lines at which O_2 and H_2 are at 1 atmosphere and identify stability field for O_2, H_2O, and H_2 under equilibrium conditions.

$$pH = 0...14 \qquad pe_{O2}(pH)= 20.78-pH \qquad pe_{H2}(pH)= -pH$$

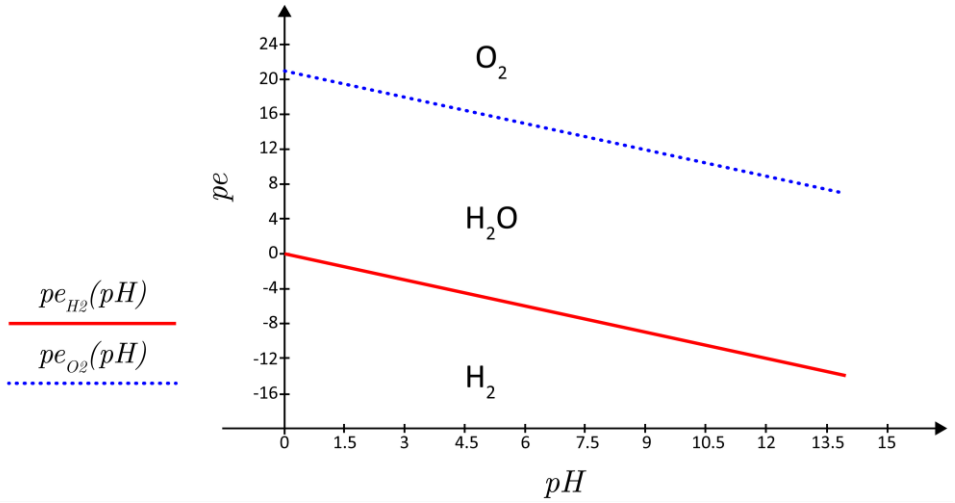

Figure Box 4-1 - Stability field for O_2, H_2O, and H_2 under equilibrium conditions.

Problem 2) Resolving the stability fields for thermodynamically stable forms of carbon

A) Start with

$$C(\text{graphite})+H_20 \leftrightarrows CO_{2\,(g)}+4\,e^- +4\,H^+ \qquad K_o=10^{-14.01}$$

Equate the molar concentration of the product over the reactants to the equilibrium coefficient.

$$\frac{[CO_2\,(g)\,][e^-]^4[H^+]^4}{[C(\text{graphite})\,]}=10^{-14.01}$$

Take the logs of the left- and right-hand sides of the equation

Substitute in $-\log[H^+]=pH$ and $-\log[e^-]=pe$

Assume $[CO_2\,(g)]$ and $[C(\text{graphite})\,]=1$

Solve for pe as a function of pH when $[CO_2(g)]=[C(\text{graphite})]$

$$pe_{CO_2\text{-Graphite}}(pH)=3.52 - pH$$

The primary forms of aqueous CO_2 are $H_2CO_3^o$ (pH<6.36), HCO_3^- (6.36<pH<10.33), and CO_3^{-2} pH>10.33. Plot the stability field of the Carbonate species and graphite on the water stability graph developed from Problem 1 and identify the areas in which the primary carbon species are graphite, $H_2CO_3^o$, HCO_3^-, and CO_3^{-2}.

B) Assuming $[CH_4](g)$ and $[C(\text{graphite})]=1$, repeat the above steps for

$$C(\text{graphite})+4\,e^-+4\,H^+ \leftrightarrow CH_{4\,(g)} \quad K_o=10^{8.9}$$

Add the lines delineating the stability field for graphite-methane to the carbon stability field plot.

$$C(\text{graphite})+H_20 \leftrightarrow CO_{2\,(g)}+4\,e^-+4\,H^+ \quad K_o=10^{-14.01}$$

$$\frac{[CO_2\,(g)\,][e^-]^4[H^+]^4}{[C(\text{graphite})\,]}=10^{-14.01}$$

$$\log[CO_2(g)\,]+4\log[e^-]+4\log[H^+]-\log[C(\text{graphite})]=-14.01$$

$$\log[CO_2(g)\,]-4\,pe-4\,pH-\log[C(\text{graphite})]=-14.01$$

Assume CO_2(g) and graphite are present at equimolar concentrations.

$$\log\left[\frac{[CO_2\,(g)\,]}{[C(\text{graphite})\,]}\right]=\log(1)=0$$

$$-4\,pe-4\,pH=-14.01$$

$$pe+ph=3.52$$

$$pe(pH)=3.52-pH$$

$$6.36,\ 10.33$$

$$C(\text{graphite})+4\,e^-+4\,H^+ \leftrightarrow CH_{4\,(g)} \quad K_o=10^{8.9}$$

$$\frac{[CH_4\,(g)\,]}{[C(\text{graphite})\,][e^-]^4[H^+]^4}=10^{8.9}$$

$$\log[CH_4\,(g)\,]-\log[C(\text{graphite})\,]-4\log[e^-]-4\log[H^+]=8.9$$

Assume methane and graphite are present in equimolar concentrations.

$$\log\left[\frac{[CH_4\,(g)\,]}{[C(\text{graphite})\,]}\right]=\log(1)=0$$

$$\log\left[\frac{[CH_4\,(g)\,]}{[C(\text{graphite})\,]}\right]-4\log[e^-]-4\log[H^+]=8.9$$

$$pe+pH=2.23$$

$$pe_{graphmeth}(pH)=2.23-pH$$

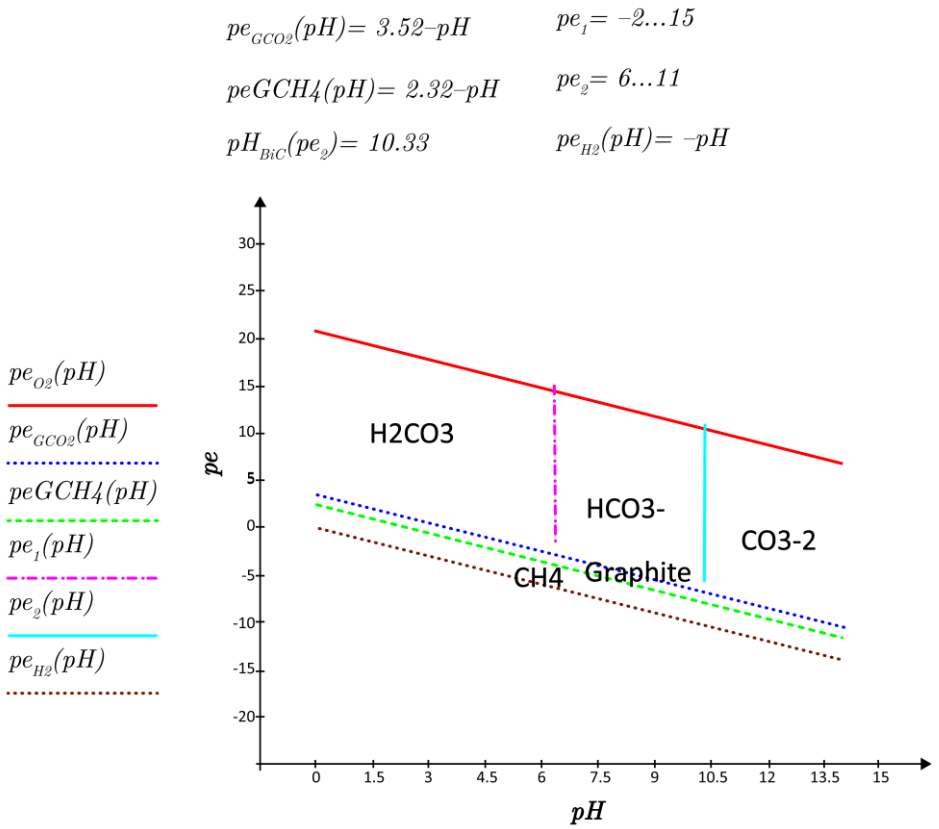

Figure Box 4-2 - Stability field for thermodynamically stable forms of carbon.

Problem 3 – Resolve the stability fields for PCE-TCE-DCE-VC

$$C_2Cl_4+H^++2e^- \leftrightarrows C_2HCl_3+Cl^- \qquad K_o=10^{21.68}$$

$$\frac{[C_2HCl_3][Cl^-]}{[C_2Cl_4][H^+][e^-]^2}=10^{21.68}$$

$$\log\frac{[C_2HCl_3]}{[C_2Cl_4]}+\log[Cl^-]-\log[H^+]-2\log[e^-]=21.68$$

Assume $[C_2HCl_3]=[C_2Cl_4]$ and $[Cl^-]=0.001$ mole/L

$$0-3+pH+2\,pe=21.68$$

$$pH+2\,pe=24.68$$

$$pe_{PCETCE}(pH)=\frac{24.68-pH}{2}$$

$$C_2HCl_3+H^++2e^- \leftrightarrows C_2H_2Cl_2+Cl^- \quad K_o=10^{21.26}$$

$$\frac{[C_2H_2Cl_2][Cl^-]}{[C_2HCl_3][H^+][e^-]^2}=10^{21.26}$$

$$\log\frac{[C_2H_2Cl_2]}{[C_2HCl_3]}+\log[Cl^-]-\log[H+]-2\log[e^-]=21.26$$

Assume $[C_2H_2Cl_2]=[C_2HCl_3]$ and $[Cl^-]=0.001$ mole/L

$$0-3+pH+2\,pe=21.68$$

$$pH+2\,pe=24.68$$

$$pe_{TCEDCE}(pH) = \frac{24.68 - pH}{2}$$

$$C_2H_2Cl_2 + H^+ + 2e^- \leftrightarrows C_2H_3Cl + Cl^- \quad K_o = 10^{17.77}$$

$$\frac{[C_2H_3Cl]\,[Cl^-]}{[C_2H_2Cl_2]\,[H^+][e^-]^2} = 10^{17.77}$$

$$\log\frac{[C_2H_3Cl]}{[C_2H_2Cl_2]} + \log[Cl^-] - \log[H^+] - 2\log[e^-] = 17.77$$

Assume $[C_2H_3Cl] = [C_2H_2Cl_2]$ and $[Cl^-] = 0.001$ mole/L

$$0 - 3 + pH + 2\,pe = 17.77$$

$$pH + 2\,pe = 20.77$$

$$pe_{DCEVC}(pH) = \frac{20.77 - pH}{2}$$

$$pe_{PCETCE}(pH) = \frac{24.68 - pH}{2} \qquad pe_{TCEDCE}(pH) = \frac{24.68 - pH}{2} \qquad pe_{DCEVC}(pH) = \frac{24.68 - pH}{2}$$

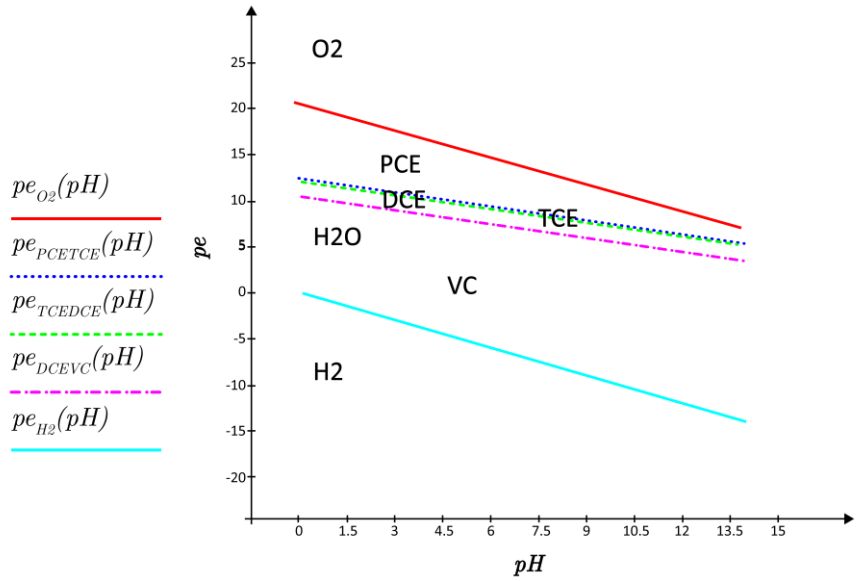

Figure Box 4-3 - Stability field for PCE, TCE, DCE, and VC.

Problem 4 – Plot common redox couple associated with subsurface remediation on the water stability pe-pH diagram

Permanganate MnO_4^{-2} is reduced Manganese(II) Mn^{+2}

Assume $\log\left(\frac{[Mn^{+2}]}{[MnO_4^{-2}]}\right)=0$

$$MnO_4^{-2}+8H^{+}+4e^{-} \leftrightarrows Mn^{+2}+4H_2O \qquad K_o=10^{118.31}$$

Nitrate-Nitrite

Assume $\log\left(\frac{[NO_2^{-}]}{[NO_3^{-}]}\right)=0$

$$NO_3^{-}+2H^{+}+2e^{-} \leftrightarrows NO_2^{-}+H_2O \qquad K_o=10^{28.64}$$

Soil Iron – Fe^{+2}

Assume $\log\left(\frac{[Fe^{+2}]}{[Fe(OH)3]}\right)=0$

$$Fe(OH)_3+3H^{+}+e^{-} \leftrightarrows Fe^{+2}+3H_2O \qquad K_o=10^{15.74}$$

Sulfate-Sulfide

Assume $\log\frac{[S^{-2}]}{[SO_4^{-2}]}=0$

$$SO_4^{-2}+8e^{-}+8H^{+} \leftrightarrows S^{-2}+4H_2O \qquad K_o=10^{20.74}$$

Zero Valent Iron – Ferrous Iron

Assume $[Fe^{o}]=1$ and $\log[Fe^{+2}]=10^{-5}$

$$Fe^{o} \leftrightarrows Fe^{+2}+2e^{-} \qquad K_o=1.04$$

$$Fe(OH)_3+3H^{+}+e^{-} \leftrightarrows Fe^{+2}+3H_2O \qquad K_o=10^{15.74}$$

$$\frac{[Fe^{+2}]}{[Fe(OH)3]\,[H^{+}]^3[e^{-}]}=10^{15.74}$$

$$\log\frac{[Fe^{+2}]}{[Fe(OH)3]} - 3\log[H^{+}] - \log[e^{-}]=15.74$$

$$3pH + pe=15.74$$

$$pe(pH)=15.74 - 3pH$$

$$SO_4^{-2}+8e^{-}+8H^{+} \leftrightarrows S^{-2}+4H_2O \qquad K_o=10^{20.74}$$

$$\frac{[S^{-2}]}{[SO_4^{-2}]\,[H^{+}]^8[e^{-}]^8}=10^{20.74}$$

$$\log\frac{[S^{-2}]}{[SO_4^{-2}]} - 8\log[H^{+}] - 8\log[e^{-}]=15.74$$

$$8pe+8pH=15.74$$

$$pe(pH)=1.97-pH$$

$$MnO_4^{-2}+8H^{+}+4e^{-} \leftrightarrows Mn^{+2}+4H_2O \qquad K_o=10^{118.31}$$

$$\frac{[Mn^{+2}]}{[MnO_4^{-2}]\,[H^{+}]^8[e^{-}]^4}=10^{118.31}$$

$$\log\frac{[Mn^{+2}]}{[MnO_4^{-2}]} - 8\log[H^{+}] - 4\log[e^{-}]=118.31$$

$$8pH+4pe=118.31$$

$$pe(pH)=29.58-2\ pH$$

$$NO_3^-+2H^++2e^- \leftrightarrow NO_2^-+H_2O \qquad K_o=10^{28.64}$$

$$\frac{[NO_2^-]}{[NO_3^-]\,[H^+]^2[e^-]^2}=10^{28.64}$$

$$\log\frac{[NO_2^-]}{[NO_3^-]}-2\log[H^+]-2\log[e^-]=28.64$$

$$2pH+2pe=28.64$$

$$pe(pH)=14.32-pH$$

Zero Valent Iron – Ferrous Iron

Assume $[Fe^o]=1$ and $\log[Fe^{+2}]=10^{-5}$

$$Fe^o \leftrightarrow Fe^{+2}+2e^- \qquad K_o=1.04$$

$$\frac{[Fe^{+2}][e^-]^2}{[Fe^0]}=10^{1.04}$$

$$\log[10^{-5}]-2pe=0.017$$

$$-2pe=5.017$$

$$pe(pH)=-2.59$$

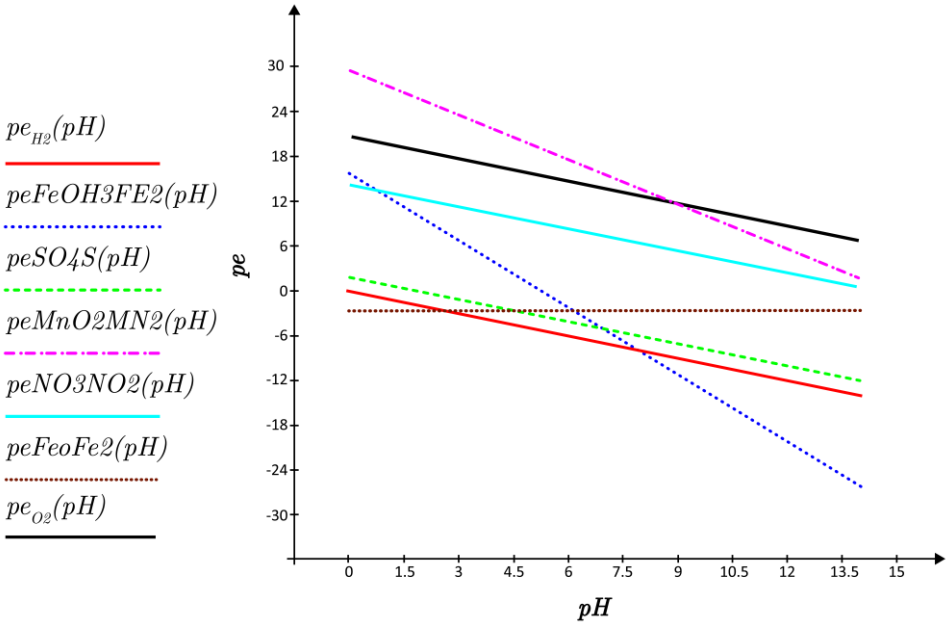

Figure Box 4-4 - Common redox couples associated with subsurface remediation plotted on the water stability pe-pH diagram.

Back to where text linked to Box 4

Box 5 - Equilibrium Partitioning Between Phases

The material in Box 5 is based on derivations developed by McWhorter for course AG638 taught at Colorado State University in 1994.

NAPL←→ Water	**Raoult's equation**	$\rho_{\mathrm{aq}_i} = \gamma_i \rho_{\mathrm{aq}_i}^{\mathrm{Pure\_NAPL}} x_{\mathrm{NAPL}_i}$
NAPL←→ Soil Gas	**Ideal Gas equation**	$\rho_{\mathrm{gas}_i} = \frac{\gamma_i P_{\mathrm{gas}_i}^{\mathrm{Pure\_NAPL}} x_{\mathrm{NAPL}_i} MW_i}{RT}$
NAPL←→ Soil Gas	**Henry's Equation**	$\rho_{\mathrm{gas}_i} = K_{\mathrm{HD}_i} \quad \rho_{\mathrm{aq}_i}$
Water←→ Sorbed	**Instantaneous equilibrium and a constant proportionality**	$\omega_{\mathrm{sorbed}_i} = f_{\mathrm{oc}} \; K_{\mathrm{oc}_i} \; \rho_{\mathrm{aq}_i}$

Figure Box-5-1 – Equilibrium partitioning.

Derivations follow McWhorter's course notes (1994)

NAPL ←→ Water

Raoult's equation (1882) for vapor pressure above a liquid at equilibrium

$$P_{gas\_Total} = \sum_{i=1}^{n} P_{gas_i}^{Pure\_liquid} x_{liquid_i}$$

or

$$P_{gas\_partial_i} = P_{gas_i}^{Pure\_liquid} x_{liquid_i}$$

P=Pressure in gas x_i=mole fraction of x in liquid mixture

Analogously, put water in place of the gas and assume the activity coefficient γ is 1

$$\rho_{aq_i} = \gamma_i \rho_{aq_i}^{Pure\_NAPL} x_{NAPL_i} \qquad (5\text{-}1)$$

ρ=mass/volume

NAPL ←→ Soil Gas

Ideal Gas Equation (Law) $PV = nRT$

First stated by Émile Clapeyron↗ in 1834

(Assumes $R = \frac{PV}{nT}$ constant for all gases)

$$\rho_{gas_i} = \frac{n_i MW_i}{V_{gas_i}} \text{ therefore } \rightarrow n_i = \frac{\rho_{gas_i} V_{gas_i}}{MW_i}$$

Substituting the definition of n into $PV = nRT$ and solving for ρ_{gas_i}

$$P_{gas_i} V_{gas_i} = \frac{\rho_{gas_i} V_{gas_i}}{MW_i} RT \rightarrow \rho_{gas_i} = \frac{P_{gas_i} MW_i}{RT}$$

Recall $P_{gas_i} = P_{gas_i}^{Pure\_NAPL} x_{NAPL_i} \gamma_{NAPL_i}$ then by substitution:

$$\rho_{gas_i} = \frac{P_{gas_i}^{Pure\_NAPL} x_{NAPL_i} \gamma_{NAPL_i} MW_i}{RT} \quad (5\text{-}2)$$

Water ←→ Soil Gas

Henry's Equation (Law of 1803) $K_H = \frac{P_{gas_i}}{[C_{aq_i}]}$

Recall $[C_{aq_i}] = \frac{\rho_{aq_i}}{MW_i}$ and

$$\rho_{gas_i} = \frac{P_{gas_i} MW_i}{RT} \rightarrow P_{gas_i} = \frac{\rho_{gas_i} RT}{MW_i}$$

By substitution $K_H = \frac{\frac{\rho_{gas_i} RT}{MW_i}}{\frac{\rho_{aq_i}}{MW_i}}$ or $\frac{K_H}{RT} = \frac{\rho_{gas_i}}{\rho_{aq_i}}$

Defining a dimensionless Henry's coefficient

$$K_{HD} = \frac{K_H}{RT} \ldots \qquad \rho_{gas_i} = K_{HD} \rho_{aq_i} \quad (5\text{-}3)$$

Water ←→ Sorbed

Assume a linear-instantaneous-equilibrium between the aqueous mass density and sorbed mass per unit dry weight soils (ω_{sorbed_i})

$$K_d = \frac{\omega_{sorbed_i}}{\rho_{aq_i}} \ldots\ldots K_d \text{ units of volume/mass}$$

K_d can be estimated as the product of the fraction of organic carbon f_{oc} and K_{oc}, (K_{oc} *is* the organic carbon – water partitioning coefficient)

$$K_d = f_{oc} K_{oc}$$

By substitution $\omega_{sorbed_i} = f_{oc} K_{oc} \rho_{aq_i}$ (5-4)

Total concentration A $\omega_{Total_i} = \frac{mass_{Total_i}}{mass_{soil}}$ mass compound per mass dry soil

Total mass

Per Cohen and Mercer (1993), the total mass of solvents in a volume of porous media is the sum of the nonaqueous, aqueous, vapor, and sorbed phases. At any point in space each of the phases is trying to equilibrate with the other phases as shown in Equation Box5-5 where ω is the mass of contaminant (e.g., chlorinated solvent) per unit mass porous media.

$$\omega_{Total_i} = \omega_{aq_i} + \omega_{gas_i} + \omega_{NAPL_i} + \omega_{sorbed_i} \tag{5-5}$$

The Aqueous phase:

$$\omega_{aq_i} = \frac{\rho_{aq_i}\phi S_w}{\rho_b} \tag{5-6}$$

S_w=water saturation (Volume water L^3 divided by Volume pore space L^3 : dimensionless)

ϕ=porosity (Volume pore space L^3 divide by Volume bulk media L^3 : dimensionless)

ρ_b=bulk soil density = $\rho_{soil}(1-\phi)$

(Mass solids M divided by Volume solids L^3 : dimensionless)

Typically assume $\rho_{soil} = 2.65$ gm/cm^3

The Gas phase:

$$\omega_{gas_i} = \frac{\rho_{gas_i}(\phi - \phi S_w - \phi S_{NAPL})}{\rho_b} \tag{5-7}$$

S_{NAPL}=Fraction of Pore space filled with NAPL (L^3/L^3 : dimensionless)

The NAPL phase:

$$\omega_{NAPL_i} = \frac{\rho_{NAPL_i}\phi S_{NAPL} x_{NAPL_i}}{\rho_b} \tag{5-8}$$

The Sorbed phase:

$$\omega_{sorbed_i} = f_{oc} K_{oc} \rho_{aq_i} \tag{5-9}$$

Equation 5-9 is the same as Equation 5-4

Substitute Equations 5-7, 5-8, and 5-9 into Equation 5-5 to obtain Equation 5-10

$$\omega_{Total_i} = \frac{\rho_{aq_i}\phi S_w}{\rho_b} + \frac{\rho_{gas_i}(\phi - \phi S_w - \phi S_{NAPL})}{\rho_b} + \frac{\rho_{NAPL_i}\phi S_{NAPL} x_{NAPL_i}}{\rho_b} + f_{oc} K_{oc} \rho_{aq_i} \tag{5-10}$$

Concentrations per volume porous media

Similarly to the total mass calculations

$$\rho_{PMTotal_i} = \rho_{aq_i} S_w \phi + \rho_{gas_i}\phi(1 - S_w - S_{NAPL}) + \rho_{NAPL_i}\phi S_{NAPL} + \omega_{sorbed_i}\rho_b \tag{5-11}$$

Substitute (5-3) in for gas concentration and (5-4) in for contaminant mass per dry mass solids.

$$\rho_{PMTotal_i} = \rho_{aq_i} S_w \phi + K_{HD} \rho_{aq_i} \phi (1 - S_w - S_{NAPL}) + \rho_{NAPL_i} \phi S_{NAPL} + f_{oc} K_{oc} \rho_{aq_i} \rho_b \quad (5\text{-}12)$$

Special cases

1) What is the maximum concentration one can have without NAPL (i.e., NAPL as a free product, or pool), or alternatively, what concentration indicates NAPL occurs at the site?

$$\omega_{Total_i} = \frac{\rho_{aq} \phi S_w}{\rho_b} + \frac{\rho_{gas_i} (\phi - \phi S_w - \phi S_{NAPL})}{\rho_b} + \frac{\rho_{NAPL_i} \phi S_{NAPL} x_{NAPL_i}}{\rho_b} + f_{oc} K_{oc} \rho_{aq}^{NAPL} \quad (5\text{-}13)$$

$$\omega_{Total_i} = \frac{\phi \rho_{aq}^{NAPL}}{\rho_b} (S_w + K_{HD}(1 - S_w) + \frac{K_d \rho_b}{\phi}) \quad (5\text{-}14)$$

$$\rho_{PMTotal_i} = \phi \rho_{aq}^{NAPL} (S_w + K_{HD}(1 - S_w \phi) + \frac{K_d \rho_b}{\phi}) \quad (5\text{-}15)$$

2) Retardation Coefficient R - $S_w = 1$ and therefore $S_{NAPL} = 0$ and $S_{gas} = 0$

3) Simplifications

$$\omega_{Total_i} = \frac{\phi \rho_{aq_i}}{\rho_b} (1 + \frac{K_d \rho_b}{\phi}) \quad (5\text{-}16)$$

$$\rho_{PMTotal_i} = \phi \rho_{aq_i} (1 + \frac{K_d \rho_b}{\phi}) \quad (5\text{-}17)$$

$$R = 1 + \frac{K_d \rho_b}{n} \quad : \text{ R=retardation coefficient} \quad (5\text{-}18)$$

4) Substituting

$$\omega_{Total_i} = \frac{\phi \rho_{aq_i}}{\rho_b} R \quad (5\text{-}19)$$

$$\rho_{PMTotal_i} = \phi \rho_{aq_i} R \text{ or } R = \frac{\rho_{PMTotal_i}}{\phi \rho_{aq_i}} \quad (5\text{-}20)$$

Back to where text linked to Box 5

Box 6 - Sorption Study Examples

Example 1: Campbell, C. (2017). Effects of capping material on longevity of degradable contaminants in sediments (master's thesis, Colorado State University, USA). Laboratory studies addressing sorption of diesel to an activated carbon reactive core mat. Campbell's MS research data. Calculations by Sale (Fall 2016).

REACTIVE CORE MAT™

WITH GRANULAR ACTIVATED CARBON CORE (GAC)

DESCRIPTION

REACTIVE CORE MAT™ GAC is an aqueous permeable composite of geotextiles and activated carbon that reliably adsorbs organics from water.

APPLICATION

REACTIVE CORE MAT™ GAC is designed for use in the following applications:

- In situ subaqueous cap for contaminated sediments or post-dredge residual sediments
- Embankment seepage control
- Groundwater remediation

BENEFITS

- REACTIVE CORE MAT™ GAC provides a reactive material that treats contaminants which are carried by advective or diffusive flow.
- Reactive cap allows for thinner cap thickness than a traditional sand cap.
- Geotextiles provide stability and physical isolation of contaminants.

REACTIVE CORE MAT™ GAC is designed to provide a simple method of placing active materials into subaqueous sediment caps.

TESTING DATA

PHYSICAL PROPERTIES		
PROPERTY	**TEST METHOD**	**RESULT**
ACTIVATED CARBON[1]		
Iodine Number	AWWA B604 or ASTM D4607	Min. 750 mg/g
FINISHED RCM PRODUCT		
Activated Carbon Mass per Area	Modified ASTM D5993	0.4 lb/ft²
Grab Strength[2]	ASTM D4632	90 lb. MARV
Permeability[3]	ASTM D 4491	1 x 10^{-3} cm/s min.

NOTES:
[1] Activated carbon properties performed prior to incorporation into the RCM
[2] All tensile testing in machine direction
[3] Permittivity at constant head of 2 inches and converted to hydraulic conductivity using Darcy's Law and RCM thickness per ASTM D5199 for geotextiles

PACKAGING

REACTIVE CORE MAT™ GAC is available in the following packaging option:

- 15' by 100' rolls, packaged on 4" PVC core tubes wrapped in polyethylene plastic

Figure Box 6-1 - Reactive Core Mat tested in the experiment.

1) Activate Carbon Reactive Core Mat

Assume $\phi := 0.5$

$\rho_b := 1 \cdot \frac{gm}{cm^3}$

$\omega_{AC} = \begin{pmatrix} 5.431\times 10^3 \\ 4.679\times 10^3 \\ 4.546\times 10^3 \\ 1.041\times 10^4 \\ 1.018\times 10^4 \\ 9.227\times 10^3 \\ 1.607\times 10^4 \\ 1.41\times 10^4 \\ 1.773\times 10^4 \\ 2.181\times 10^4 \\ 2.158\times 10^4 \\ 2.359\times 10^4 \\ 3.514\times 10^4 \\ 4.188\times 10^4 \\ 4.741\times 10^4 \\ 4.517\times 10^4 \\ 3.807\times 10^4 \\ 3.577\times 10^4 \\ 4.222\times 10^4 \\ 3.808\times 10^4 \\ 3.921\times 10^4 \\ 3.578\times 10^4 \\ 4.47\times 10^4 \end{pmatrix} \frac{mg}{kg}$ $\rho_{aq} = \begin{pmatrix} 0.998 \\ 1.03 \\ 0.666 \\ 2.504 \\ 1.74 \\ 0.732 \\ 3.323 \\ 4.097 \\ 5.88 \\ 6.707 \\ 6.452 \\ 5.583 \\ 8.243 \\ 12.583 \\ 14.221 \\ 13.535 \\ 9.867 \\ 13.847 \\ 18.062 \\ 13.027 \\ 11.415 \\ 10.852 \\ 17.297 \end{pmatrix} \frac{mg}{L}$

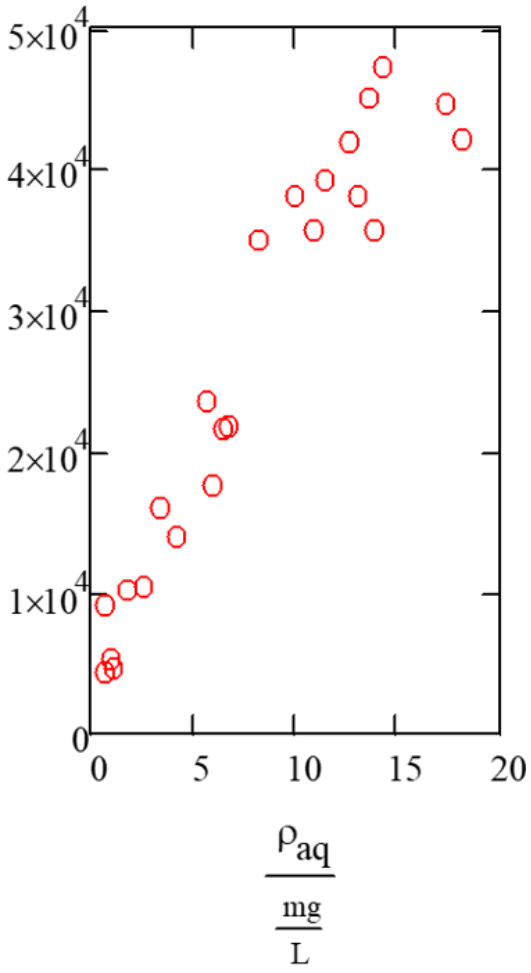

Linear

$$m_{\mathrm{ACLinear}} = \mathrm{slope}(\rho_{\mathrm{aq}}, \omega_{\mathrm{AC}}) = 2.552 \times 10^3 \frac{\mathrm{mL}}{\mathrm{gm}} \quad K_{d\mathrm{AC}} := m_{\mathrm{ACLinear}} = 2.552 \times 10^3 \frac{\mathrm{mL}}{\mathrm{gm}}$$

$$y_{\mathrm{ACLinear}} = \mathrm{intercept}(\rho_{\mathrm{aq}}, \omega_{\mathrm{AC}}) = 5.943 \times 10^3 \frac{\mathrm{mg}}{\mathrm{kg}}$$

$$R_{\mathrm{coor}} = \mathrm{corr}(\rho_{\mathrm{aq}}, \omega_{\mathrm{AC}}) = 0.955 \qquad R_{\mathrm{corr2}} = \mathrm{corr}(\rho_{\mathrm{aq}}, \omega_{\mathrm{AC}})^2 = 0.912$$

$$\omega_{\mathrm{ACLinear}}(\rho_{\mathrm{aq}}) = K_{d\mathrm{AC}} \rho_{\mathrm{aq}}$$

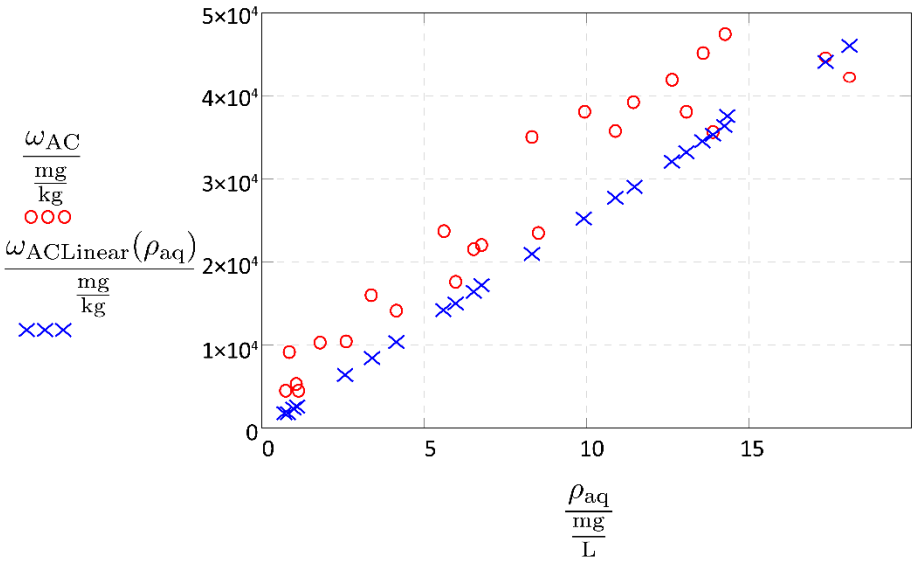

Freundlich

$$m_{\text{ACFreund}} = \text{slope}\left(\log\left(\rho_{\text{aq}}\frac{\text{L}}{\text{mg}}\right), \log\left(\omega_{\text{AC}}\right)\right) = 0{\cdot}704 \qquad n = m_{\text{ACFreund}}$$

$$y_{\text{ACFreund}} = \text{intercept}\left(\log\left(\rho_{\text{aq}}\frac{\text{L}}{\text{mg}}\right), \log\left(\omega_{\text{AC}}\right)\right) = -2{\cdot}194 \qquad K_{\text{FreundAC}} = 10^{y_{\text{ACFreund}}}$$

$$R_{\text{corr}^2\text{Freund}} = \text{corr}\left(\log\left(\rho_{\text{aq}}\frac{\text{L}}{\text{mg}}\right), \log\left(\omega_{\text{AC}}\right)\right) = 0{\cdot}968$$

$$R_{\text{corr}^2\text{Freund}} = \text{corr}\left(\log\left(\rho_{\text{aq}}\frac{\text{L}}{\text{mg}}\right), \log\left(\omega_{\text{AC}}\right)\right)^2 = 0{\cdot}938$$

$$\omega_{\text{ACFreund}}(\rho_{\text{aq}}) = K_{\text{FreundAC}}\rho_{\text{aq}}^{n}$$

Methods follows recommendations of Calista Campbell

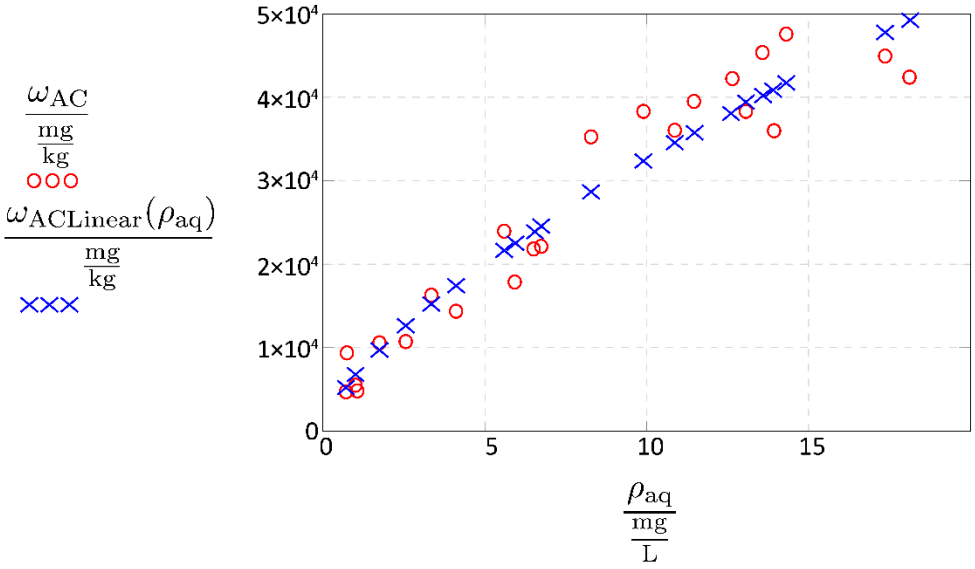

Langmuir

$\Gamma_{\max} = .085$ $K_L = 7 \times 10^4 \frac{\text{mL}}{\text{gm}}$ Parameters by iteration

$$\omega_{\text{ACLang}}(\rho_{\text{aq}}) = \frac{\Gamma_{\max} K_L \rho_{\text{aq}}}{1 + K_L \rho_{\text{aq}}}$$

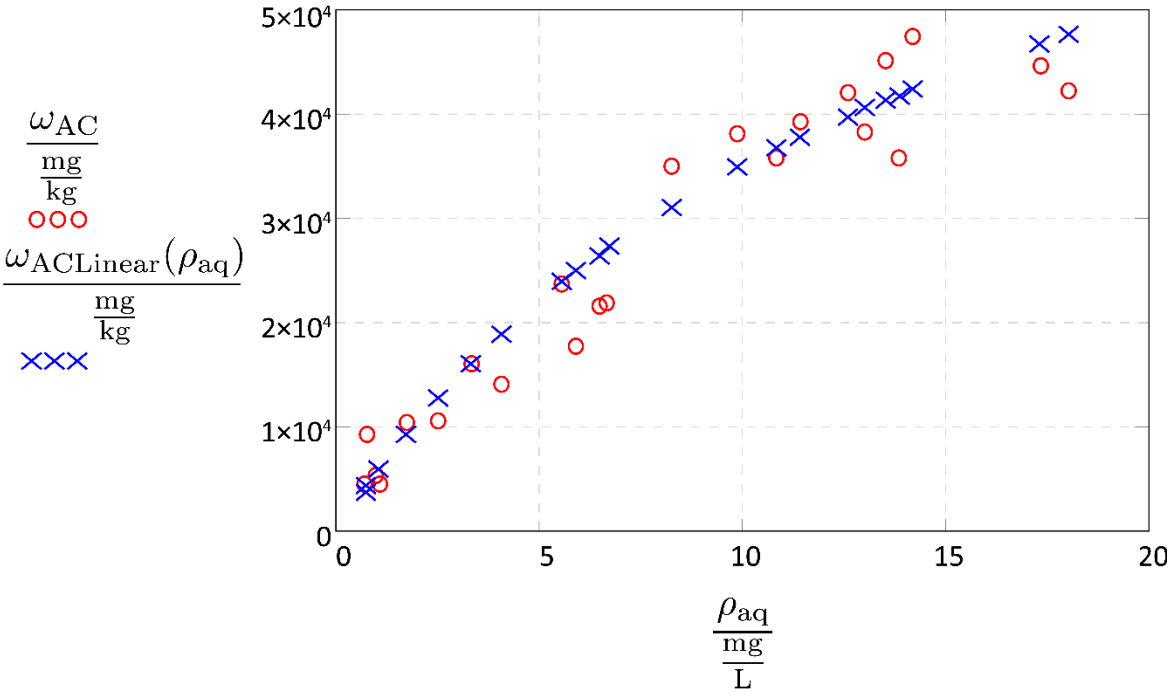

Example 2: McSpadden, R. (2016). Method development for long-term laboratory studies evaluating contaminant assimilation processes (master's thesis, Colorado State University). Laboratory studies were conducted to evaluate the fate of contaminants into low-*k* zones.

Figure Box-6-2 - Ampule vial setup with field soils and lab-grade soil.

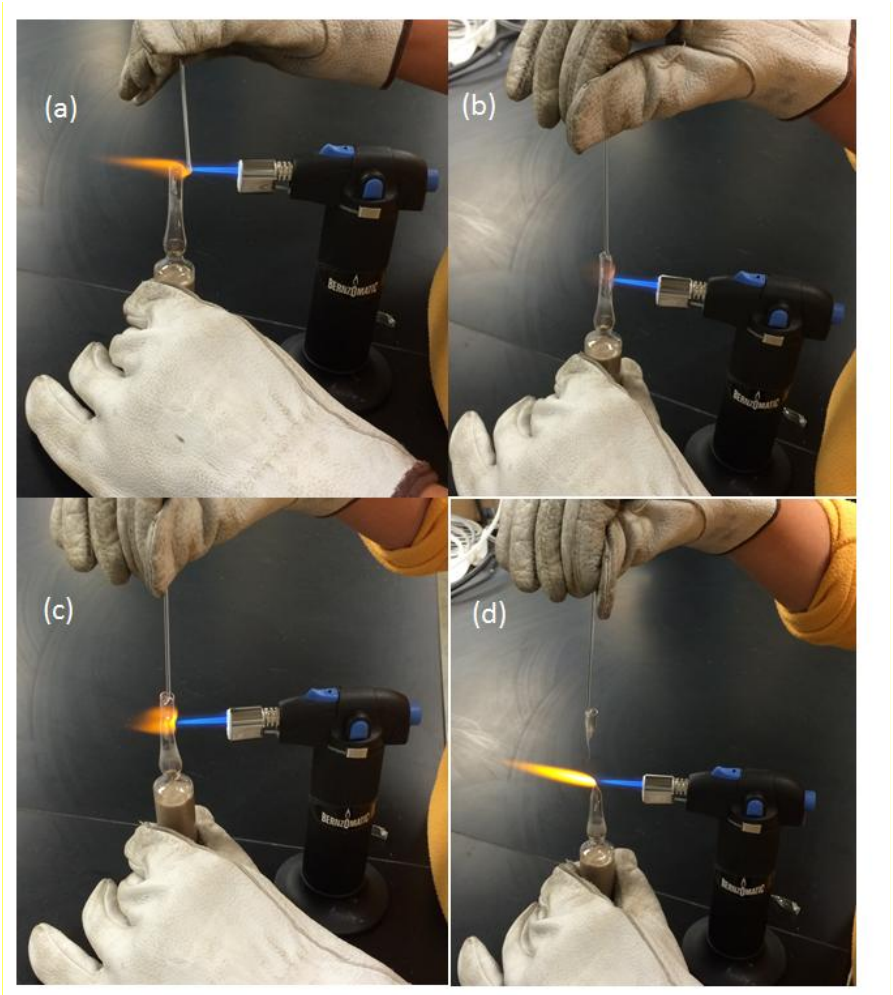

Figure Box 6-3 – Sealing ampule vials.

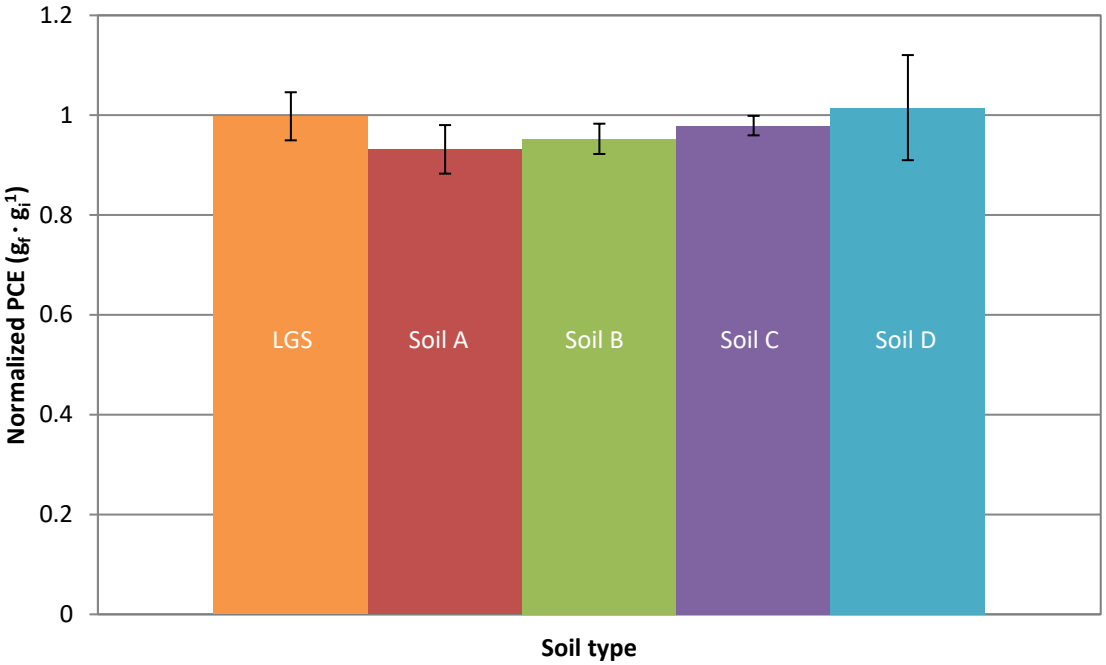

Figure Box 6-4 – Normalized PCE recovery for each soil type (final mass in grams over initial mass in grams) from ampules methanol extraction method with LGS and the four field soils.

Back to where text linked to Box 6

10 Exercise Solutions

Solution Exercise 1

- Only one of 14 compartments are informed by groundwater monitoring well data (i.e., the aqueous transmissive zone within the source).
- Only one of 14 compartments are informed by groundwater monitoring well data (i.e., the aqueous transmissive zone within the plume)

Return to Exercise 1
Return to where text linked to Exercise 1

Solution Exercise 2

Yes. If only two of 14 compartments are informed by data from groundwater monitoring wells, it seems likely that important aspects of the site conceptual model are not understood using only groundwater monitoring wells.

Return to Exercise 2
Return to where text linked to Exercise 2

Solution Exercise 3

Advection, diffusion, and reactions are the three primary processes governing transport in heterogeneous aquifers.

Return to Exercise 3
Return to where text linked to Exercise 3

Solution Exercise 4

Transmissive zones provide preferential flow paths. With equivalent gradients across low-*k* zones, their lower permeability results in lower rates of flow.

Return to Exercise 4
Return to where text linked to Exercise 4

Solution Exercise 5

Depositional environments inform stylistic occurrences of transmissive and low-*k* zones, including likely nature of occurrences of contaminants in transmissive and low-*k* zones, as well as the general distribution of biogeochemical conditions governing reactions.

Return to Exercise 5
Return to where text linked to Exercise 5

Solution Exercise 6

In addition to heterogeneous permeability, the following properties are also typically heterogeneous: natural organic material (NOM) that governs sorption, contaminant phases, contaminant concentrations, and biogeochemical conditions governing reactions.

Return to Exercise 6
Return to where text linked to Exercise 6

Solution Exercise 7

It is useful to embrace mathematics when studying transport of contaminants in subsurface media because it is a language wherein

- defined variables are critical vocabulary concepts, and
- solutions describe relationships between contaminant concentrations and physical attributes of sites.

Return to Exercise 7
Return to where text linked to Exercise 7

Solution Exercise 8

In the field, aquifers have preferential flow paths (transmissive zones) so contaminants arrive sooner at a fixed point as compared to arrival times in a homogeneous classroom aquifer.

Return to Exercise 8
Return to where text linked to Exercise 8

Solution Exercise 9

Even a stylistic concept of transmissive and low-k zones leads to embracing

- early arrival of plumes via transport in preferential flow paths,
- assimilation of contaminants into low-k zones while sources are active, and
- slow releases of contaminants from low-k zones that sustain plumes for extended periods, after sources have been removed.

Return to Exercise 9
Return to where text linked to Exercise 9

Solution Exercise 10

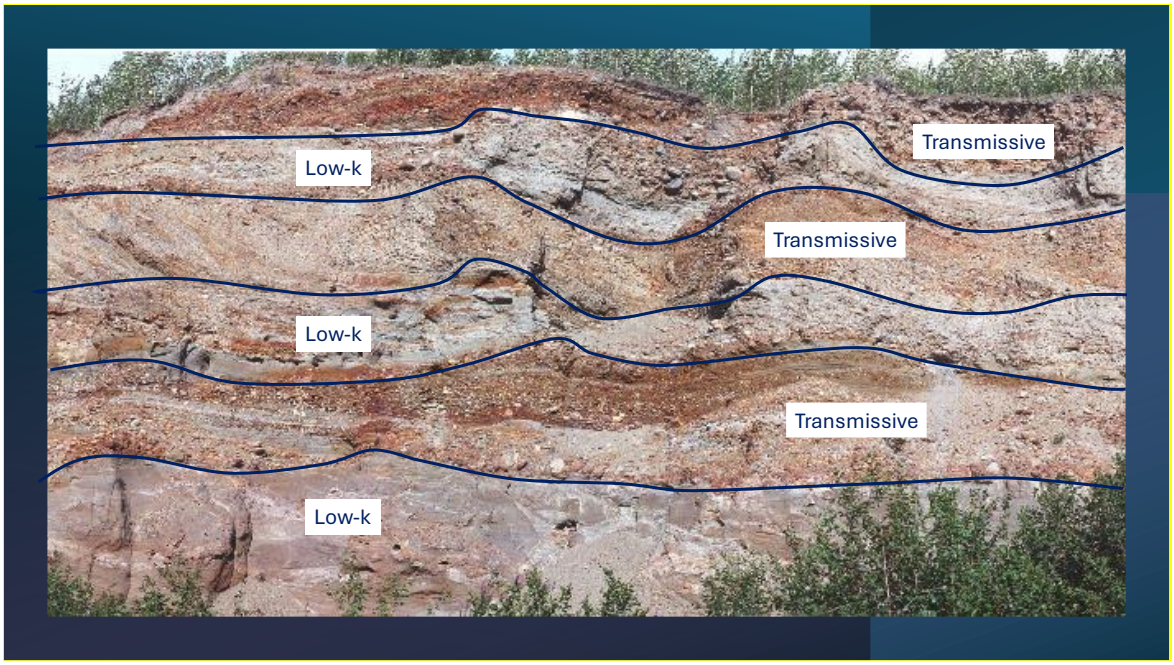

Return to Exercise 10
Return to where text linked to Exercise 10

Solution Exercise 11

- Smaller f_T values will lead to earlier arrival times. Arrival would be twice as fast for f_T of 0.5 and ten times faster for f_T of 0.1.
- Nine flow tubes contribute to well 1. One tube has water with a concentration of 100 ug/L and the others have a concentration of zero. Assuming no reactions and significant time, 1/9 (100 ug/L) + 8/9 (0 ug/L) = 11.1 ug/L.
- Uptake of TCE in low-*k* zones via diffusion will reduce concentrations at well 1 while the source is active and cause concentrations to remain above zero longer after the source is removed.
- If the source had been present for a significant time, concentration at the well would begin to decline and release of contaminants from low-*k* zones in the plume would begin to occur which would extend the period of contamination of well 1.

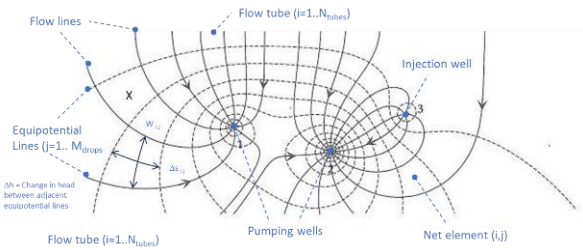

Return to Exercise 11
Return to where text linked to Exercise 11

Solution Exercise 12

No. Preferential flow of NAPLs through transmissive zones, with low-displacement pressures, will likely preclude movement of NAPLs into low-*k* zones with high-displacement pressures.

Return to Exercise 12
Return to where text linked to Exercise 12

Solution Exercise 13

Tubes associated with plants and animals or fractures associated with settlement can have larger openings than the matrix blocks of the low-*k* zones and low displacement pressures, allowing NAPL entry into low-*k* zones.

Return to Exercise 13
Return to where text linked to Exercise 13

Solution Exercise 14

Yes. If air–water capillary pressures are less than the displacement pressures, low-*k* zones above the water table can be fully saturated with water.

Return to Exercise 14
Return to where text linked to Exercise 14

Solution Exercise 15

Capillary pressures must be greater than displacement pressures for a nonwetting phase to displace a wetting phase in a saturated media.

Return to Exercise 15
Return to where text linked to Exercise 15

Solution Exercise 16

Having multiple immiscible fluids coexisting in pores leads to relative permeabilities for all fluid phases being less than 1 and, correspondingly, reduced capacity for conduction of all fluids.

Return to Exercise 16
Return to where text linked to Exercise 16

Solution Exercise 17

Models for multiple immiscible fluids, while not always accurate from a quantitative perspective, provide stylistic understanding of how the system functions.

Return to Exercise 17

Return to where text linked to Exercise 17

Solution Exercise18

- Up to three immiscible fluids can be present in pore spaces.
- Differential pressures between immiscible fluids known as capillary pressures govern fluid saturations.
- Fluid saturations govern relative permeability values that are always less than 1, with 1 being the saturated permeability.

Return to Exercise 18

Return to where text linked to Exercise 18

Solution Exercise 19

Two processes govern diffusion.

1. Molecules in solutions have kinetic energies that are temperature dependent, resulting in molecules having random velocity vectors distributed around a mean value.
2. Net contaminant fluxes occur in the direction of decreasing molecule velocities.

Return to Exercise 19

Return to where text linked to Exercise 19

Solution Exercise 20

The low-*k* zone will have a larger effective diffusion coefficient. Effective diffusion coefficients are a function of porosity. Zones with greater porosity will have larger effective diffusion coefficients.

Return to Exercise 20

Return to where text linked to Exercise 20

Solution Exercise 21

Loading into low-*k* zones is a function of historical, time-dependent, concentration gradients at transmissive–low-*k* zone boundaries. Factors governing concentration gradients at transmissive–low-*k* zone boundaries include groundwater velocity in the transmissive zone and source strength through time. After the effect of source removal reaches a point at a transmissive–low-*k* zone boundary, contaminants at the boundary begin to diffuse back into the transmissive zone, while contaminants farther into low-*k* zone continue to move into the low-*k* zone.

Return to Exercise 21
Return to where text linked to Exercise 21

Solution Exercise 22

The time it takes to release contaminants from low-*k* zones is typically far greater than the time it takes to load contaminants into low-*k* zones. Concurrent outward and inward diffusion in low-*k* zones after source removal or depletion can lead to tailing concentrations of contaminants in transmissive zones for long, often problematic periods of time.

Return to Exercise 22
Return to where text linked to Exercise 22

Solution Exercise 23

Sorption in low-*k* zones increases gradients driving contaminants into low-*k* zones. Correspondingly, sorption increases the total mass of contaminants in low-*k* zones. Once sources are removed, sorption in low-*k* zones increases the time over which contaminants can be released from low-*k* zones.

Return to Exercise 23
Return to where text linked to Exercise 23

Solution Exercise 24

Low-*k* zones commonly have greater sorptive capacities because they are usually deposited in quiescent environments in which greater amounts of natural organic carbon (NOM) are likely to be present, such as swamps or lacustrine deposits.

Limited transport of oxygen into low-*k* zones is likely to increase the stability/longevity of NOM deeper into low-*k* zones.

Return to Exercise 24
Return to where text linked to Exercise 24

Solution Exercise 25

No. Given the absence of low-*k* zones in classroom aquifers, there is *no* storage and release of contaminants in classroom aquifers in plumes.

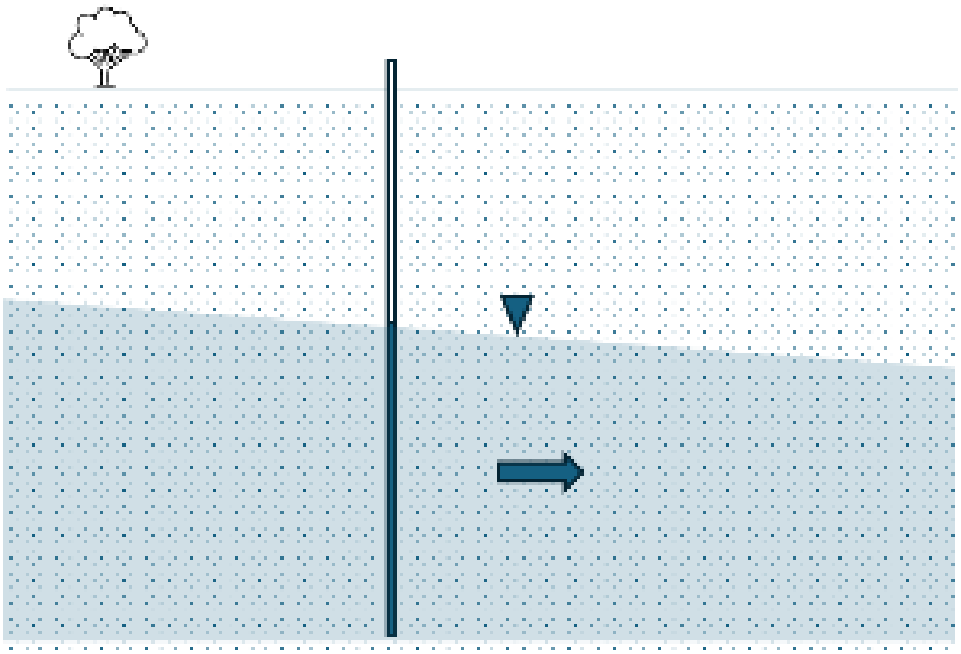

Return to Exercise 25

Return to where text linked to Exercise 25

Solution Exercise 26

Three field phenomena that are not observed in classroom aquifers include:

1. erroneous late arrival times of contaminants at points of interest in plumes,
2. missed early assimilation of contaminant concentrations in plumes by low-*k* zones, and
3. persistent tailing contaminant concentrations after sources are removed.

Return to Exercise 26

Return to where text linked to Exercise 26

Solution Exercise 27

A plume can have stable extent when loading from sources are constant and contaminants are moving in the plume if ongoing reactions in the plume destroy contaminants at the same rate that contaminants are added to the plume.

Return to Exercise 27

Return to where text linked to Exercise 27

Solution Exercise 28

Field evidence for NAPL dissolution

- presence of soluble NAPLs
- near-constant contaminant mass discharge from source zones

Field evidence for sorption

- retarded advancement of plumes
- for organic compounds, high levels of natural organic carbon

Field evidence for transformation

- favorable thermodynamic conditions
- observations of reaction byproducts
- shifts in ratios of stable contaminant isotopes

Return to Exercise 28

Return to where text linked to Exercise 28

Solution Exercise 29

If investigation at a contaminated site looked only for CoCs in groundwater then, contaminants in other phases (i.e., NAPL, sorbed, and gases) in transmissive zones would be missed and all contaminant phases in low-*k* zones would be missed.

Return to Exercise 29

Return to where text linked to Exercise 29

Solution Exercise 30

As our models for reactions are based on simplifications of complex settings and governing processes, they should not be viewed as rigorous forecasts of dissolution, sorption, or transformation in heterogeneous field settings.

Return to Exercise 30

Return to where text linked to Exercise 30

Solution Exercise 31

Yes, there significant uncertainties associated with the input parameters used for our reaction models. It is difficult to accurately measure input parameters (e.g., effective diffusion coefficients), and the true spatial variations of input parameters in heterogeneous aquifers is often unknowable.

Return to Exercise 31

Return to where text linked to Exercise 31

Solution Exercise 32

Three general approaches to modeling are:

- empirical,
- analytical, and
- numerical.

Return to Exercise 32

Return to where text linked to Exercise 32

Solution Exercise 33

Long-term forecasts of contaminant concentrations in plumes are likely to be more flawed than short-term forecasts. Accumulating errors associated with model assumptions, flawed estimates of parameter inputs, and missed processes are likely to grow with time.

Return to Exercise 33

Return to where text linked to Exercise 33

Solution Exercise 34

Numerical methods create numerical dispersion that has nothing to do with contaminant transport when discretization of time and/or space are so large that truncated (dropped) terms in series approximations of derivatives are large.

Return to Exercise 34

Return to where text linked to Exercise 34

Solution Exercise 35

Two mathematical approaches that can capture preferential transport in transmissive zones, diffusive exchanges of contaminants between transmissive and low-*k* zones, and spatially varying reactions in transmissive and low-*k* zones are:

- analytical solutions where separate PDEs are used for transmissive and low-*k* zones and equations are linked by equating contaminant fluxes and/or concentrations at transmissive–low-*k* zone boundaries; and
- high-resolution numerical models where insufficient discretization of time and space is demonstrated by iteratively reducing discretization until solutions converge to constant values.

Return to Exercise 35

Return to where text linked to Exercise 35

Solution Exercise 36

Models are useful for:

- building stylistic understanding of governing processes to support decisions for managing subsurface releases, and
- sharing best understandings of sites with broad audiences.

Return to Exercise 36

Return to where text linked to Exercise 36

Solution Exercise 37

Models are not useful for accurately forecasting future conditions at large times.

Return to Exercise 37

Return to where text linked to Exercise 37

Solution Exercise 38

Yes. It is amazing that Theis foresaw the problems we would be confronted with through the 1970s,1980s, 1990s, 2000s, and 2010s.

Return to Exercise 38

Return to where text linked to Exercise 38

Solution Exercise 39

We can move forward by employing the observational approach as outlined by Peck, including these elements:

- site investigation sufficient to establish a general site conceptual model, but not necessarily in detail.
- assessing the most probable conditions (extent, transport, and fate of contaminants) and the most unfavorable conceivable deviations from these conditions.
- establishing the remedial design based on a working hypothesis of behavior anticipated under the most probable conditions.
- selecting parameters and locations to be observed as remediation proceeds and calculating anticipated values based on the working hypothesis.
- selecting in advance of contingency plans for foreseeable significant deviation.
- measuring parameters to be observed and evaluating actual conditions.
- modifying the plans for remediation considering the observational results.

Return to Exercise 39

Return to where text linked to Exercise 39

11 Notations

A = slope of a uniform water surface in the x direction (dimensionless)

α_L = longitudinal dispersivity (L)

A_T = cross-sectional area normal to transport (L^2)

α_T = transverse dispersivity (L)

B = slope of a uniform water surface in the y direction (dimensionless)

b = aquifer saturated thickness (L) – also used as in next row

b = for the Dandy–Sale model (DSM), source distribution constant (L^{-1}) – also used as in previous row

$b``$ = space between two plates an equivalent fracture aperture (L)

b_{pool} = height of a NAPL pool (L)

C = integration constant (units per equation of interest)

C_{aq} = mole-based aqueous phase solute mass concentration (moles L^{-3})

C_{g_i} = molar gas phase concentration of compound ***i*** (moles L^{-3})

CL = chloride

$D_{e_{aq}}$ = effective aqueous phase diffusion coefficient (L^2T^{-1})

D_{e_g} = effective gas phase diffusion coefficient (L^2T^{-1}

$D_{m_{aq}}$ = aqueous phase molecular diffusion coefficient (L^2T^{-1})

D_{m_g} = gas phase molecular diffusion coefficient (L^2T^{-1})

D_{m_i} = molecular diffusion coefficient for compound ***i*** (L^2T^{-1})

D_t = transmissive zone transverse diffusion coefficient (L^2T^{-1})

$D_t`$ = low-k zone transverse diffusion coefficient (L^2T^{-1})

E = potential (cell or redox) ($ML^2T^{-3}I^{-1}$) typically in volts

E_h = redox potential ($ML^2T^{-3}I^{-1}$) typically in volts

F = Farday's Constant ($TI\ mole^{-1}$) typically in coulomb per mole

f_{lk} = low-permeability formation fraction (dimensionless)

f_{oc} = weight basis organic carbon porous media fraction (dimensionless)

f_T = transmissive formation fraction (dimensionless)

γ_i = activity coefficient for compound i (dimensionless)

G_m = contaminant source strength ($MT^{-1}L^{-3}$)

g = gravitational constant (LT^{-2})

ΔG_r = Gibbs free energy of reaction (ML^2T^{-2} $mole^{-1}$) typically in joules/mole

ΔG_f = Gibbs free energy of formation (ML^2T^{-2} $mole^{-1}$)

$\Delta G_a z$ = Gibbs free energy of activation (ML^2T^{-2} $mole^{-1}$)

h_i = head, potential energy driving flow of fluid I (L)

h_j = head, potential energy driving flow of fluid j (L)

Δh_{Tube} = change in head between equipotential lines in a flow net (L)

θ_w = angle between a wetting phase and a solid (degrees)

θ_w = angle between air-water and water-solid interfaces (degrees)

i = subscript denotes a compound or CoC (dimensionless)

j = subscript denotes a fluid (dimensionless)

k = permeability (L^2)

$k_{T_A}^0$ = zero-order rate constant for the total contaminant mass of compound A ($ML^{-3}T^{-1}$)

$k_{T_A}^1$ = first-order rate constant for total contaminant mass of compound A (T^{-1})

K = hydraulic conductivity (LT^{-1})

K^o = dissociation constants measured under standard conditions (dimensionless)

K_{H_i} = Henry's coefficient for compound i (MT^{-2} mole)

K_{HD_i} = dimensionless Henry's coefficient for compound i (dimensionless)

K_{oc_i} = octanol water portioning coefficient for compound i (L^3M^{-1})

J_{ad_i} = advective flux of compound i ($ML^{-2}T^{-1}$)

$J_{ad_{i,j}}$ = advective flux of compound i due to advection of fluid j ($ML^{-2}T^{-1}$)

J_{D_i} = diffusive flux of compound i ($ML^{-2}T^{-1}$)

J_{T_i} = total solute mass flux ($ML^{-2}T^{-1}$)

K = hydraulic conductivity (LT^{-1})

K_{aq} = hydraulic conductivity to water (LT^{-1})

K_{NAPL} = NAPL conductivity (LT^{-1})

k = permeability (L^2)

K_{d_i} = sorption coefficient (L^3M^{-1})

k_{r_i} = relative permeability for fluid i (dimensionless)

k_{r_j} = relative permeability for fluid j (dimensionless)

k_{rw} = relative permeability to wetting phase (dimensionless)

k_{rnw} = relative permeability to nonwetting phase (dimensionless)

λ = first-order decay rate constant (T^{-1})

λ = Brooks–Corey model fitting parameter factor (dimensionless)

L = position in the direction of flow or transport (L)

L = length of a NAPL pool in the direction of flow (L)

$\dot{M}_{ad_i}$ = CoC mass discharge due to advection in fluid i (MT^{-1})

$\dot{M}_{Source}$ = CoC mass discharge from a source (MT^{-1})

$\dot{M}$ = CoC mass discharge (MT^{-1})

$\dot{M}_{pool}$ = rate of dissolution from a NAPL pool (MT^{-1})

M_R = total contaminant mass released (M)

M_{t_i} = total contaminant mass in a plume at time t_i (M)

MW_i = molecular weight for compound i (amu) atomic mass units

m_A = mass of particle A (M)

m_B = mass of particle B (M)

μ_{aq} = water viscosity ($ML^{-1}T^{-1}$)

μ_i = viscosity of fluid $\boldsymbol{i}$ ($ML^{-1}T^{-1}$)

μ_j = viscosity of fluid ***j*** ($ML^{-1}T^{-1}$)

μ_{NAPL} = NAPL viscosity ($ML^{-1}T^{-1}$)

μ_g = gas viscosity ($ML^{-1}T^{-1}$)

n = number of moles (dimensionless)

$N_{Elements}$ = number of elements in a flow net (dimensionless)

N_{tubes} = number of stream tubes in a flow net (dimensionless)

ω_{aq} = aqueous solute contaminant mass per dry mass porous media (dimensionless)

ω_{g_i} = gas phase mass of compound i per dry mass porous media (dimensionless)

$\omega_{NAPL-Thresh}$ = total mass of compound i per dry mass porous media, above which NAPLs are present (dimensionless)

ω_{s_i} = sorbed mass of compound i per dry mass porous media (dimensionless)

ω_{T_i} = total mass of compound i per dry mass porous media (dimensionless)

ϕ = transmissive zone porosity (dimensionless)

ϕ` = low-*k* zone porosity (dimensionless)

π = constant pi (dimensionless)

P = pressure ($ML^{-1}T^{-2}$)

P_c = capillary pressure ($ML^{-1}T^{-2}$)

P_d = displacement pressure ($ML^{-1}T^{-2}$)

P_{nw} = fluid pressure in a nonwetting fluid ($ML^{-1}T^{-2}$)

P_{iw} = fluid pressure in an intermediate wetting fluid ($ML^{-1}T^{-2}$)

P_w = fluid pressure in wetting fluid ($ML^{-1}T^{-2}$)

ρ_{aq_s} = saturated aqueous phase solute concentration (ML^{-3})

$\overline{\rho_{aq}}$ = vertically averaged aqueous concentrations from a monitoring well (ML^{-3})

ρ_{aq_i} = mass-based aqueous phase solute concentration for compound ***i*** (ML^{-3})

$\rho_{aq_{ei}}$ = effective solubility of mass-based aqueous solute concentration for compound ***i*** (ML^{-3}) given multiple NAPLs

$\rho_{aq_{si}}$ = saturated mass-based aqueous solute concentration for compound ***i*** (ML^{-3})

ρ_b = dry-weight porous media bulk density for the transmissive zone (ML^{-3})

ρ_b` = Dry-weight porous media bulk density for the low-*k* (ML^{-3})

ρ_{g_i} = mass-based gas phase solute concentration for compound *i* (ML^{-3})

$\rho_{i,j}$ = mass-based concentration for compound *i* in fluid *j* (ML^{-3})

ρ_i = density of fluid *i* (ML^{-3})

ρ_{j_i} = mass-based concentration of CoC *j* in fluid *i* (ML^{-3})

ρ_{NAPL} = nonaqueous phase liquid density (ML^{-3})

$P_{gas_i}^{NAPL}$ = partial pressure of compound of i in a gas adjacent to a NAPL ($ML^{-1}T^{-2}$)

pH = -log[H^+] proton activitity (dimensionless)

pe = -log[e^-] electron activity (dimensionless)

ρ_0 = constant or initial mass based aqueous concentration (ML^{-3})

ρ_{PMT_i} = total mass of compound ***i*** per volume of porous media (M/L^3)

ρ_w = water density (ML^{-3})

σ = interfacial forces ($ML^{-1}T^{-2}$)

σ_{sw} = solid-water interfacial tension (MLT^{-2})

σ_{sa} = solid-air surface tension (MLT^{-2})

σ_{wa} = water-air surface tension (MLT^{-2})

Q = volumetric fluid discharge (L^3T^{-1})

Q_r = reaction quotient (dimensionless)

Q_{Tube_i} = volumetric discharge in stream tube ***i*** in a flow net (L^3T^{-1})

Q_{well} = volumetric discharge from a well (L^3T^{-1})

q = volumetric flux ($L^3L^{-2}T^{-1}$ or LT^{-1})

q_{aq} = Darcy or volumetric water flux ($L^3L^{-2}T^{-1}$ or LT^{-1})

q_g = Darcy or volumetric gas flux ($L^3L^{-2}T^{-1}$ or LT^{-1})

q_{ad_i} = volumetric advective flux of fluid i in porous media ($L^3L^{-2}T^{-1}$)

q_{ad_j} = volumetric advective flux of fluid j in porous media ($L^3L^{-2}T^{-1}$)

$q``_{ad_i}$ = volumetric advective flux of fluid i in a fracture ($L^3L^{-2}T^{-1}$)

q_{NAPL} = Darcy or volumetric NAPL flux (L^3/L^2T or L/T)

R = ideal gas constant ($ML^2T^{-2}\Theta^{-1}$) typically in joules per mole-Kelvin

R_i = transmissive zone retardation factor for compound i (dimensionless)

$R`_i$ = low-*k* zone retardation factor for compound $\boldsymbol{i}$ (dimensionless)

R_{aq} = aqueous phase solute retardation factor (dimensionless)

R_g = gas phase solute retardation factor (dimensionless)

$\dot{R}_{plume}$ = rate of total contaminant losses in a plume (MT^{-1})

R_m = contaminant source strength ($MT^{-1}L^{-3}$)

r = radial distance (L)

S = storage coefficient (dimensionless)

S_r = irreducible wetting phase saturation (dimensionless)

S_{wd} = saturation of the wetting phase under drainage (dimensionless)

S_{wi} = saturation of the wetting phase under wetting phase imbibition (dimensionless)

S_e = effective wetting phase saturation (dimensionless)

S_m = saturation at which a nonwetting phase becomes discontinuous (dimensionless)

s = distance along a streamline in the middle of a stream tube parallel to flow (L)

S_g = gas saturation (dimensionless)

S_{NAPL} = NAPL saturation (dimensionless)

S_w = water or wetting phase saturation (dimensionless)

S_s = specific storage coefficient (L^{-1})

SSA = specific surface area (L^3L^{-2} or L)

T = temperature (Θ) typically degrees Kelvin or Celsius

T_{aq} = transmissivity to water (L^2T^{-1})

T_{NAPL} = transmissivity to NAPL (L^2T^{-1})

t = time (T)

t' = source off time (T)

$t_{elememt_{i,j}}$ = time to traverse flow net element i, j (T)

$t_{source\ to\ well}$ = time to traverse from source to well in a flow net

τ = tortuosity (dimensionless)

V = volume (L^3)

v_{aq} = aqueous phase (water) seepage velocity (LT^{-1})

v_{ad_i} = advective velocity of CoC i (LT^{-1})

$\bar{v}_A$ = mean velocities of particles A (LT^{-1})

$\bar{v}_B$ = mean velocities of particles B (LT^{-1})

W = width of a NAPL pool or source (L)

w_c = upgradient width of a pumping wells capture zone (L)

$W_{i,j}$ = midpoint stream tube width transverse to flow (L)

x = spatial position (L) horizontal or in direction of advective transport

χ_i = mole fraction of compound i (dimensionless)

χ_{NAPL_i} = mole fraction of compound i in a NAPL (dimensionless)

x_s = distance to a stagnation point down gradient of a pumping well (L)

y = horizontal spatial position (L) transverse to the direction of advective transport

z = vertical spatial position (L)

z_c = height of capillary rise (L)

12 About the Authors

Tom Sale is an emeritus professor in the department of civil and environmental engineering at Colorado State University, US. His 43-year career includes extensive consulting engineering, research, teaching, and commercialization of technologies with a focus on working with industry and government to manage the environmental impacts of our modern lifestyles. Dr. Sale has followed a path of interdisciplinary studies with BA degrees in chemistry and geology (Miami University of Ohio), an MS in watershed hydrology (University of Arizona), and a PhD in agricultural engineering (Colorado State University). Dr. Sale is the founder and former director of the Center for Contaminant Hydrology in Civil and Environmental Engineering at Colorado State University and a former associate director of the University Consortium for Field-Focused Groundwater Research. Primary funding for Dr. Sale's research has come from Chevron, DuPont, Suncor Energy, ExxonMobil, DOW, Boeing, the US Department of Defense, and Colorado State University, including revenue from patents. In 2024, Dr. Sale received the Colorado State University 2024 STRATA Innovator of the Year award.

Joe Scalia joined the department of civil and environmental engineering at Colorado State University in 2015 and is currently an associate professor. He holds an MS and PhD in geological engineering from the University of Wisconsin-Madison and a BS in civil and environmental engineering from Bucknell University. He is a principal investigator at the University Consortium for Field-Focused Groundwater Research, and a founding member and CSU site director of the Tailings Center. His research and teaching focus on tailings and mine waste, contaminant transport, geo-hydrotechnics, and unsaturated terramechanics. In 2021, Dr. Scalia received the inaugural Robert and Mitchell Landreth Steward of the Environment award.

Please consider signing up for the GW-Project mailing list to stay informed about new book releases, events, and ways to participate in the GW-Project. When you sign up for our email list, it helps us build a global groundwater community. Sign up↗.